Function and modulation of TRPM2 channels

Zou, Jie

Submitted in accordance with the requirements for the
Degree of Doctor of Philosophy

The University of Leeds, School of Biomedical Sciences

September, 2013

The candidate confirms that the work submitted is her own and that appropriate credit has been given where reference has been made to the work of others.

Acknowledgments

Firstly, I would like to express my sincerest gratitude to Dr. Lin-Hua Jiang, my supervisor, who has provided knowledge, understanding and patience to support me throughout my PhD study. Before I started my Ph.D project in University of Leeds, I had little idea about my study about ion channels because of my background in physics. Without his patient training and instructions over the past few years, I can hardly get improvement in my scientific research. I also would like to thank my co-supervisor, Prof. David J Beech, and my assessor, Dr. Nikita Gamper, for their assistance at every steps of my research project. I also would like to thank the other members of our group, Dr. Wei Yang, Ms Alicia Sedo, who provided their helpful assistance throughout my project.

I would like to thank the University of Leeds and China Scholarship Council for providing a scholarship funding my tuition fee and living cost, respectively. Also, I want to thank the School of Biomedical Sciences at the University of Leeds, for providing research facilities. Many thanks are also due to Dr. Jing Li, Prof. Asipu Sivaprasadarao, Dr. Christopher J Cockcroft, Dr. Yasser Majeed, Mr. Hongsen Peng and Ms. Hon-Lin Rong, for their help in the lab.

Especially, I would like to thank my parents, my husband and my friends for supporting and encouraging me through my entire life.

Abstract

Melastatin-related transient receptor potential 2 (TRPM2) channel is a Ca^{2+}-permeable cation channel that is gated by ADP-ribose (ADPR) and also activated by reactive oxygen species (ROS) such as H_2O_2. TRPM2 channel are shown to be critically involved in several physiological and pathological cell processes.

Previous studies have reported inhibition of the human TRPM2 channel by extracellular acidic pH. However, the underlying mechanism is not fully understood. In the present study, I performed patch-clamp recordings to examine the effect of extracellular acidic pH on ADPR-induced currents in HEK293 cells heterogeneously expressing human TRPM2 (hTRPM2) or mouse TRPM2 (mTRPM2) channels. The results showed that the inhibition was substantially reversible upon brief exposure to acidic pH but became irreversible after prolonged exposure, supporting the mechanism in which protons bind to and inhibit the open TRPM2 channel and the proton-binding induces further conformational changes leading to channel inactivation. Furthermore, the mTRPM2 channel exhibited a lower sensitivity to, and slower kinetics of, inhibition, than the hTRPM2 channel. A residue in the pore region (His-995 in hTRPM2 and Gln-992 in mTRPM2) had a crucial role in determining such species differences.

The pharmacology of the TRPM2 channel is poor, with no specific inhibitor. Here, I examined the effects of 48 hit compounds identified from screening chemical libraries on hTRPM2 channels expressed in HEK293 cells. Four compounds inhibited H_2O_2-induced Ca^{2+}-response with a micromolar to submicromolar potency and abolished ADPR-induced currents at 10 μM, indicating that they act as TRPM2 channel inhibitors.

The TRPM2 channel was reported to be functionally expressed in macrophage cells, but its role in mediating ROS-induced Ca^{2+} signalling and cell death is largely unclear. This study examined the contribution and mechanism of the TRPM2 channel in H_2O_2-induced Ca^{2+}-responses and cell death in RAW264.7 and differentiated THP-1 macrophage cells and peritoneal macrophage cells isolated from $TRPM2^{+/+}$ and $TRPM2^{-/-}$ mice. The results showed that TRPM2 channels operated as cell surface Ca^{2+}-permeable channels and constituted the principal Ca^{2+} signalling mechanism, but played a limited role in cell death.

In summary, the results from my study provided useful information to advance the understanding of the pharmacology and functional roles of the TRPM2 channels.

Contents

ACKNOWLEDGMENTS ····· **2**

ABSTRACT ····· **3**

CONTENTS ····· **4**

LIST OF FIGURES ····· **8**

LIST OF TABLES ····· **10**

LIST OF ABBREVIATIONS ····· **11**

LIST OF AMINO ACIDS ····· **17**

CHAPTER 1 GENERAL INTRODUCTION ····· **18**

1.1 TRP CHANNEL SUPERFAMILY ····· 19

1.1.1 TRPC subfamily ····· *22*

1.1.2 TRPV subfamily ····· *24*

1.1.3 TRPA subfamily ····· *26*

1.1.4 TRPM subfamily ····· *26*

1.1.5 TRPML subfamily ····· *28*

1.1.6 TRPP subfamily ····· *29*

1.2 TRPM2 CHANNELS ····· 31

1.2.1 Molecular cloning and cellular/ tissue distribution ····· *31*

1.2.2 Molecular or structural properties ····· *32*

1.2.2.1 Functional properties of the TRPM2 channels ····· 32

1.2.2.2 Channel assembly ····· 33

1.2.2.3 Other domains ····· 38

1.2.3 Alternative splicing isoforms ····· *39*

1.2.4 Subcellular location ····· *40*

1.2.5 Pharmacology of TRPM2 channels ····· *41*

1.2.5.1 Channel activators ····· 41

1.2.5.1.1 ADPR ····· 41

1.2.5.1.2 Nicotinic acid adenine dinucleotide phosphate (NAADP) ····· 43

1.2.5.1.3 NAD ····· 44

1.2.5.1.4 cADPR ····· 44

1.2.5.1.5 Ca^{2+} ····· 45

1.2.5.1.6 Reactive oxygen species ····· 46

1.2.5.1.7 Temperature ····· 48

1.2.5.2 Inhibitors ····· 49

1.2.5.2.1 N-(p-amylcinnamoyl) anthranilic acid (ACA) 49
1.2.5.2.2 Flufenamic acid (FFA) and its homologue 49
1.2.5.2.3 Clotrimazole and econazole 50
1.2.5.2.4 2-APB 52
1.2.5.2.5 Adenosine monophosphate (AMP) 52
1.2.5.2.6 Divalent cations 53
1.2.5.2.7 Acidic pH 53
1.2.6 Modulation of TRPM2 channel functions by interacting proteins 55
1.2.6.1 Protein tyrosine phosphatase-L1 (PTPL1) 55
1.2.6.2 Calmodulin and EF-hand domain-containing (EFHC) protein 1 56
1.2.7 Physiological functions 57
1.2.7.1 Cytokine production 57
1.2.7.2 Insulin secretion 59
1.2.8 Pathological functions 62
1.2.8.1 ROS-induced increases in endothelial permeability 62
1.2.8.2 ROS-induced cell death 63
1.2.8.3 Cancer cell proliferation 64
1.2.9 TRPM2 channels in diseases 64
1.2.9.1 Alzheimer's disease 64
1.2.9.2 Amyotrophic lateral sclerosis and Parkinsonism-dementia 65
1.3 AIM OF THE CURRENT STUDY 66
CHAPTER 2 MATERIALS AND METHODS 67
2.1 MATERIALS 68
2.1.1 Mammalian cells lines 68
2.1.2 E.Coli strains 68
2.1.3 Plasmids and primers 68
2.1.4 Animals 68
2.1.5 Chemicals 69
2.1.6 Antibodies 69
2.1.7 Solutions 69
2.1.8 Growth medium for mammalian cells and E.Coli cells 69
2.2 METHODS 70
2.2.1 Mammalian cell culture 70
2.2.1.1 Maintenance 70
2.2.1.2 Induction of tetracycline-inducible HEK293 cells stably expressing the hTRPM2 70
2.2.1.3 Differentiation of THP-1 cells 70
2.2.1.4 Cell passage 71
2.2.1.5 Restoration of frozen cells 72
2.2.1.6 Freezing cells 72

2.2.2 Isolation of mouse peritoneal macrophage *72*
2.2.3 Cell counting *72*
2.2.4 Cell preparation *73*
2.2.5 Transient transfection *73*
2.2.6 Polymerase chain reaction *74*
2.2.7 Site-directed mutagenesis *74*
2.2.7.1 Primer design 74
2.2.7.2 Restriction enzyme digestion 75
2.2.8 Agarose gel electrophoresis *75*
2.2.8.1 Agarose gel preparation 75
2.2.8.2 Gel electrophoresis 75
2.2.9 Heat shock transformation *76*
2.2.10 Mini-preparation of plasmid DNA *76*
2.2.11 DNA sequencing *77*
2.2.12 Immunofluorescent confocal imaging *77*
2.2.13 Patch clamp recording *78*
2.2.13.1 Principles 78
2.2.13.2 Solutions for TRPM2 channel current recordings 81
2.2.13.3 Procedures for whole-cell TRPM2 channel current recording 82
2.2.14 Calcium imaging using fluorescent dyes *83*
2.2.14.1 Principle 83
2.2.14.2 Solutions 83
2.2.14.3 Procedures of single cell calcium imaging 84
2.2.14.4 Procedure of Flex-station experiments 84
2.2.15 XTT assay *85*
2.2.16 Trypan blue exclusion assay *85*
2.2.17 Data analysis *86*

CHAPTER 3 A RESIDUE IN THE TRPM2 CHANNEL OUTER PORE IS CRUCIAL IN DETERMINING SPECIES-DEPENDENT SENSITIVITY TO EXTRACELLULAR ACIDIC PH 88

3.1 INTRODUCTION 89
3.2 RESULTS 90
3.2.1 Inhibition of H_2O_2-induced increases in the $[Ca^{2+}]_c$ and ADPR-induced currents by ACA in HEK293 cells expressing hTRPM2 channel *90*
3.2.2 Exposure duration-dependent reversibility of hTRPM2 channel inhibition *92*
3.2.3 Differential inhibition of the mTRPM2 and hTRPM2 channel currents by acidic pH *92*
3.2.4 Accelerated kinetics of, and increased sensitivity to, inhibition by acidic pH by His substitution of pore residue Gln-992 in mTRPM2 channel *98*

3.2.5 Decelerated kinetics of inhibition by acidic pH by reciprocal mutation of His-995 in the hTRPM2 channel ····· *102*

3.3 DISCUSSION ····· 107

CHAPTER 4 CHARACTERIZATION OF NOVEL TRPM2 CHANNEL INHIBITORS ····· 110

4.1 INTRODUCTION ····· 111

4.2 RESULTS ····· 112

4.2.1 Inhibition of H_2O_2-induced increases in $[Ca^{2+}]_c$ by the TRPM2 inhibitor candidates ····· 112

4.2.2 Potency of select TRPM2 inhibitor candidates ····· 120

4.2.3 Inhibition of ADPR-induced currents by TRPM2 inhibitor candidates ····· 120

4.2.4 Derivatives of No.13 and No.07 ····· 126

4.3 DISCUSSION ····· 137

CHAPTER 5 EXPRESSION OF TRPM2 CHANNELS AND THEIR ROLE IN H_2O_2-INDUCED CA^{2+} RESPONSES AND CELL DEATH IN MACROPHAGE CELLS ····· 140

5.1 INTRODUCTION ····· 141

5.2 RESULTS ····· 143

5.2.1 Optimization of the working conditions of anti-TRPM2 antibody ····· 143

5.2.2 TRPM2 protein expression in RAW264.7, PMA-differentiated THP-1 and peritoneal macrophage cells ····· 143

5.2.3 H_2O_2-induced increases in the $[Ca^{2+}]_c$ in macrophage cells mainly result from extracellular Ca^{2+} influx and are temperature dependent ····· 146

5.2.4 Functional expression of the TRPM2 channels in peritoneal macrophage cells ····· 150

5.2.5 Contribution of TRPM2 channel in H_2O_2-induced cell death in RAW264.7, PMA-differentiated THP-1 and peritoneal macrophage cells ····· 154

5.3 DISCUSSION ····· 161

CHAPTER 6 SUMMARY AND CONCLUSIONS ····· 164

6.1 SUMMARY OF FINDINGS ····· 165

6.1.1 The crucial contribution of a pore residue in determining species-dependent inhibition of TRPM2 channels by extracellular acidic pH ····· 165

6.1.2 Identification of novel and potent TRPM2 channel inhibitors ····· 166

6.1.3 Expression of TRPM2 channels and their role in H_2O_2–induced Ca^{2+} responses and cell death in macrophage cells ····· 167

6.2 GENERAL DISCUSSION ····· 168

6.3 CONCLUSIONS ····· 170

REFERENCES ····· 171

List of figures

FIGURE 1.1 THE FAMILY TREE OF THE MAMMALIAN TRP CHANNEL PROTEINS..... 20

FIGURE 1.2 SCHEMATIC REPRESENTATION OF THE MAIN STRUCTURAL FEATURES OF THE MEMBERS OF THE SIX MAMMALIAN TRP CHANNEL SUBFAMILIES 21

FIGURE 1.3 TRPM2 AMINO ACID SEQUENCE ALIGNMENTS..... 36

FIGURE 1.4 THE TOPOLOGY AND STRUCTURAL FEATURES OF THE TRPM2 CHANNEL SUBUNIT..... 37

FIGURE 1.5 STRUCTURES OF TRPM2 ACTIVATORS..... 42

FIGURE 1.6 STRUCTURES OF TRPM2 INHIBITORS 51

FIGURE 1.7 THE PATHWAY OF TRPM2 CHANNELS ACTIVATION AND FUNCTION 60

FIGURE 2.1 CELL-ATTACHED AND WHOLE-CELL CONFIGURATIONS OF THE PATCH-CLAMP RECORDING..... 79

FIGURE 2.2 THE EQUIVALENT CIRCUIT OF THE WHOLE-CELL PATCH CLAMP RECORDING..... 80

FIGURE 3.1 CHARACTERIZATION OF THE INHIBITORY EFFECT OF ACA ON TRPM2 CHANNEL FUNCTIONS..... 91

FIGURE 3.2 EXPOSURE DURATION-DEPENDENT REVERSIBILITY OF INHIBITION OF THE HTRPM2 CHANNEL CURRENTS BY PH 5.5 94

FIGURE 3.3 CHARACTERIZATION OF THE MTRPM2 AND HTRPM2 CHANNEL CURRENTS INDUCED BY ADPR . 95

FIGURE 3.4 DIFFERENTIAL INHIBITION OF ADPR-INDUCED CURRENTS MEDIATED BY THE HTRPM2 AND MTRPM2 CHANNELS BY EXTRACELLULAR ACIDIC PH 97

FIGURE 3.5 ADPR-INDUCED WHOLE-CELL CURRENTS IN THE HEK293 CELLS EXPRESSING WT AND PORE MUTANT HTRPM2 AND MTRPM2 CHANNELS 99

FIGURE 3.6 ACCELERATED KINETICS OF, AND INCREASED SENSITIVITY TO, INHIBITION BY ACIDIC PH BY MUTATION OF GLN-992 BUT NOT SER-958 IN THE MTRPM2 CHANNEL.....101

FIGURE 3.7 DECELERATED KINETICS OF, AND INCREASED SENSITIVITY TO, INHIBITION BY ACIDIC PH BY MUTATION OF HIS-995 BUT NOT ARG-961 IN THE HTRPM2 CHANNEL.....104

FIGURE 3.8 A CRUCIAL ROLE OF HIS-995 IN THE HTRPM2 CHANNEL AND GLN-992 IN THE MTRPM2 CHANNEL FOR SPECIES-DEPENDENT INHIBITION BY ACIDIC PH. 106

FIGURE 4.1 EFFECTS OF HIT COMPOUNDS AT 10 μM ON H_2O_2-INDUCED INCREASES IN THE $[CA^{2+}]_C$.....115

FIGURE 4.2 SUMMARY OF INHIBITION OF H_2O_2-INDUCED INCREASES IN THE $[CA^{2+}]_C$ BY COMPOUNDS AT 10 μM.....116

FIGURE 4.3 EFFECTS OF HIT COMPOUNDS AT 1 μM ON H_2O_2-INDUCED INCREASES IN THE $[CA^{2+}]_C$ 118

FIGURE 4.4 SUMMARY OF INHIBITION OF H_2O_2-INDUCED INCREASES IN THE $[CA^{2+}]_C$ BY COMPOUNDS AT 1 μM.....119

FIGURE 4.5 CONCENTRATION-DEPENDENT INHIBITION OF H_2O_2-INDUCED INCREASES IN THE $[CA^{2+}]_C$ 124

FIGURE 4.6 IC_{50} VALUES OF THE TESTED COMPOUNDS INHIBITING H_2O_2-INDUCED INCREASES IN THE $[CA^{2+}]_C$ 125

FIGURE 4.7 EFFECTS OF TESTED COMPOUNDS ON ADPR-INDUCED TRPM2 CHANNELS CURRENTS 128

FIGURE 4.8 INHIBITION OF ADPR-INDUCED WHOLE CELL CURRENTS BY TESTED COMPOUNDS 129

FIGURE 4.9 THE CHEMICAL STRUCTURES OF THE DERIVATIVES OF COMPOUNDS NO.13 AND NO.07.....132

FIGURE 4.10 THE EFFECTS OF THE DERIVATIVES OF NO.13 AND NO.07 ON H_2O_2-INDUCED CA^{2+} RESPONSES135

FIGURE 4.11 THE IC_{50} VALUES OF THE DERIVATIVES OF COMPOUNDS NO.13 AND NO.07 IN INHIBITING H_2O_2-INDUCED INCREASES IN THE $[CA^{2+}]_C$.....136

FIGURE 5.1 IMMUNOFLUORESCENCE IN HEK293 CELLS TRANSIENTLY TRANSFECTED WITH HTRPM2 PLASMID 144

FIGURE 5.2 EXPRESSION OF TRPM2 PROTEINS IN MACROPHAGE CELLS 145

FIGURE 5.3 EXPOSURE TO H_2O_2 ELEVATES THE $[CA^{2+}]_C$ IN MACROPHAGE CELLS. 147

FIGURE 5.4 H_2O_2-INDUCED INCREASES IN THE $[CA^{2+}]_C$ IN MACROPHAGE CELLS PRIMARILY RESULTS FROM EXTRACELLULAR CA^{2+} INFLUX. 148

FIGURE 5.5 H_2O_2-INDUCED INCREASES IN THE $[CA^{2+}]_C$ IN MACROPHAGE CELLS ARE FACILITATED BY BODY TEMPERATURE.....149

FIGURE 5.6 TRPM2 CHANNEL MEDIATES H_2O_2-INDUCED EXTRACELLULAR CA^{2+} INFLUX IN MACROPHAGE CELLS. 152

FIGURE 5.7 ADPR-INDUCED WHOLE-CELL CURRENTS IN PERITONEAL MACROPHAGE CELLS.....153

FIGURE 5.8 PJ-34 ATTENUATES H_2O_2-INDUCED REDUCTION IN MACROPHAGE CELL VIABILITY. 157

FIGURE 5.9 TRPM2 DEFICIENCY SUPPRESSES H_2O_2-INDUCED REDUCTION IN MACROPHAGE CELL VIABILITY. 158

FIGURE 5.10 H_2O_2-INDUCED NECROSIS IN MACROPHAGE CELLS 160

List of tables

TABLE 2.1 GROWTH MEDIUM FOR MAMMALIAN CELLS **71**

TABLE 2.2 CELL PREPARATION FOR DIFFERENT EXPERIMENTS **73**

TABLE 2.3 SEQUENCES OF THE PRIMERS USED IN THIS STUDY **75**

TABLE 2.4 BUFFERS FOR MINI-PREPARATION OF PLASMIDS **77**

TABLE 2.5 SOLUTIONS IN IMMUNOFLUORESCENT CONFOCAL IMAGING **78**

TABLE 2.6 SOLUTIONS IN PATCH-CLAMP RECORDING (IN MM) **82**

TABLE 2.7 SOLUTIONS IN CA^{2+} IMAGING (IN MM) **84**

List of abbreviations

$[Ca^{2+}]_c$	Cytoplasmic Ca^{2+}concentration
2-APB	2-aminoethoxydiphenyl borate
3-MFA	3-aminoethoxydiphenyl borate
ACA	N-(p-amylcinnamoyl)anthranilic acid
AD	Alzheimer's disease
ADPKD	Autosomal dominant polycystic kidney diseases
ADPR	Adenosine diphosphate ribose
ADPRase	ADPR pyrophosphatase
ALS	Amyotrophic lateral sclerosis
AMP	Adenosine monophosphate
ANOVA	Analysis of variance
Arf6	ADP-ribosylation factor 6
ATP	Adenosine triphosphate
Aβ	Amyloid β-peptide
BAPTA	1,2-bis(o-aminophenoxy)ethane- N,N,N',N'-tetraacetic acid
BD	Bipolar disorder
BFU-E	Burst-forming unit-erythroid
BMDM	Bone marrow derived macrophage
cADPR	Cyclic adenosine diphosphate ribose
CaM	Calmodulin
Ca_v	Voltage-gated Ca^{2+} channel
cGMP	Cyclic guanosine monophosphate
CHO	Chinese hamster ovary

C_m	Membrane capacitance
CXCL	C-X-C motif ligand
DAG	Diacylglycerol
DAPI	4',6-diamidino-2-phenylindole
DMEM	Dulbecco's modified Eagle's medium
DMSO	Eimethyl sulfoxide
DNA	Deoxyribonucleic acid
dNTP	Deoxy-(adenosine/guanine/thiamine/cytosine)-triphosphate
DRG	Dorsal root ganglion
EB	Ethidium bromide
EC_{50}	The concentration evoking half of the maximal effects
ECaC	Epithelial Ca^{2+} channel
EDTA	Ethylenediaminetetraacetic acid
EFHC1	EF-hand motif-containing protein
EGTA	Ethyleneglycoltetraacetic acid
ER	Endoplasmic reticulum
ERK	Extracellular signal-regulated protein kinase
FBS	Foetal bovine serum
FFA	Flufenamic acid
FITC	Fluorescent isothiocyanate
fMLP	Formyl-methionyl-leucyl-phenylalanine
FOXO3a	Forkheadbox O3
FSK	Forskolin
Ga	Gauge
G-CSF	Granulocyte colony-stimulating factor

GFP	Green fluorescent protein
GLP-1	Glucagon-like peptide 1
GluT2	Glucose transporter 2
GPCR	G-protein coupled receptors
GΩ	Giga ohm
H_2O_2	Hydrogen peroxide
HEK293	Human embryonic kidney 293
HEPES	4-(2-hydroxyethyl)-1-piperazineethanesulfonic acid
HPAE	human pulmonary artery endothelial cells
IC_{50}	Concentration for half maximum inhibition
IL	Interleukin
INFγ	Interferon-γ
IP_3	Inositol 1,4,5-trisphosphate
I-V	Current-voltage
K_{ATP}	ATP-sensitive potassium channel
$K_{Ca}3.1$	Ca^{2+}-activated K^+ channel 3.1
K_d	Binding affinity
LB	lysogeny broth
LM	*Listeria monocytogenes*
LPS	Lipopolysaccharides
MAPK	Mitogen-activated protein kinases
MCP-1	Macrophage-chemoattractant protein-1
MEK	MAPK/ERK kinase
MIP-2	Macrophage inflammatory peptide-2
MLIV	Tomucolipidosis type IV

mM	Millimolar
mV	Millivolt
nA	Nanoamp
NAADP	Nicotinic acid adenine dinucleotide phosphate
NAD	Nicotinamide adenine dinucleotide
NADase	NAD nucleosidase
NDP	Nimodipine
NF-κB	Nuclear factor kappa-light-chain-enhancer of activated B cells
ng	Nanogram
nM	Nanomolar
NUDT9-H	Nudix (nucleoside diphosphate linked moiety X)-type motif 9-homology
OD value	Optical density values
Orai	Calcium release-activated calcium channel protein
PAR	Poly (ADP-ribose)
PARG	Poly (ADP-ribose) glycohydrolase
PARP	Poly-ADPR polymerases
PBS	Phosphate buffered saline
PD	Parkinson's disease
PIP_2	Phosphatidylinositol 4,5-bisphosphate
PKC	Protein kinase C
PKD	Polycystic kidney disease
PLA_2	Phospholipase A2
PLC	Phospholipase C
PMA	Phorbol 12-myristate 13-acetate

PMN	Polymorphonuclear leukocyte
PMS	N-methylphenazonium methyl sulphate
PTPL1	Protein tyrosine phosphatase-L1
P_x	x cation permeability
Pyk2	Proline-rich tyrosine kinase 2
Ras	Rat sarcoma
R_m	Membrane resistance
$R_{pipette}$	Pipette resistance
R_{seal}	Seal resistance
RNS	Reactive nitrogen species
ROS	Reactive oxygen species
RTK	Receptor tyrosine kinases
RT-PCR	Reverse transcription-polymerase chain reaction
SBS	Standard bath solution used for fluorescent Ca^{2+} imaging
shRNA	Short hairpin RNA
siRNA	Small interfering RNA
SM	Sulfur mustard
SOC	Store-operated Ca^{2+} channel
SOCE	Store-operated Orai1/STIM1-mediated Ca^{2+} entry
SOD2	superoxide dismutase 2
Src	sarcoma
STIM1	Stromal interaction molecule 1
TER	transendothelial electrical resistance
TG	Trigeminal ganglion
TNF-α	Tumor necrosis factor alpha

TRP	Transient receptor potential
TRPM2	Transient receptor potential melastatin channel 2
hTRPM2	Human TRPM2 channel
mTRPM2	Mouse TRPM2 channel
V-ATPase	vacuolar-type H^+-ATPase
WT	Wild-type
µg	Microgram
µl	Microlitre
µM	Micromolar
µm	Micrometre

List of amino acids

G	Gly	Glycine	W	Trp	Tryptophan
P	Pro	Proline	H	His	Histidine
A	Ala	Alanine	K	Lys	Lysine
V	Val	Valine	R	Arg	Arginine
L	Leu	Leucine	Q	Gln	Glutamine
I	Ile	Isoleucine	N	Asn	Asparagine
M	Met	Methionine	E	Glu	Glutamic Acid
C	Cys	Cysteine	D	Asp	Aspartic Acid
F	Phe	Phenylalanine	S	Ser	Serine
Y	Tyr	Tyrosine	T	Thr	Threonine

Chapter 1

General introduction

1.1 TRP channel superfamily

The transient receptor potential (TRP) channel was originally identified in a genetic study of the photoreceptors in the fruitfly *Drosophila* (Hardie and Minke, 1992). In contrast with the persistent receptor potential response in the wild-type (WT) fly to constant bright light, a spontaneous mutant fly showed a transient receptor potential response and named the *trp* mutant (Cosens and Manning, 1969, Minke et al., 1975, Hardie and Minke, 1992). The responsible *trp* gene was identified later by molecular cloning, and the encoded TRP protein was shown as a membrane protein located in the membrane of photoreceptor cells (Montell and Rubin, 1989). Subsequent studies further demonstrated that the TRP protein formed a Ca^{2+}-permeable channel (Montell and Goodman, 1989, Hardie and Minke, 1992). Up to now, 28 homologues of the *Drosophila* TRP proteins in mammalian cells have been identified, and constitute a large superfamily that can be divided into 6 subfamilies based on their amino acid sequence homology. These subfamilies are TRPC (classical), TRPM (melastatin), TRPV (vanilloid), TRPA (ankyrin), TRPML (mucolipin) and TRPP (polycystin) (Pedersen et al., 2005) (Fig. 1.1). According to their homology to the *Drosophila* TRP, the mammalian TRPs can also be broadly categorized into two groups (Fig. 1.2). The proteins of the TRPC, TRPV, TRPM, TRPA subfamilies show high amino acid relatedness with the *Drosophila* TRP and constitute group 1, while the proteins of the TRPP and TRPML subfamilies exhibit low sequence homology to the *Drosophila* TRP and form group 2 (Venkatachalam and Montell, 2007). All members of the TRP superfamily share a similar membrane topology, having intracellular C- and N-terminus, six transmembrane segments (S1-S6), and a re-entrant loop between the S5 and S6 that forms the ion-permeating pore (Montell, 2005, Pedersen et al., 2005, Venkatachalam and Montell, 2007) (Fig. 1.2).

The second member of the TRPM subfamily, TRPM2, is the major topic of my study. In the following sections, I will first provide a brief overview of all the other TRP channels and present a more detailed discussion of our current knowledge regarding the TRPM2 channel.

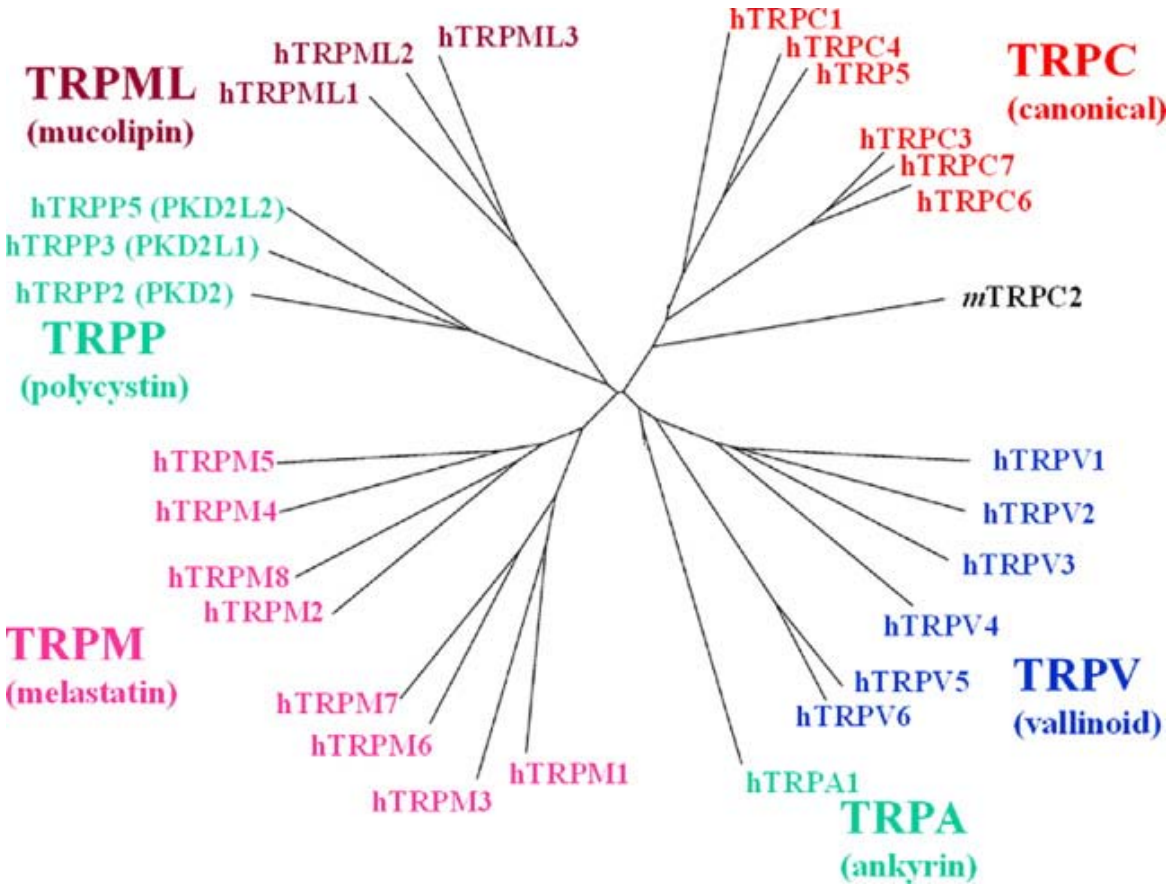

Figure 1.1 The family tree of the mammalian TRP channel proteins

The tree shows the homology of human TRP proteins. The mouse TRPC2 protein is shown, as the gene encoding the human TRPC2 is a pseudogene (Nilius et al., 2007). (The permission for using this figure in a thesis, which has been verified on the website of Copyright Clearance Center's RightsLink™, is not required.)

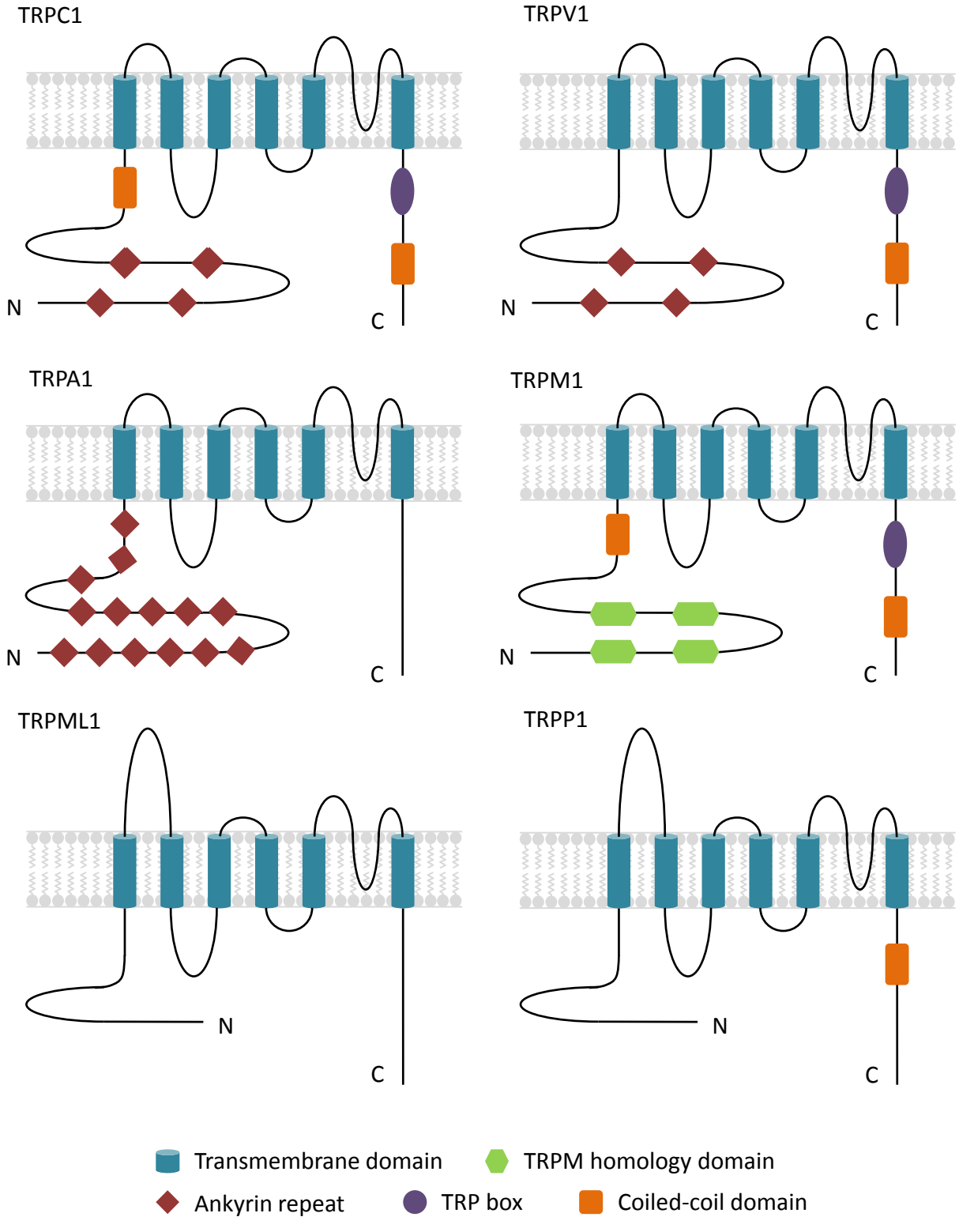

Figure 1.2 Schematic representation of the main structural features of the members of the six mammalian TRP channel subfamilies

1.1.1 TRPC subfamily

There are seven mammalian TRPC members, TRPC1-7 (Fig. 1.1). As illustrated for TRPC1 in Fig. 1.2, these proteins have multiple ankyrin repeats, 33-residue motifs forming helix-loop-helix and mediating protein-protein interactions, in the N-terminus. There is a TRP domain adjacent to the intracellular part of S6, which is composed of 23-25 highly conserved residues. Two coiled-coil domains locate in the N- and C-terminus, respectively. The coiled-coil domain is composed of a-helix forming heptad repeats (*abcdefg*), in which residues at positions *a* and *d* are preferentially hydrophobic and mediate protein-protein interactions (Cohen and Parry, 1990).

TRPCs have been cloned from human (Nagamine et al., 1998) and rodents (Xu et al., 2001, Nakayama et al., 2006). They are extensively expressed in tissues and cells, such as brain (Sossey-Alaoui et al., 1999, Nagamine et al., 1998), heart (Nakayama et al., 2006), testis (Sutton et al., 2004), spleen (Uehara, 2005), vascular smooth muscle (Wang et al., 2004), kidney (Wissenbach et al., 2000), liver (Chen and Barritt, 2003) and endothelial cells (Wang et al., 2009). Among of them, TRPC3, TRPC4 and TRPC5, are distributed in abundance in neurons (Lee-Kwon et al., 2005, Crousillac et al., 2003, Riccio et al., 2009, Sossey-Alaoui et al., 1999, Davare et al., 2009).

All TRPC channels are Ca^{2+} permeable cationic channels and activated by phospholipase C (PLC) signal transduction pathway. Activation of PLC by G-protein coupled receptors (GPCR) results in hydrolysis of membrane lipid phosphatidylinositol 4,5-bisphosphate (PIP_2) into inositol 1,4,5-trisphosphate (IP_3), an agonist for the IP_3 receptor that is located on the endoplasmic reticulum (ER) and mediates Ca^{2+} release from the ER, and diacylglycerol (DAG), a physiological activator of protein kinase C (PKC).

The TRPC1 channel has been proposed as a candidate of store-operated channel (SOC). It can be activated by Ca^{2+} depletion in the ER as a result of activation of the IP_3 receptor. Furthermore, associating with STIM1 (stromal interaction molecule 1) and Orai1 (calcium release-activated calcium channel protein 1), TRPC1 can modulate the store-operated Orai1/STIM1-mediated Ca^{2+} entry (SOCE) (Worley et al., 2007).

The TRPC4 and TRPC5 proteins have high sequence homology (64%) (Ramsey et al., 2006). They can form homotetramers which are regarded as receptor-operated channels (ROC) that can be stimulated by activation of GPCRs and receptor tyrosine kinase (RTK) (Odell et al., 2005, Schaefer et al., 2000, Plant and Schaefer, 2003). In addition, TRPC4 and TRPC5 proteins can also assemble heteromeric channels with each other, and also with TRPC1 and TRPC3 proteins (Plant and Schaefer, 2003, Poteser et al., 2006). The TRPC4 channels are involved in vasodilatation (Plant and Schaefer, 2003) and neurotransmitter release (Munsch et al., 2003), meanwhile the TRPC5 channels are shown to play a role in cardiovascular remodeling (Nath et al., 2009) and metabolic syndrome (Wuensch et al., 2010).

The TRPC3, TRPC6 and TRPC7 share 70–80% sequence homology with each other (Hofmann et al., 1999). All of them can be stimulated by DAG (Kiselyov et al., 1998, Philipp et al., 1998, Venkatachalam et al., 2003, Lievremont et al., 2005, Hofmann et al., 1999). The TRPC3 channel also couples with the IP_3 receptor after its conformational change caused by binding with IP_3 and calmodulin. Thus, it is involved in modulating depletion of intracellular Ca^{2+} store in the ER and SOCE, and is likely to depolarize the membrane potential and further activate the voltage-gated Ca^{2+} (Ca_v) channels (Groschner and Rosker, 2005). The TRPC6 channel activity can be modulated by redox (Graham et al., 2010), phosphorylation by PKC (Bousquet et al., 2010) and Src (sarcoma) family PTK (Hisatsune et al., 2004), and activation of GPCRs (Cayouette et al., 2004). There are many lines of evidence to support the involvement of the TRPC6 channel in promoting neuron survival (Du et al., 2010) and controlling contraction of smooth muscles and vessels (Ding et al., 2011, Monet et al., 2012). The TRPC7 channels can be modulated by cGMP (cyclic guanosine monophosphate)-dependent protein kinase and are involved in mediating carbachol-induced Ca^{2+} influx (Yuasa et al., 2011). However, the physiological function of the TRPC7 channel is still poorly understood.

The TRPC2 is unique among the TRPCs, as the full-length genes have only been identified from rodents and bovine (Zufall, 2005). In mice, TRPC2 is expressed in brain, testis and sperm, and is important in regulating sexual and social behaviors of the animals (Zufall et al., 2005). However, in human, the complete TRPC2 gene is lost and the remnants form a pseudogene (Yildirim and Birnbaumer, 2007, Lof et al., 2011).

1.1.2 TRPV subfamily

There are six members, TRPV1-6, in the TRPV subfamily (Fig. 1.1). The TRPVs contain multiple ankyrin repeats in the intracellular N-terminal region, and a TRP domain in the proximal part of the C-terminus, similar to the TRPCs (Fig. 1.2). The TRPV1 and TRPV4 proteins, but not other TRPVs, contain a C-terminal coiled-coil domain (Tominaga and Tominaga, 2005, Nilius et al., 2003b).

The TRPV1-4 proteins are abundantly expressed in neuronal tissues, including hippocampus (Planells-Cases et al., 2005), cerebral cortex (Pingle et al., 2007), hypothalamus (Planells-Cases et al., 2005), midbrain (Smith et al., 2002), dorsal root ganglion (DRG) (Derbenev et al., 2004, Derbenev et al., 2006, Xing and Li, 2007), trigeminal ganglion (TG) (Derbenev et al., 2004) and nodose ganglion (Derbenev et al., 2006, Planells-Cases et al., 2005, Pingle et al., 2007), as well in other types of cells, such as granulocytes, macrophages, endothelial cells (Strotmann et al., 2000, Liedtke, 2006), keratinocytes and smooth muscle cells (Muraki et al., 2003, Montell et al., 2002, Beech et al., 2004).

The TRPV1-4 channels show remarkable thermo-sensitivity (Smith et al., 2002, Caterina et al., 1997, Peier et al., 2002b). Among them, the TRPV1 and TRPV2 channels respond to noxious heat (>42°C), while the TRPV3 and TRPV4 channels are stimulated by non-painful warm temperature (25°C-42°C).

In physiological conditions, the TRPV1 channels are stimulated by heat at approximate 43°C, whereas the threshold is reduced to body temperature in inflammatory conditions, since pro-inflammatory factors, such as macrophage-chemoattractant protein-1 (MCP-1), IL (interleukin)-1β, IL-6 and TNF-α (tumor necrosis factor-α), can all enhance the sensitivity of the TRPV1 channel to heat (Okada et al., 2011, Zhang et al., 2005, Caterina et al., 2000, Bishnoi et al., 2011). Besides heat, the TRPV1 channel can be activated by capsaicin (Tominaga et al., 1998) and extracellular acidic pH (<6.0) (Jordt et al., 2000). It plays a critical role in nociception and thermo-sensing (Caterina et al., 2000, Walker et al., 2003). The TRPV2 channel responds to noxious heat or temperature of higher than 52°C (Caterina et al., 1997). Activation of the TRPV2 channel by chemical ligands shows striking species specificity. For instance, 2-aminoethoxydiphenyl borate (2-APB) potently activates the

rodent TRPV2 channel, but does not activate the human TRPV2 channel at concentrations up to 1 mM (Neeper et al., 2007, Hu et al., 2004). Several studies show that the TRPV2 channel activity is up-regulated after tissue injury or inflammation, suggesting its role in pain sensation (Frederick et al., 2007, Shimosato et al., 2005).

The TRPV3 and TRPV4 channels respond to moderate temperatures in the range of 34°C-38°C (Smith et al., 2002, Xu et al., 2002) and 27°C-34°C (Guler et al., 2002), respectively. TRPV3 can also be activated by 2-APB and camphor (Vogt-Eisele et al., 2007). Intriguingly, the TRPV3 channel activation by warm temperature or 2-APB results in a biphasic response. The first phase shows a gradual increase in the TRPV3 channel currents, followed by the second phase characterized by an abrupt enhancement in the current amplitude and loss of the outward rectification (Hu et al., 2004, Chung et al., 2005). Besides heat, the TRPV4 channel can be activated by hypotonic cell swelling (Nilius et al., 2003b, Vriens et al., 2005), and chemical stimuli, such as anandamide and arachidonic acid (Watanabe et al., 2003, Nilius et al., 2003b, Nilius et al., 2004).

The TRPV5 and TRPV6 channels were initially named ECaC1 (epithelial Ca^{2+} channel 1) and ECaC2, respectively. They have been identified in kidney (Nijenhuis et al., 2003), small intestine (van de Graaf et al., 2006), placenta (Bernucci et al., 2006), pancreas, brain and rectum (Hoenderop et al., 2000). Distinct from other members of the TRP superfamily, the TRPV5 and TRPV6 channels exhibit strong inward rectification and a high Ca^{2+} selectivity with the P_{Ca} (permeability of Ca^{2+}) /P_{Na} value being over 100 (Nilius et al., 2000, Nilius et al., 2001a, Vennekens et al., 2000). The TRPV5 and TRPV6 channels are constitutively active (den Dekker et al., 2003). The most efficient blockers of the TRPV5 channels are ruthenium red and econazole (Nilius et al., 2001b). The TRPV5 channel also can be blocked by extracellular divalent cations, including Pb^{2+}, Cu^{2+}, Zn^{2+}, Co^{2+} and Fe^{2+}, with IC_{50} (the half maximal inhibitory concentration) values between 1-10 μM (Nilius et al., 2001b). The TRPV6 channel is inhibited by ruthenium red with the potency approximate 100-fold lower than that for TRPV5. In addition, Mg^{2+} inhibits TRPV5 and TRPV6 channels from both extracellular and intracellular sides and in a voltage-dependent manner (Nilius, 2007). The TRPV5 and TRPV6 channels are thought to contribute to Ca^{2+} absorption/reabsorption in kidney and intestine (Nijenhuis et al., 2005, Hoenderop et al., 2003, Hoenderop et al., 2005).

1.1.3 TRPA subfamily

The TRPA1 protein is the sole member of the TRPA subfamily (Fig. 1.1). The protein contains 14 ankyrin repeats in the intracellular N-terminal domain (Fig. 1.2). TRPA1 mRNA expression is detected in several tissues, but the functional TRPA1 channel is only observed in sensory neurons such as DRG and TG (Kobayashi et al., 2005, Story et al., 2003), and hair cells of the inner ear (Nagata et al., 2005, Corey et al., 2004). The TRPA1 channel can be activated by cold temperature (Bandell et al., 2004, Story et al., 2003) as well as a variety of pungent chemicals, such as mustard oil, allicin, wasabi and acrolein (Bandell et al., 2004). Intracellular Ca^{2+} can also stimulate the TRPA1 channel (Zurborg et al., 2007, Doerner et al., 2007). The contribution of the TRPA1 channel in cold sensation is still disputable. Some groups have shown that exogenously expressed TRPA1 channels are activated by noxious cold (<15°C) (Bandell et al., 2004, Story et al., 2003) and that the cold sensitivity is reduced to very low temperatures (-10°C) in the TRPA1-deficient mice in tail flick test, in which the mice flick tail when they feels pain caused by cold (Karashima et al., 2009). However, other groups have failed to observe such changes in the cold sensitivity (Bautista et al., 2006, Karashima et al., 2009).

1.1.4 TRPM subfamily

The TRPM subfamily is composed of eight members, TRPM1-8 (Fig. 1.1). Like the TRPC proteins, they all contain a TRP domain and a coiled-coil domain in the C-terminus (Fig. 1.2). Unique to the TRPM proteins is the presence of four highly homologous regions among the TRPM subfamily (thus called TRPM-homology regions) in the N-terminus that bear no sequence homology to any other known proteins (Eisfeld and Luckhoff, 2007).

The TRPM1, TRPM3-5, and TRPM7-8 channels have been identified in various tissues, such as kidney (Grimm et al., 2003), DRG neurons (Babes et al., 2004, Kobayashi et al., 2005), lung epithelia (Sabnis et al., 2008), pancreas (Wagner et al., 2008), retina (Schmidt, 2009), vascular smooth muscles (Naylor et al., 2010) and testis (De Blas et al., 2005). In contrast, the TRPM6 channel is almost exclusively expressed in epithelial cells (Chubanov et al., 2004, Wolf et al., 2010).

The TRPM1 protein forms an outwardly-rectifying non-selective cation channel (Oancea et al., 2009). This channel has been shown to mediate synaptic transmission in rod bipolar cells of the retina and probably contribute to production of melanin pigment (Devi et al., 2009). Loss of the functional TRPM1 channels results in melanomas and night blindness in human (Duncan et al., 1998, Venkatachalam et al., 2006).

The TRPM3 channel is a Ca^{2+} permeable non-selective cation channel that exhibits constitutive activity and strong outward rectification (Naylor et al., 2010, Oberwinkler et al., 2005). The TRPM3 channel activity can be increased by extracellular pregnenolone sulphate, osmolarity and Ca^{2+} depletion in the ER (Naylor et al., 2010, Wagner et al., 2008). The TRPM3 channel has been shown to contribute to renal Ca^{2+} homeostasis and steroid-induced insulin secretion from pancreatic β-cells (Lee et al., 2003, Wagner et al., 2008).

The TRPM4 and TRPM5 channels exhibit similar channel activation and ion permeation properties. Different from other TRP or TRPM channels, they are monovalent cation-selective and are impermeable to divalent cations such as Ca^{2+} but they can be activated by intracellular Ca^{2+} (>1 μM). However, the TRPM4 channel can be inactivated in the constant presence of intracellular Ca^{2+} (Nilius et al., 2003a). The TRPM4 and TRPM5 channels are also activated by IP_3-triggered Ca^{2+} depletion in the ER (Hofmann et al., 2003, Perez et al., 2002), positive membrane potential (Hofmann et al., 2003, Liman, 2007) and heat (Talavera et al., 2005). Both TRPM4 and TRPM5 channels contribute to generation of action potential in atria cardiomyocytes and taste cells (Hofmann et al., 2003, Simard et al., 2013). The TRPM4 channel has been shown to play an important role in determining dendritic cell migration (Barbet et al., 2008), and the TRPM5 channel contributes in taste, such as sweet, bitter and umami (Hofmann et al., 2003, Liu and Liman, 2003, Talavera et al., 2005).

The TRPM6 and TRPM7 proteins show high sequence homology, and both form non-selective cation channels with substantial Mg^{2+}-permeability. The TRPM6 channel currents are characterized by strong outward rectification. The channel can be inhibited by internal Mg^{2+} (Gwanyanya et al., 2004), ATP (Thebault et al., 2008) and acidic pH (Gwanyanya et al., 2004). The TRPM7 channel is constitutively active, and can be inhibited by internal MgATP (Mishra et al., 2009) and acidic pH (Gwanyanya et al., 2004). The TRPM6 and TRPM7 channels play an important role in Mg^{2+} homeostasis (Bodding, 2007, Nijenhuis et al., 2006),

and be also involved in cell apoptosis (Nadler et al., 2001), adhesion (Su et al., 2006), and migration (Kuras et al., 2012) as well as detrusor smooth muscle contraction (Nomoto et al., 2008).

TRPM8 is present in many cells and tissues, including sperm and prostate (Henshall et al., 2003, Tsavaler et al., 2001). The TRPM8 channel can be activated by low temperature with a threshold of about 25°C, and a variety of cooling compounds, such as menthol, icilin and eucalyptol (Behrendt et al., 2004, Brauchi et al., 2004). Menthol and icilin show a high potency with an EC_{50} (the concentration evoking half of the maximal effects) of 80 μM and 0.36 μM, respectively (McKemy et al., 2002, Peier et al., 2002a). The sensitivity of the TRPM8 channel to cold or menthol can be increased by inflammatory factors such as bradykinin and prostaglandin E2 (Linte et al., 2007, Premkumar et al., 2005). TRPM8 has been shown to be involved in cool sensing and cold nociception as well as inflammatory process (Premkumar et al., 2005, Tsukimi et al., 2005, Marchand et al., 2005).

1.1.5 TRPML subfamily

Three proteins, TRPML1-3, make up the TRPML subfamily (Fig. 1.1). The TRPML proteins contain a large serine lipase active site on the large loop between the S1 and S2 (Fig. 1.2). The function of this domain is still unclear, but it has been speculated that it may regulate membrane remodeling (LaPlante et al., 2011). In contrast with the TRPs in group 1, the TRPMLs contain no coiled-coil domain, ankyrin repeats and the TRP domain (Montell, 2005) (Fig. 1.2). Perhaps most distinctively, the TRPMLs form non-selective cation channels in the membranes of lysosome.

TRPML1, also named mucolipin (MLN) 1, is the founding member of TRPML subfamily. It was cloned during a genetic study searching for the gene responsible for mucolipidosis type IV (MLIV), a childhood neurodegenerative disease (Bargal et al., 2000). The TRPML1 channel is located in the late lysosomes and endosomes, and appears to be involved in lysosome formation and recycling (Campbell and Fares, 2010, LaPlante et al., 2011, Piper and Luzio, 2004). Mutations of the TRPML1 proteins lead to the MLIV. To date, at least 15 mutations are identified in the human TRPML1 gene (Dong et al., 2008, Sun et al., 2000).

TRPML2, also called MLN2, is abundantly expressed in the endosome and lysosome, and can be detected at a lower level in the plasma membranes (Venkatachalam et al., 2006). The heterogeneously expressed TRPML2 channel is constitutively active and characterized by inward rectification. The TRPML2 channel has been reported to be involved in trafficking and regulation of Arf6 (ADP-ribosylation factor 6) -associated pathway as well as cell apoptosis (Karacsonyi et al., 2007, Lev et al., 2010).

TRPML3, also called MLN3, shows a broad tissue expression, including skin (Bargal et al., 2002), stereocilia and inner ear (Atiba-Davies and Noben-Trauth, 2007, Di Palma et al., 2002, Kim et al., 2008). The TRPML3 proteins are localized in the membranes of the early- and late-endosomes, lysosome, as well as on the cell surface (Kim et al., 2009). The TRPML3 channel is an inwardly-rectifying non-selective cation channel and inhibited by extracellular pH (Kim et al., 2008). TRPML3 has been reported to play a role in regulating cargo trafficking along the endosomal pathway and autophagy (Kim et al., 2009, Martina et al., 2009). Mutations in the TRPML3 channel have been reported to result in embryonic lethality and deafness (Noben-Trauth, 2011).

1.1.6 TRPP subfamily

TRPP proteins are identified in the search for the gene(s) responsible to the autosomal dominant polycystic kidney diseases (ADPKDs) (Mochizuki et al., 1996). ADPKDs are mainly caused by mutations in two separate genes, pkd1 and pkd2. Pkd1 encodes PKD-1 protein (polycystic kidney disease protein 1), and pkd2 encodes TRPP2 protein. The PKD-1 protein is a large integral plasma membrane protein that has 11 transmembrane segments and an extracellular N-terminus and an intracellular C-terminus. The function of PKD-1 is not fully understood. Several lines of independent evidence support that PKD-1 binds with TRPP2 to form a hetero-multimeric ion channel complex that plays a critical role in kidney development.

The TRPP2 protein is a member of the TRPP subfamily (Fig. 1.1). It is expressed in many tissues, including kidney, liver and pancreatic cysts (Gattone et al., 2002). The TRPP2 protein contains a coiled-coil domain in the C-terminus, but no ankyrin repeats and no TRP domain. Similar to TRPMLs, the TRPP2 protein contains a large domain between the S1 and

S2 (Zhu et al., 2011, Feng et al., 2011) (Fig. 1.2) The TRPP2 protein is located in the plasma membrane and the membrane of the ER, and form a Ca^{2+} permeable non-selective cation channel (Inoue et al., 2006). The channel responds to activation of GPCRs and RTKs (Foggensteiner et al., 2000), and mechanical stimuli, such as fluid shear stress (Nauli et al., 2003). It is well known that mutations of TRPP2 contribute to ADPKD. However, there is still a lack of knowledge of the physiological function of the TRPP2 channels.

Two TRPP2 homologues, TRPP3 and TRPP5, have been identified to date. The TRPP3 channel has been detected in numerous tissues, such as retina (Nomura et al., 1998), brain (Wu et al., 1998), hair cell (Huang et al., 2006) and taste receptor cells in the tongue (Ishimaru et al., 2006, LopezJimenez et al., 2006). The TRPP3 channel is a Ca^{2+}-activated non-selective cation channel and responds to extracellular hypo-osmotic solutions and extracellular acidification (Murakami et al., 2005). The TRPP3 channel plays a role in sour tasting (Ishimaru et al., 2006, LopezJimenez et al., 2006) and development of retina (Nomura et al., 1998). The TRPP5 channel is expressed in testis, brain and kidney (Guo et al., 2000), and could be involved in spermiogenesis, cell proliferation and apoptosis (Chen et al., 2008, Xiao et al., 2010). However, the role of the TRPP5 channel in the physiological processes is still far from being understood (Xiao et al., 2010).

1.2 TRPM2 channels

1.2.1 Molecular cloning and cellular/ tissue distribution

TRPM2, previously named TRPC7 (Nagamine et al., 1998) or long TRPC2 (LTRPC2) (Perraud et al., 2001), is the second member of the TRPM subfamily (Fig. 1.1). The genes encoding TRPM2 protein have been cloned from human (Nagamine et al., 1998), rat (Kraft et al., 2004) and mouse (Okada et al., 1999). The predicted full-length human, rat and mouse TRPM2 proteins have 1503, 1508 and 1506 amino acid residues, respectively (Fig.1.3), with a molecular weight of approximately 170 kDa (Hill et al., 2006, Nagamine et al., 1998). The human TRPM2 (hTRPM2) gene is located in the chromosome 21q22.3, composed of 32 exons, and spanning approximately 90 kb (Nagamine et al., 1998).

An early study using Northern blotting and reverse transcription-polymerase chain reaction (RT-PCR) showed that TRPM2 mRNA of approximate 6.5 kb is abundantly expressed in many regions in the brain, including cerebral cortex, occipital pole, frontal lobe, amygdala, caudate nucleus and hippocampus (Nagamine et al., 1998). To date, both TRPM2 mRNA and protein have been revealed in several other types of cells, such as neutrophil granulocytes (Heiner et al., 2003), microglia (Fonfria et al., 2006), monocyte cells (Yamamoto et al., 2008), pancreatic β-cells (Togashi et al., 2006, Uchida and Tominaga, 2011) and endothelial cells (Hecquet et al., 2008, Hill et al., 2006, Wehrhahn et al., 2010).

Furthermore, using patch clamp recording and fluorescent Ca^{2+} imaging, functional expression of the TRPM2 channels has been identified in various types of cells, such as hippocampal neurons (Olah et al., 2009, Perraud et al., 2001), striatal neurons (Perraud et al., 2001), DRG neurons (Naziroglu et al., 2011), peritoneal macrophages (Kashio et al., 2012), microglia (Fonfria et al., 2006, Hill et al., 2006, Kraft et al., 2004), T lymphocytes (Beck et al., 2006, Magnone et al., 2012), neutrophil granulocytes (Beck et al., 2006, Heiner et al., 2003), pancreatic β-cells (Togashi et al., 2006, Uchida and Tominaga, 2011) and endothelial cells (Hecquet et al., 2008, Hill et al., 2006, Wehrhahn et al., 2010).

1.2.2 Molecular or structural properties

As shown in Fig. 1.4, TRPM2 subunit contains six transmembrane segments, a pore-forming region between the S5 and S6, and intracellular N- and C-terminus like all other members of the TRP superfamily. The functional TRPM2 channel is homo-tetrameric, composed of four subunits. The results from a study using transmission electron microscopy shows a bell-shaped three-dimensional structure of the tetrameric TRPM2 channel with 18 nm in width and 25 nm in height (Maruyama et al., 2007). The extracellular part of this bell-shaped molecule is small, dense and dome-like; while the intracellular part is large, sparse and double-layered.

The N-terminus of the TRPM2 protein (amino acid residues 1-730) contains an IQ-like motif, comprising of amino acid residues 406–416 (Tong et al., 2006). The N-terminus also contains a coiled-coil domain, which is located in the amino acid sequence from residues 654-681 (Mei and Jiang, 2009) (Fig. 1.3 and Fig. 1.4). The significant noticeable variation between TRPM2 and other TRP proteins or the unique feature of the TRPM2 proteins is that the C-terminus (amino acid residues 1236-1503) has an enzyme domain, which shares 39% homology to the NUDT9 (Nudix (nucleoside diphosphate linked moiety X)-type motif 9) ADPR (adenosine diphosphate ribose) hydrolases and thus is termed the NUDT9-H domain (Shen et al., 2003). This domain serves as a binding site for ADPR and confers specific activation of the TRPM2 channels by ADPR. The C-terminus of TRPM2 protein also contains a coiled-coil domain (amino acid residues 1171-1200) and a highly conserved TRP domain (amino acid residues 1062-1067) (Sumoza-Toledo and Penner, 2011) (Fig. 1.3 and Fig. 1.4).

1.2.2.1 Functional properties of the TRPM2 channels

The TRPM2 channel currents exhibit a linear current-voltage (I-V) relationship. The reversal potential in physiological solutions is about 0 mV, indicating that the TRPM2 channel is non-selective and permeable to cations such as Na^+, K^+ and Ca^{2+}. The relative permeability, P_K/P_{Na} and P_{Ca}/P_{Na}, is about 1.1 and 0.9, respectively (Xia et al., 2008), although a much higher P_{Ca}/P_{Na} value of 5.83 has also been reported (Togashi et al., 2006). According to the results of single-channel patch clamp recording, the conductance of the single TRPM2 channel is 50-80 pS (Inamura et al., 2003, Perraud et al., 2001, Sano et al., 2001, Kraft et al.,

2004). The single-channel recordings also show sustained channel opening that can last up to minutes (Kraft et al., 2004, Perraud et al., 2001, Sano et al., 2001).

There are several amino acid residues and segments that have been demonstrated to be involved in determining the TRPM2 channel functional properties. A previous study using site-directed mutagenesis in our lab demonstrated that Glu-960, Gln-981, Asp-987, and Glu-1022 in the pore-forming loop contribute to the gating and divalent cation permeation of the hTRPM2 channel (Fig. 1.4). Whole-cell recordings in this study showed that mutation of Glu-960 eliminates the channel activation by ADPR. The reduction in ADPR-induced currents was also observed in the D987E and E1022A mutant channels. Further experiments revealed augmentation of the Ca^{2+} permeability by Q981E and D987E mutations, as well as the increase in Mg^{2+} permeability by E1022A mutation (Xia et al., 2008). Another site-directed mutagenesis study reported that substitution of two conserved Cys residues, Cys-996 and Cys-1008 in the pore region of the hTRPM2 channel (Fig.1.4) by Ala or Ser dramatically reduced or completely abolished ADPR-induced currents. Furthermore, Biotin labeling and co-immunoprecipitation analysis showed no change in total protein expression, membrane trafficking and localization, or subunit interactions. These results suggest an essential role of these two Cys residues in the channel function (Mei et al., 2006a). The TRPM2 channel currents decline in the continuous or prolonged exposure to ADPR, a phenomenon called current rundown, often observed in the inside-out configuration of patch-clamp recording. Such current rundown is presumably due to irreversible inactivation of the TRPM2 channels through conformational changes in the pore region. Consistent with this hypothesis, a recent study has demonstrated that, in the TRPM2 pore region, insertion of a Leu residue between residues 983 and 984 and substitution of Gly-984 and Tyr-985 residues (Fig. 1.4) with Asp and Glu present in the corresponding pore region of the TRPM5 channel, which showed no current rundown, almost completely abolished the rundown of the TRPM2 channel currents (Toth and Csanady, 2012).

1.2.2.2 Channel assembly

As described above, a coiled-coil domain is located in the C-terminus of the TRPM2 protein (Fig. 1.4), and its sequence is presented in Fig. 1.3. This domain is highly conserved among the TRPM subfamily. A previous study has reported that this coiled-coil domain is essential

```
                1
hTRPM2     MEPSALRKAGSEQEEGFEGLPRRVTDLGMVSNLRRSNSSLFKSWRLQCPFGNNDKQESLSSWIPENIKKKECVYFVESSK    80
mTRPM2     MESLDRRRTGSEQEEGFGVQSRRATDLGMVPNLRRSNSSLCKSRRFLCSFSS-EKQENLSSWIPENIKKKECVYFVESSK    79
rTRPM2     MEPLDQRRTDSDQEEGFGVQSRRATDLGMVPNLRRSNSSLCKSRRLLCSFSS-EKQENLSSWIPENIKKKECVYFVESSK    79

hTRPM2     LSDAGKVVCQCGYTHEQHLEEATKPHTFQGTQWDPKKHVQEMPTDAFGDIVFTGLSQKVKKYVRVSQDTPSSVIYHLMTQ    160
mTRPM2     LSDAGKVVCACGYTHEQHLEVAIKPHTFQGKEWDPKKHVQEMPTDAFGDIVFTDLSQKVGKYVRVSQDTPSSVIYQLMTQ    159
rTRPM2     LSDAGKVVCECGYTHEQHIEVAIKPHTFQGKEWDPKKHVHEMPTDAFGDIVFTGLSQKVGKYVRLSQDTSSIVIYQLMTQ    159

hTRPM2     HWGLDVPNLLISVTGGAKNFNMKPRLKSIFRRGLVKVAQTTGAWIITGGSHTGVMKQVGEAVRDFSLSSSYKEGELITIG    240
mTRPM2     HWGLDVPNLLISVTGGAKNFNMKLRLKSIFRRGLVKVAQTTGAWIITGGSHTGVMKQVGEAVRDFSLSSSCKEGEVITIG    239
rTRPM2     HWGLDVPSLLISVTGGAKNFNMKLRLKSIFRRGLVKVAQTTGAWIITGGSHTGVMKQVGEAVRDFSLSSSCKEGDVITIG    239

hTRPM2     VATWGTVHRREGLIHPTGSFPAEYILDEDGQGNLTCLDSNHSHFILVDDGTHGQYGVEIPLRTRLEKFISEQTKERGGVA    320
mTRPM2     VATWGTIHNREGLIHPMGGFPAEYMLDEEGQGNLTCLDSNHSHFILVDDGTHGQYGVEIPLRTKLEKFISEQTKERGGVA    319
rTRPM2     IATWGTIHNREALIHPMGGFPAEYMLDEEGQGNLTCLDSNHSHFILVDDGTHGQYGVEIPLRTKLEKFISEQTKERGGVA    319

hTRPM2     IKIPIVCVVLEGGPGTLHTIDNATTNGTPCVVVEGSGRVADVIAQVANLPVSDITISLIQQKLSVFFQEMFETFTESRIV    400
mTRPM2     IKIPIVCVVLEGGPGTLHTIYNAINNGTPCVIVEGSGRVADVIAQVATLPVSEITISLIQQKLSIFFQEMFETFTENQIV    399
rTRPM2     IKIPIVCVVLEGGPGTLHTIYNAITNGTPCVIVEGSGRVADVIAQVAALPVSEITISLIQQKLSVFFQEMFETFTENQIV    399
                     406  IQ-motif
hTRPM2     EWTKKIQDIVRRRQLLTVFREGKDGQQDVDVAILQALLKASRSQDHFGHENWDHQLKLAVAWNRVDIARSEIFMDEWQWK    480
mTRPM2     EWTKKIQDIVRRRQLLTIFREGKDGQQDVDVAILQALLKASRSQDHFGHENWDHQLKLAVAWNRVDIARSEIFTDEWQWK    479
rTRPM2     EWTKKIQDIVRRRQLLTVFREGKDGQQDVDVAILQALLKASRSQDHFGHENWDHQLKLAVAWNRVDIARSEIFTDEWQWK    479
                                                                                  535
hTRPM2     PSDLHPTMTAALISNKPEFVKLFLENGVQLKEFVTWDTLLYLYENLDPSCLFHSKLQKVLVEDPERPACAPAAPRLQMHH    560
mTRPM2     PADLHPMMTAALISNKPEFVRLFLENGVRLKEFVTWDTLLCLYENLEPSCLFHSKLQKVLAEE-QRLAYASATPRLHMHH    558
rTRPM2     PSDLHPMMTAALISNKPEFVRLFLENGVRLKEFVTWDTLLCLYENLEPSCLFHSKLQKVLAEEHERLAYASETPRLQMHH    559
```


hTRPM2 VAQVLRELLGDFTQPLYPRPRHNDRLRLLLPVPHVKLNVQGVSLRSLYKRSSGHVTFTMDPIRDLLIWAIVQNRRELAGI 640
mTRPM2 VAQVLRELLGDSTQLLYPRPRYTDRPRLSMTVPHIKLNVQGVSLRSLYKRSTGHVTFTIDPVRDLLIWAVIQNHRELAGI 638
rTRPM2 VAQVLRELLGDSTQLLYPRPRYTDRPRLSLPMPHIKLNVQGVSLRSLYKRSTGHVTFTIDPVRDLLIWAIIQNHRELAGI 639
654 658 coiled-coil domain
hTRPM2 IWAQSQDCIAAALACSKILKELSKEEEDTDSSEEMLALAEEYEHRAIGVFTECYRKDEERAQKLLTRVSEAWGKTTCLQL 720
mTRPM2 IWAQSQDCTAAALACSKILKELSKEEEDTDSSEEMLALADEFEHRAIGVFTECYRKDEERAQKLLVRVSEAWGKTTCLQL 718
rTRPM2 IWAQSQDCTAAALACSKILKELSKEEEDTDSSEEMLALADEFEHRAIGVFTECYRKDEERAQKLLVRVSEAWGKTTCLQL 719
762 S1 796
hTRPM2 ALEAKDMKFVSHGGIQAFLTKVWWGQLSVDNGLWRVTLCMLAFPLLLTGLISFREKRLQDVGTPAARARAFFTAPVVVFH 800
mTRPM2 ALEAKDMKFVSHGGIQAFLTKVWWGQLCVDNGLWRIILCMLAFPLLFTGFISFREKRLQALCRP-ARVRAFFNAPVVIFH 797
rTRPM2 ALEAKDMKFVSHGGIQAFLTKVWWGQLCVDNGLWRIILCMLAFPLLFTGFISFREKRLQALCRP-ARVRAFFNAPVVIFY 798
S2 847 868 N-x-x-D motif
hTRPM2 LNILSYFAFLCLFAYVLMVDFQPVPSWCECAIYLWLFSLVCEEMRQLFYDPDECGLMKKAALYFSDFWNKLDVGAILLFV 880
mTRPM2 MNILSYFAFLCLFAYVLMVDFQPSPSWCEYLIYLWLFSLVCEETRQLFYDPDGCGLMKMASLYFSDFWNKLDVGAILLFI 877
rTRPM2 LNILSYFAFLCLFAYVLMVDFQPSPSWCEYLIYLWLFSLVCEETRQLFYDPDGCGLMKMASLYFSDFWNKLDVGAILLFI 878
S3 914 S4 930 933 S5 952 958 960
hTRPM2 AGLTCRLIPATLYPGRVILSLDFILFCLRLMHIFTISKTLGPKIIIVKRMMKDVFFFLFLLAVWVVSFGVAKQAILIHNE 960
mTRPM2 VGLTCRLIPATLYPGRIILSLDFIMFCLRLMHIFTISKTLGPKIIIVKRMMKDVFFFLFLLAVWVVSFGVAKQAILIHNE 957
rTRPM2 AGLTCRLIPATLYPGRIILSLDFIMFCLRLMHIFTISKTLGPKIIIVKRMMKDVFFFLFLLAVWVVSFGVAKQAILIHNE 958
961 964 981 984/5 987 994/5/6 1002 1008 1017 1022
hTRPM2 RRVDWLFRGAVYHSYLTIFGQIPGYIDGVNFNPEHCSPNGTDPYKPKCPESDATQQRPAFPEWLTVLLLCLYLLFTNILL 1040
mTRPM2 SRVDWIFRGVVYHSYLTIFGQIPTYIDGVNFSMDQCSPNGTDPYKPKCPESDWTGQAPAFPEWLTVTLLCLYLLFANILL 1037
rTRPM2 SRVDWIFRGVIYHSYLTIFGQIPTYIDGVNFSMDQCSPNGTDPYKPKCPESDWTGQAPAFPEWLTVTLLCLYLLFANILL 1038
S6
hTRPM2 LNLLIAMFNYTFQQVQEHTDQIWKFQRHDLIEEYHGRPAAPPPFILLSHLQLFIKRVVLKTPAKRHKQLKNKLEKNEEAA 1120
mTRPM2 LNLLIAMFNYTFQEVQEHTDQIWKFQRHDLIEEYHGRPPAPPPLILLSHLQLLIKRIVLKIPAKRHKQLKNKLEKNEETA 1117
rTRPM2 LNLLIAMFNYTFQEVQEHTDQIWKFQRHDLIEEYHGRPPAPPPLILLSHLQLLIKRIVLKIPAKRHKQLKNKLEKNEEAA 1118

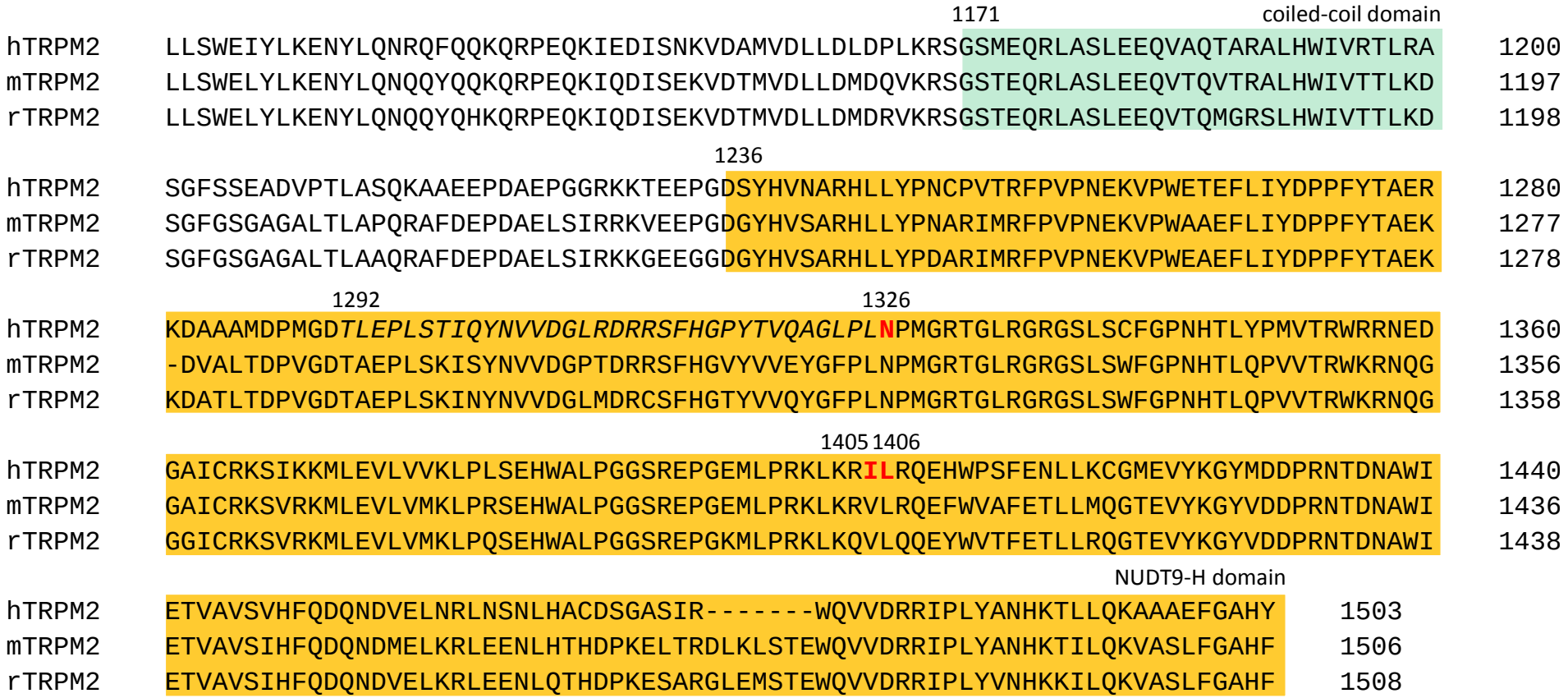

Figure 1.3 TRPM2 amino acid sequence alignments

Amino acid sequence alignments of human (hTRPM2), mouse (mTRPM2) and rat (rTRPM2) TRPM2 proteins. Different functional domains are highlighted in different background colours (*Blue*, transmembrane segments; *Yellow*, pore region; *Orange*, NUDT9-H domain; *Purple*, IQ-moif; *Green*, coiled-coil domain; *Navy*, N-x-x D motif; *Pink*, TRP domain). The sequences in italics present the truncation of amino acids residues in splice variants. The amino acids labelled in red are subjected to site-direct mutagenesis studies.

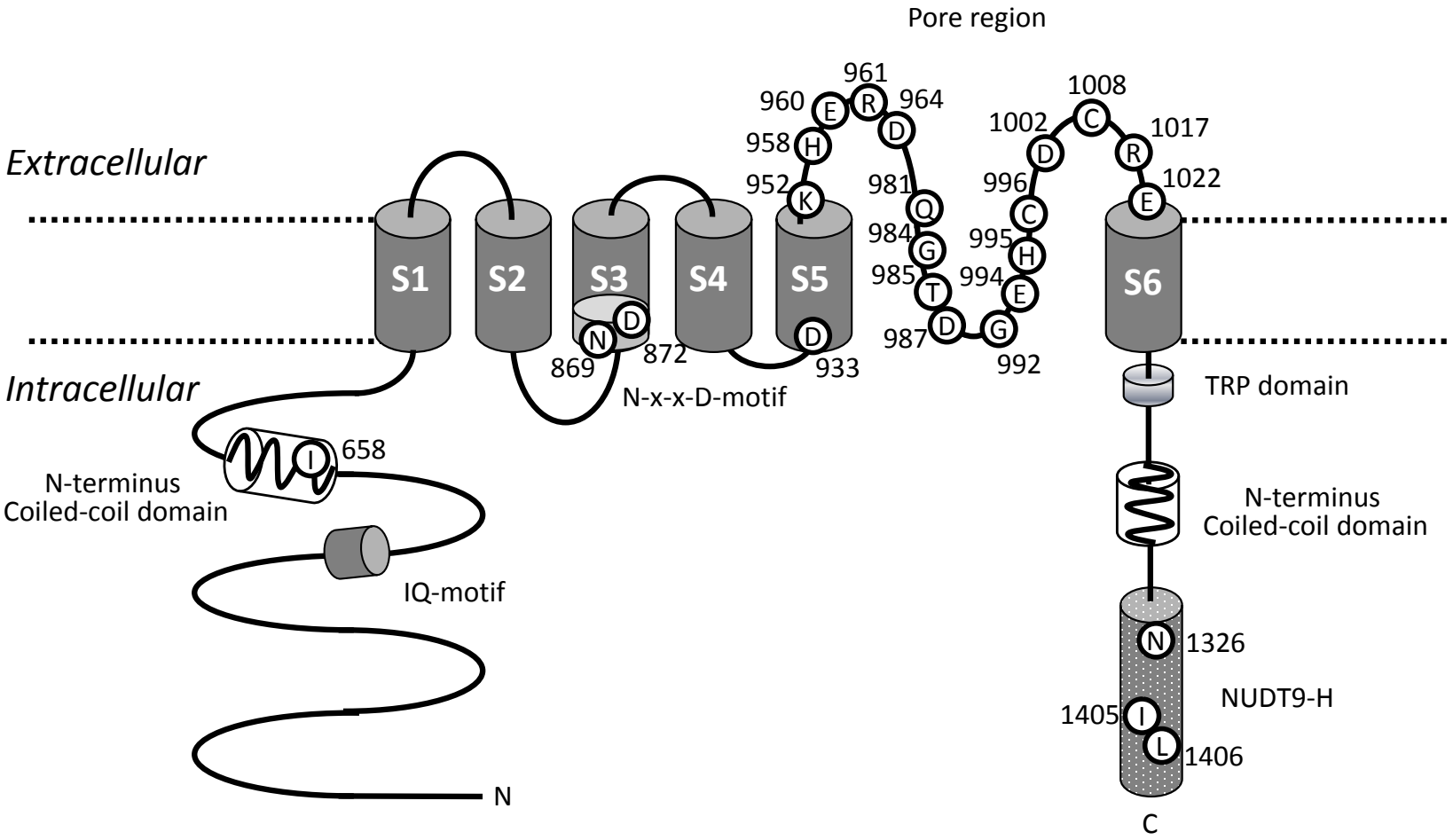

Figure 1.4 The topology and structural features of the TRPM2 channel subunit

Different functional domains are highlighted in different symbol denoted in the figure. The amino acids presented in the figure are subjected to site-direct mutagenesis studies.

for the TRPM8 channel assembly (Tsuruda et al., 2006). A study has revealed that the coiled-coil domain also plays an important role in the TRPM2 channel assembly (Mei et al., 2006b). Biotin labeling and Western blotting results demonstrated that there was no difference in the total protein expression level between the TRPM2 mutant with the C-terminal coiled-coil domain being deleted (ΔCC) and WT TRPM2 protein, whereas the cell surface expression level of the ΔCC mutant protein was only about half of the WT protein. The co-immunoprecipitation experiments also showed a dramatic reduction in the interaction between the ΔCC mutant proteins. Furthermore, much smaller ADPR-induced currents were observed in HEK293 (human embryonic kidney 293) cells expressing the ΔCC mutant protein than in cells expressing the WT protein. Thus, these observations led to the conclusion that the C-terminal coiled-coil domain is required in functional TRPM2 channel assembly. However, low level interactions between the ΔCC mutant proteins themselves and between the ΔCC mutant and WT proteins were observed, suggesting involvement of additional regions in the TRPM2 channel assembly (Mei et al., 2006b).

1.2.2.3 Other domains

Besides the C-terminal coiled-coil domain, the TRPM2 protein contains another coil-coiled domain in the N-terminus (Fig. 1.4) with its sequence showed in Fig. 1.3. The deletion of this N-terminal coiled-coil domain dramatically reduced the TRPM2 protein expression, and completely abolished ADPR-induced whole-cell current. Furthermore, introduction of I658Q mutation in the coiled-coil domain abolished ADPR-induced current without significant change in the protein expression and subunit interaction (Mei and Jiang, 2009) (Fig. 1.4). Thus, in contrast to contribution of the C-terminal coiled-coil domain in the TRPM2 channel assembly, the N-terminal coiled-coil domain plays a role in the TRPM2 channel expression and function, with minimal involvement in the channel assembly.

An N-x-x-D motif (amino acid 869-872) is present in the intracellular end of the S3 (Fig. 1.4). Substitution of Asp-872 with Asn resulted in complete loss of ADPR-induced currents, but caused no change in the cell surface expression level of TRPM2 protein , suggesting potential involvement in the TRPM2 channel gating (Winking et al., 2012).

Besides the functional regions mentioned above, there is a TRP domain located in the C-terminus of the TRPM2 protein (Fig. 1.4). However, the functional significance of this domain in the TRPM2 channel is unknown.

1.2.3 Alternative splicing isoforms

In addition to the full-length TRPM2 subunit (TRPM2-L in short), there are several alternative splice isoforms (Fig. 1.3). The TRPM2-S (short TRPM2) isoform results from introduction of a premature stop codon (TAG) at the splice junction between exons 16 and 17, leading to truncation of amino acid residues 847-1053; thus TRPM2-S lacks the last four transmembrane segments and the whole C-terminus (Fig. 1.3). This isoform is expressed in human hematopoietic cells (Du et al., 2009b, Zhang et al., 2003). Endogenous expression of both the TRPM2-L and TRPM2-S isoforms have been identified in human BFU-E (burst-forming unit-erythroid)-derived cells. Both are targeted to the plasma membrane as shown by immunofluorescent confocal microscopy. Heterologous expression of the TRPM2-S isoform in HEK293 cells exhibits a similar subcellular localization as the TRPM2-L, but results in no functional channel. Co-expression and co-immunoprecipitation showed that TRPM2-L and TRPM2-S isoforms can interact directly. However, co-expression with the TRPM2-S isoform suppresses H_2O_2 (hydrogen peroxide)-induced Ca^{2+} responses and inhibits H_2O_2-induced cell death mediated by the TRPM2-L isoform (Zhang et al., 2003).

Another short isoform is called SSF-TRPM2, as it was originally identified in the striatum (Uemura et al., 2005) (Fig. 1.3). Its transcription begins with the start codon in the fourth intron. The SSF-TRPM2 protein lacks the first 214 amino acid residues in the N-terminus (Fig. 1.3), but can still form a functional channel that mediates H_2O_2-induced Ca^{2+} influx. However, the Ca^{2+} influx amplitude is smaller than that mediated by the TRPM2-L channel.

Additional alternative splicing isoforms have been found, including loss of part of exon 11 and skipping of exon 27, resulting in deletion of amino acid residues 537–556 and 1292–1325 in the N- and C-terminus, respectively, or TRPM2-ΔN and TRPM2-ΔC isoforms (Fig. 1.3). The TRPM2-ΔC isoform was initially identified in neutrophils and Hela cells, and cannot be activated by ADPR or cADPR (cyclic ADPR) (Numata et al., 2012, Wehage et al., 2002, Du et al., 2009a). Using whole-cell patch clamp, Du and his colleagues have revealed that the

TRPM2-ΔC isoform can be stimulated by intracellular Ca^{2+}, requiring the calmodulin (CaM)-binding domain (the IQ-motif) in the N-terminus. This result suggests the TRPM2 channel gating by Ca^{2+} in an ADPR-independent manner (discussed further in section 1.2.5.1.5 and 1.2.6.2) (Du et al., 2009a). A recent study has proposed the TRPM2-ΔC channel to mediate the hypertonic stress-induced currents in Hela cell as both exhibit similar I-V relationships and Ca^{2+} permeability (Numata et al., 2012). The TRPM2-ΔN channels exhibited no activation by ADPR and H_2O_2 (Kuhn et al., 2009, Du et al., 2009a). However, Du demonstrated that the whole-cell TRPM2-ΔN channel current can be evoked by intracellular Ca^{2+} (Du et al., 2009a).

1.2.4 Subcellular location

As mentioned above, the TRPM2 channels were thought as Ca^{2+}-permeable cation channels. Many studies have provided functional evidence supporting that the TRPM2 channels are localized in the plasma membrane and mediate extracellular Ca^{2+} influx in diverse types of cells, such as monocyte cells (Yamamoto et al., 2008), T lymphocytes (Beck et al., 2006, Magnone et al., 2012), pancreatic β-cells (Togashi et al., 2008, Uchida and Tominaga, 2011), endothelial cells (Hecquet et al., 2008) and neurons (Chung et al., 2011, Ishii et al., 2006a, Ishii et al., 2006b, Kolisek et al., 2005, Olah et al., 2009, Perraud et al., 2005). TRPM2-mediated Ca^{2+} influx results in increases in the cytosolic Ca^{2+} concentrations ($[Ca^{2+}]_c$) that plays a role in a variety of cell functions such as cytokine generation, insulin release, and cell death (discussed in detail in section 1.2.7-1.2.8).

Recent studies have reported that the TRPM2 channels are also or exclusively present in the membranes of intracellular organelles and function as intracellular Ca^{2+}-release channels. The study by Lange and his colleagues demonstrated that, besides acting as a plasma membrane Ca^{2+} channel, the TRPM2 channel contributed to ADPR-induced intracellular Ca^{2+}-release from the lysosome in TRPM2-expressing HEK293 cells and also in rat insulinoma cell line INS-1 endogenously expressing TRPM2 channels (Lange et al., 2009). Lange and his colleagues showed using immunofluorescent confocal microscopy that the TRPM2 proteins were localized in the lysosome but not in the ER. The Ca^{2+} storage in the lysosome is maintained by the proton gradient across the lysosomal membrane that is generated by

vacuolar-type H^+-ATPase (V-ATPase). V-ATPase is an enzyme located in the lysosomal membrane and pumps intracellular protons into the lysosomes, endosomes and secretory vesicles (Haller et al., 1996, Christensen et al., 2002). Bafilomycin A, a type of macrolide antibiotic, is a specific blocker of the V-ATPase and can induce Ca^{2+} depletion in the lysosome (Kinnear et al., 2008, Kinnear et al., 2004). Lange further showed that intracellular ADPR induced- Ca^{2+} release in INS-1 β cells can be abolished by pre-treatment with bafilomycin A. These results indicate the TRPM2 channels to function as lysosomal Ca^{2+} release channels in INS-1 β cells (Lange et al., 2009). A recent study using immunofluorescent confocal microscopy and Ca^{2+} imaging has shown the TRPM2 channel to be exclusively localized in the late endosomes and lysosomes, mediating Ca^{2+} release from the lysosome in mouse dendritic cells (Sumoza-Toledo and Penner, 2011).

1.2.5 Pharmacology of TRPM2 channels

1.2.5.1 Channel activators

Several chemical and physical activators of the TRPM2 channels have been found over the past few years. Structures of some chemical activators are shown in Fig. 1.5.

1.2.5.1.1 ADPR

ADPR (Fig. 1.5) activates the TRPM2 channels in a concentration-dependent manner. The EC_{50} value varies in the range of 1-90 μM, depending on the cell types examined. For instance, studies reported the EC_{50} to be 1.1, 7, 10 and 90 μM in neutrophils (Lange et al., 2008), Jurkat T cells (Beck et al., 2006), TRPM2-expressing HEK293 cells (Kolisek et al., 2005, Starkus et al., 2007) and CRI-G1 insulinoma cells (Inamura et al., 2003), respectively. The concentration for maximal activation is about 300-500 μM. ADPR activates the TRPM2 channels by directly binding to the above-mentioned TRPM2-specific NUDT9-H domain in the distal part of the intracellular C-terminus. The binding affinity (K_d) of ADPR to the NUDT9-H domain, when expressed alone, is 100-130 μM (Kuhn and Luckhoff, 2004). Using sited-directed mutagenesis, Kühn and his colleagues have revealed that Asn-1326, Ile-1405 and Leu-1406 in the NUDT9-H domain (Fig. 1.3) play a crucial role in activation of TRPM2 channel by ADPR (Kuhn and Luckhoff, 2004).

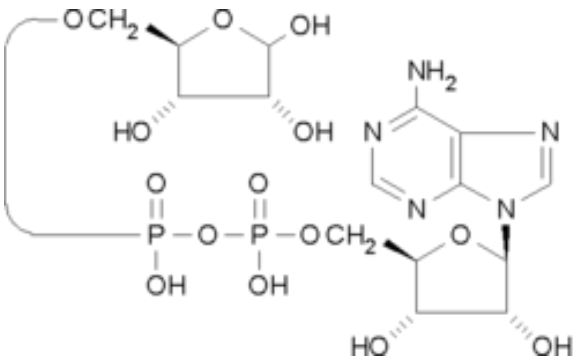

ADPR

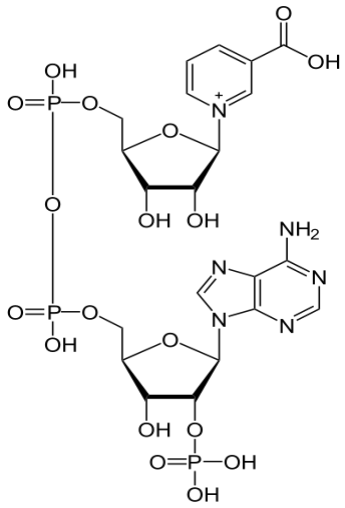

NAADP

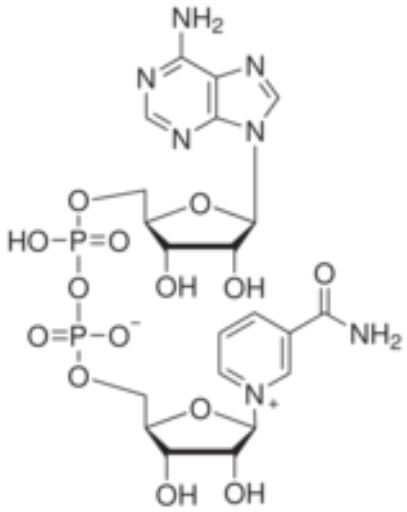

NAD

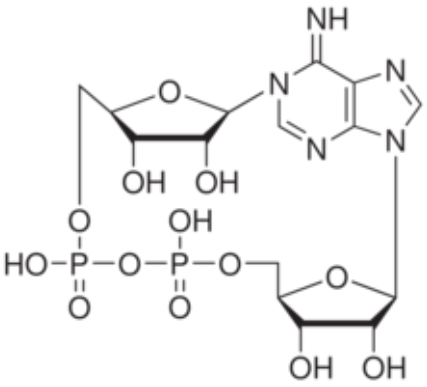

cADPR

Figure 1.5 Structures of TRPM2 activators

It has been proposed that ADPR is generated from nicotinamide adenine dinucleotide (NAD) in the nucleus or in the mitochondria of the cells in response to ROS (reactive oxygen species) and reactive nitrogen species (RNS) (Fig. 1.7). In the nucleus, ROS/RNS-induced DNA-damages initiate the DNA repair process, in which poly(ADPR) polymerases (PARP) are activated to polymerize ADPR using donor NAD into poly(ADPR) (PAR) chain on acceptor proteins, including PARP itself and, subsequently, the PAR chain is hydrolyzed to ADPR by poly(ADPR) glycohydrolase (PARG) (Kim et al., 2005). In the mitochondria, ROS/RNS-activated NAD nucleosidase (NADase) catalyzes hydrolysis of NAD to ADPR and nicotinamide (Guse, 2005, Wehage et al., 2002) (Fig. 1.7). ADPR presumably diffuses via yet known mechanisms to the cytosol from either the nucleus or the mitochondria, and bind to the TRPM2 channels. ADPR can be also generated extracellularly by CD38, a multifunctional ectoenzyme, using NAD as the substrate (Fig. 1.7). CD38 can convert NAD to cADPR or ADPR (Fig. 1.7) via its ADP-ribosylcyclase and NAD glycohydrolase activities, respectively. Cyclic ADPR can be further converted to ADPR by CD38 via its cADPR hydrolase activity. In addition to CD38, CD38-like enzymes BST-1 and CD157 are also involved in the metabolism of NAD, cADPR and ADPR (Lund et al., 2006, Lund et al., 1995, Malavasi et al., 2006). Partida-Sanchez has shown increases in the $[Ca^{2+}]_c$ and chemotaxis in mouse bone marrow neutrophils in response to cytokine and bacterial chemoattractant, formyl-methionyl-leucyl-phenylalanine (fMLP). Furthermore, using CD38-deficient mice, he also demonstrated that the deficiency of CD38 dramatically suppressed these two processes via reducing production of cADPR and ADPR (Partida-Sanchez et al., 2007, Partida-Sanchez et al., 2001). However, the roles of CD38 and CD38-like enzymes in regulating the intracellular level of ADPR are still not well established, because it is unclear how ADPR generated extracellularly can be transported into the cytosol in order to bind the NUDT9-H domain of the TRPM2 channels (Hecquet and Malik, 2009, Takahashi et al., 2011).

1.2.5.1.2 Nicotinic acid adenine dinucleotide phosphate (NAADP)

NAADP (Fig. 1.5) elicits TRPM2 channel currents in a concentration-dependent manner in several types of cells, such as neutrophils (Lange et al., 2008), Jurkat T cells (Beck et al., 2006) and TRPM2-expressing *Xenopus* oocytes (Toth and Csanady, 2010). The EC_{50}s are 95 and

730 µM in neutrophils and Jurkat T cells, respectively; under the same experimental conditions, the EC_{50}s for ADPR are 1.1 and 7 µM in these two types of cells, suggesting that the potency of NAADP is approximately 100-fold lower than that of ADPR (Beck et al., 2006, Lange et al., 2009). Furthermore, NAADP induced TRPM2 channel currents in inside-out recording of *Xenopus* oocytes heterogeneously expressing the TRPM2 channels, indicating that NAADP can directly activate the TRPM2 channels (Toth and Csanady, 2010).

1.2.5.1.3 NAD

NAD, shown in Fig. 1.5, is the substrate for ADPR generation (Fig. 1.7). An early study using inside-out patch clamp recording however revealed that intracellular NAD can directly trigger the TRPM2 channels to open but it has a low potency with an EC_{50} of about 1 mM in TRPM2-expressing HEK293 cells (Sano et al., 2001). Activation of the TRPM2 channels by NAD in whole-cell patch clamp recordings exhibited a significant delay (50-150 s) (Kolisek et al., 2005, Sano et al., 2001). However, another study showed failure of NAD to activate the TRPM2 channels (Wehage et al., 2002). In a recent study, Toth and Csanady showed that commercially available NAD is contaminated with a detectable amount of ADPR using thin layer chromatography, and suggested the activation of the TRPM2 channels by NAD could be induced by the contaminated ADPR (Toth and Csanady, 2010). Thus, the function of NAD as a TRPM2 activator is still an open question.

1.2.5.1.4 cADPR

Several studies also show activation of the TRPM2 channels by cADPR (Fig. 1.5). Intracellular cADPR has been shown using whole-cell patch clamp recording to induce the TRPM2 channel currents in a concentration-dependent manner in several types of cells, such as TRPM2-expressing HEK293 cells (Kolisek et al., 2005), neutrophils (Lange et al., 2009) and Jurkat T cells (Beck et al., 2006). The sensitivity differs substantially with EC_{50}s of about 700 µM, 44 µM and 60 µM, respectively in these three cell types. Furthermore, inside-out patch clamp recordings confirm direct activation of the TRPM2 channels by cADPR (Beck et al., 2006), but the underlying mechanism is unclear. It has been proposed that cADPR interacts with a site that is different from the ADPR binding-site in the NUDT9-H domain (Kolisek et al., 2005). However, several other studies have failed to demonstrate cADPR as a

TRPM2 channel agonist (Hara et al., 2002, Wehage et al., 2002, Heiner et al., 2006). In a recent study using inside-out patch clamp recordings in TRPM2-expressing *Xenopus* oocytes, the TRPM2 channel currents can induced by the commercially sourced cADPR but not the purified cADPR (Toth and Csanady, 2010), supporting the notion that cADPR does not directly activate the TRPM2 channels on its own.

A series of chemicals contained adenine dinucleotide group, including ADPR, NAADP, NAD and cADPR, have been reported to show a synergy in activation of the TRPM2 channels (Kolisek et al., 2005, Lange et al., 2009). For instance, using whole-cell patch clamp recording in neutrophils, the EC_{50}s of NAADP and cADPR are reduced from 95 μM to 1 μM and from 44 μM to 3 μM, respectively, in the presence of 100 nM ADPR (Lange et al., 2009). In addition, the TRPM2 channels can be activated by co-application of 300 μM NAD and 10 μM cADPR, which cannot activate on their own, suggesting a synergistic effect (Kolisek et al., 2005). However, ADPR-induced TRPM2 channel currents were not enhanced by co-application with cADPR in TRPM2-expressing *Xenopus* oocytes (Toth and Csanady, 2010). This could result from different type of cells used, or, according to the authors, from the fact that the ADPR contamination in the commercial cADPR samples, but not the cADPR, leads to TRPM2 channel activation (Toth and Csanady, 2010).

1.2.5.1.5 Ca^{2+}

ADPR-induced TRPM2 channel currents were significantly increased in the presence of extracellular Ca^{2+}. Furthermore, ADPR-induced currents in the presence of extracellular Ca^{2+} can be attenuated by intracellular application of BAPTA (1,2-bis(o-aminophenoxy)ethane-N,N,N',N'-tetraacetic acid), a Ca^{2+}chelator, to lower the $[Ca^{2+}]_c$. Since Ca^{2+} can enter into the cell through the open TRPM2 channels, these results suggest that intracellular Ca^{2+} is required for full activation of the TRPM2 channels. Further whole-cell patch clamp recordings show that the up-regulation of the ADPR-induced TRPM2 channel currents by Ca^{2+} is concentration-dependent, with an EC_{50} of 340 nM and a threshold of 100 nM (McHugh et al., 2003). Such a concentration-dependent activation by intracellular Ca^{2+} is confirmed in a subsequent study by inside-out patch clamp recordings of ADPR-induced currents in TRPM2-expressing *Xenopus* oocytes, with an EC_{50} of 22.4 μM, which is noticeably

higher due to perhaps the different concentrations of ADPR used (Csanady and Torocsik, 2009).

Besides the enhancement of ADPR-induced TRPM2 channel activation by Ca^{2+}, a recent study, using whole-cell and single-channel patch clamp recording, also showed that intracellular Ca^{2+} alone is sufficient to activate the TRPM2 channels. In particular, the study showed robust Ca^{2+}-induced TRPM2 channel currents in HEK293 cells heterologously expressing the ADPR-insensitive TRPM2-ΔC splice isoform, presenting compelling evidence to support the notion that intracellular Ca^{2+} can activate the TRPM2 channels independently of ADPR. The same study also shows that, in cells expressing the ADPR-sensitive TRPM2 channels, ADPR can enhance Ca^{2+}-induced activation and that co-application of ADPR reduces the EC_{50} for Ca^{2+} from 16.9 μM to 0.49 μM (Du et al., 2009a).

1.2.5.1.6 Reactive oxygen species

The free oxygen radicals or ROS all have oxygen ion or peroxide. There are several types of ROS, such as hydroxyl radical (HO•), superoxide anion ($•O_2^-$) and H_2O_2. ROS is generated by a variety of enzymes, including NADPH oxidase located in the plasma and ER membranes, xanthine oxidases and cytochrome p450 enzymes in the cytosol. ROS can also result from reactions with oxygen of electrons leaked from the mitochondrial electron transport chain at the complex I or complex III (Bae et al., 2011). Historically, ROS is considered as a harmful chemical, leading to a series of damages to DNA, RNA, lipids and proteins. Recent studies have proposed ROS as a physiological signaling molecule in many cell processes, such as cell migration, proliferation, and apoptosis (Tsutsui et al., 2011). ROS has been reported to be involved in aging and in many diseases, such as cancers, Parkinson's diseases (PD), Alzheimer's disease (AD) (Valko et al., 2007), myocardial infarction (Yang et al., 2006), lichen planus (Aly and Shahin, 2010) and fragile X syndrome (Halliwell, 2007).

There are numerous studies showing contribution of H_2O_2 in the TRPM2 channel activation and functions. Extracellular H_2O_2 can concentration-dependently induce the increase in the $[Ca^{2+}]_c$ in TRPM2-expressing HEK293 cells, with an EC_{50} of about 30 μM (Fonfria et al., 2004, Hara et al., 2002, Perraud et al., 2005, Wehage et al., 2002). H_2O_2-induced increases in the $[Ca^{2+}]_c$ have also been observed in several types of cells, such as endothelial cells (Hecquet

et al., 2008), microglia (Kraft et al., 2004), neutrophils (Lange et al., 2009) and rat insulinoma RIN-5F cells (Ishii et al., 2006a, Ishii et al., 2006b). While activation of the TRPM2 channels by H_2O_2 is consistently observed, the underlying mechanism remains still controversial. There is evidence to support direct stimulation of the TRPM2 channels by H_2O_2. Using whole-cell patch clamp recording, Kolisek and his colleagues showed that application of H_2O_2 in the micropipette solution induced currents in TRPM2-expressing HEK293 cells but the current amplitude is only about 5% of that induced by ADPR. Thus, these authors have proposed that H_2O_2 activates the TRPM2 channels independently with ADPR generation (Kolisek et al., 2005). The more solid evidence for ADPR-independent activation of the TRPM2 channel by H_2O_2 came from a study by Wehage and his colleagues (Wehage et al., 2002). They showed that H_2O_2 and ADPR evoked currents in HEK293 cells heterologously expressing the WT TRPM2 channel, whereas H_2O_2, but not ADPR, can induce currents in cells expressing the TRPM2-ΔC channel, suggesting direct activation of the TRPM2 channel by H_2O_2 is independent of ADPR. However, a subsequent study failed to observe H_2O_2-evoked increases in the $[Ca^{2+}]_c$ or currents in HEK293 cells expressing the TRPM2-ΔC channels (Perraud et al., 2005).

Most of the experimental results suggest that H_2O_2 induces activation of the TRPM2 channels by promoting generation of ADPR in the mitochondria and nucleus, as discussed above (see section 1.2.1.5.1 and Fig. 1.7). In TRPM2-expressing HEK293 cells, H_2O_2-induced increases in the $[Ca^{2+}]_c$ can be strongly suppressed by pre-treatment with 5[H]-phenanthridin-6-one, GPI16539 (Perraud et al., 2005), PJ34 and SB750139-B (Fonfria et al., 2004) to inhibit PARP activation and thereby to prevent accumulation of ADPR. H_2O_2-induced TRPM2 channel currents can be also attenuated by hydrolysis of ADPR by overexpression of cytNUDT9, a non-compartmentalized form of the ADPR pyrophosphatase (Perraud et al., 2005). These results indicate that elimination of ADPR accumulation prevents activation of TRPM2 channel by H_2O_2. A recent study, using inside-out patch clamp recordings, also has shown that H_2O_2 cannot directly activate the TRPM2 channels heterogeneously expressed in *Xenopus* oocytes (Toth and Csanady, 2010). All these studies support an indirect mechanism of TRPM2 channel activation by H_2O_2.

1.2.5.1.7 Temperature

The TRPM2 channel is sensitive to temperature. Using fluorescent Ca^{2+} imaging, heterologous expression of the TRPM2 channels in HEK293 cells conferred significant increase in the $[Ca^{2+}]_c$ in response to heat, with a threshold of about 40°C (Togashi et al., 2006). A recent study has also shown similar heat-evoked increases in the $[Ca^{2+}]_c$, with a higher average threshold of about 47°C in TRPM2-expressing HEK293 cells (Kashio et al., 2012). Such heat-evoked increases in the $[Ca^{2+}]_c$ were also observed in pancreatic β-cells and insulinoma RIN-5F cells, which were almost completely abolished by reducing TRPM2 expression using TRPM2 siRNA (small interfering RNA) (Togashi et al., 2006). Heat evoked whole-cell currents that exhibited typical linear TRPM2 I-V relationships, and further inside-out single-channel recordings showed that heat elicited currents with a threshold of about 34°C and maximum channel activation at 36°C in TRPM2-expressing HEK293 cells (Togashi et al., 2006). The mechanism underlying TRPM2 channel activation by heat is still unclear. According to a recent thermodynamic study using cold-activated TRPM8 channel and heat-activated TRPC5 channel as two examples, the thermo-sensitivity of TRP channels results from the conformational changes (Clapham and Miller, 2011). However, the direct evidence supporting this hypothesis for the sensitivity of TRPM2 channels to heat is still lacking.

Besides activation of TRPM2 channel by heat alone, heat also can dramatically facilitate the TRPM2 channel activation by agonists, such as ADPR, NAD and cADPR (Kashio et al., 2012, Togashi et al., 2006). In TRPM2-expressing HEK293 cells, the currents induced by cADPR at body temperature (37°C) are significantly larger than those by cADPR at room temperature or by raising temperature from 25°C to 37°C in the absence of cADPR. These results have revealed a synergistic effect of heat with agonists on the TRPM2 channel activation (Togashi et al., 2006). In addition, a recent study has also demonstrated that, in macrophages, the threshold of temperature inducing increases in the $[Ca^{2+}]_c$ is reduced from about 47°C to about 41°C or 36°C by pre-exposure of the cells to 100 μM or 3 mM H_2O_2, respectively (Kashio et al., 2012). H_2O_2-induced increases in the thermo-sensitivity of the TRPM2 channel was eliminated by substituting Met-214 with Ala in the intracellular N-terminus of the TRPM2 channel, leading to the proposal that Met oxidation by H_2O_2 has a role in increasing the TRPM2 channel sensitivity to temperature (Kashio et al., 2012). However, in

the same study, it was shown such sensitization by H_2O_2 was dramatically reduced by pre-treatment with PJ34 (Kashio et al., 2012), a PARP inhibitor; such the result seems to be consistent with the idea that H_2O_2-induced ADPR generation and the resultant synergy between ADPR and temperature are important in increasing the temperature sensitivity of the TRPM2 channels.

1.2.5.2 Inhibitors

Several structurally different inhibitors of the TRPM2 channels have been found over the past few years. Their chemical structures are shown in Fig. 1.6.

1.2.5.2.1 N-(p-amylcinnamoyl) anthranilic acid (ACA)

ACA belongs to the class of N-cinnamoyl-anthranilic acids (Fig. 1.6). In TRPM2-expressing HEK293 cells, extracellular application of ACA suppressed H_2O_2-induced increases in the $[Ca^{2+}]_c$ in a concentration-dependent manner with an IC_{50} of about 1.7 μM. ACA at 20 μM fully abolished ADPR-induced currents. The current inhibition was largely reversible upon washout (Kraft et al., 2004). Single-channel patch clamp recordings showed no significant change in single-channel conductance by ACA, implying that the current inhibition is mainly due to decrease in the channel open probability. ACA has been shown to inhibit endogenously expressed TRPM2 channels in DT40 B lymphocytes, human U937 cells and INS-1E β-cells (Bari et al., 2009, Kraft et al., 2004, Song et al., 2008). ACA is known to inhibit phospholipase A2 (PLA_2) (Harteneck et al., 2007). However, two other PLA_2 inhibitors, p-bromophenacyl bromide and arachidonyltrifluoromethyl ketone showed no inhibition of ADPR-induced TRPM2 channel activation, suggesting that ACA-induced inhibition of the TRPM2 channels is not related to PLA_2 inhibition (Kraft et al., 2004). Besides the TRPM2 channels, ACA can inhibit several other TRP channels, such as TRPC6 and TRPM8 (Harteneck et al., 2007, Kraft et al., 2004).

1.2.5.2.2 Flufenamic acid (FFA) and its homologue

FFA is a non-steroidal anti-inflammatory drug (Fig. 1.6). Extracellular application of FFA inhibits ADPR-induced currents in TRPM2-expressing HEK293 cells (Chen et al., 2012, Hill et al., 2004a). An early study showed that FFA inhibited the TRPM2 channels in an all-or-none

manner in the range of concentrations from 50 μM to 1000 μM (Hill et al., 2004a). However, a recent study demonstrated that the inhibition is concentration-dependent with an IC_{50} of 70 μM (Chen et al., 2012). The inhibition of ADPR-induced currents by FFA was reversible upon washout, but the reversibility is exposure duration-dependent in TRPM2-expressing HEK293 cells (Hill et al., 2004a). In contrast, in CRI-G1 insulinoma cells endogenously expressing the TRPM2 channels, the inhibition by FFA was strongly reversed even after prolonged exposure to high concentrations (1 mM for 3 min) (Hill et al., 2004a). In addition to the TRPM2 channel, FFA can inhibit TRPM3 (Klose et al., 2011), TRPM4 and TRPM5 channels (Ullrich et al., 2005), whereas it activates other TRP channels. For example, TRPA1 can be stimulated by FFA in a concentration-dependent manner with an EC_{50} of about 78 μM in TRPA1-expressing *Xenopus oocytes* (Hu et al., 2010). Furthermore, FFA can induce intracellular Ca^{2+} release in *Aplysia* Bag Cell Neurons (Gardam et al., 2008).

A novel analogue of FFA has been reported recently, 3-aminoethoxydiphenyl borate (3-MFA), in which the trifluoromethyl group in 2-phenylamino ring of FFA is substituted by a methyl. 3-MFA showed a concentration-dependent inhibition of ADPR-induced currents with an IC_{50} of 76 μM. Furthermore, 3-MFA did not elicit Ca^{2+} release, suggesting 3-MFA is more selective than FFA (Chen et al., 2012).

1.2.5.2.3 Clotrimazole and econazole

1-[(2-chlorophenyl) diphenylmethyl]-1H-imidazole (clotrimazole) and 1-[2-[4-chlorophenyl) methoxy]-2-(2,4-dichlorophenyl)ethyl]-1H-imidazole (econazole) are imidazole related antifungal agents (Fig. 1.6) and are widely used in clinical and veterinary treatments of fungal infection (Fromtling, 1988). Both compounds, when applied extracellularly at the concentrations ranging from 3 μM to 30 μM, almost completely inhibited ADPR-induced currents in TRPM2-expressing HEK293 cells, and also in CRI-G1 insulinoma cells. The inhibition of ADPR-induced currents by clotrimazole was partially reversible in CRI-G1 insulinoma cells, but irreversible in TRPM2-expressing HEK293 cells. The inhibition of ADPR-induced by econazole in TRPM2-expressing HEK293 cells was also irreversible (Hill et al., 2004b). Econazole can also inhibit TRPM8 (Malkia et al., 2009) and P2Y2 receptors (Bahra et al., 2004), and clotrimazole blocks TRPV4 (Bai and Lipski, 2010) and Ca^{2+}-activated K^+ channels ($K_{Ca}3.1$) (Turner and Sontheimer, 2013).

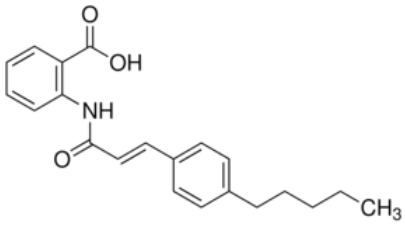

ACA

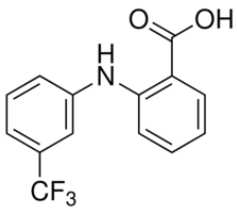

FFA

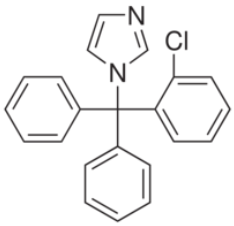

Clotrimazole

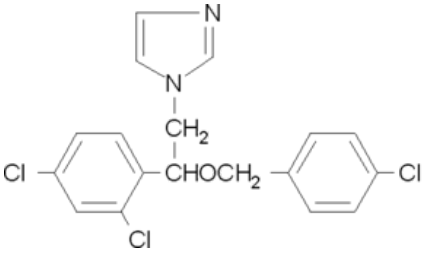

Econazole

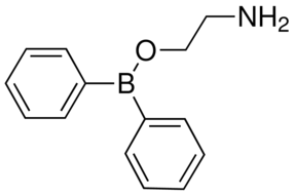

2-APB

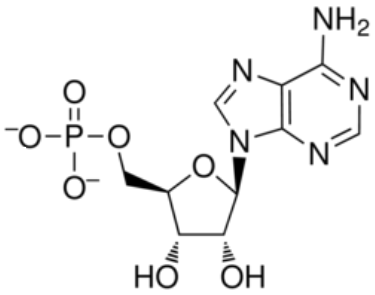

AMP

Figure 1.6 Structures of TRPM2 inhibitors

1.2.5.2.4 2-APB

2-APB can inhibit TRPM2 channels (Fig. 1.6). In TRPM2-expressing HEK293 cells, extracellular application of 2-APB caused a rapid and reversible inhibition of ADPR-induced currents in a concentration-dependent manner with an IC_{50} of 1.2 μM. In DRG neurons, 2-APB at 50 μM almost completely and reversibly blocked H_2O_2-induced whole-cell currents and dramatically suppressed H_2O_2-induced increases in the $[Ca^{2+}]_c$ (Naziroglu et al., 2011). 2-APB also completely inhibited cADPR-elicited TRPM2 channel currents (Chen et al., 2012). 2-APB is a non-specific blocker that acts on a variety of ion channels, including IP_3 receptors (Vázquez-Martínez O, 2003), TRPV6 channel (Kovacs et al., 2012), TRPM7 channel (Chokshi et al., 2012) and most of the TRPC channels (Rychkov and Barritt, 2007, Harteneck and Gollasch, 2011).

1.2.5.2.5 Adenosine monophosphate (AMP)

ADPR can be hydrolyzed to AMP and ribose-5'-phosphate by ADPR pyrophosphatase (Bessman et al., 1996). Ribose-5'-phosphate does not have any effect, whereas AMP has effect on inhibition of the TRPM2 channel activation (Fig. 1.6). Intracellular application of AMP inhibited ADPR-induced currents in TRPM2-expressing HEK293 cells in a concentration-dependent manner with an IC_{50} of 70 μM. AMP at 500 μM also completely abolished the whole-cell currents induced by NAD or cADPR (Kolisek et al., 2005). AMP has been shown to bind to the NUDT9-H domain in the C-terminus of the TRPM2 protein with a K_d of about 166 μM (Grubisha et al., 2006), and the inhibition of the TRPM2 channel by AMP is thus thought to be via a mechanism in which AMP competitively binds to the NUDT9-H domain and replaces the ADPR binding. Since the NUDT9-H domain has the activity of ADPR pyrophosphatase, AMP is proposed to form a negative feedback in regulating the TRPM2 channel activation by ADPR.

So far specific TRPM2 channel inhibitors are still lacking but required to study the physiological and pathological functions of hTRPM2 channels. Thus, chapter 4 in my thesis will describe our efforts to search for potential hTRPM2 channel inhibitors.

1.2.5.2.6 Divalent cations

Several recent studies have examined the effects of divalent cations such as Zn^{2+}, Cu^{2+} and Pb^{2+}, on the TRPM2 channels. Extracellular Zn^{2+} completely inhibited ADPR-induced currents in the range of concentrations down to 30 μM in TRPM2-expressing HEK293 cells. This inhibition was irreversible upon prolonged exposure, suggesting that Zn^{2+} induces the TRPM2 channel inactivation. There are 20 residues located in the pore-forming region of the TRPM2 protein that may potentially interact with Zn^{2+}, including His, Cys, Lys, Gln and Asn. A site-directed mutagenesis study showed that K952A and D1002A mutations strongly suppressed channel inhibition caused by Zn^{2+}. This study further showed that the inhibition kinetics is concentration and species-dependent. The mouse TRPM2 (mTRPM2) channels exhibit much slower response to Zn^{2+} than the hTRPM2 channels. Change of Gln-992 in the mTRPM2 channel to His in the hTRPM2 channel dramatically accelerated the kinetics of Zn^{2+}-evoked inhibition; conversely, the reciprocal mutation H995Q in the hTRPM2 channel decelerated the inhibition kinetics (Yang et al., 2011). Zeng and his colleagues have demonstrated that extracellular application of Cu^{2+} inhibited ADPR-induced TRPM2 channel currents in a concentration-dependent manner with an IC_{50} of 2.59 μM (Zeng et al., 2012). Furthermore, Hg^{2+} Pb^{2+}, Fe^{2+} and Se^{2+} also inhibited ADPR-induced currents in TRPM2-expressing HEK293 cells (Sukumar and Beech, 2010, Zeng et al., 2012).

1.2.5.2.7 Acidic pH

Extracellular acidic pH has been shown to significantly inhibit the TRPM2 channel by three independent studies (Du et al., 2009b, Starkus et al., 2010, Yang et al., 2010). However, the pattern of inhibition and the underlying mechanisms are inconsistent. In TRPM2-expressing HEK293 cells, the studies by Du and Starkus using whole-cell patch clamp recordings showed that inhibition of ADPR-induced currents or open TRPM2 channels by acidic pH was concentration-dependent with IC_{50} values of pH 5.3 (Du et al., 2009b) or pH 6.5 (Starkus et al., 2010), respectively. Differing from these two studies, the study from our lab showed that inhibition of the TRPM2 channel by extracellular acidic pH was state-dependent in whole-cell patch clamp recordings (Yang et al., 2010); ADPR-induced currents or open channels is completely, irreversibly and voltage-independently blocked by acidic pH in the range of pH 4.0–6.0, whereas exposure of the closed channels to acidic pH reduced the

channel activation in a pH-dependent manner with an IC_{50} for pH 4.7 (Yang et al., 2010). These results suggest two sequential steps in TRPM2 channel inhibition by extracellular acidic pH, which was due to initial blockage of the open channels and subsequent conformational changes leading to inactivation of the open channels. Furthermore, single-channel recordings from Du's and Yang' studies suggest that acidic pH decreased the single-channel conductance (Du et al., 2009b, Yang et al., 2010). Starkus et al examined the effects of acidic pH on single channel conductance in neutrophil cells endogenously expressing the TRPM2 channels, and found a similar effect (Starkus et al., 2010).

In contrast to the voltage-independent inhibition (Du et al., 2009b), Starkus et al showed that the inhibition was voltage-dependent, with stronger inhibition at negative membrane potential and that the kinetics of inhibition by extracellular acidic pH was decelerated by holding more acidic intracellular pH (Starkus et al., 2010). They have therefore proposed that extracellular protons permeate the open channels into the cells and results in inactivation of the TRPM2 channels by binding at an intracellular site. However, the other two studies suggest that the inhibition of TRPM2 channels by acidic pH is due to binding of protons to the extracellular pore region of the TRPM2 channels. In Yang's study, substitution with Ala of two residues in the pore-forming region, Lys-952 and Asp-1002 (Fig. 1.4), significantly slowed down or reduced pH-induced inhibition (Yang et al., 2010). Du et al showed by site-directed mutagenesis that H958Q, D964N and E994Q introduced into the pore-forming region, resulted in an increase in the pH sensitivity and reduction in the single-channel conductance (Du et al., 2009a). These results suggest that extracellular acidic pH or protons can interact with the extracellular vestibule of the pore to initially inhibit the open channel and subsequently to induce conformational changes leading to the channel inactivation.

Intriguingly, several early studies showed that extracellular acidic pH accelerated the inhibition kinetics of other blockers (Chen et al., 2012, Hill et al., 2004a, Hill et al., 2004b, Kraft et al., 2004). For instance, the inhibition of ADPR-induced current by 100 μM FFA at pH 6.0 was about 10-times faster than at pH 7.4 (Hill et al., 2004a). These studies proposed that this phenomenon could be resulted from the change of the proportion of the charged form to the uncharged form of the inhibitors by pH. However, according to the effects of

extracellular acidic pH revealed in the studies as discussed above, the acceleration of the inhibition kinetics could be in part due to the inhibition of acidic pH itself.

Intracellular acidic pH also can block TRPM2 channels. The inhibition of ADPR-induced currents by intracellular acidic pH was concentration-dependent with an IC_{50} of pH 6.7 (Du et al., 2009b). Using inside-out single-channel recordings, Starkus and his colleagues showed that the channel open probability was reduced when intracellular pH was changed from 7.0 to 6.0 (Starkus et al., 2010). Both studies from Du and Starkus observed no change in single channel conductance by intracellular acidic pH (Du et al., 2009b, Starkus et al., 2010). Furthermore, substitution of Asp-933 with Glu, His, Lys and Ala, reduced the IC_{50} from pH 6.7 to about pH 5, suggesting that Asp-933 plays a critical role in the sensitivity to intracellular acidic pH (Du et al., 2009b).

As discussed above, despite that these studies have shown that extracellular acidic pH can inhibit the TRPM2 channels; the underlying mechanisms are still not fully understood. In chapter 3, I will conduct further experiments to study the inhibition of the human and mouse TRPM2 channels by extracellular acidic pH.

1.2.6 Modulation of TRPM2 channel functions by interacting proteins

Protein-protein interaction is a commonly used mechanism by which ion channel function is modulated. In this section, I will discuss several intracellular proteins that have been shown to interact with and regulate the TRPM2 channels.

1.2.6.1 Protein tyrosine phosphatase-L1 (PTPL1)

PTPL1, also called PTP-BAS (Maekawa et al., 1994), PTP1E (Banville et al., 1994) or FAP-1 (Sato et al., 1995), is a widely expressed tyrosine phosphatase that remove the phosphate group from phosphorylated tyrosine residues. PTPL1 has been reported to be involved in protecting Fas (folic acid synthesis)-mediated apoptosis and up-regulating Ewing's Sarcoma tumor genesis (Abaan et al., 2005). Using Western blotting, Zhang and his colleagues showed an increased TRPM2 protein phosphorylation level in response to H_2O_2 or TNF-α (Zhang et al., 2006). Increases in H_2O_2 or TNF-α-induced TRPM2 phosphorylation and the

$[Ca^{2+}]_c$ were significantly reduced by PTPL1 overexpression in TRPM2-expressing HEK293 cells. Conversely, down-regulation of endogenous PTPL1 expression by siRNA enhanced both TRPM2 phosphorylation and H_2O_2-induced increases in the $[Ca^{2+}]_c$. In addition, co-immunoprecipitation showed a direct interaction between TRPM2 and PTPL1 proteins in HEK293 cells heterologously co-expressing, and U937 cells endogenously expressing, these two proteins (Zhang et al., 2006). These results suggest an important role of PTPL1 in modulating the TRPM2 channel function.

1.2.6.2 Calmodulin and EF-hand domain-containing (EFHC) protein 1

CaM is a small protein that is ubiquitously expressed and regulates diverse Ca^{2+}-dependent cell processes (Crivici and Ikura, 1995, Hoeflich and Ikura, 2002). CaM contains four EF-hand motifs, each of which provides one Ca^{2+}-binding site with a high affinity. As mentioned above, intracellular Ca^{2+} is important in TRPM2 channel activation. Overexpression of wild-type CaM cannot alter H_2O_2- or TNF-α-induced increases in the $[Ca^{2+}]_c$ (Tong et al., 2006) or Ca^{2+}-stimulated currents (Du et al., 2009a), presumably because the endogenous CaM expression level is sufficient. Whereas, overexpression of Ca^{2+}-binding deficient mutant CaM (CaM_{MUT}), significantly reduced both H_2O_2- or TNF-α-induced Ca^{2+} responses and intracellular Ca^{2+}-induced TRPM2 channel currents (Du et al., 2009a, Tong et al., 2006). Furthermore, co-immunoprecipitation demonstrated a direct interaction between CaM and TRPM2 via the N-terminus, and such interaction strongly depended on Ca^{2+} (Tong et al., 2006). These results suggest that CaM binds with the channels, and acts as a Ca^{2+} sensor that renders the TRPM2 channel to be activated by Ca^{2+}.

The N-terminus of the TRPM2 protein contains an IQ-like motif (see Fig. 1.4 and section 1.2.2). Disruption of this motif by point mutagenesis (IQ_{MUT}) reduced the interaction of TRPM2 with CaM as assessed by co-immunoprecipitation and gel shift experiments (Tong et al., 2006). Furthermore, IQ_{MUT} was shown to significantly reduce H_2O_2- or TNF-α-induced increases in the $[Ca^{2+}]_c$ (Tong et al., 2006) and almost completely abolished Ca^{2+}-stimulated TRPM2 channel currents (Du et al., 2009a). These results suggested that this IQ-motif plays an important role in the TRPM2 channel activation. However, binding of CaM to the TRPM2 protein was reduced but not completely abolished by mutational disruption of the IQ-like

motif, suggesting that more than one CaM-binding site is present in the TRPM2 channel (Tong et al., 2006).

EFHC1 has also been shown to modulate the TRPM2 channels. Katano and his colleagues showed co-expression of EFHC1 and TRPM2 proteins in mouse brain using in-situ hybridization and direct protein-protein interaction between these two proteins by co-immunoprecipitation (Katano et al., 2012). In TRPM2-expressing HEK293 cells, both H_2O_2-induced increases in the $[Ca^{2+}]_c$ and ADPR-stimulated currents can be enhanced by co-expression of EFHC1 (Katano et al., 2012). Therefore, EFHC1 plays a role in regulating TRPM2 channel activation through direct binding. However, it is unclear whether EFHC1 has a role in providing Ca^{2+}-binding site to facilitate activation of the TRPM2 channels by Ca^{2+}.

1.2.7 Physiological functions

In the past decade, many studies by pharmacological inhibition of the TRPM2 channel function and genetic manipulation of the TRPM2 protein expression, and particularly using TRPM2 deficient transgenic mice, provide evidence to show that the TRPM2 channels contribute to several physiological functions.

1.2.7.1 Cytokine production

Cytokines are small signal proteins or peptides, such as IL-1, IL-6, cytokine (C-X-C motif) ligand 8 (CXCL8) and TNF-α. They are produced by immune cells, including lymphocytes, dendritic cells, monocytes and macrophages, and play an essential role in immune responses (Lacy and Stow, 2011). CXCL8, the human cytokine also called IL-8, and CXCL2, the rodent functional homolog (Sonoda et al., 1998), are responsible for recruitment of inflammatory cells, such as macrophages and neutrophils, to the sites of tissue injured or infected. It is well-known that H_2O_2 induces secretion of CXCL8 but the underlying mechanism remains not well established (Chiu et al., 2007, Josse et al., 2001). Several recent studies have revealed that TRPM2 channels are critically involved in H_2O_2-induced CXCL8 release. Release of CXCL8 by H_2O_2 in human monocyte cells was dramatically suppressed by siRNA knockdown of TRPM2 protein expression (Yamamoto et al., 2008). Consistently, H_2O_2-evoked CXCL2 release in monocytes isolated from TRPM2 deficient mice

was significantly inhibited. Removal of extracellular Ca^{2+} by EGTA (ethyleneglycoltetraacetic acid) abolished H_2O_2-evoked Ca^{2+} influx and led to almost complete inhibition of CXCL8 release in U937 cells. These data suggest a critical role of TRPM2 channels in H_2O_2-evoked CXCL8 release via mediating Ca^{2+} influx (Yamamoto et al., 2008). Furthermore, this study also showed the inhibition of H_2O_2-evoked CXCL8 release by pre-treatment with PD98059, a MEK (MAPK (mitogen-activated protein kinase) / ERK (extracellular signal-regulated protein kinases) kinase) inhibitor, and PDTC, a NF-κB (nuclear factor kappa-light-chain-enhancer of activated B cells) inhibitor. H_2O_2 has been also showed to enhance the activation of ERK and its upstream signal molecular Pyk2 (proline-rich tyrosine kinase 2) and Ras (rat sarcoma). Furthermore, activation of these molecules, were all strongly suppressed by removal of extracellular Ca^{2+} or TRPM2 specific siRNA transfection, suggesting that TRPM2 channel-mediated Ca^{2+} influx plays an essential role in activation of ERK pathway and nuclear translocation of the NF-κB by H_2O_2 (Yamamoto et al., 2008). In human blood monocytes, mouse splenocytes and mouse paw, the production of CXCL8/CXCL2 was evoked by lipopolysaccharides (LPS), *listeria monocytogenes* (*LM*) and carrageenan, respectively. Such LPS-induced CXCL8 generation was suppressed by TRPM2-specific siRNA transfection; and the *LM*/carrageenan-evoked CXCL2 generation was significantly decreased in the $TRPM2^{-/-}$ mice (Haraguchi et al., 2012, Knowles et al., 2011, Wehrhahn et al., 2010). As summarized in Fig. 1.7, H_2O_2-induced CXCL8 generation results from TRPM2-mediated Ca^{2+} influx and subsequent activation of the signaling pathway engaging Pyk2 (proline-rich tyrosine kinase 2), Ras, MEK and ERK, leading to nuclear translocation of NF-κB and initiation of expression of CXCL8 (Yamamoto et al., 2008).

Besides CXCL8/CXCL2, TRPM2 channels have been reported to be involved in production of other cytokines. Wehrhahn has shown that exposure of human acute monocytic leukemia THP-1 cells to LPS strongly enhanced both mRNA and protein expression levels of IL-6, IL-10, IL-12, IL-17, interferon-γ (INFγ), macrophage inflammatory peptide 2 (MIP-2) and TNF-α, which were partially suppressed by reducing TRPM2 expression using shRNA (short hairpin RNA) (Wehrhahn et al., 2010). Another recent study has also showed that LPS evoked production of MIP-2, TNF-α and IL-6 from mouse lung, and release of theses cytokines was dramatically reduced in $TRPM2^{-/-}$ mice (Di et al., 2012). In addition, *LM*-induced production of INFγ and IL-12 was decreased in serum of $TRPM2^{-/-}$ mice (Knowles et

al., 2011). Production of IL-2, INFγ and IL-17 induced by anti-CD3/CD28 from mouse $CD4^+$ T cells was attenuated by pre-treatment with ACA or in $TRPM2^{-/-}$ mice (Melzer et al., 2012). Taken together, these data indicate that TRPM2 channels play an important role in mediating production of several types of cytokines. However, the mechanisms underlying such TRPM2-mediated production of these cytokine are still not fully understood. There are studies investigating the signalling mechanism underlying TNF-α production. In THP-1 cells LPS-induced increases in the $[Ca^{2+}]_c$ were strongly suppressed by TRPM2 specific shRNA and removal of extracellular Ca^{2+} led to reduction, but not complete abolition of LPS-evoked TNF-α production (Wehrhahn et al., 2010). A recent study revealed sulfur mustard (SM)-induced increases in the $[Ca^{2+}]_c$ and production of TNF-α in human neutrophils. In this study, it was further shown that the phosphorylation level of p38 MAPK was increased by SM treatment but such increase was abolished by removal of extracellular Ca^{2+}, implying an important role of p38 MAPK activity in SM-induced TNF-α production. Consistent with this idea, application of SB203580, a p38 MAPK inhibitor, was dramatically attenuated SM-induced TNF-α production. In addition, SM-induced elevation in the $[Ca^{2+}]_c$ was strongly reduced by TRPM2 channel inhibitors, FFA, clotrimazole or econazole (Ham et al., 2012). These data suggest the TRPM2-mediated increases in the $[Ca^{2+}]_c$ and Ca^{2+}-dependent activation of the p38 MAPK pathway plays an important role in mediating TNF-α production.

1.2.7.2 Insulin secretion

Insulin, a peptide hormone, plays a central role in regulating glucose metabolism via eliciting absorption of blood glucose by tissues such as liver and skeletal muscles. It is produced in, and released from, pancreatic β-cells. When the level of glucose is increased in the blood and interstitial fluid, glucose is transported into β-cells by GluT2 (glucose transporter 2), and is degraded in the tricarboxylic acid cycle to generate ATP. Elevated concentration of ATP in turn closes the ATP-sensitive potassium (K_{ATP}) channels on the β-cell surface, causes membrane depolarization leading to activation of Ca_v and Ca^{2+} influx; subsequently, increase in the $[Ca^{2+}]_c$ triggers insulin secretion by exocytosis (Koster et al., 2005, Olson and Terzic, 2010).

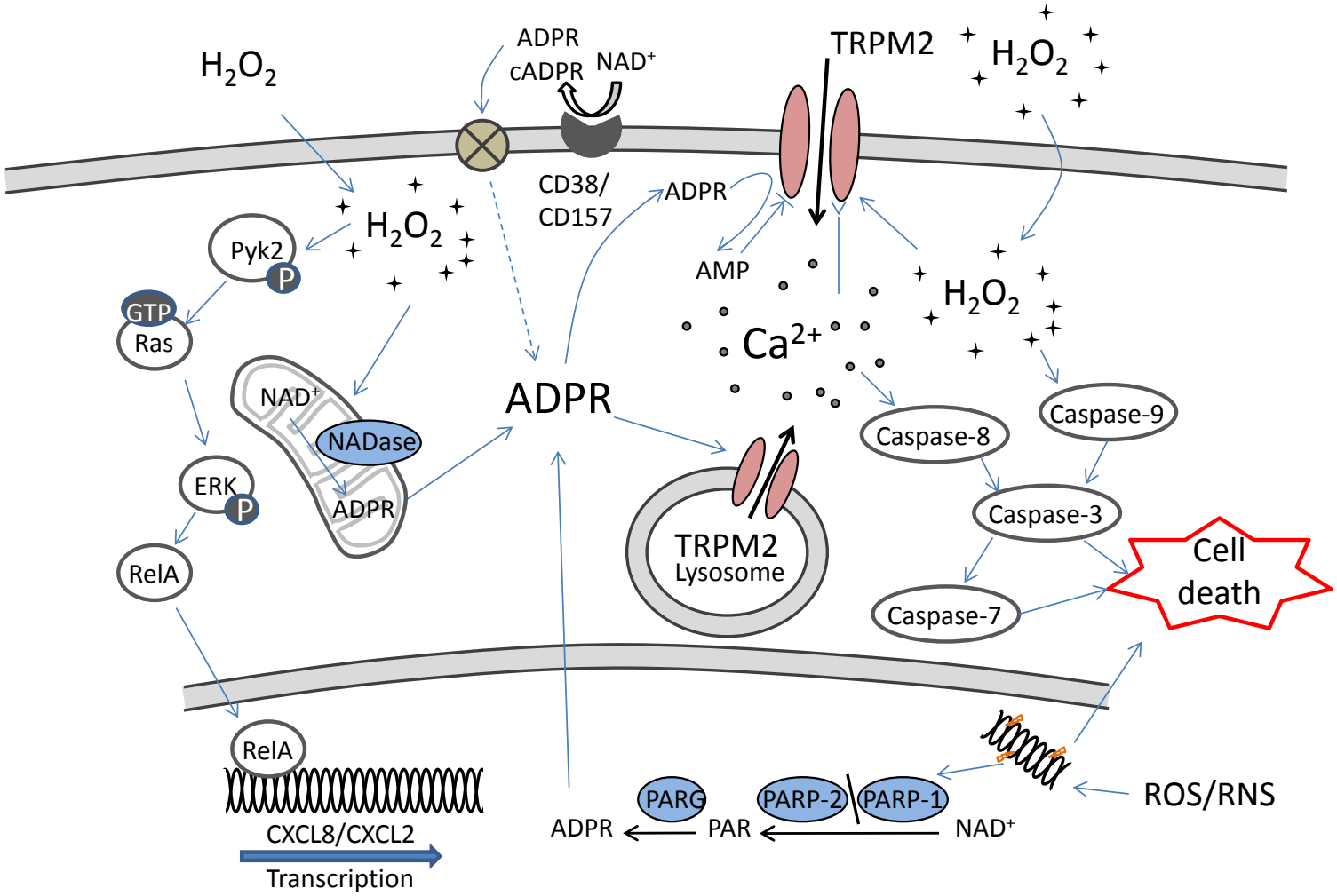

Figure 1.7 The pathway of TRPM2 channels activation and function

The signalling pathway of TRPM2 channel activation and related cell functions. This figure is based on the figure in a review paper from Takahashi (Takahashi et al., 2011).

Besides the classical K_{ATP} channel-dependent signaling pathway for insulin secretion, K_{ATP} channel-independent pathway has been documented. Several recent studies have provided consistent evidence to support critical involvement of the TRPM2 channels in the K_{ATP} channel-independent pathway. As described above (see section 1.2.5.1.7), heat can evoke TRPM2 channel activation. In pancreatic β-cells, heat at 40°C enhanced glucose-induced insulin secretion that was significantly reduced by either treatment with TRPM2 channel inhibitors, FFA and 2-APB, or with TRPM2-specific siRNA. In addition, in the presence of nimodipine, a Ca_v blocker, glucose-induced insulin secretion was still suppressed by TRPM2-specific siRNA, suggesting the existence of K_{ATP} channel-independent pathway in insulin secretion and TRPM2 channels have a part in this pathway (Togashi et al., 2006). In a recent study, glucose-induced insulin secretion was strongly attenuated in pancreatic β-cells from $TRPM2^{-/-}$ mice. Furthermore, TRPM2-deficiency reduced glucose-induced insulin secretion in the presence of diazoxide, K_{ATP} activator, and high concentration of extracellular potassium (Uchida and Tominaga, 2011). These data provide further evidence to support a role for the TRPM2 channels in insulin secretion via K_{ATP}-independent pathway.

The mechanism(s) by which the TRPM2 channels mediate glucose-induced insulin secretion is (are) not clear. There is evidence to imply that cAMP-PKA pathway is involved. Glucose-induced insulin secretion was enhanced by treatment with FSK (forskolin), an adenylyl cyclase activator, to increase intracellular cAMP level, and FSK-induced enhancement of insulin secretion was partially reduced by TRPM2-spesific siRNA (Togashi et al., 2006). Glucagon-like peptide 1 (GLP-1), produced in the intestinal cells, stimulates insulin secretion from β-cells and suppresses glucagon secretion from α-cells (Hong et al., 2002). Togashi and his colleagues also showed that exendin-4, an agonist of GLP-1 receptor, enhanced glucose-induced insulin secretion and such an effect was partially inhibited by TRPM2-spesific siRNA (Togashi et al., 2006). Consistently, enhancement of insulin secretion by exendin-4 was reduced by TRPM2 siRNA and TRPM2 knockout (Uchida et al., 2011, Uchida and Tominaga, 2011). Taken together, these data have hypothesized that GLP-1 receptor activation leads to TRPM2 channel phosphorylation by cAMP-PKA and thereby increase glucose-induced insulin secretion from pancreatic β-cells. However, whether the TRPM2 channel is phosphorylated by cAMP-PKA and how this phosphorylation leads to increase in insulin secretion are still not unclear.

1.2.8 Pathological functions

The TRPM2 channel has been reported to be involved in several pathological processes.

1.2.8.1 ROS-induced increases in endothelial permeability

Endothelial cells, forming the cell monolayer that lines the interior surface of the blood and lymphatic vessels, provide the physical barrier to prevent the transvascular movement of circulating cells into tissues in normal conditions. The dysfunction of endothelial barrier, associated with endothelial hyperpermeability, allows diffusion of pathogens and leukocytes into tissues, leading to infection and inflammation, respectively. The hyperpermeability caused by interendothelial cell gap formation, which can be determined experimentally by measuring the transendothelial electrical resistance (TER), can be caused by many factors including oxidative stress and ischemia.

As described above (1.2.1), TRPM2 channels are expressed in endothelial cells. Hecquet and his colleague have shown that, in human pulmonary artery endothelial cells (HPAE), H_2O_2 evokes whole-cell currents and concentration-dependent decreases of TER. Both the current and the TER reduction can be attenuated by using siRNA to reduce TRPM2 expression, overexpressing the non-functional isoform, TRPM2-S, or treating with DPQ (3,4-Dihydro-5[4-(1-piperindinyl)butoxy]-1(2H)-isoquinoline), the PARP inhibitor, to suppress production of ADPR (Hecquet et al., 2008). These results indicate the involvement of TRPM2 channels in H_2O_2-induced endothelial hyperpermeability.

Early studies have been shown that H_2O_2-induced increases in the $[Ca^{2+}]_c$ plays an important role in endothelial hyperpermeability (Moore et al., 1998, Siflinger-Birnboim et al., 1996). It has been reported that this H_2O_2-induced Ca^{2+} influx can be suppressed by TRPM2-specific antibody, TRPM2 siRNA and expression of TRPM2-S, suggesting that TRPM2 channels via mediating Ca^{2+} influx plays a critical role of H_2O_2-induced endothelial hyperpermeability (Dietrich and Gudermann, 2008, Hecquet et al., 2010, Hecquet et al., 2008).

1.2.8.2 ROS-induced cell death

It is well known that ROS, such as H_2O_2, can induce cell death via a complex signaling transduction network.

The TRPM2 channel is proposed to be one candidate in mediating H_2O_2-induced cell death in several types of cells, such as hippocampal neurons (Verma et al., 2012), B lymphoblast cells (Roedding et al., 2012), endothelial cells (Sun et al., 2012), pancreatic β-cells (Ishii et al., 2006b), cardiomyocytes (Yang et al., 2006), as well as HEK293 cells (Hara et al., 2002, Katano et al., 2012) and Chinese hamster ovary (CHO) cells (Naziroglu et al., 2013) heterologously expressing TRPM2 channels. For instance, in isolated striatal neurons, H_2O_2-induced cell death was dramatically suppressed by TRPM2-specific siRNA or blockage of ADPR generation with SB-750139, a PARP inhibitor (Fonfria et al., 2005). A recent study has reported that apoptotic endothelial H5V cell death induced by H_2O_2 was attenuated by knocking down TRPM2 protein expression using shRNA (Sun et al., 2012). In insulinoma RIN-5F cells, loss of the cell viability evoked by H_2O_2 was reversed by treatment with TRPM2-specific antisense oligonucleotides (Ishii et al., 2006b). All these results consistently provide evidence to support contribution of the TRPM2 channels in mediating H_2O_2-induced cell death.

The mechanisms by which TRPM2 channels mediate cell death induced by H_2O_2 are still poorly understood. As described above (1.2.5.1.6), TRPM2 channels mediate increase in the $[Ca^{2+}]_c$ induced by H_2O_2. This Ca^{2+} response is considered to be involved in H_2O_2-induced cells death. In U937 cells, removal of intracellular Ca^{2+} by pre-treatment with BAPTA, a Ca^{2+} chelator, led to partial reduction of H_2O_2-induced cell death (Sun et al., 2012). It was mentioned above (1.2.5.1.5) that TRPM2 channel activation by Ca^{2+} is through binding to CaM tethered to the IQ-motif in the TRPM2 protein (Tong et al., 2006). H_2O_2-induced cell death was significantly reduced in cells expressing the TRPM2 proteins carrying mutation disrupting the IQ-motif. These results implies requirement of intracellular Ca^{2+} via Ca^{2+}-CaM binding to IQ-motif in TRPM2 proteins in TRPM2-mediated cell death.

Furthermore, TRPM2-mediated cell death induced by H_2O_2 has been reported to engage the caspase pathway. Treatment of U937 cells with H_2O_2 induced increases in the level of

caspase-8, -9, -3 and -7 as shown using Western blotting (Zhang et al., 2006). A recent study has presented similar results to show that H_2O_2 enhanced expression levels of caspase-9 and activated caspase-8 and -3 in H5V cells, which was mitigated by TRPM2 specific shRNA (Sun et al., 2012). These results suggest that activation of the caspase-9 and caspase-8 pathways, as the signaling cascade downstream of TRPM2 channel activation and elevation in the $[Ca^{2+}]_c$, is involved in H_2O_2-induced cell death.

Although the functional expression of TRPM2 channels has been identified in macrophages, the role of TRPM2 channels in mediating H_2O_2-induced cell death is still not fully understood. In the last results chapter, I will study the role of TRPM2 channels in H_2O_2-induced Ca^{2+}-responses and macrophage cell death.

1.2.8.3 Cancer cell proliferation

TRPM2 protein expression has been shown in normal prostate epithelial cells (RWPE-1), benign prostate cancer cells (BPH-1) and cancerous prostate cancer cells (PC-3 and DU-145), using immunofluorescent confocal microscopy and Western blotting (Zeng et al., 2010). In RWPE-1 and BPH-1 cells, the TRPM2 proteins were mainly located closely to the plasma membranes. In contrast and intriguingly, a substantial amount of the TRPM2 proteins in PC-3 and DU-145 cells were aggregated in the nucleus. Reduction of the TRPM2 protein expression using siRNA strongly slowed proliferation of the cancerous cells (PC-3 and DU-145), but not the non-cancerous cells (BPH-1 and RWPE-1). These findings suggest that TRPM2 channel may play role in prostate cancer cell proliferation (Zeng et al., 2010).

1.2.9 TRPM2 channels in diseases

TRPM2 channels have been implied to contribute to several disease conditions.

1.2.9.1 Alzheimer's disease

Alzheimer's disease (AD), firstly described by Alois Alzheimer, is a type of neurodegenerative disorder and the most common cause of senile dementia, which affects about 36 million people in the world (Bergeron, 1990, Gilbert, 2013). It manifests as gradual decline of memory and cognition functions (Price et al., 1993). One of the histopathological hallmarks

of AD is accumulation of amyloid β-peptide (Aβ), a peptide of 36-43 amino acids, in the senile plaques (Gilbert, 2013). Fonfria and his colleagues showed that Aβ induced increases in the $[Ca^{2+}]_c$, generation of ROS and cell death in rat primary striatal neurons. Furthermore, they showed that Aβ-induced increase in the $[Ca^{2+}]_c$, ROS generation and cell death were strongly suppressed by TRPM2 siRNA, , PARP inhibitor SB-750139 and expression of TRPM2-S isoform (Fonfria et al., 2005). These data imply a role for the TRPM2 channel in Aβ-induced neurotoxicity in AD.

1.2.9.2 Amyotrophic lateral sclerosis and Parkinsonism-dementia

Amyotrophic lateral sclerosis (ALS) and Parkinsonism-dementia (PD) are another two types of neurodegenerative disorders. ALS is caused by motor neuron death, and its clinical manifestations include muscle weakness and atrophy. About 120,000 ALS patients are diagnosed annually worldwide (Parakh et al., 2013). PD, resulting from dopaminergic neuron death, is characterized by tremor, hypokinesia and rigidity. It affects about 1 million individuals around the world (McGhee et al., 2013). Hermosura has, using genotyping, identified P1018L mutation in the S6 of the TRPM2 protein in a subset of Guamanian ALS and PD cases. Functional studies have shown that, unlike the WT TRPM2 channel, the P1018L mutant channel exhibited rapid channel inactivation. In addition, H_2O_2-induced increases in the $[Ca^{2+}]_c$ was almost abolished in HEK293 cells expressing the P1018L mutant channel (Hermosura et al., 2008). These results imply critical contribution of loss of the TRPM2 channel function to the pathogenesis of ALS and PD.

1.3 Aim of the current study

The overall aim of my study is to increase our understanding of theTRPM2 channels in terms of functional regulation, pharmacology and physiological roles. My study is composed of three parts.

The first part described in chapter 3 was to investigate how extracellular acidic pH regulate the TRPM2 channels using whole-cell patch clamp recording, and to elucidate the molecular basis determining the distinct sensitivity of the human and mouse TRPM2 channels to extracellular acid pH, in combination of sited-directed mutagenesis and patch clamp recording.

The second part presented in chapter 4 focused on characterization of compounds as novel TRPM2 inhibitors. This was achieved by examining the effects of 48 hit compounds identified from screening of a chemical library on H_2O_2-induced increase in $[Ca^{2+}]_c$ using fluorescent Ca^{2+} imaging and ADPR-induced TRPM2 channel currents using whole-cell patch clamp recording.

The last part detailed in chapter 5, was to study functional expression of the TRPM2 channels and the role in H_2O_2-evoked Ca^{2+}-response in macrophage cells, using immunofluorescent confocal microscopy, single cell Ca^{2+} imaging and whole-cell patch clamp recording, in conjunction of pharmacological inhibition and gene ablation. The role of the TRPM2 channels in H_2O_2-induced macrophage cell death was also investigated by performing XTT and trypan blue exclusion assays.

Chapter 2

Materials and Methods

2.1 Materials

2.1.1 Mammalian cells lines

HEK293 cells and THP-1 cells were available in our lab, and RAW264.7 cells were kindly supplied by Dr. J Sim (University of Manchester, UK). The tetracycline-inducible HEK293 cells stably expressing the hTRPM2 were kindly provided by Prof. D Beech (University of Leeds, UK).

2.1.2 E.Coli strains

Competent DH5α strains of *E.Coli* cells used for site-directed mutagenesis and plasmid amplification were purchased from BioLine.

2.1.3 Plasmids and primers

The cDNA encoding the hTRPM2 protein with a C-terminal FLAG epitope tag was kindly provided by Dr. AM Scharenberg (University of Washington, USA). The cDNAs encoding the hTRPM2 subunit with a C-terminal EE- or FLAG-tag were subcloned into pcDNA3.1 vector (Promega) in our previous study (Mei et al., 2006a). The mTRPM2 cDNA in pCI-neo vector (Promega) was kindly provided by Dr. Y Mori (Kyoto University, Japan). Primers shown in Table 2.3 were custom made by Geneservice.

2.1.4 Animals

The $TRPM2^{+/+}$ (WT) C57BL/6J mice were purchased from Harlan Lab. The$TRPM2^{-/-}$transgenic C57BL/6J mice were generated in the lab, in collaboration with Prof DJ Beech and Dr JF Ainscough. The $TRPM2^{-/-}$ mice express non-functional TRPM2 isoform lacks amino acid residuals from Leu-843 to Met-931 (Zou et al., 2011, Zan et al., 2003). All the mice were maintained in the Centre Biomedical Services, University of Leeds. They were sacrificed by Ms Alicia Sedo according to the animal usage procedures approved by the University of Leeds.

2.1.5 Chemicals

All the general chemicals were purchased from Sigma at the analytical reagent grade.

All the compounds tested as the TRPM2 inhibitors in this study were provided by Dr Richard Foster, in the School of Chemistry, University of Leeds. The sources and full chemical structure information of these compounds are held in Dr Lin-Hua Jiang's laboratory in the School of Biomedical Sciences (l.h.jiang@leeds.ac.uk) and also Dr Richard Foster's laboratory and available upon request with prior confidentiality agreement.

2.1.6 Antibodies

Primary anti-TRPM2 antibody produced in rabbit and secondary FITC (fluorescein isothiocyanate)-conjugated anti-rabbit IgG antibody antibody were commercially obtained from Bethyl (catalog number: A300-413A) and Sigma (product number: F0382), respectively.

2.1.7 Solutions

The solutions used for whole-cell patch-clamp recording and calcium imaging were prepared in Milli-Q deionized water and the pH values were adjusted to pH 7.3 by 4M NaOH or to the pH indicated in the experiments by 4M NaOH or 37% (w:w) hydrochloric acid. The solutions for cell culture were commercially obtained in sterilized condition or were sterilized by autoclaving or filtering through 0.22 μm syringe filters.

2.1.8 Growth medium for mammalian cells and E.Coli cells

The growth medium for mammalian cells was prepared by adding 10% (v:v) foetal bovine serum (FBS) (GIBCO-BRL) and the indicated antibiotics into appropriate media (GIBCO-BRL) as listed in Table 2.1 and described in detail in sections 2.2.1. The medium was stored at 4°C prior to use.

LB (lysogeny broth) growth medium for *E.Coli* cells were prepared by dilution 1.5% (w:v) LB powder (Sigma) into Milli-Q deionized water. The LB medium was autoclaved and stored at 4°C prior to use.

In order to make LB-agar plate, 1% (w:v) agar (Sigma) was added into the LB growth medium. After the solution was autoclaved and cooled down, 100 μg/ml ampicillin (Sigma) was added into the solution. The solution was poured into 100-mm Petri dishes and solidified at room temperature to form LB-agar plates. The plates were stored at 4°C prior to use.

2.2 Methods

2.2.1 Mammalian cell culture

2.2.1.1 Maintenance

All the following cell culture operations were carried in a tissue culture hood (Wolf laboratories Awra-B6). RAW264.7, THP-1 and HEK293 cells and tetracycline-inducible HEK293 cells stably expressing the hTRPM2 were maintained in appropriate growth media (Table 2.1) at 37°C in a humidified 5% CO_2 incubator.

2.2.1.2 Induction of tetracycline-inducible HEK293 cells stably expressing the hTRPM2

HEK293 cells stably transfected with tetracycline-inducible cytomegalovirus-driven FLAG-tagged TRPM2 were maintained at 37°C in a humidified 5% CO_2 incubator in Dulbecco's modified Eagle's medium (DMEM)/F12 (DMEM-Ham's F-12 growth medium containing L-glutamax) and supplemented with 5 μg/ml blasticidin (InvivoGen) and 0.4 mg/ml zeocin (InvivoGen). Tetracycline (Sigma) at 1 μg/ml (Table 2.1) was applied to induce TRPM2 protein expression 18-48 hr prior to use.

2.2.1.3 Differentiation of THP-1 cells

THP-1 cells were maintained at 37°C in a humidified 5% CO_2 incubator in RPMI-1640 growth medium (Table 2.1), 100 ng/ml PMA (phorbol 12-myristate 13-acetate) (Calbiochem) was applied for 24 hr to induce differentiation to macrophage cells before use (Schwende et al., 1996).

Table 2.1 Growth medium for mammalian cells

Cell type	Medium
Peritoneal macrophage cells	RPMI-1640 supplemented with 10% (v:v) FBS, 100 U/ml penicillin and 100 μg/ml streptomycin
RAW264.7	RPMI-1640 supplemented with 10% (v:v) FBS
THP-1	RPMI-1640 supplemented with 10% (v:v) FBS
HEK293	DMEM containing L-glutamax supplemented with 10% (v:v) FBS
Tetracycline-inducible TRPM2-expressing HEK293 cells (maintaining medium)	DMEM/F12 supplemented with 10% (v:v) FBS, 5 μg/ml blasticidin and 0.4 mg/ml zeocin
Tetracycline-inducible TRPM2-expressing HEK293 cells (inducing medium)	DMEM/F12 supplemented with 10% (v:v) FBS and 1 μg/ml tetracycline

2.2.1.4 Cell passage

All these cells were passed every 3-4 days as they became confluent.

THP-1 cells are non-adherent cells, which were cultured in 30 ml media in 75-cm^2 tissue culture flasks. When the cells became confluent, 5 ml of cell suspension was moved to a fresh flask, and fresh growth medium was added to a final volume of 30 ml.

RAW264.7, HEK293 and tetracycline-inducible TRPM2-expressing HEK293 cells are adherent. The cells were maintained in 5 ml media in 25-cm^2 tissue culture flasks till they became confluent. After rinsing with phosphate buffered saline (PBS), RAW264.7 cells were removed from the bottom of the flasks by a sterilized cell scraper. HEK293 and tetracycline-inducible TRPM2-expressing HEK293 cells were detached by incubating the cells in 1-2 ml trypsin-EDTA (ethylenediaminetetraacetic acid) at 37 °C for about 2 min. Then, 1-2 ml fresh growth medium was added to inactivate trypsin. Then, the cell suspension was transferred into a 15-ml centrifuge tube and the cells were collected by centrifugation at 130 × *g* for 5 min. After the supernatant was removed, the cells pellet was resuspended in 3 ml of fresh medium and then, 0.5 ml of cell suspension was moved into a new 25-cm^2 flask. 5 ml of fresh growth medium was added into the flask to maintain the cells.

2.2.1.5 Restoration of frozen cells

A vial of frozen cells was taken out from a liquid nitrogen cryostat and thawed quickly in a 37°C bath for about 2 min. For adherent cells, the cell suspension was transferred into a 25-cm^2 flask with 5 ml growth medium and cultured for 24 hr to allow cells to adhere to the bottom of the flask before the growth medium was replaced. For non-adherent cells, the cell suspension was centrifuged at 130 × *g* for 5 min. Then, the cells were resuspended in fresh growth medium in a 25-cm^2 flask. All the cells were cultured as described above for 1-2 weeks before use.

2.2.1.6 Freezing cells

Cells were cultured in 75-cm^2 flasks till when they were more than 80% confluent. Then, the cells were detached from the bottom of the flasks as described in the section of cell passage, and collected by centrifugation at 130 × *g* for 5 min. The cell pellets were resuspended in 3 ml of FBS mixed with 10% (v:v) DMSO (dimethyl sulfoxide) (Sigma) and divided into three 2-ml cryostat vials. The vials were placed in an isopropanol-containing box at -70°C overnight, and moved into a liquid nitrogen cryostat.

2.2.2 Isolation of mouse peritoneal macrophage

Mice, 4-6 weeks old, were sacrificed by cervical dislocation. The skin covering the abdomen was cut off and about 10 ml of ice-cold PBS was injected into the abdominal cavity using a syringe with 24 Ga needle. After gentle massage, the PBS was removed from abdominal cavity by a syringe with 18 Ga needle, and, then, centrifuged at 130 × *g* for 15 min. The cell pellets were resuspended in RPMI-1640 with 10% (v:v) FBS and penicillin (100 U/ml)-streptomycin (100 μg/ml) (GIBCO-BRL) and seeded onto the 15-mm coverslips in 35-mm Petri dish. After overnight culture, macrophage cells were easily purified by washing three times with pre-warmed PBS, because of strong adhesion of macrophage cells.

2.2.3 Cell counting

The counting chamber of the hemocytometer and its paired coverslip were carefully cleaned with ethanol and left to dry. After the coverslip was placed on the top of the

hemocytometer, 10 µl of cell suspension was injected into the counting chamber through the V-shaped well. Using the microscope with 10× objective, the cells in 5 large squares (four large squares in the corner and one in the middle) and on the left and top edges of these squares in the counting grid were counted. This number was multiplied by 50,000 to obtain the number of cells per ml.

2.2.4 Cell preparation

Cells were detached from the bottom of flasks as described in the section of cell passage, and harvested by centrifugation at 130 × *g* for 5 min. Cells were added into the indicated container with growth medium in appropriate volume (Table 2.2) and incubated at 37°C in a humidified 5% CO_2 incubator prior to use.

Table 2.2 Cell preparation for different experiments

Experiment	Number of cells	container	Volume of medium
Immunofluorescent confocal imaging	50,000 -100,000	35-mm Petri dish containing 4 15-mm coverslips	2 ml
Whole-cell patch clamp recording	40,000 - 50,000	35-mm Petri dish containing 4 15-mm coverslips	2 ml
Single cell Ca^{2+} imaging	50,000 -100,000	15-mm coverslip in each well of 24-well plates	0.5 ml
Flex-station	25,000-30,000	Each well of 96-well plates	0.1 ml
XTT assay	10,000 - 20,000	Each well of 96-well plates	0.1 ml
Trypan blue exclusion assay	10,000 – 15,000	Each well of 24-well plates	0.5 ml

2.2.5 Transient transfection

One day before transfection, HEK293 cells were seeded in a 35-mm Petri dish in growth medium so that they would be 80-90% confluent at the time of transfection. The transfection was carried out with Lipofectin2000® reagent (GIBCO-BRL) following the

manufacturer's instructions. For each transfection, 1 µg plasmid DNA alone or with 0.1 µg plasmid DNA encoding green fluorescent protein (GFP), and 3 µl Lipofectin2000® reagent were diluted separately in 100 µl of OPTI-MEM I reduced serum medium (GIBCO-BRL). Then two solutions were mixed and incubated at room temperature for 20-30 min to allow plasmid DNA and Lipofectin2000® reagent to form DNA-liposome complex. The mixture was added into the Petri dish with HEK293 cells after removal of the old medium. Then, 800 µl of fresh growth medium was added into each dish to a final volume of 1 ml. The cells were incubated at 37°C overnight. On the next day, the cells were detached by trypsin-EDTA. 50 µl of cell suspension was added into a 35-mm Petri dish containing four 15-mm coverslips. 2 ml of fresh growth medium was added into each dish. Cells were cultured overnight prior to use.

2.2.6 Polymerase chain reaction

Polymerase chain reaction (PCR) was performed using a thermocycler (Eppendorf) in a reaction volume of 25 µl. The 25 µl reaction sample, set up in a 0.5-ml thin-wall Eppendorf tube, was composed of 0.75 µl of 10 µM each primer (forward and reversal primers) (Table 2.2), 2.5 µl of 10 x Pfu Ultra reaction buffer (Stratagene), 2.5 µl of 2 mM dNTP mixture, 0.5 µl of 0.1 µg/µl DNA template and 0.5 µl of 2.5 U/µl Pfu Ultra polymerase (Stratagene), and was adjusted to a final volume of 25 µl with Milli-Q water.

The PCR sample was gently mixed and incubated at 95°C for 1 min to denature the double-stranded DNA templates. Then, 18 cycles of PCR were executed; each cycle was composed of 95°C for 50 s, 60°C for 50 s and 68°C for 20 min. Incubation at 4°C was applied after the final cycle.

2.2.7 Site-directed mutagenesis

2.2.7.1 Primer design

The oligonucleotide primers for site-directed mutagenesis were individually designed, depending on the location of mutations. The nucleotide sequences of the forward and reversal primers used in this study are listed in Table 2.3 below.

Table 2.3 Sequences of the primers used in this study

Primer name	5’ to 3’ Sequences
hTRPM2 R961S forward primer	5’- CATCCACAACGAGAGCCGGGTGGACTGG -3’
hTRPM2 R961S reversal primer	5’- CCAGTCCACCCGGCTCTCGTTGTGGATG -3’
hTRPM2 H995Q forward primer	5’- CTTCAACCCGGAGCAGTGCAGCCCCAATGG -3’
hTRPM2 H995Q reversal primer	5’- CCATTGGGGCTGCACTGCTCCGGGTTGAAG -3’
mTRPM2 S958R forward primer	5’- ATACATAACGAGCGCCGCGTGGACTGG -3’
mTRPM2 S958R reversal primer	5’- CCAGTCCACGCGGCGCTCGTTATGTAT -3’
mTRPM2 Q992H forward primer	5’- TTCAGCATGGACCACTGCAGCCCCAAT -3’
mTRPM2 Q992H reversal primer	5’- ATTGGGGCTGCAGTGGTCCATGCTGAA -3’

2.2.7.2 Restriction enzyme digestion

PCR using pair of designed primers was performed to create and amplify the plasmid containing mutation. The method was shown in 2.2.6. Then, each PCR sample was gently mixed with 0.5 µl of 10 U/µl DpnI (Promega), and incubated in a 37°C water bath for 1 hr.

2.2.8 Agarose gel electrophoresis

2.2.8.1 Agarose gel preparation

Agarose gels (1%) were prepared by dissolving 1% (w:v) agarose powder (Melford) into TAE buffer (Table 2.4) by heating in a microwave. After the gel solution was cooled down to 50-60°C, ethidium bromide (EB) was added to a final concentration at 0.5 µg/ml. Then, the gel solution containing EB was poured into a plastic gel cast pre-assembled with a well-forming comb and left to solidify at room temperature.

2.2.8.2 Gel electrophoresis

The loading samples were made by blending the PCR sample with 1/6 volume of 6 × loading buffer. Then, the PCR samples and suitable DNA markers at 0.5 µg/µl were loaded into

individual wells side by side. Gel electrophoresis was carried out at 70 V for 90 min. Finally, the product was visualized and photoed using a BioRad Gel Doc system (BioRad, UK) under the UV light.

2.2.9 Heat shock transformation

Competent *E. coli* cells are able to take up nucleic acids including plasmid DNA in the presence of Ca^{2+} in the extracellular surroundings (Hanahan, 1983). The DH5α strain of *E. coli* cells was used for transformation; 1 µl of the PCR sample was transferred into 50 µl of freshly thawed competent *E. coli* cells and incubated on ice for 30 min. The mixture was shocked at 42°C for 45 s, and then returned onto ice and incubated for 2 min. The cells were mixed with 950 µl of LB growth medium and incubated at 37°C for 1 hr with a shaking incubator at 200 rpm. The cell suspension was centrifuged at 7,000 × *g* for 5 min. After removal of 800 µl of supernatant, the cells were resuspended and spread on LB agar plates. The agar plates were incubated at 37°C overnight. On the next day, four single colonies for each mutation were selected and individually inoculated into 5 ml of LB medium containing 50 µg/ml of ampicillin. The *E. coli* cells were incubated at 37°C with shaking at 250 rpm overnight.

2.2.10 Mini-preparation of plasmid DNA

Mini-preparations of plasmid DNA were carried out by a QIAprep®Miniprep kit (QIAGEN). *E. coli* were collected from overnight cell cultures by centrifugation at 5,000 × *g* for 3 min. After the supernatant was removed, the *E. coli* cells were resuspended in 250 µl of Buffer P1 (Table 2.4) and transferred into a fresh Eppendorf tube. After 250 µl of Buffer P2 (Table 2.4) was added into the tube, the cell suspension was thoroughly mixed by gently inverting the tubes 4–6 times, and then 350 µl of Buffer N3 (Table 2.4) was added into the cell suspension after the solution turned blue, and mixed thoroughly by inverting the tube 4-6 times again. The cell suspension was centrifuged at 13,000 × *g* for 10 min. The supernatant was moved into a QIAprep spin column placed in a 1.5-ml Eppendorf tube, and centrifuged at 13,000 × *g* for 1 min. The column was washed by adding 0.75 ml of Buffer PE and centrifuged at 13,000 × *g* for 1 min twice to remove the residual liquid. The column was moved into a fresh 1.5-ml Eppendorf tube, and the DNA was eluted by adding 50 µl of Buffer EB (Table 2.4) onto the

spin column and centrifugation at 13,000 × *g* for 1 min. The plasmid was stored at 4°C in a frost-free refrigerator prior to use.

Table 2.4 Buffers for mini-preparation of plasmids

TAE buffer	40 mM Tris-Oac, 0.114% (v:v) glacial acetic acid, and 1 mM EDTA pH 8.0
Buffer P1	50 mM Tris·Cl, pH 8.0, 10 mM EDTA, 100 μg/ml RNAase
Buffer P2	200 mM NaOH and 1% (w:v) sodium dodecyl sulfate (SDS)
Buffer N3	3 M potassium acetate, pH 5.5 (adjust pH with glacial acetic acid)
Buffer EB	10 mM Tris·Cl, pH 8-8.5

2.2.11 DNA sequencing

The DNA plasmids were sequenced by Geneservice in Cambridge, and the mutations were verified by sequence alignment to the WT human or mouse TRPM2 sequence using the Clustal W software (http://www.ebi.ac.uk/Tools/clustalw/).

2.2.12 Immunofluorescent confocal imaging

Cells were prepared as described in section 2.2.5. After gently rinsed with PBS three times, the cells on the coverslips were fixed using pure methanol for 5 min at -20°C. The cells were washed three times with PBS-T (Table 2.5) for 5 min each to remove methanol and enhance cell membrane permeability. The cells were incubated in the blocking solution (Table 2.5) at room temperature for 30 min. The primary anti-TRPM2 antibody was diluted in the antibody dilution buffer to the indicated concentrations detailed in chapter 5, and incubated with the cells at 4°C overnight. On the next day, after washing with PBS-T three times, the cells were incubated with the secondary FITC-conjugated anti-rabbit IgG antibody in the indicated concentrations detailed in chapter 5 for 1 hr at room temperature in the dark. After washing three times with PBS-T, each coverslip was dried on tissue paper, mounted inversely on a glass slide with a 3-μl drop of anti-fade fluorescent mounting medium containing 4',6-diamidino-2-phenylindole (DAPI) which was used to show all of the cells in view, as it can pass through the cell membrane and strongly bind onto DNA, and exhibit

fluorescence at 461 nm. Then, the coverslips were sealed by nail polish on the edge. The slides were labelled and kept in a slide container at 4°C to be protected from light.

The Zeiss LSM510 META upright confocal fluorescence microscope housed in the Faculty of Biological Science, University of Leeds was used to capture images. The 63x/1.4 oil plan-apochromat objective was used with prior addition of immersion oil on the coverslip. A 25mW 405 nm diode laser and a 30mW argon ion were applied to excite the DAPI at 405 nm and the FITC group in anti-rabbit IgG antibody at 488 nm, respectively. After an appropriate cell sample was found under the microscope, the fluorescence was captured by a Zeiss AxioCam HRc high resolution microscope camera. The photographing progress was controlled by the software Zen 2009. Then, the data were analyzed using the Zeiss LSM Image software (version 4.3.0.121).

Table 2.5 Solutions in immunofluorescent confocal imaging

PBS	8 g/l NaCl, 0.2 g/l KCl, 1.44 g/l Na_2PO_4, and 0.24 g/l KH_2PO_4 in water, pH7.4 with HCl
PBS-T	0.4% (v:v) Trition X- 100 dissolved in PBS
Blocking solution/ antibody dilution buffer	Freshly prepared by mixing PBS-T and 10% (w:v) bovine serum albumin

2.2.13 Patch clamp recording

2.2.13.1 Principles

The patch-clamp recording technique, which was developed about thirty years ago (Hamill et al., 1981, Hille, 1992, Neher and Sakmann, 1992), provides a research tool for ion transportation through membrane proteins, since it has a high resolution (Numberger and Draguhn, 1996) in detecting transmembrane ionic movements or currents, even through a single channel molecule.

Whole-cell patch clamp recording is one configuration of the patch-clamp recording, together with the others, including cell-attached, inside-out and outside-out configurations. As illustrated in Fig. 2.1, a glass micropipette which has an open sharp tip of about one square micron is used. After the tip is pressed against the cell membrane, a small suction is

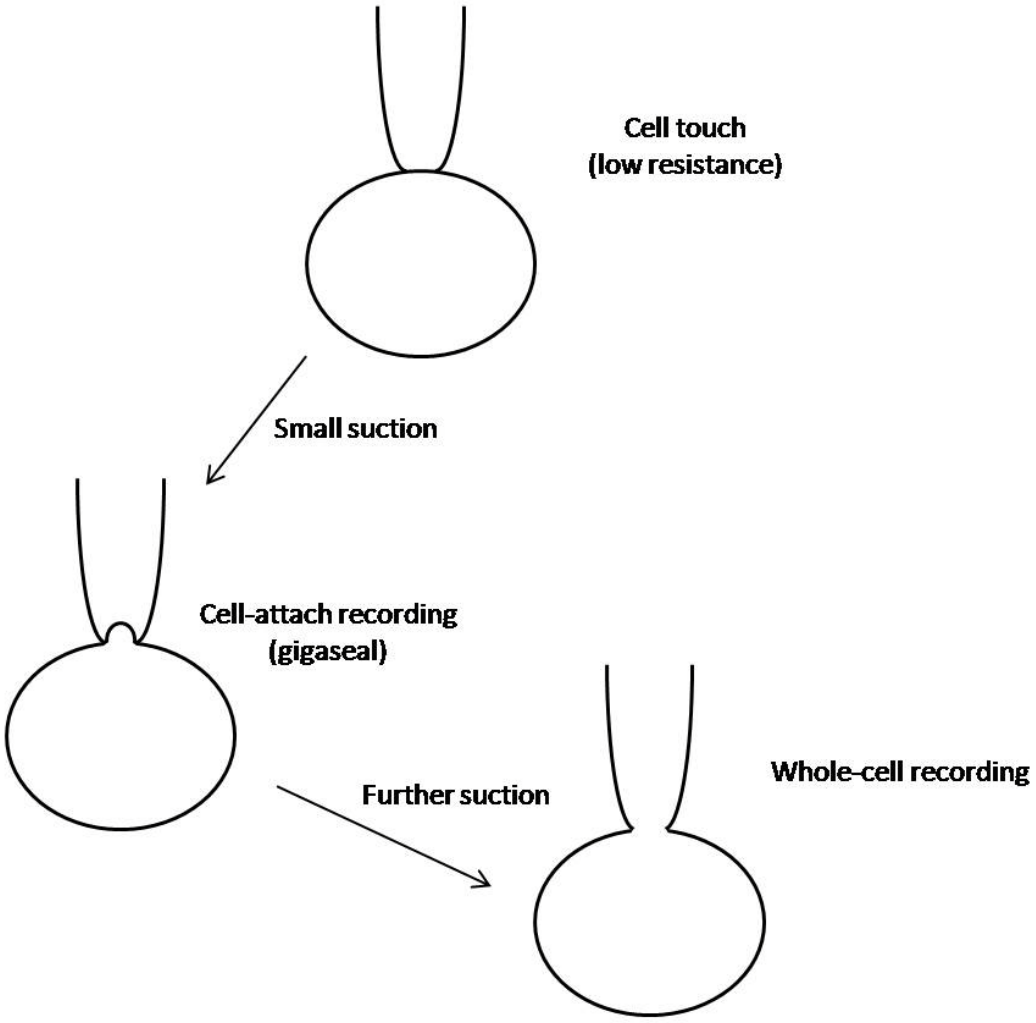

Figure 2.1 Cell-attached and whole-cell configurations of the patch-clamp recording

This electrode is pressed against the cell surface to form a high resistance seal (gigaseal) with the plasma membrane by a small suction; this is cell-attached configuration. After a further gentle suction is applied, the plasma membrane is rupture to form the whole-cell configuration.

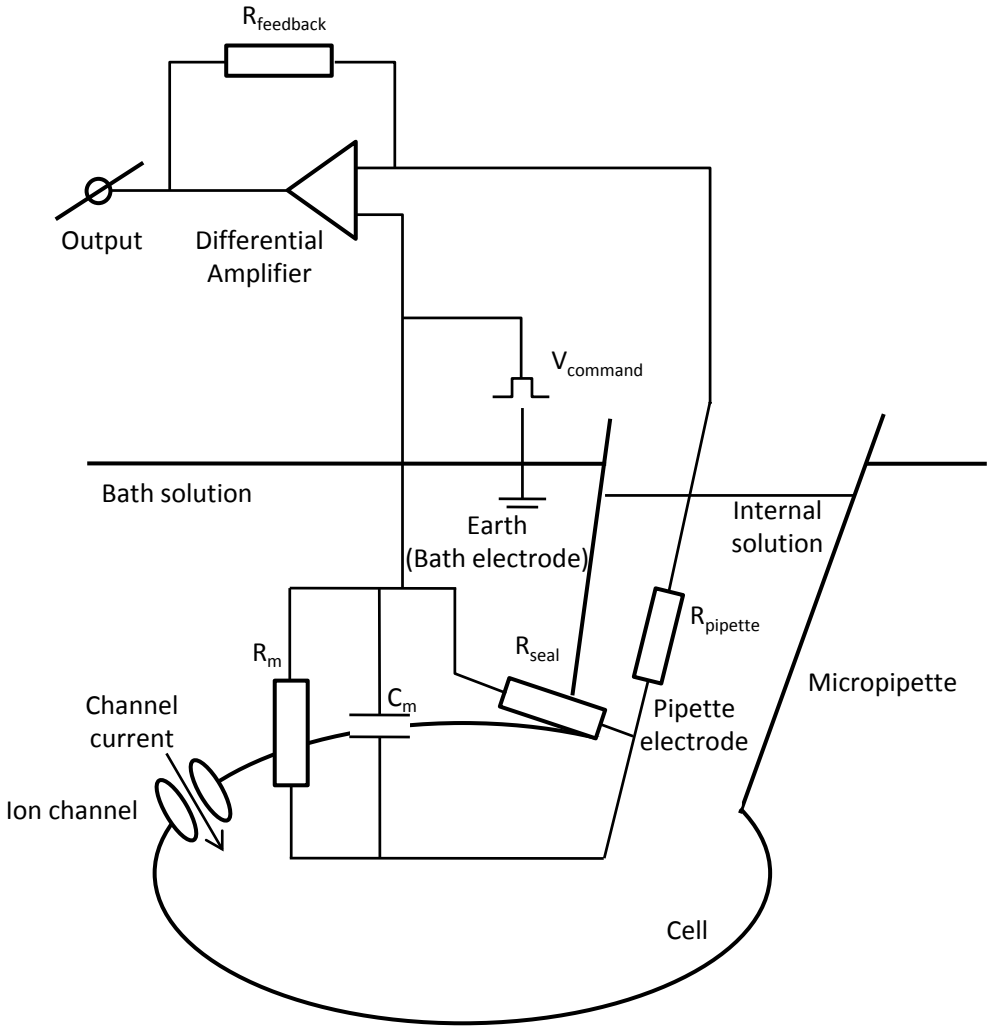

Figure 2.2 The equivalent circuit of the whole-cell patch clamp recording

The plasma membrane potential, which is equal to the voltage between the two electrodes in an ideal situation, is clamped at $V_{command}$ by the differential amplifier connected with a feedback resistance. The change of the current flowing between the electrodes is detected and reflected on the current change through the feedback resistance.

applied to form a high resistance seal (in excess of GΩ) between the tip and the cell membrane, which is called the "gigaseal". Then, a further suction is applied in order to rupture the membrane underneath the tip.

Fig. 2.2 shows the equivalent circuit of the whole-cell patch clamp recording. The recording electrode is mad e of a silver chloride-coated silver wire inserted in the micropipette, which is back-filled with micropipette solution. The other electrode is placed in the bath to set the zero level. These two electrodes are connected onto a differential amplifier that can amplify the difference in voltage between the two electrodes. Through connecting a feedback resistance linked back onto the micropipette electrode, the differential amplifier clamps the voltage between the two electrodes at $V_{command}$ and detects the shift of the current flowing between them, which reflects on the current change through the feedback resistance. Since the plasma membrane sits between the electrodes, the membrane potential is equal to the voltage between the electrodes in the ideal situation. In addition, because the gigaseal suppresses the noise to the negligible level, the current change between the two electrodes is essentially composed by the variation of the transmembrane currents, such as the increase of the channel current when ion channel opens.

2.2.13.2 Solutions for TRPM2 channel current recordings

The standard external solution for whole-cell TRPM2 channel current recording is shown in Table 2.6 and pH was adjusted to 7.3 by 4 mM NaOH (Yang et al., 2010). Other external solutions with different acidic pH indicated in chapter 3 were adjusted with 37% (w:w) hydrochloric acid. ACA and test compounds were made as 20 mM and 10 mM stock solutions in DMSO, respectively. All these compounds were freshly diluted to final concentrations in the external solution just before use, at the concentrations indicated in the result chapters. DMSO alone at related concentrations was used as solvent control. ADPR and Na_2ATP were added into the micropipette solution (Table 2.6) at the beginning of the day when recordings were made. A rapid solution changer RSC-160 system (Biologic Science Instruments) was used to change the external solutions.

Table 2.6 Solutions in patch-clamp recording (in mM)

Solution	NaCl	KCl	$MgCl_2$	$CaCl_2$	Glucose	HEPES	EGTA	Na_2ATP	ADPR
External solution	147	2	1	2	13	10			
Micropipette solution	145			1	0	10	0.05	1	1

2.2.13.3 Procedures for whole-cell TRPM2 channel current recording

Cells were prepared as shown in section 2.2.5. The borosilicate glass capillaries (World Precision Instruments) were used to the produce micropipettes using a two-stage vertical puller (PP-830, Narishige Scientific Instruments), and back-filled with the micropipette solution (Table 2.6) before it was amounted onto the probe of the amplifier. In the external solution, the resistance of the micropipette was approximate 4-6 MΩ.

ADPR-induced current recordings, from single peritoneal macrophage cells, tetracycline-inducible TRPM2-expressing HEK293 cells, or single GFP-positive HEK293 cells transiently transfected with TRPM2 plasmids identified under an UV fluorescent microscope (Zeiss), were performed using an Axopach200B amplifier and Digidata 1332A (Axon Instruments). The pClamp9 software (Axon Instruments) was used to acquire and analyse the data. The micropipette was moved toward and positioned on the cells using micromanipulators. The membrane potential of the cells was held at -40 mV. Recordings started, using voltage ramp protocols from -120 mV to 80 mV with 1-s duration applied every 5 s. The whole-cell configuration was established by the small suction via a syringe connected to the micropipette and informed by a sudden increase in the transient capacitive currents.

After the stable current was established, ACA at 10 μM or test compounds at 10 μM and acid pH indicated in the result chapter were added into the external solution. All the test compounds were applied up to 5 min. Acidic pH was continuously provided till the current became steady. ACA was applied at the end of recordings to verify the TRPM2 current.

2.2.14 Calcium imaging using fluorescent dyes

2.2.14.1 Principle

Calcium imaging is usually used to monitor the $[Ca^{2+}]_c$ using fluorescent calcium indicator molecules, such as Fura-2. Fura-2/AM (Fura-2-acetoxymethyl ester) is a membrane permeable derivative of Fura-2 and is Ca^{2+}-insensitive. It readily penetrates the cell membranes and is converted to the Ca^{2+}-sensitive free Fura-2 in the cytosol upon removal of acetoxymethyl group by an endogenously expressed esterase. Free Fura-2, can be excited by a light with peak value at 362 nm, and exhibits an emission peak of around 505 nm. Upon binding with Ca^{2+}, the excitation peak is shifted to 335 nm, whereas the emission peak remains the same (Grynkiewicz et al., 1985). Thus, upon binding of Ca^{2+}, the emission intensity excited by the excitation at 335 nm is enhanced and the emission intensity excited by 362 nm is reduced. In practice, 340 nm and 380 nm are used as excitation wavelengths, and the fluorescent emission intensities at 510 nm (F_{340} and F_{380}) are measured. The ratio of F_{340} to F_{380} (F_{340}/F_{380}) is used to indicate the $[Ca^{2+}]_c$, as it is proportional to the $[Ca^{2+}]_c$. The change of F_{340}/F_{380} ($\Delta F_{340}/F_{380}$) is used to represent as the change in the $[Ca^{2+}]_c$ in this study.

2.2.14.2 Solutions

The standard bath solution (SBS) (Table 2.7) used for Ca^{2+} imaging experiments was adjusted to pH 7.4 by 4 mM NaOH. In some experiments, Ca^{2+}-free SBS were used, which contained 0.4 mM EGTA, but no $CaCl_2$ (Table 2.7). In some experiments, the SBS and the Ca^{2+}-free SBS were preheated to 22°C or 37°C in a water bath. The Fura-2/AM solution was prepared by diluting 4 µl Fura-2/AM (prepared as 1 mM stock solution in DMSO) (Calbiochem) and 1 µl plutonic acid (prepared as 10% (v:v) stock solution in DMSO) into 1 ml SBS before use.

H_2O_2 was diluted in the SBS or Ca^{2+}-free SBS to 0.3 mM from 30% (v:v) H_2O_2 stock solution for single cell calcium imaging, and diluted to 4 mM for Flex-station. ACA and test compounds were made as 20 mM and 10 mM stock solutions in DMSO, respectively. PJ-34 was dissolved in Milli-Q water to 10 mM. All these compounds were diluted in bath solutions to the final concentrations indicated in the result chapters. DMSO alone was used as solvent control.

Table 2.7 Solutions in Ca^{2+} imaging (in mM)

Solution	NaCl	KCl	$MgCl_2$	$CaCl_2$	Glucose	HEPES	EGTA
SBS	134	5	1.2	1.5	8	10	
Ca^{2+}-free SBS	134	5	1.2		8	10	0.4

2.2.14.3 Procedures of single cell calcium imaging

Cells were prepared as shown in section 2.2.5. After the medium was removed from the wells, the cells were rinsed three times with SBS, and incubated in 250 µl of 4 µM Fura-2/AM solution. After fully covered with aluminium foil, the plates were kept at 37°C in a tissue culture incubator for 1 hr. The cells were then rinsed three times with SBS and left in 250 µl of SBS alone or SBS containing 10 µM of PJ-34 for 30 min. The coverslip was mounted onto the bottom of the home-made silica gel plate with a hole in its central part, and the plate was placed in the recording chamber on the microscope stage and the home-made gravity-fed perfusion system was connected. SBS alone or SBS containing 300 µM of H_2O_2 were applied to cells after establishment of the baseline.

The fluorescence was measured using an inverted S100 microscope with 40× objective (Zeiss). The excitation light source was provided by a Xenon arc lamp (Ushio), and the wavelength at 340 nm or 380 nm was selected by a monochromator (Till Photonics). The emission was collected via a 510-nm filter and sampled by a CCD camera (Orca ER; Hamamatsu). Images were taken in every 6 or 10 s by Openlab 2 software (Image Processing & Vision Company Ltd) as described by Zeng and his colleagues (Zeng et al., 2004).

2.2.14.4 Procedure of Flex-station experiments

Cells were prepared as shown in section 2.2.5. The cells in each well were rinsed three times with SBS after removal of the culture medium. Then 50 µl of 4 µM Fura-2/AM solution was added into each well, and the plates were wrapped with aluminium foil and kept at 37°C in a tissue culture incubator for 1 hr. The cells were then rinsed three times with SBS, and then, kept in 120 µl of SBS with DMSO at related concentrations, or SBS containing ACA or test compound at the concentrations indicated in chapter 4 for 30 min.

The solution plate was prepared by adding 250 µl of SBS alone or SBS containing 4 mM H_2O_2 into each well of the U-bottom 96-well plate.

The fluorescence was measured using a Flex-Station II^{384} (Molecular Devices). After setting the working temperature at 37°C and placing the pipette tip pack, solution plate and cell plate into the allocated chambers, the recording began following the set sampling program. In brief, the basal $[Ca^{2+}]_c$ was recorded for 1 min and, subsequently, 40 µl of SBS alone or SBS containing 4 mM H_2O_2 was transferred from the solution plate into each well in the cell plate. The working concentration of H_2O_2 was 1 mM.

2.2.15 XTT assay

The cell viability was assessed using XTT assay kits (Biotium). XTT, 2,3-bis-(2-methoxy-4-nitro-5-sulfophenyl)-2H-tetrazolium-5-carboxanilide, can be converted to a highly water-soluble product, which exhibits an reflection peak of around 475 nm, in the live cells by the active mitochondrial enzymes that become inactivated shortly after cell death (Nargi and Yang, 1993). Thus, the optical density value (OD value) at 475 nm is measured to represent the number of live cells.

Cells were prepared as shown in section 2.2.5. After exposure to test compounds or 10 µM PJ-34 for 30 min, the cells were exposed to H_2O_2 at the concentrations and duration detailed in the result chapters. After wash once with fresh medium, 100 µl of growth medium, 50 µl of XTT solution and 0.25 µl of activation reagent PMS (N-methylphenazonium methyl sulphate) were added into each well, and three extra blank wells. After incubation for 3 hr, the OD value at 475 nm in each well was measured using Varioskan Flash (Thermo Fisher Scientific Inc). OD value at 650 nm was also determined as non-specific reading.

2.2.16 Trypan blue exclusion assay

Cells were prepared as shown in section 2.2.5. After treatment with H_2O_2 at the indicated concentrations shown in the result chapters, cells were incubated in 0.4% (w:v) of trypan blue solution (Sigma) for 5min. The images in transmission light were captured using an Olympus IX51 microscope and software Cell^F (Olympus). The dye-stained cells indicate the

necrotic cells. ImagJ 1.43u software (National Institutes of Health, USA) was used for cell counting.

2.2.17 Data analysis

For the whole-cell current recordings, representative ADPR-induced currents at -80 mV are illustrated and analyzed in the result chapters. The inhibition kinetics of the TRPM2 channel currents by acidic pH or test compounds was estimated by the time required to produce ≥ 90% of the current inhibition ($\tau_{90\%}$). The inhibition and the current recovery from inhibition were determined by expressing the residual current and the currents recovered upon wash, as the percentage of the control currents.

For the single cell calcium imaging, representative recordings illustrated in the result chapters represent the F_{340}/F_{380} values that were normalized to the basal value at the time when in the solution perfusion started. The changes in the $[Ca^{2+}]_c$ were estimated by the $\Delta F_{340}/F_{380}$ before and after exposure to H_2O_2 at the times indicated in the result chapters.

For the Flex-station experiments, the mean values of F_{340}/F_{380} from 3-5 wells are shown in the result chapters. The changes in the $[Ca^{2+}]_c$ were estimated by the $\Delta F_{340}/F_{380}$ values at 5 min after exposure to H_2O_2. The inhibition of the H_2O_2-induced increases in the $[Ca^{2+}]_c$ by test compounds was defined as the reduction in $\Delta F_{340}/F_{380}$ value in the presence of test compounds as percentage of the $\Delta F_{340}/F_{380}$ in matched control cells. The following Hill equation was used to fit the concentration-inhibition data:

$$y = 100 \times IC_{50}^{\ n} / (x^n + IC_{50}^{\ n})$$

or, if there was significant residual or compound-insensitive component:

$$y = (100 - A) \times IC_{50}^{\ n} / (x^n + IC_{50}^{\ n}) + A.$$

Where n is Hill coefficient, x and y represent as the concentration of the test compound and the percentage of H_2O_2-induced increases in the $[Ca^{2+}]_c$ in the control group in which the cells were exposed to SBS containing DMSO, respectively. IC_{50} is the concentration producing 50% inhibition by the test compound. A represents the residual component. The

R value, which reflects the accuracy of the data fitting, was greater than 0.9 for all the data described in the result chapters.

For the XTT assays, all the values were expressed as percentage of the average value of the control groups of cells that were not exposed to H_2O_2.

For the trypan blue exclusion assays, the cell necrosis was defined as the percentage of trypan blue-positive cells in the total number of cells examined.

Results are presented, where appropriate, as mean ± s.e.m. (standard error mean). The numbers shown in the brackets in the figures represent the number of cells recorded in whole-cell current recording, single cell calcium imaging and trypan blue exclusion assay, or the number of wells in Flex-station experiments and XTT assays. Statistical significance were analyzed using Student's t-test between two groups and ANOVA (analysis of variance) (post-hoc Tukey) among multiple groups, with significance at the level of $p < 0.05$.

Chapter 3

A residue in the TRPM2 channel outer pore is crucial in determining species-dependent sensitivity to extracellular acidic pH

3.1 Introduction

As discussed in detail in the introduction chapter (section 1.2.5.2.7), acidic pH is an important parameter regulating ion channel activity and its biological function, including TRPV1 (Buijs et al., 2004), TRPV2 (Neeper et al., 2007), TRPA1 (Chen and Kym, 2009, Klionsky et al., 2007), P2X4 (Garcia-Guzman et al., 1997), and P2X7 (Jiang et al., 2000, Roger et al., 2010). Several recent studies including one from our lab have shown the inhibition of hTRPM2 channel by extracellular acidic pH (Du et al., 2009b, Starkus et al., 2010, Yang et al., 2010). However, there is significant discrepancy, particularly in terms of the reversibility of the inhibition and the underlying mechanisms. I conducted further experiments as described in this chapter to better understand the inhibition of the hTRPM2 channel by acidic pH.

Mice, including transgenic mice, and the cells from them, are of paramount importance to infer the physiological functions of human proteins and the mechanisms responsible for associated pathologies and conduct preclinical testing of new therapeutic drugs (Chen and Kym, 2009). Therefore I compared the effects of extracellular acidic pH on the hTRPM2 and mTRPM2 channels. My results showed striking difference in the inhibition of the TRPM2 channels by extracellular acidic pH in that the mTRPM2 channel exhibited a much lower sensitivity to, and slower kinetics of, inhibition, than the hTRPM2 channel. By introducing reciprocal mutations of species-specific residues in the outer pore in the human and mouse TRPM2 channels, I have identified a crucial role for one residue in the outer pore region in determining such species differences. In addition, such findings provide further evidence to support the conclusion that interaction of protons with the outer pore region underlies the inhibition of the TRPM2 channels by extracellular acidic pH (Yang et al., 2010). Overall, these results help increase our understanding of how the TRPM2 channels in different species are functionally regulated by acidic pH.

3.2 Results

3.2.1 Inhibition of H_2O_2-induced increases in the $[Ca^{2+}]_c$ and ADPR-induced currents by ACA in HEK293 cells expressing hTRPM2 channel

ACA has been identified as a potent TRPM2 channel inhibitor (see section 1.2.5.2.1). Thus, I began with experiments studying the effects of ACA on the TRPM2 channel mediated responses, as it would be used as a control in the experiments that to be described later. Using Flex-station and tetracycline-inducible hTRPM2 channel-expressing HEK293 cells, I firstly investigated the effect of ACA on H_2O_2-induced increases in the $[Ca^{2+}]_c$. As the results shown in Fig. 3.1A, H_2O_2 at 0.3 mM evoked significant elevation in the $[Ca^{2+}]_c$ in the tetracycline-induced TRPM2-expressing HEK293 cells (black square), but not in the un-induced cells (blue-triangle). This Ca^{2+}-response was suppressed by pre-treatment with ACA for 5 min in a concentration-dependent manner with an IC_{50} of 1.87 μM (Fig. 3.1A), which is similar as reported in a previous study (Kraft et al., 2004), and was completely blocked by ACA at 10 μM. However, ACA at 30 μM evoked a strong increase in the basal $[Ca^{2+}]_c$. ACA at 10-20 μM also resulted in strong inhibition without altering the basal $[Ca^{2+}]_c$ and thus was used to inhibit the TRPM2 channel activation in the rest of experiments described in this thesis. Next, I studied whether ACA at 20 μM inhibited ADPR-induced current in the tetracycline-induced TRPM2-expressing HEK293 cells using whole-cell patch clamp recordings. Fig. 3.1B shows the results. ADPR at 1 mM induced a strong and sustained current, with the typical linear I-V relationship curve of the TRPM2 channels with the reversal potential at approximately 0 mV. This ADPR-induced current was quickly and completely inhibited by ACA.

Since HEK293 cells transiently transfected with WT and mutant hTRPM2 and mTRPM2 plasmid were used in the following experiments in this chapter, I also investigated the inhibition of ADPR-induced current by ACA in HEK293 cells transiently transfected with the WT hTRPM2 plasmid. A representative recording is illustrated in Fig. 3.1C, showing that 20 μM ACA can rapidly and completely block the ADPR-induced current as observed in the tetracycline-induced HEK293 cells (Fig. 3.1B).

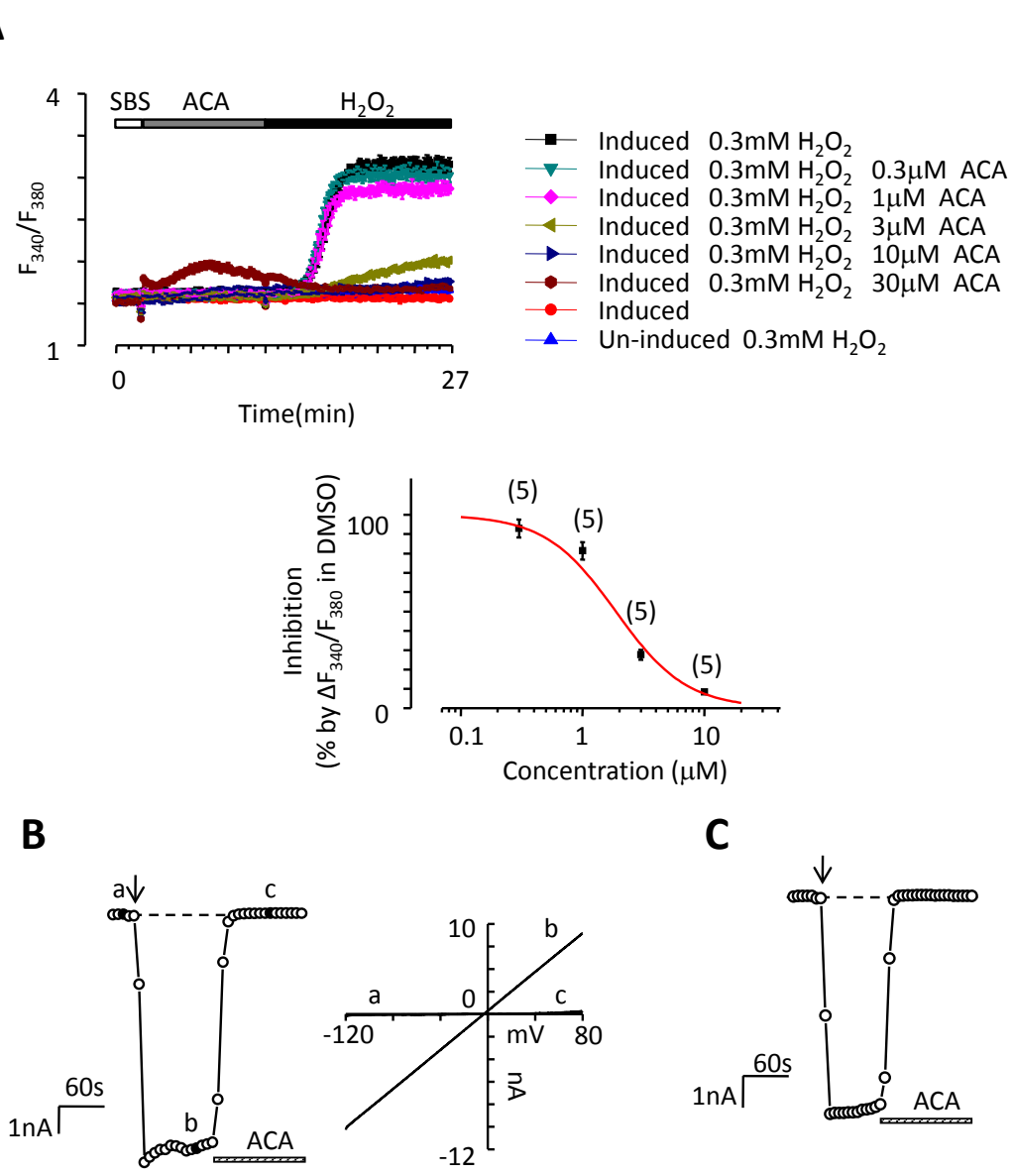

Figure 3.1 Characterization of the inhibitory effect of ACA on TRPM2 channel functions

A, *upper*, the time course of the effects of ACA at different concentrations H_2O_2-induced increases in the $[Ca^{2+}]_c$ in Ca^{2+}-containing SBS in tetracycline-inducible hTRPM2-expressing HEK293 cell examined using Flex-station. The different cell preparations and ACA concentrations are indicated with different symbols or colours. *Bottom*, the concentration-inhibition relationship curve was fit to the Hill equation to determine the IC_{50}. The numbers of wells examined in each concentration are indicated in parenthesis. **B**, representative recording of 1 mM ADPR-induced currents at -80 mV (*left*) and the I-V relationship curves (*right*) recorded from tetracycline-induced hTRPM2-expressing HEK293 cells, using 1-s voltage ramps of -120 to +80 mV applied every 5 s. 20 μM ACA was applied to inhibit the currents. **C**, representative recording of 1 mM ADPR-induced current at -80 mV in HEK293 cells transiently transfected with the hTRPM2 plasmid. The dotted lines in B and C indicate the baseline.

3.2.2 Exposure duration-dependent reversibility of hTRPM2 channel inhibition

In order to investigate the inhibitory effect of extracellular acidic pH on the hTRPM2 channel and, particularly, the mechanisms underlying the reversibility, I examined the kinetics of the recovery from the inhibition following various exposure durations in HEK293 cells transiently transfected with the hTRPM2 plasmid. Fig. 3.2A-E show representative recordings and the mean data for pH 5.5. The exposure duration, denoted by the open bar above the recording traces, was defined as the time starting from the point when the complete inhibition was obtained. Fig. 3.2F illustrates the percentage of the current recovery in individual cells. While the data are scattered but still exhibit a discernible pattern in that the short exposure durations (0 and 30 s) led to greater current recovery whereas there was little or no recovery after the longer exposure durations (60, 90 and 120 s). Fig. 3.2G plots the current recovery against the exposure duration; the data were fit reasonably well with exponential (R=0.7), yielding an inactivation time constant of approximately 30 s. Taken together, these results suggest that the early or initial inhibition of ADPR-induced currents by extracellular acidic pH is largely reversible, but became steady and irreversible after long exposure duration.

3.2.3 Differential inhibition of the mTRPM2 and hTRPM2 channel currents by acidic pH

For the reasons outlined in the introduction, it is interesting to know whether acidic pH inhibits the mTRPM2 channel in a similar fashion. Therefore, I went on to investigate the effects of acidic pH on the mTRPM2 channel currents in HEK293 cells transiently transfected with the mTRPM2 plasmid. Application of intracellular ADPR (1 mM) induced robust current responses, which displays a typical linear I-V relationship and complete inhibition by ACA, indicating that the mTRPM2 channel exhibits similar functional properties as the hTRPM2 channel. Similar to our previous study for the inhibition of the hTRPM2 channel currents by acidic pH (Yang et al., 2010), the steady-state inhibition of the mTRPM2 currents by extracellular acidic pH (4.5-5.5) was complete, irreversible and pH-independent (Fig. 3.3). The inhibition kinetics was also pH-dependent, as described for the hTRPM2 channel

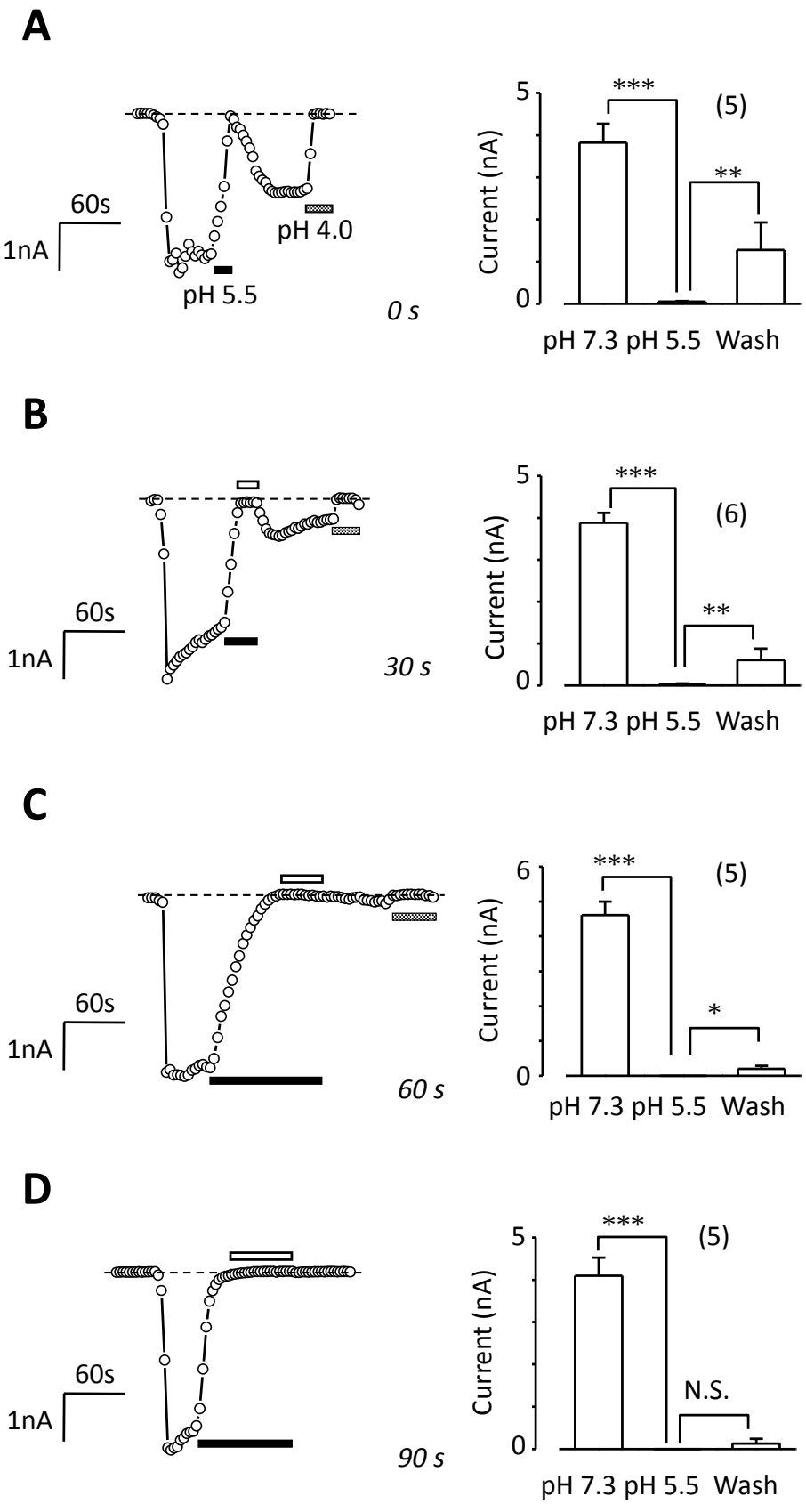
A
60s
1nA
pH 5.5
pH 4.0
0 s
Current (nA)
5
0
***
**
(5)
pH 7.3 pH 5.5 Wash
B
60s
1nA
30 s
Current (nA)
5
0
***
**
(6)
pH 7.3 pH 5.5 Wash
C
60s
1nA
60 s
Current (nA)
6
0
***
*
(5)
pH 7.3 pH 5.5 Wash
D
60s
1nA
90 s
Current (nA)
5
0
***
N.S.
(5)
pH 7.3 pH 5.5 Wash

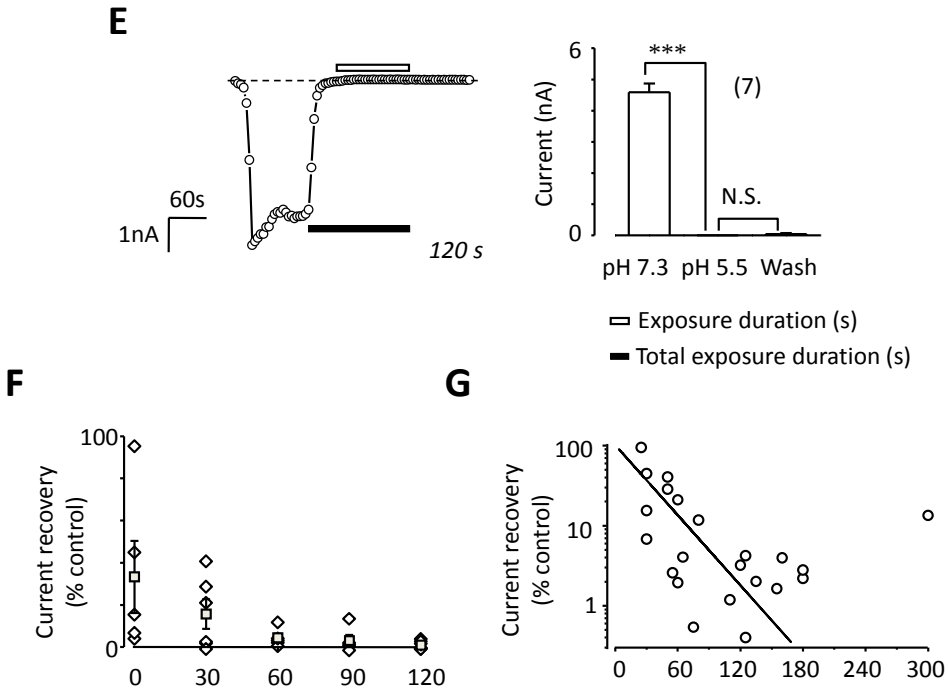

Figure 3.2 Exposure duration-dependent reversibility of inhibition of the hTRPM2 channel currents by pH 5.5

A-E, representative recordings (*left*) and summary (*right*) of the 1 mM ADPR-induced whole-cell currents are shown. The currents at 80 mV were recorded in HEK293 cells expressing the hTRPM2 channels, using 1-s voltage ramps of −120 to 80 mV applied every 5 s in extracellular pH 7.3 before exposure to pH 5.5, after the indicated time of exposure to pH 5.5, recovered upon return to pH 7.3 (*left*). The open bars on top of each trace show the duration (0, 30, 60, 90, and 120 s) from attainment of complete inhibition, and the black bars the total duration of exposure to pH 5.5. The dotted lines indicate the baseline. The ***p<0.001, **p<0.01, and *p<0.05 between the paired groups. The numbers of cells examined in each case are indicated in parenthesis. **F**, summary of the percentage of current recovery in individual cells (diamond symbols) and the mean values (filled squares) in each group as those shown in **A-E**. **G,** Relationship of the percentage of current recovery to the total exposure duration (denoted by the black bars in **A-E**). The straight line shows an exponential fit to the data with a time constant of approximately 30 s (R = 0.7)

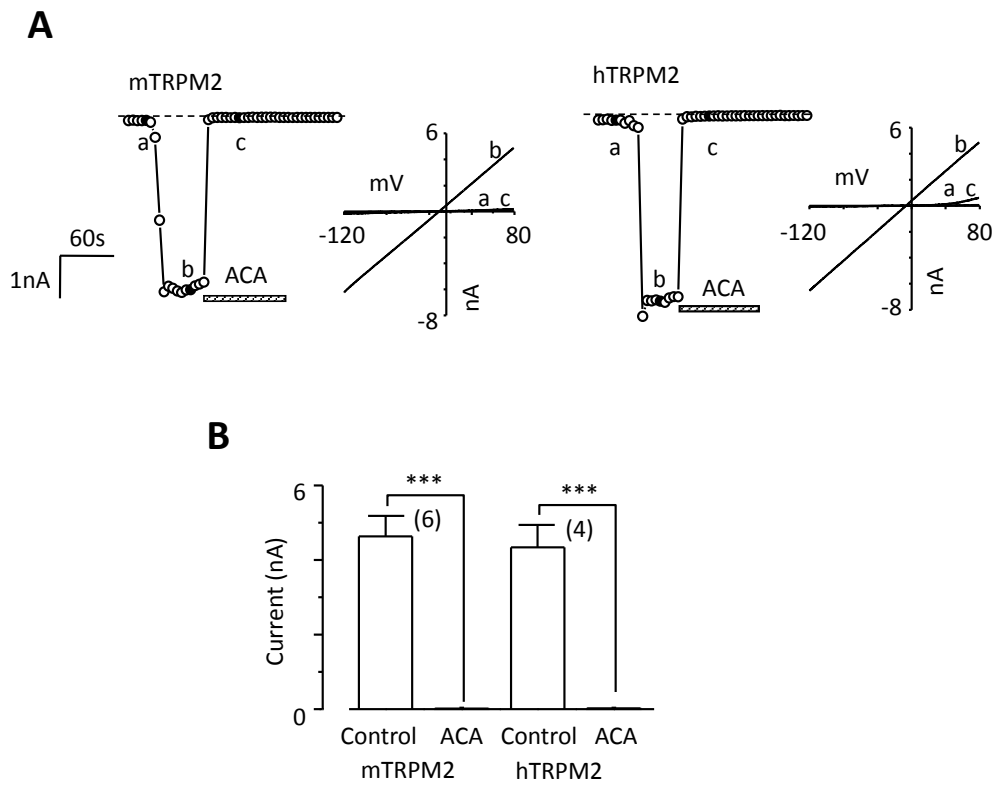

Figure 3.3 Characterization of the mTRPM2 and hTRPM2 channel currents induced by ADPR

A, representative 1 mM ADPR-induced currents at −80 mV and I -V relationship curves were recorded from HEK293 cells transiently transfected with WT mTRPM2 (*left*) or hTRPM2 (*right*) plasmid, using 1-s voltage ramps of −120 to 80 mV applied every 5 s. The currents were inhibited by application of 20 μM ACA. The dotted lines indicate the baseline. **B**, summary of the currents before and after application of ACA as shown in **A**. The numbers of cells recorded in each case are indicated in parenthesis. ***p<0.005 between the paired groups.

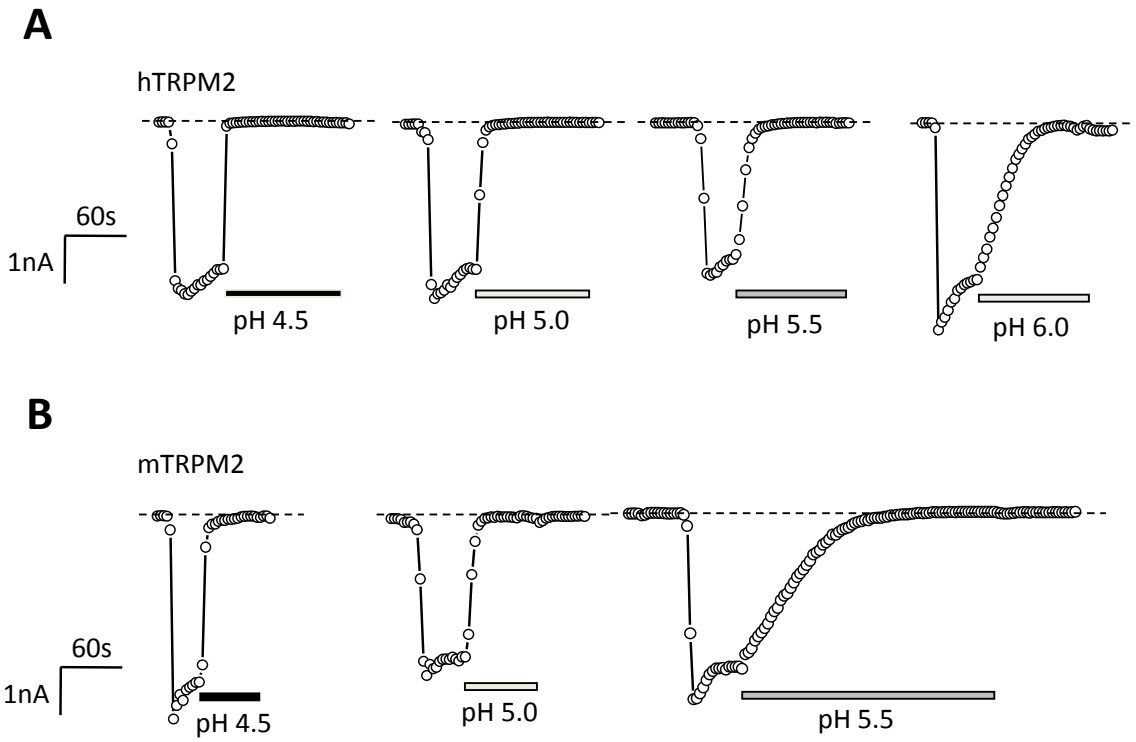
A
hTRPM2
60s
1nA
pH 4.5
pH 5.0
pH 5.5
pH 6.0
B
mTRPM2
60s
1nA
pH 4.5
pH 5.0
pH 5.5

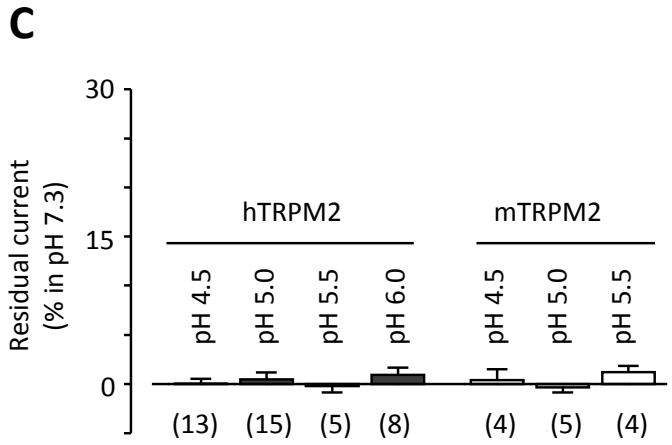
C
Residual current
(% in pH 7.3)
30
15
0
hTRPM2
mTRPM2
pH 4.5
pH 5.0
pH 5.5
pH 6.0
pH 4.5
pH 5.0
pH 5.5
(13)
(15)
(5)
(8)
(4)
(5)
(4)

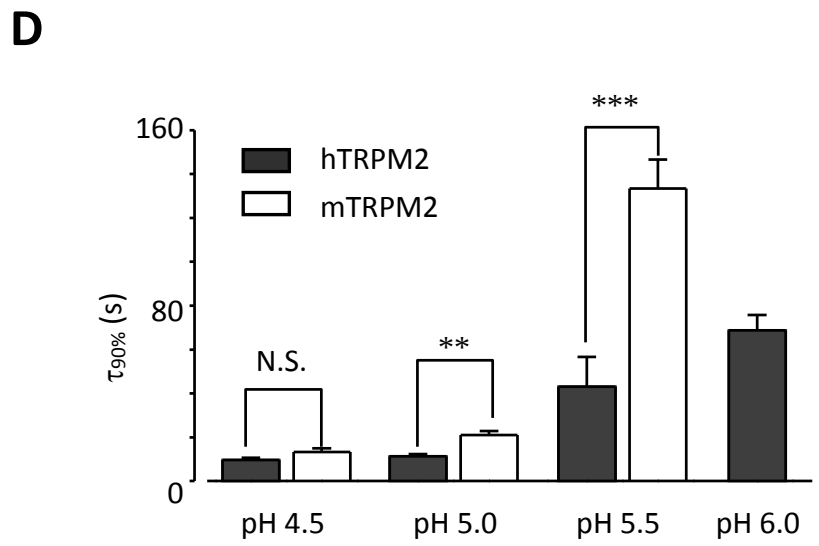

Figure 3.4 Differential inhibition of ADPR-induced currents mediated by the hTRPM2 and mTRPM2 channels by extracellular acidic pH

A-B, 1 mM ADPR-induced currents are recorded from HEK293 cells transiently transfected with the WT hTRPM2 (**A**) and mTRPM2 (**B**) plasmid, first in extracellular pH 7.3 and then in indicated extracellular acidic pH. The dotted lines indicate the baseline. **C-D**, summary of the residual currents in the steady state, expressed by percentage of the currents in pH 7.3 before solution change (**C**), and the kinetics of inhibition (**D**), indicated by $\tau_{90\%}$. The numbers of cells examined in each case are indicated in parenthesis in C. **p<0.01 and ***p<0.005 between the paired groups, and N.S., no significant difference.

currents. However, the inhibition kinetics was significantly slower than that of the hTRPM2 channel currents, particularly by pH 5.5 (Fig. 3.4). Furthermore, in contrast with the complete inhibition of the hTRPM2 channel currents, there was little inhibition by pH 6.0 of the mTRPM2 channel currents. In summary, these results provided clear evidence to indicate species-dependent modulation of the TRPM2 channels by acidic pH.

3.2.4 Accelerated kinetics of, and increased sensitivity to, inhibition by acidic pH by His substitution of pore residue Gln-992 in mTRPM2 channel

Our previous site-directed mutagenesis study shows that inhibition of the human TRPM2 channel by acidic pH results from interactions of protons with residues in the outer pore domain (Yang et al., 2010). In order to understand the molecular mechanism that is responsible for the difference in inhibition of the hTRPM2 and mTRPM2 channels by acidic pH, I compared the amino acid sequences of the pore domain in the hTRPM2 and mTRPM2 channels. As shown earlier in Fig. 1.3, there are three proton-interacting candidate residues in the hTRPM2 protein, Arg-961, His-995 and Arg-1017, which are substituted by Ser-958, Gln-992 and Ala-1014 in the mTRPM2 protein. The R1017A mutation in the hTRPM2 protein was shown to accelerate, rather than slow down, the inhibition by acidic pH in our previous study (Yang et al., 2010). I investigated the role of Ser-958 and Gln-992 in the mTRPM2 channel by mutating them individually to the residues in the hTRPM2 channel. Both S958R and Q992H mutations had no effect on the amplitude of the ADPR-induced whole cell currents (Fig. 3.5), as well as the TRPM2 channel properties such as the linear I-V relationship (Fig. 3.6). The S958R mutant mTRPM2 channel showed similar steady-state and kinetics of the inhibition by acidic pH, and by contrast, the Q992H mutation conferred dramatically accelerated inhibition kinetics or $\tau_{90\%}$ (see section 2.2.16) in response to pH 4.5-5.5, without changing the steady-state inhibition (Fig. 3.6 and Fig. 3.8). More strikingly, in contrast with the insensitivity of the WT mTRPM2 channel currents, the Q992H mutant mTRPM2 channel currents were completely inhibited by pH 6.0 (Fig. 3.6), as found for the hTRPM2 channel (Fig. 3.4). These results indicate that Gln-992 residue is crucial in determining the slower kinetics of, and lower sensitivity to, the inhibition of the mTRPM2 channel by extracellular acidic pH.

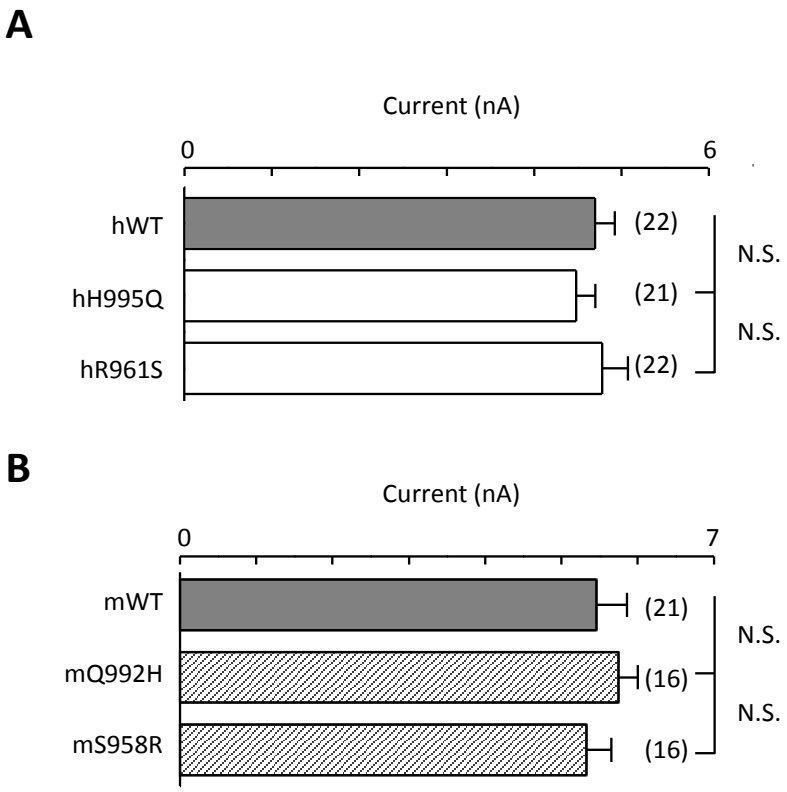

Figure 3.5 ADPR-induced whole-cell currents in the HEK293 cells expressing WT and pore mutant hTRPM2 and mTRPM2 channels

A-B, mean amplitude of 1 mM ADPR-induced currents recorded in single cells transiently transfected with indicated WT (gray bar) and mutant hTRPM2 (**A**) (open bars) and mTRPM2 (**B**) plasmid (oblique line bars). The numbers of cells recorded in each case are indicated in parenthesis. N.S. represents no significant difference compared to WT.

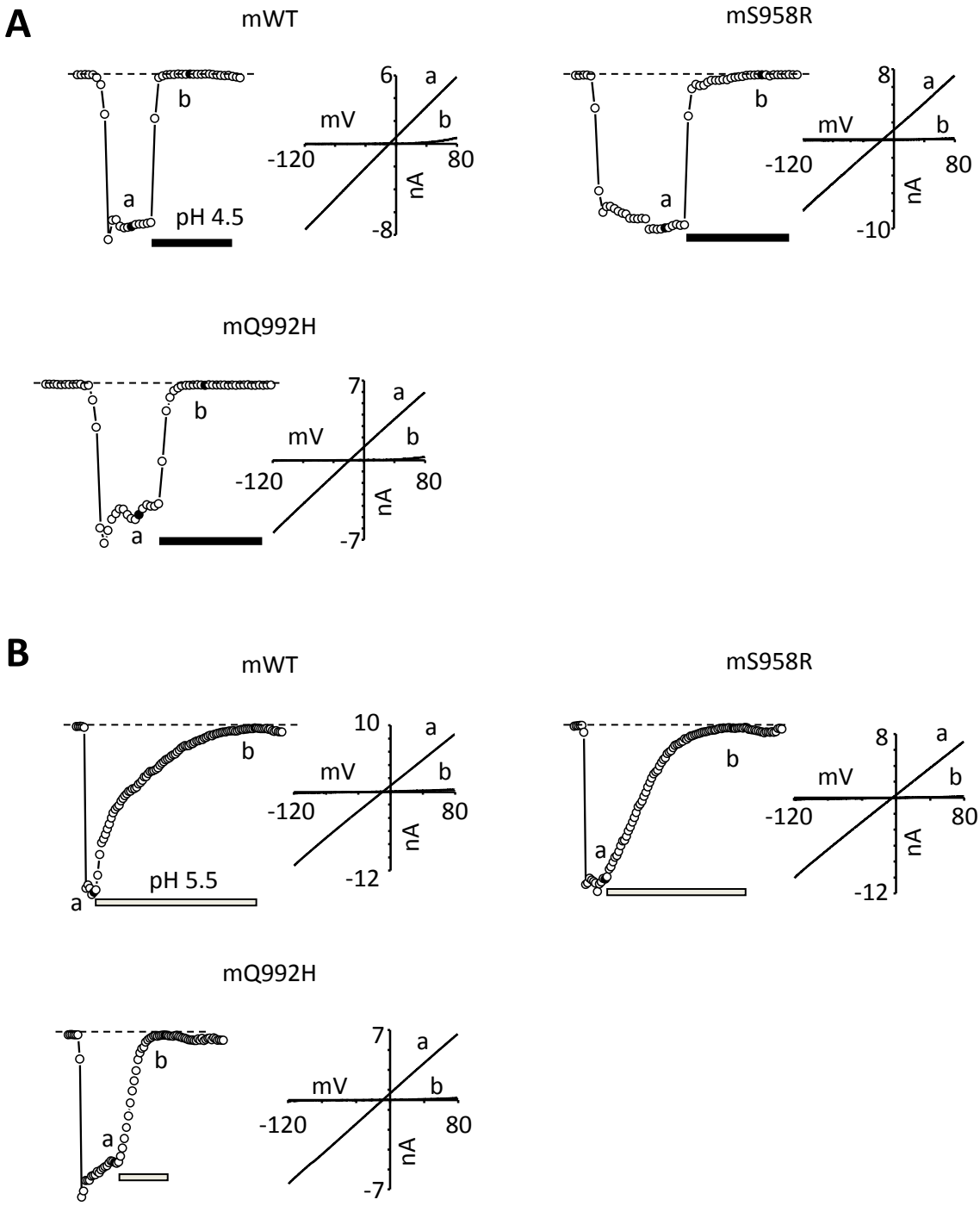
A
mWT
mS958R
mQ992H
B
mWT
mS958R
mQ992H
pH 4.5
pH 5.5
mV
nA
a
b
-120
80
6
-8
8
-10
7
-7
10
-12

C

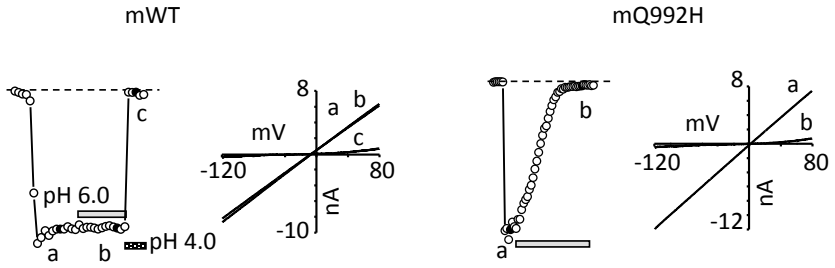

Figure 3.6 Accelerated kinetics of, and increased sensitivity to, inhibition by acidic pH by mutation of Gln-992 but not Ser-958 in the mTRPM2 channel

A-C, 1 mM ADPR-induced currents at−80 mV and I -V relationship curves are recorded in HEK293 cells transiently transfected with the WT or S958R or Q992H mutant mTRPM2 plasmid in response to extracellular acidic pH 4.5 (**A**), 5.5 (**B**) and 6.0 (**C**). Note that the mutation Q992H greatly accelerates the inhibition by pH 5.5 and confers complete inhibition by pH 6.0 without change in the I-V relationship curves.

3.2.5 Decelerated kinetics of inhibition by acidic pH by reciprocal mutation of His-995 in the hTRPM2 channel

To further verify the role of Gln-992 residue in the mTRPM2 channel and the equivalent His-995 residue in the hTRPM2 channel in determining the species difference in the inhibition of the TRPM2 channels by acidic pH, I introduced the reciprocal mutations, R961S and H995Q, in the hTRPM2 channel. Again, like the mutations in the mTRPM2 channel, both R961S and H995Q mutations did not alter the amplitude of ADPR-induced currents (Fig. 3.5) and the linear I-V relationship (Fig. 3.7). Like the S958R mutation in the mTRPM2 channel, the R961S mutation in the hTRPM2 channel failed to change both the steady-state inhibition by extracellular acidic pH and the inhibition kinetics (Fig. 3.7 and Fig. 3.8). While the steady-state inhibition by pH 5.5-6.0 remained unchanged, the kinetics of inhibition was remarkably decelerated when the H995Q mutant hTRPM2 channel was compared to the WT hTRPM2 channel (Fig. 3.8). These results, taken together with the results from the mTRPM2 channel, indicate that His-995/Gln-992 residue in the pore region is critical in determining the differential responses of the human and mouse TRPM2 channels to extracellular acidic pH.

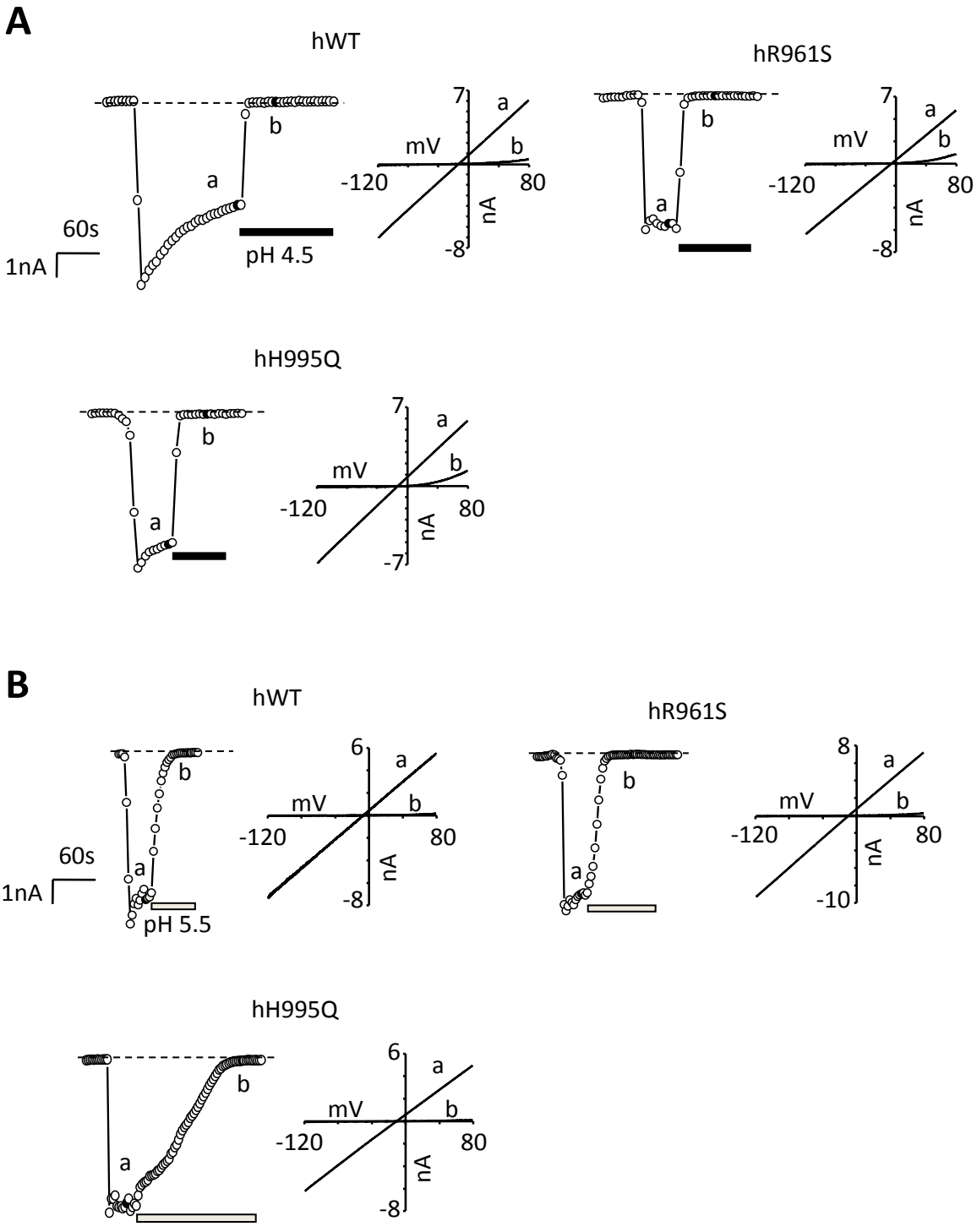
A
hWT
hR961S
hH995Q
60s
1nA
pH 4.5
mV
nA
-120
80
7
-8
-7
a
b
B
hWT
hR961S
hH995Q
60s
1nA
pH 5.5
6
8
-10

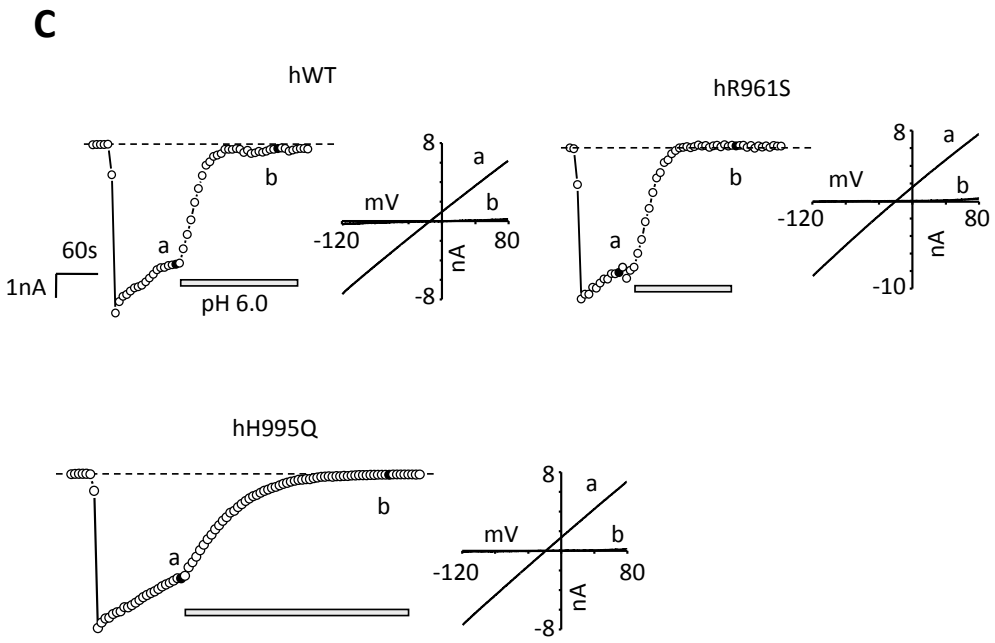

Figure 3.7 Decelerated kinetics of, and increased sensitivity to, inhibition by acidic pH by mutation of His-995 but not Arg-961 in the hTRPM2 channel

A-C, 1 mM ADPR-induced currents at−80 mV and I -V relationship curves are recorded in HEK293 cells transiently transfected with the WT or R961S or H995Q mutant hTRPM2 plasmid in response to extracellular acidic pH 4.5 (**A**), 5.5 (**B**) and 6.0 (**C**). Note that mutation H995Q strikingly slows down the inhibition by pH 5.5 and pH 6.0 without change in the I-V relationship curves.

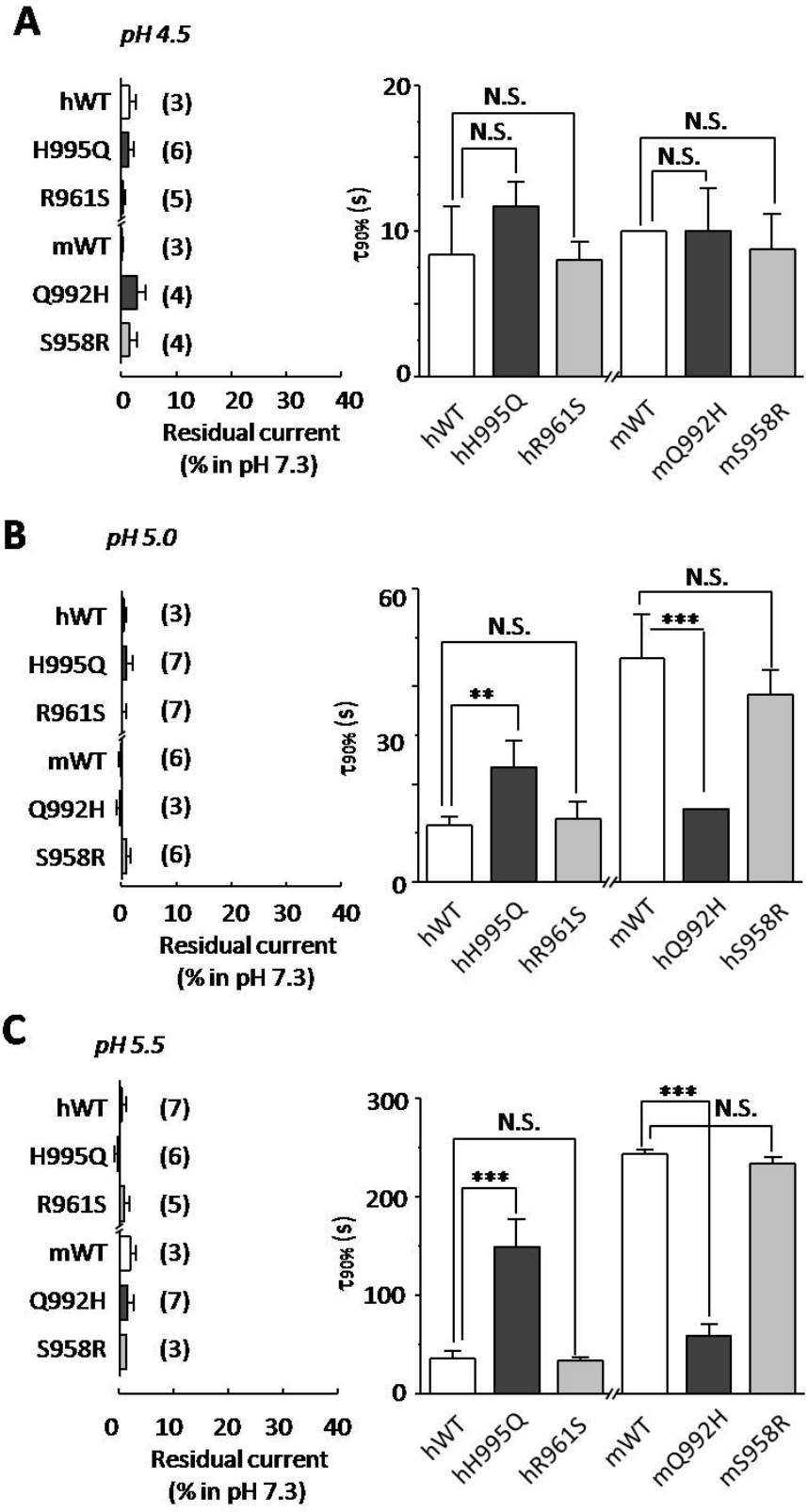
A
pH 4.5
hWT (3)
H995Q (6)
R961S (5)
mWT (3)
Q992H (4)
S958R (4)
0 10 20 30 40
Residual current
(% in pH 7.3)
τ90% (s)
20
10
0
N.S.
N.S.
N.S.
N.S.
hWT
hH995Q
hR961S
mWT
mQ992H
mS958R
B
pH 5.0
hWT (3)
H995Q (7)
R961S (7)
mWT (6)
Q992H (3)
S958R (6)
0 10 20 30 40
Residual current
(% in pH 7.3)
τ90% (s)
60
30
0
N.S.
**
N.S.
***
hWT
hH995Q
hR961S
mWT
hQ992H
hS958R
C
pH 5.5
hWT (7)
H995Q (6)
R961S (5)
mWT (3)
Q992H (7)
S958R (3)
0 10 20 30 40
Residual current
(% in pH 7.3)
τ90% (s)
300
200
100
0
N.S.
***
***
N.S.
hWT
hH995Q
hR961S
mWT
mQ992H
mS958R

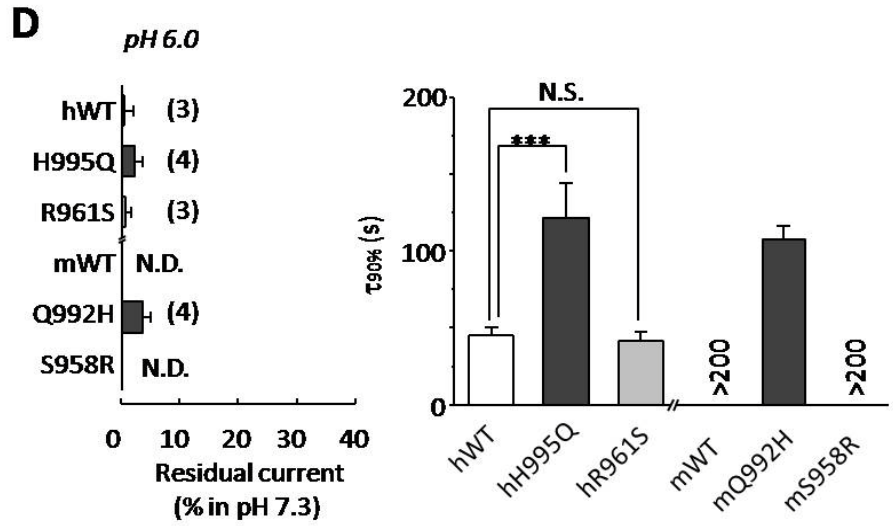

Figure 3.8 A crucial role of His-995 in the hTRPM2 channel and Gln-992 in the mTRPM2 channel for species-dependent inhibition by acidic pH.

A-D, summary of the residual currents induced by 1 mM ADPR in the steady state as percentage of the currents in pH 7.3 before solution change (*left*) and the kinetics of inhibition (indicated by $\tau_{90\%}$; *right*) in extracellular pH 4.5 (**A**), 5.0 (**B**), 5.5 (**C**), and 6.0 (**D**). The numbers of cells examined in each case are indicated in parenthesis in the left panel. *p<0.05, **p<0.01, and ***p<0.005 between the paired groups, N.S., no significant difference, and N.D., not determined.

3.3 Discussion

In this chapter I have shown that the initial inhibition of the hTRPM2 channel currents by extracellular acidic pH exhibited substantial reversibility but the steady-state inhibition became irreversible. Similar to the hTRPM2 channel currents, the steady-state inhibition of the mTRPM2 channel currents was irreversible and pH-independent within pH 4.0–5.5, with strong pH-dependent kinetics of inhibition. However, there was a significant difference between the hTRPM2 and mTRPM2 channels; compared to the hTRPM2 channel currents, the mTRPM2 channel currents exhibited much slower kinetics of inhibition by pH 5.0–5.5 and lack of inhibition by pH 6.0. Furthermore, the results from site-directed mutagenesis and functional study provide clear evidence to show that species-specific residue His-995/Gln-992 in the outer pore region of the TRPM2 channels is crucial in determining the difference between hTRPM2 and mTRPM2 channels in the sensitivity to extracellular acidic pH.

The finding that the reversibility of the inhibition of the hTRPM2 channel currents strongly depends upon the exposure duration was important in two folds. Firstly, the inhibition showed substantial reversibility upon returning to pH 7.3 immediately after exposure that just sufficed complete inhibition, but such reversibility progressively diminished as the exposure duration was prolonged to ≥ 60 s (Fig. 3.2A-F). These results provide clear evidence to indicate that extracellular protons induces initial reversible inhibition and evokes conformational changes leading to subsequent irreversible inhibition or channel inactivation, as was proposed previously (Yang et al., 2010). Detailed analysis further revealed that the inactivation occurs with a time constant of 30 s (Fig. 3.2G). Secondly, as mentioned in the introduction, a fundamentally different mechanism had been proposed to account for both the reversible and irreversible inhibition of the hTRPM2 channel currents by extracellular acidic pH; the inhibition is thought to result from binding of extracellular protons, after permeating through the open channels, to an intracellular binding site (Csanady and Torocsik, 2009, Starkus et al., 2007). It is also worth mentioning that there is no evidence for the permeability of the TRPM2 channels to protons. This intracellular mechanism underlying the reversible inhibition and particularly the irreversible inhibition appears difficult to be reconciled with the strong dependence of the reversibility on the

duration, starting after no further proton influx, if one presumes that protons can permeate through the open TRPM2 channels (Fig. 3.2A-E).

The steady-state inhibition of the mTRPM2 channel currents was complete, irreversible, and pH-independent (pH 4.0-5.5) with clear pH-dependent kinetics. These inhibitory features are similar to those for the hTRPM2 channel currents (Fig. 3.4A-C). However, the kinetics of inhibition by pH 5.0–5.5 for the mTRPM2 channel currents was noticeably slower than that for the hTRPM2 channel currents (Fig. 3.4D). Furthermore, in contrast with the complete inhibition of the hTRPM2 channel currents, the mTRPM2 channel currents showed little or no inhibition by pH 6.0. Such differences in the kinetics and particularly the sensitivity to pH 6.0 could bear significant functional implications, because the TRPM2 channels at the cell surface could experience extracellular acidic pH, e.g., at the site of inflammation (Lardner, 2001), or within the lysosome where the luminal pH was highly acidic (Lange et al., 2009). In addition, as discussed below, the effects of extracellular acidic pH engage proton–outer pore interactions, and thus the species-dependence provides an indication of some local structural difference in the outer pore, which could have a profound impact on development of antagonists.

Our previous study have identified several residues in the outer pore, including Lys-952 and Asp-1002, to be critical in determining the sensitivity to, and the kinetics of, the reversible inhibition and inactivation of the hTRPM2 channel currents, leading to the notion that the effects of extracellular acidic pH originates from interactions of protons with the outer pore (Yang et al., 2010). Yue and her colleagues have proposed a similar molecular mechanism for the reversible inhibition (Du et al., 2009b) that, however, has been subsequently challenged (Csanady and Torocsik, 2009, Starkus et al., 2007). They introduced the H995Q mutation in the hTRPM2 channel but found no significant effect on the reversible inhibition (Du et al., 2009b). In the present study, the H995Q mutation in the hTRPM2 channel remarkably slowed down, and the reciprocal Q992H mutation in the mTRPM2 channel accelerated, the kinetics of the channel inhibition or inactivation (Fig. 3.6, Fig. 3.7 and Fig. 3.8). Moreover, the Q992H mutation conferred complete inactivation by pH 6.0 to the mTRPM2 channel, which was otherwise insensitive (Fig. 3.6). We simply failed to produce such opposing effects by introducing reciprocal mutations of another pair of residues, Arg-961 in the hTRPM2 channel and Ser-958 in themTRPM2 channel (Fig. 3.8), supporting that

the mutational effects of H995Q in the hTRPM2 channel and Q992H in the mTRPM2 channel is specific. Taken together, the results described in this chapter suggest that His-995 confers greater sensitivity to and faster kinetics of inactivation of the hTRPM2 channel by extracellular acidic pH. One simple and plausible interpretation of the striking differences between the hTRPM2 and mTRPM2 channels and the opposing effects from reciprocal mutations of His-995/Gln-992 is that protonation at His-995 in the WT hTRPM2 channel, or the His residue engineered in the equivalent position of the Q992H mutant mTRPM2 channel, introduces electrostatic interactions with other charged residues nearby such as Asp-1002 (Yang et al., 2010) and particularly Asp-987 (Wehrhahn et al., 2010), and thereby evokes conformational changes leading to inactivation of the ion-conducting pore. Such an interpretation is consistent with a previous study proposing that the P1018L mutation in the outer pore, identified in Guamanian Western Pacific amyotrophic lateral sclerosis and Parkinsonism dementia patients, renders the hTRPM2 channel to inactivate via conformational changes in the outer pore (Hermosura et al., 2008).

In summary, I have shown in the study described in this chapter that extracellular acidic pH induces initial reversible inhibition and subsequent irreversible inactivation of the human TRPM2 channels. I have also revealed the strong difference of the sensitivity to, and kinetics of, the inhibition by extracellular acidic pH between the human and mouse TRPM2 channels, and have identified residue His-996 in the outer pore of the hTRPM2 channel and equivalent Gln-992 in the mTRPM2 channel as a crucial determinant for such species difference. These findings provide new insight into the responses of the TRPM2 channels to extracellular acidic pH.

Chapter 4

Characterization of novel TRPM2 channel inhibitors

4.1 Introduction

As discussed in detail in the introduction chapter, many compounds have been demonstrated to inhibit the TRPM2 channels, such as ACA, FFA and 2-APB (section 1.2.5.2). In the previous chapter, I have also presented evidence to show that acidic pH can also inhibit the TRPM2 channels. However, all of these chemicals are able to have various effects on a range of ion channels. For example, ACA acts as an inhibitor of calcium-activated chloride channels and 2-APB inhibit the IP_3 receptors and other TRP channels (Diver et al., 2001, Gwanyanya et al., 2010, Xu et al., 2005). Besides these non-specific TRPM2 channel inhibitors, some other chemicals can indirectly influence the TRPM2 channel activation, such as PJ-34 which is an inhibitor of PARPs and thus suppresses the TRPM2 channel activation by blocking PARP-mediated generation of ADPR (Fonfria et al., 2004, Kashio et al., 2012). Currently, there is no specific blocker for the TRPM2 channels, which makes difficulties if it is impossible to study the physiological functions of the hTRPM2 channel. In addition, several recent studies show that transgenic TRPM2 deficient mice are fertile and exhibit no significant detrimental phenotype but such mice show strong protection from oxidative stress-induced colitis (Knowles et al., 2011), and mitigate obesity and metabolic disorders (Zhang et al., 2012), suggesting development of hTRPM2 channel specific inhibitors is a promising therapeutic strategy. In order to develop new TRPM2 inhibitors, our lab has collaborated with Dr. R Foster, Medicinal Chemistry and Chemical Biology (MCCB) Technology Group Leader in the School of Chemistry in the University of Leeds. They have screened 14,000 compounds by testing the effects on H_2O_2-induced increases in the $[Ca^{2+}]_c$ in the tetracycline-induced hTRPM2-expressing HEK293 cells and identified 48 hit compounds. In this chapter, I will describe a detailed characterization of the effects on H_2O_2-induced Ca^{2+} responses and ADPR-induced currents by these compounds. I have shown that several compounds can inhibit the TRPM2 channels with a micromolar or submicromolar potency.

4.2 Results

4.2.1 Inhibition of H_2O_2-induced increases in $[Ca^{2+}]_c$ by the TRPM2 inhibitor candidates

I began with examining the effects of 48 compounds at 10 μM on the increases in the $[Ca^{2+}]_c$ induced by 1 mM H_2O_2 in the tetracycline-induced HEK293 cells expressing the hTRPM2 channels. The cells were loaded with Fura-2/AM, and the fluorescence intensity, excited with 340 nm and 380 nm and emitted at 510 nm, was measured using Flex-station (see section 2.2.13). After 1 min recording to establish the baseline, cells were exposed to H_2O_2, and the recording continued for 5min. As shown in Fig. 4.1, for the cells in the control group (treated with the solvent DMSO) in Ca^{2+}-containing SBS, H_2O_2 evoked, with a delay of about 1 min, strong increases in the $[Ca^{2+}]_c$ that reached the steady-state level within 1-3 min. Pre-treatment with 10 μM ACA for 30 min substantially inhibited H_2O_2-induced increases in the $[Ca^{2+}]_c$. Similar pre-treatment with each of the 48 compounds exhibited various effects. Some of the compounds, including No.13, No.35, No.37, No.42, No.02 and No.07, completely or almost completely eliminated H_2O_2-induced increases in the $[Ca^{2+}]_c$, many other compounds, such as No.15, No.17, No.34 and No.09, had partial inhibition, whereas some compounds, such as No.18 and No.44, showed little or no inhibition. Fig. 4.2 summarizes the mean inhibitions of all 48 compounds, arranged in a descending order.

Of notice, several compounds such as No.31 and No.12 substantially altered the baseline before addition of H_2O_2 (Fig. 4.1), which prevents or complicates accurate determination of the inhibition by such compounds. The baseline shift could be caused by many reasons, for example, alteration in the membrane permeability to allow extracellular Ca^{2+} influx or release of intracellular Ca^{2+}, or interference of the fluorescent properties of Fura-2. To mitigate the effect on the baseline, these compounds at 1 μM were tested for their effects on H_2O_2-induced Ca^{2+} responses. The time course of the effects and the mean inhibition are shown in Fig. 4.3 and Fig. 4.4, respectively. The shifts in the basal $[Ca^{2+}]_c$ by most of the compounds tested, such as No.04, No.10 and No.33, were reduced or completely abolished. In addition, some of these compounds, including No.22 and No.45, still exhibited substantial, but attenuated, changes in the basal $[Ca^{2+}]_c$, but elimination of the increases in the $[Ca^{2+}]_c$ by

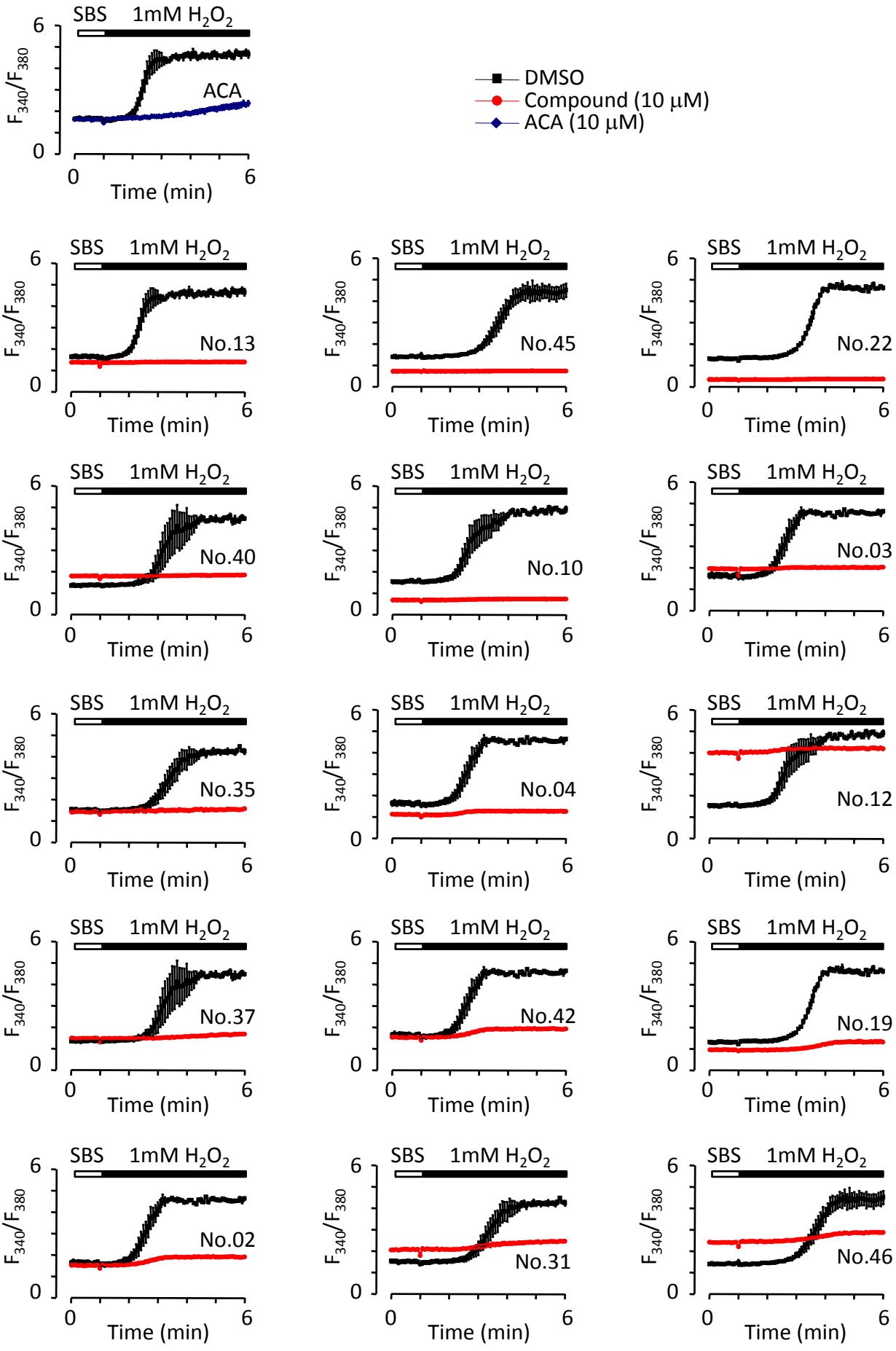
SBS
1mM H2O2
ACA
F340/F380
Time (min)
DMSO
Compound (10 μM)
ACA (10 μM)
No.13
No.45
No.22
No.40
No.10
No.03
No.35
No.04
No.12
No.37
No.42
No.19
No.02
No.31
No.46

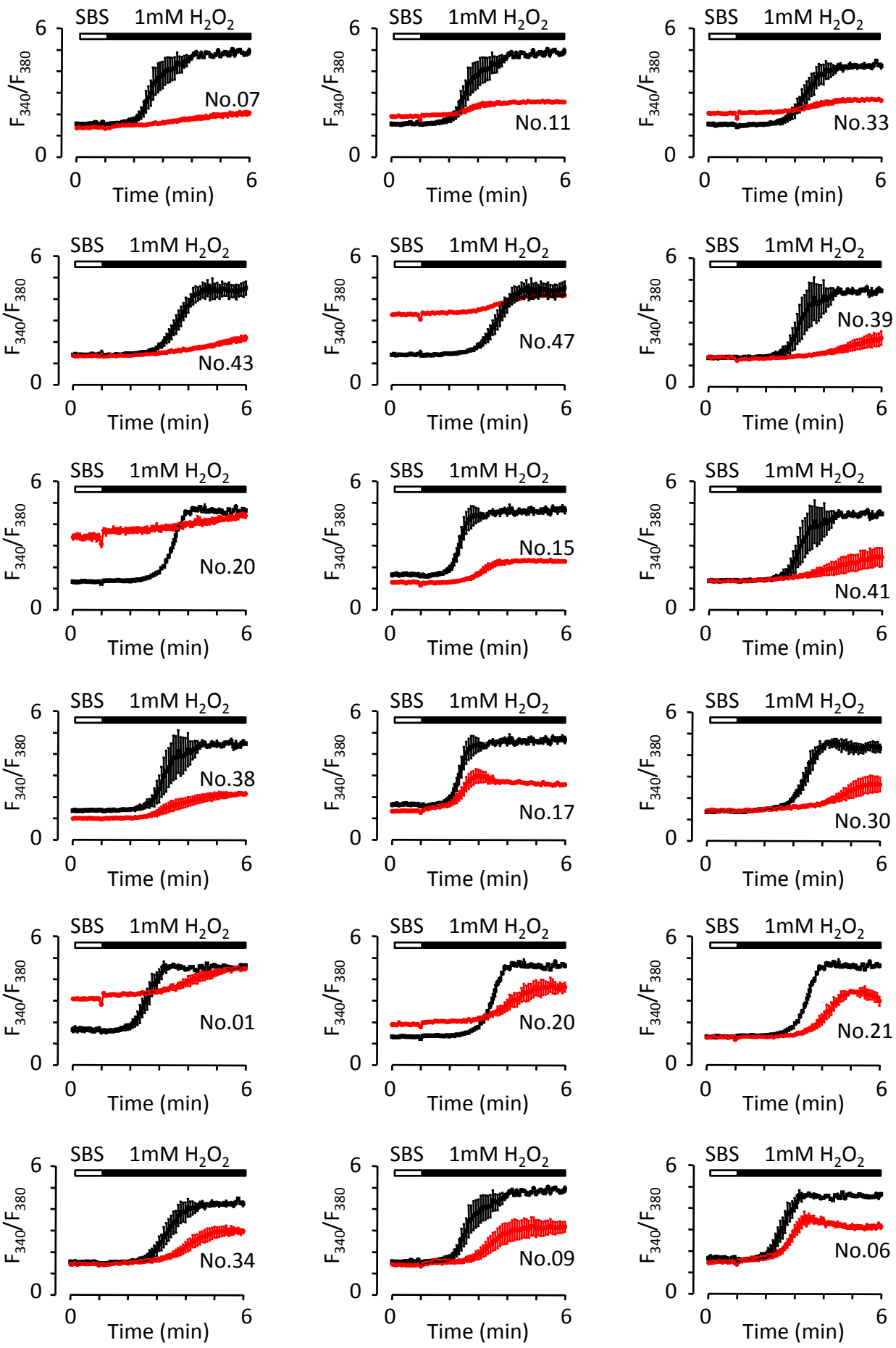
SBS
1mM H2O2
F340/F380
6
0
0
6
Time (min)
No.07
No.11
No.33
No.43
No.47
No.39
No.20
No.15
No.41
No.38
No.17
No.30
No.01
No.20
No.21
No.34
No.09
No.06

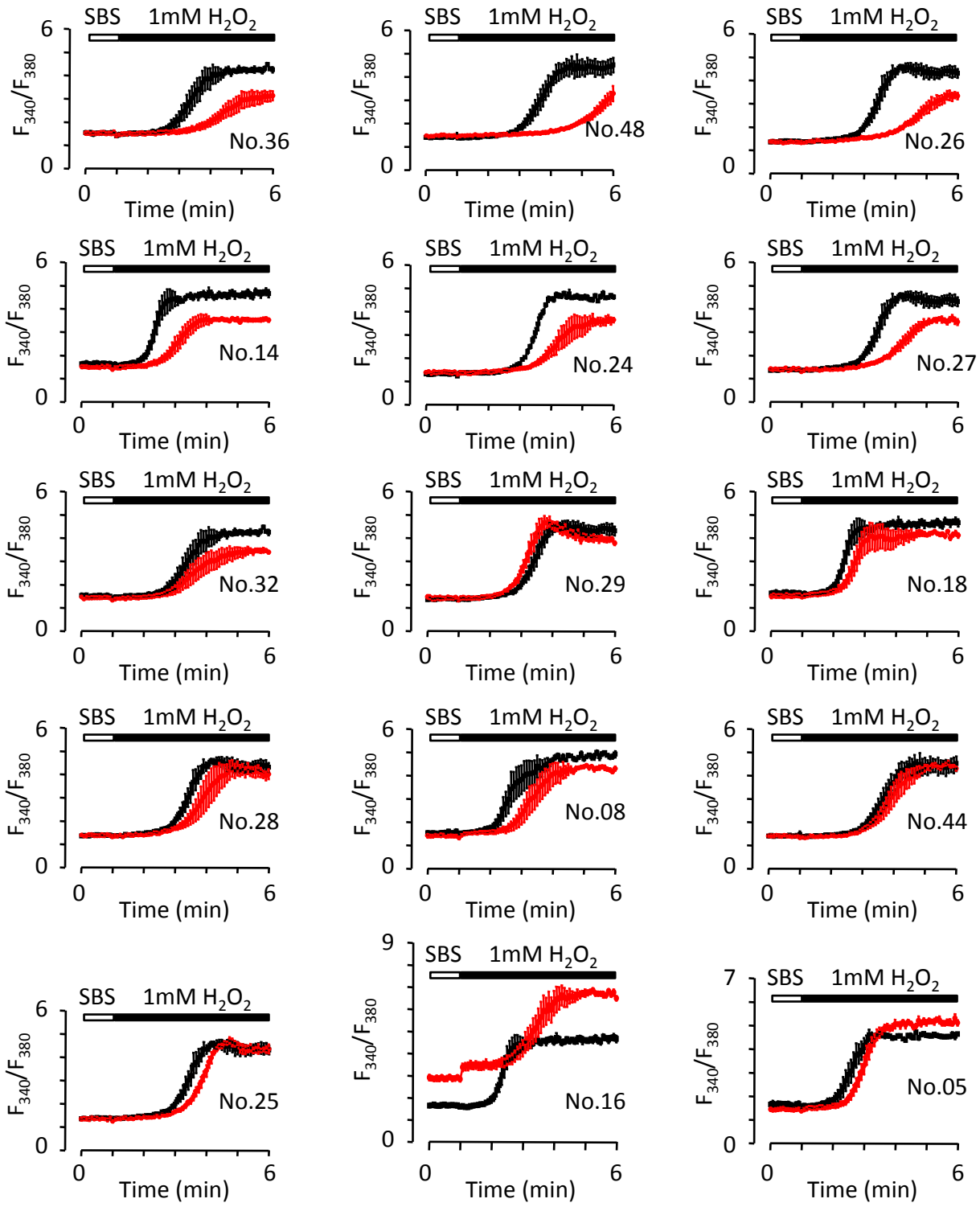

Figure 4.1 Effects of hit compounds at 10 μM on H_2O_2-induced increases in the $[Ca^{2+}]_c$

The time courses of the effects on H_2O_2-induced Ca^{2+} responses by individual compounds (indicated in the figure) in tetracycline-induced hTRPM2-expressing HEK293 cells in Ca^{2+}-containing SBS using Flex-station. Cells were pre-treated with DMSO (black square), 10 μM ACA (navy diamond) or 10 μM compounds (red circle) for 30 min, and then exposed to 1 mM H_2O_2 for 5 min. The compounds are arranged according to the percentage of inhibiting H_2O_2-induced Ca^{2+} responses in a descending order. The data show mean ± sem; the number of wells examined for each compound are indicated in parenthesis in Fig.4.2.

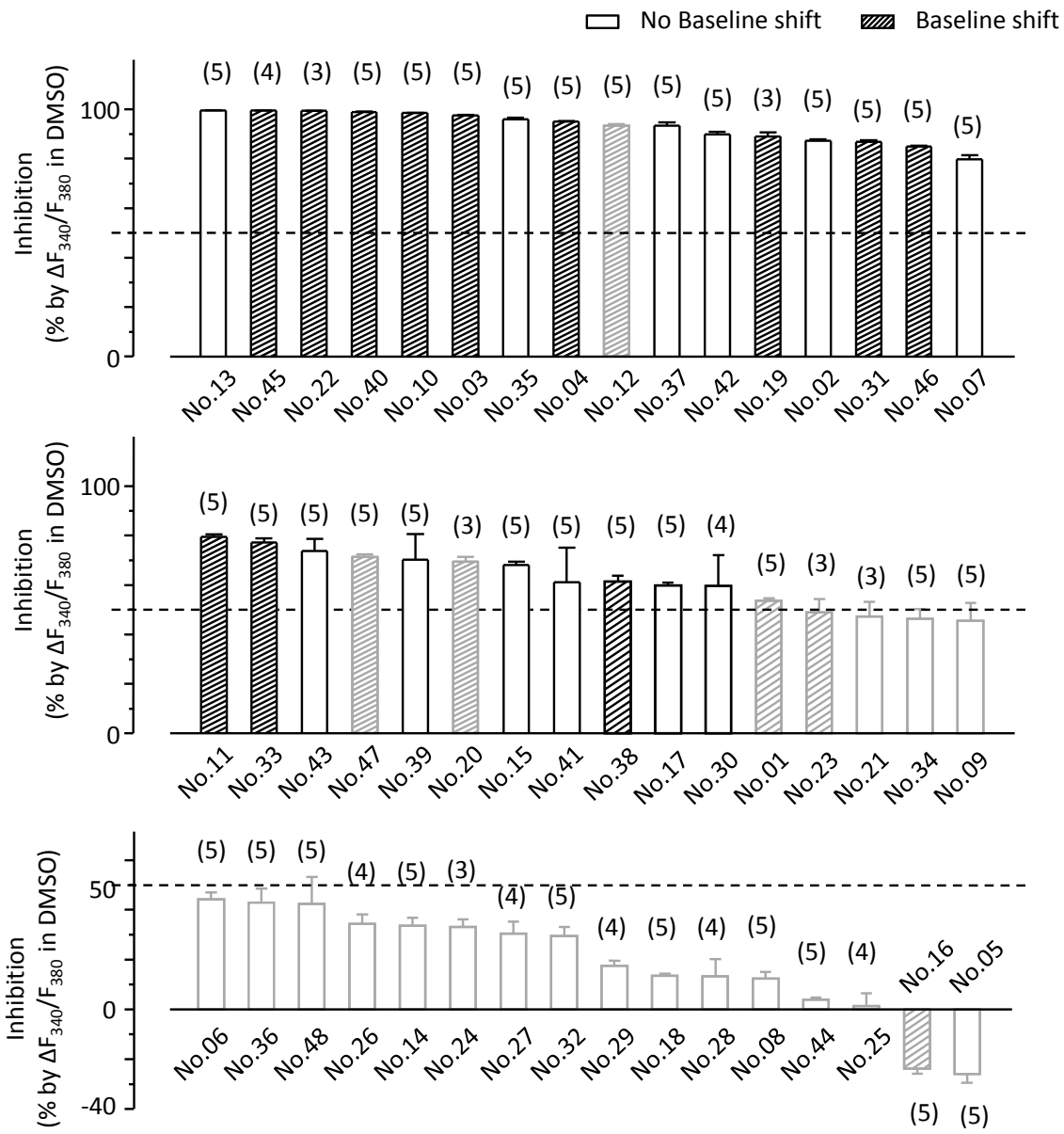

Figure 4.2 Summary of inhibition of H_2O_2-induced increases in the $[Ca^{2+}]_c$ by compounds at 10 μM

Summary of the inhibition of 1 H_2O_2-induced Ca^{2+} responses by individual compounds 10 μM in tetracycline-induced hTRPM2-expressing HEK293 cells as illustrated in Fig. 4.1. The compounds are arranged according to their percentage of inhibiting H_2O_2-induced Ca^{2+} responses in a descending order. The dotted-line shows 50% inhibition. The compounds before the double-line induce >50% inhibition. The oblique line bars indicate that the compounds cause a substantial change in the basal $[Ca^{2+}]_c$. The data show mean ± sem; the number of wells examined for each compound are indicated in parenthesis.

A

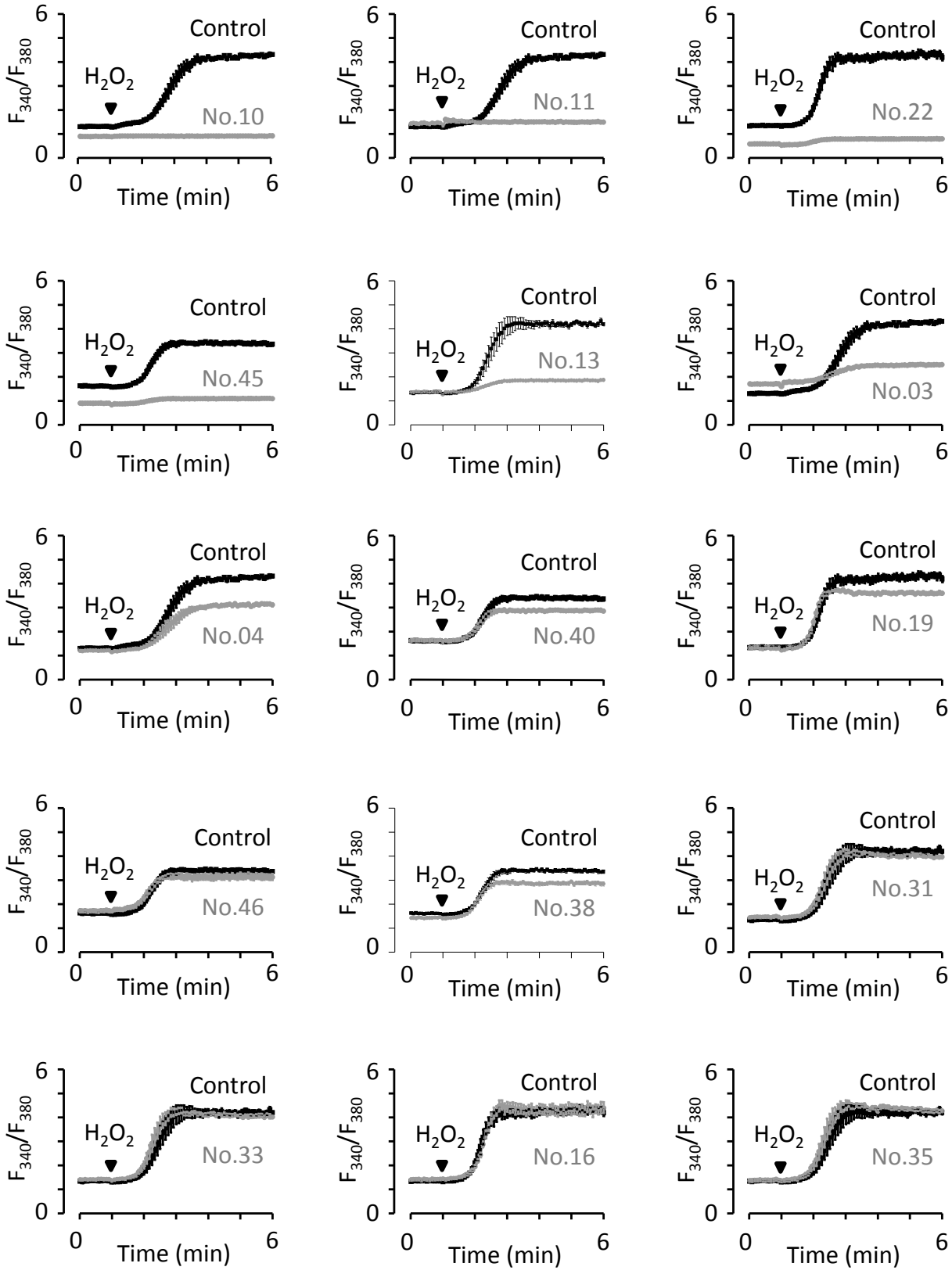
Control
H_2O_2
No.10
No.11
No.22
No.45
No.13
No.03
No.04
No.40
No.19
No.46
No.38
No.31
No.33
No.16
No.35
F_{340}/F_{380}
Time (min)
0
6

B

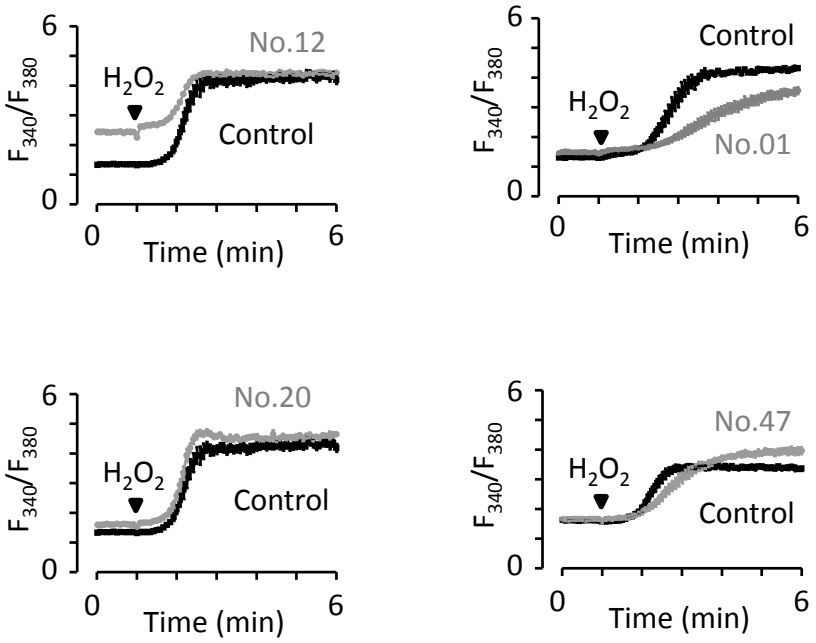

Figure 4.3 Effects of hit compounds at 1 μM on H_2O_2-induced increases in the $[Ca^{2+}]_c$

A-B, the time courses of the effects on H_2O_2-induced Ca^{2+} responses by individual compounds (indicated in the figure) in tetracycline-induced hTRPM2-expressing HEK293 cells in Ca^{2+}-containing SBS using Flex-station. Cells were pre-treated with DMSO (black square) or 1 μM indicated compounds (grey circle) for 30 min, and then exposed to 1 mM H_2O_2 for 5 min. Panel **B** shows the compounds which exhibited modest or no effects on the basal $[Ca^{2+}]_c$ and no inhibition of H_2O_2-induced Ca^{2+} responses. The compounds are arranged according to the percentage of inhibiting H_2O_2-induced Ca^{2+} responses in a descending order. The data show mean ± sem; the numbers of wells examined for each compound are indicated in parenthesis in Fig. 4.4.

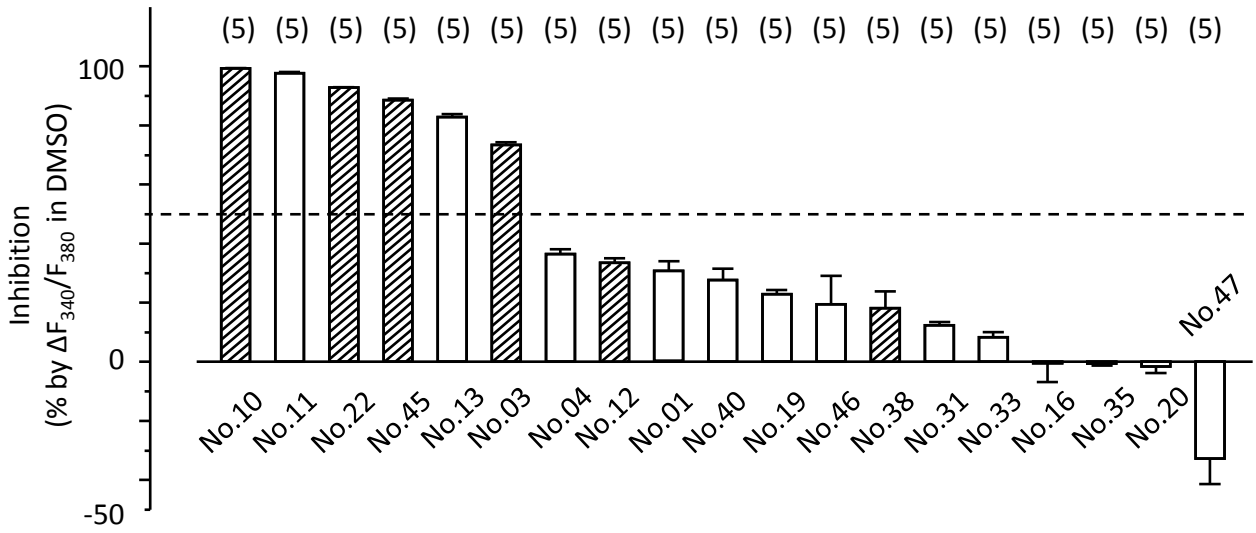

Figure 4.4 Summary of inhibition of H_2O_2-induced increases in the $[Ca^{2+}]_c$ by compounds at 1 μM

Summary of the inhibition of 1 mM H_2O_2-induced Ca^{2+} responses by 1 μM individual compounds in tetracycline-induced hTRPM2-expressing HEK293 cells. The compounds are arranged according to the percentage of inhibiting H_2O_2-induced Ca^{2+} responses in a descending order. The dotted-line shows 50% inhibition. The oblique line bars indicate that the compounds cause a substantial change in the basal $[Ca^{2+}]_c$. The data show mean ± sem; the number of wells examined for each compound are indicated in parenthesis.

these compounds at 1 μM suggested a high potency of inhibiting the TRPM2 channels. In contrast, some other compounds (Fig 4.3B), No.01, No.12, No.20 and No.47, at 1 μM showed modest or no effects on the basal $[Ca^{2+}]_c$ and at the same time they lost their inhibition of H_2O_2-induced increases in the $[Ca^{2+}]_c$. Thus, 24 compounds, which showed strong inhibition of H_2O_2-induced Ca^{2+}responses with modest or no effect on the basal $[Ca^{2+}]_c$ were subjected to further characterization (showing in black in Fig. 4.2).

4.2.2 Potency of select TRPM2 inhibitor candidates

I next examined the potency of the 24 compounds by determining the inhibition of H_2O_2-induced increase in the $[Ca^{2+}]_c$ at more than 5 different concentrations and fitting the data to Hill equation (section 2.2.16) to derive the IC_{50}. Fig. 4.5 shows the mean data and the fitting curves, and Fig. 4.6 summarizes the derived IC_{50}s. Three compounds (No.30, No.17 and No.15) exhibited a relatively low potency with an IC_{50} of higher than 5 μM. The IC_{50}s of all other compounds were lower than 5 μM, suggesting a high sensitivity of H_2O_2-induced increase in the $[Ca^{2+}]_c$ to these compounds; among them, six compounds (No.03, No.40, No.10, No.13, No.22 and No.45) have a very high potency, with an IC_{50} of less than 1 μM. However, two compounds, No.41 and No.43, were ineffective, resulting in partial inhibition of H_2O_2-induced Ca^{2+} response at 10 μM, and thus, their IC_{50}s were not calculated.

4.2.3 Inhibition of ADPR-induced currents by TRPM2 inhibitor candidates

The whole-cell patch-clamp recording was performed to investigate whether the suppression of H_2O_2-induced increases in the $[Ca^{2+}]_c$ by these compounds were due to direct inhibition of the hTRPM2 channel activation. I focused on the 19 compounds, whose IC_{50}s were lower than 5 μM (Fig. 4.6), and determined their effects at 10 μM on the currents induced by 1 mM ADPR in the tetracycline-induced HEK293 cells stably expressing the hTRPM2 channels. The individual compound was applied to the patched cells for up to 5 min after stable ADPR-induced currents were established (Fig. 4.7). ACA at 20 μM was applied to any residual currents at the end of the recordings to verify that the currents were mediated by the TRPM2 channels. The representative currents at -80 mV and the mean data are shown in Fig. 4.7 and Fig. 4.8, respectively. The effects of these compounds on the

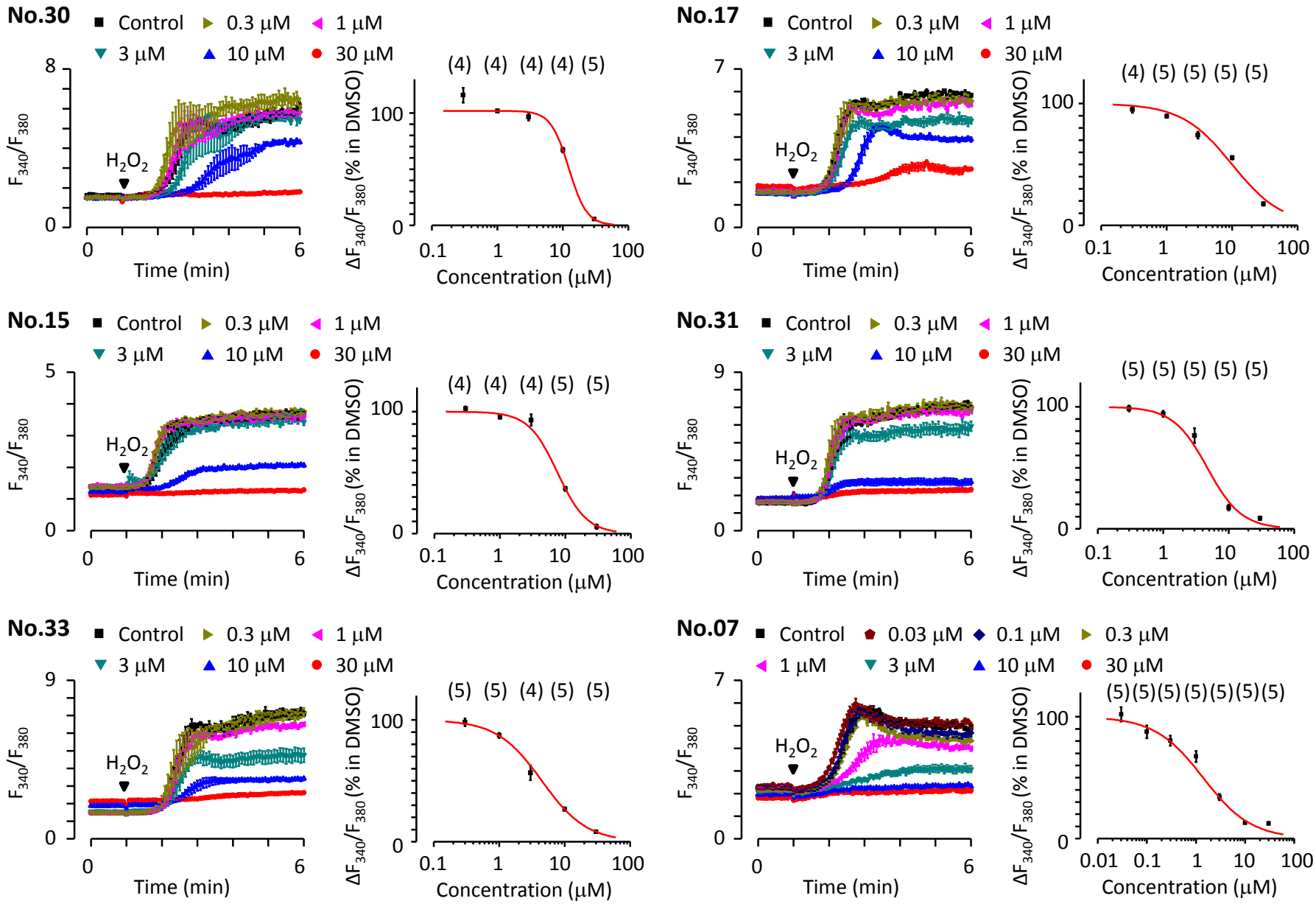
No.30
Control
0.3 μM
1 μM
3 μM
10 μM
30 μM
F_{340}/F_{380}
H_2O_2
Time (min)
(4) (4) (4) (4) (5)
$\Delta F_{340}/F_{380}$ (% in DMSO)
Concentration (μM)
No.17
(4) (5) (5) (5) (5)
No.15
(4) (4) (4) (5) (5)
No.31
(5) (5) (5) (5) (5)
No.33
(5) (5) (4) (5) (5)
No.07
0.03 μM
0.1 μM
(5)(5)(5)(5)(5)(5)(5)

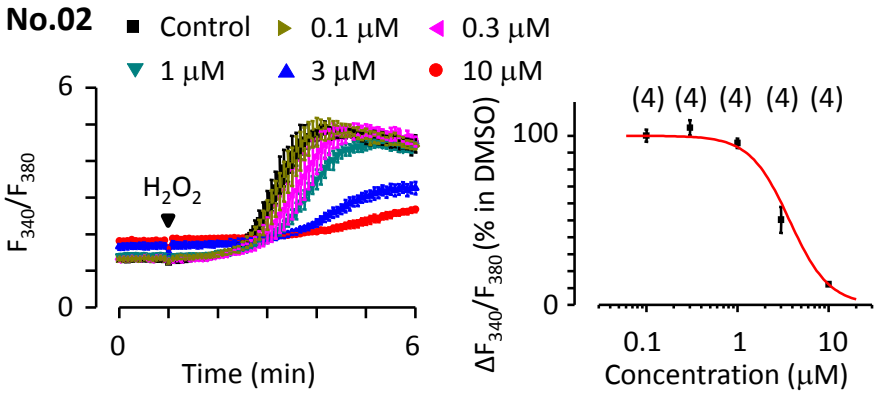
No.02
Control
0.1 μM
0.3 μM
1 μM
3 μM
10 μM
H_2O_2
F_{340}/F_{380}
Time (min)
(4) (4) (4) (4) (4)
$\Delta F_{340}/F_{380}$ (% in DMSO)
Concentration (μM)

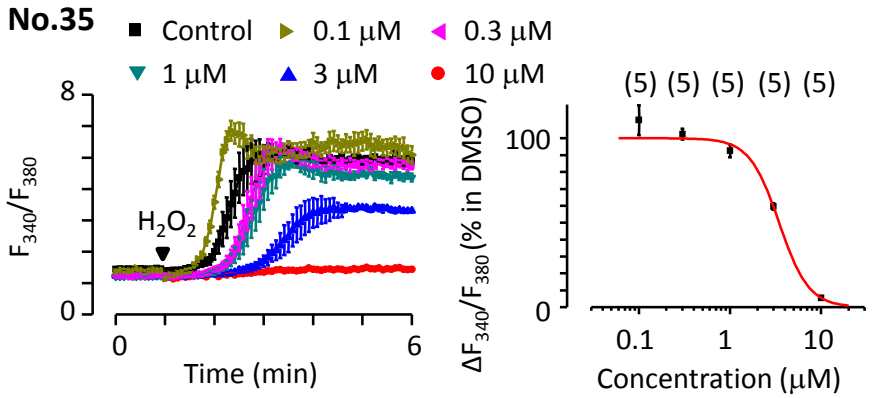
No.35
Control
0.1 μM
0.3 μM
1 μM
3 μM
10 μM
H_2O_2
F_{340}/F_{380}
Time (min)
(5) (5) (5) (5) (5)
$\Delta F_{340}/F_{380}$ (% in DMSO)
Concentration (μM)

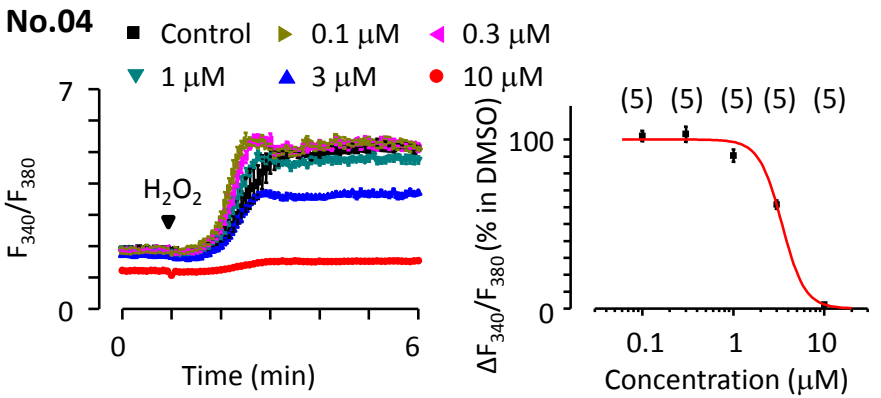
No.04
Control
0.1 μM
0.3 μM
1 μM
3 μM
10 μM
H_2O_2
F_{340}/F_{380}
Time (min)
(5) (5) (5) (5) (5)
$\Delta F_{340}/F_{380}$ (% in DMSO)
Concentration (μM)

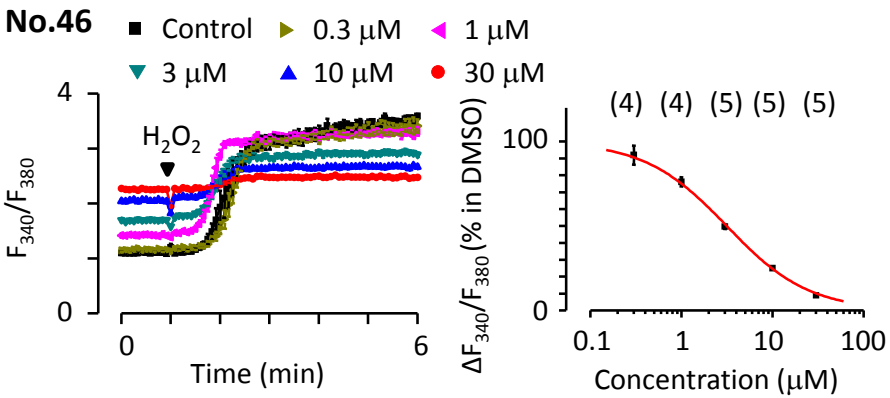
No.46
Control
0.3 μM
1 μM
3 μM
10 μM
30 μM
H_2O_2
F_{340}/F_{380}
Time (min)
(4) (4) (5) (5) (5)
$\Delta F_{340}/F_{380}$ (% in DMSO)
Concentration (μM)

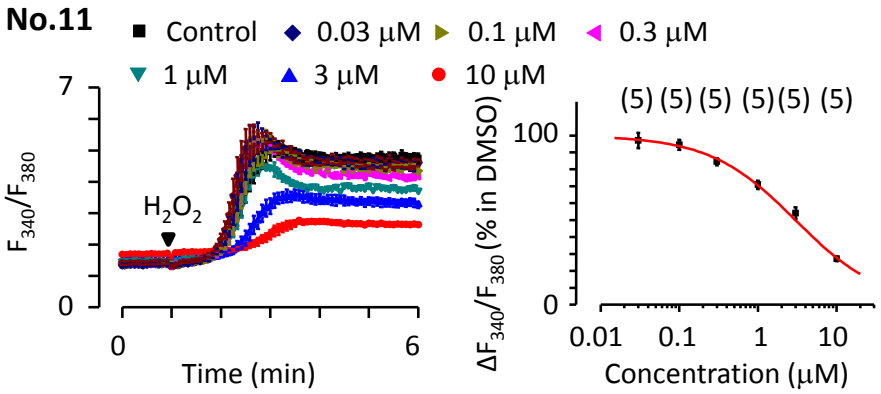
No.11
Control
0.03 μM
0.1 μM
0.3 μM
1 μM
3 μM
10 μM
H_2O_2
F_{340}/F_{380}
Time (min)
(5) (5) (5) (5)(5) (5)
$\Delta F_{340}/F_{380}$ (% in DMSO)
Concentration (μM)

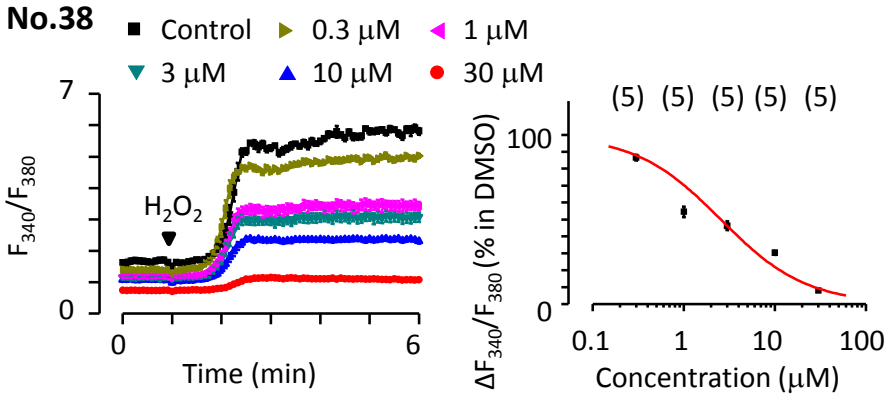
No.38
Control
0.3 μM
1 μM
3 μM
10 μM
30 μM
H_2O_2
F_{340}/F_{380}
Time (min)
(5) (5) (5) (5) (5)
$\Delta F_{340}/F_{380}$ (% in DMSO)
Concentration (μM)

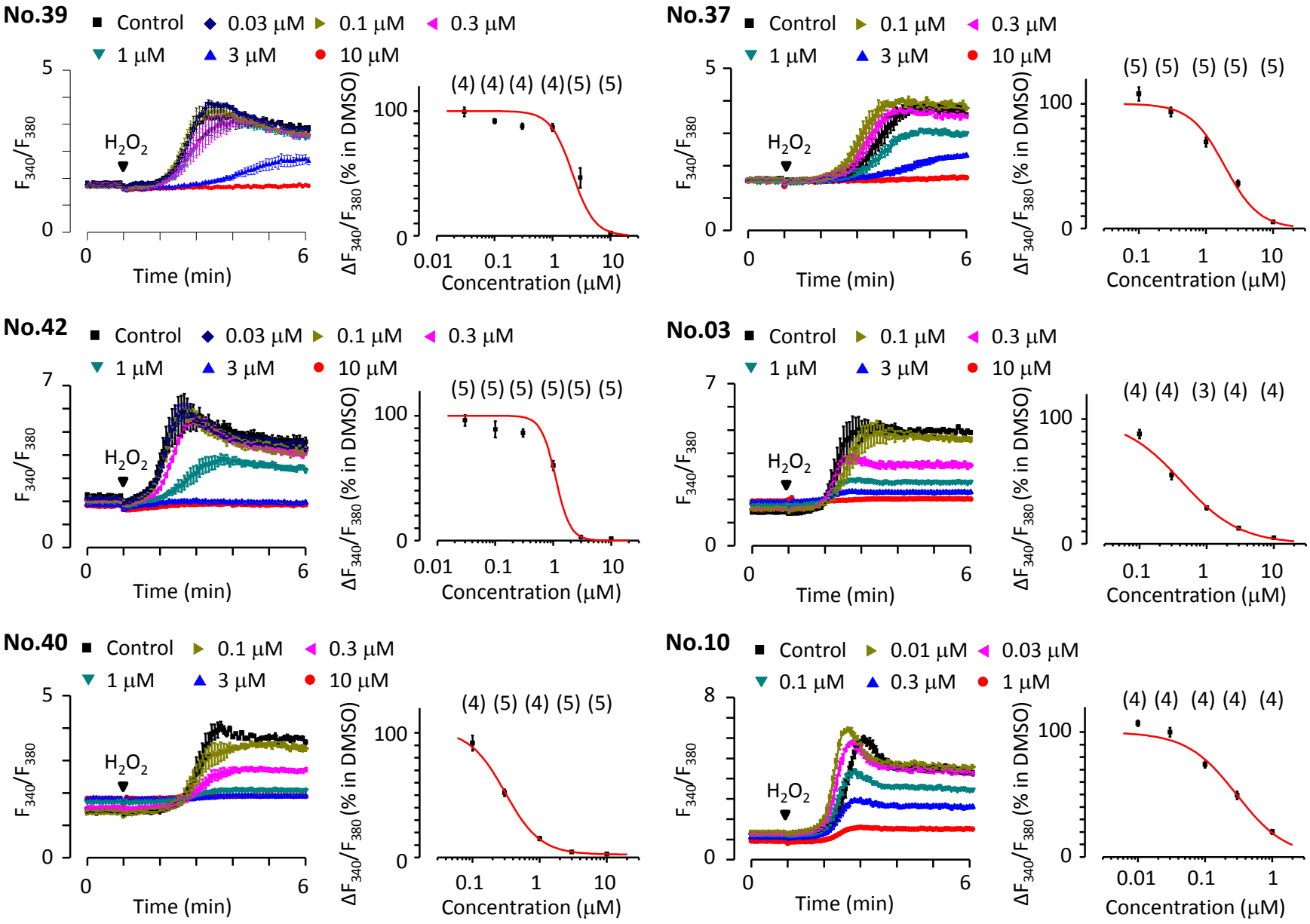
No.39
Control
0.03 μM
0.1 μM
0.3 μM
1 μM
3 μM
10 μM
H2O2
F340/F380
Time (min)
ΔF340/F380 (% in DMSO)
(4) (4) (4) (4) (5) (5)
Concentration (μM)
No.37
(5) (5) (5) (5) (5)
No.42
(5) (5) (5) (5) (5) (5)
No.03
(4) (4) (3) (4) (4)
No.40
(4) (5) (4) (5) (5)
No.10
0.01 μM
(4) (4) (4) (4) (4)

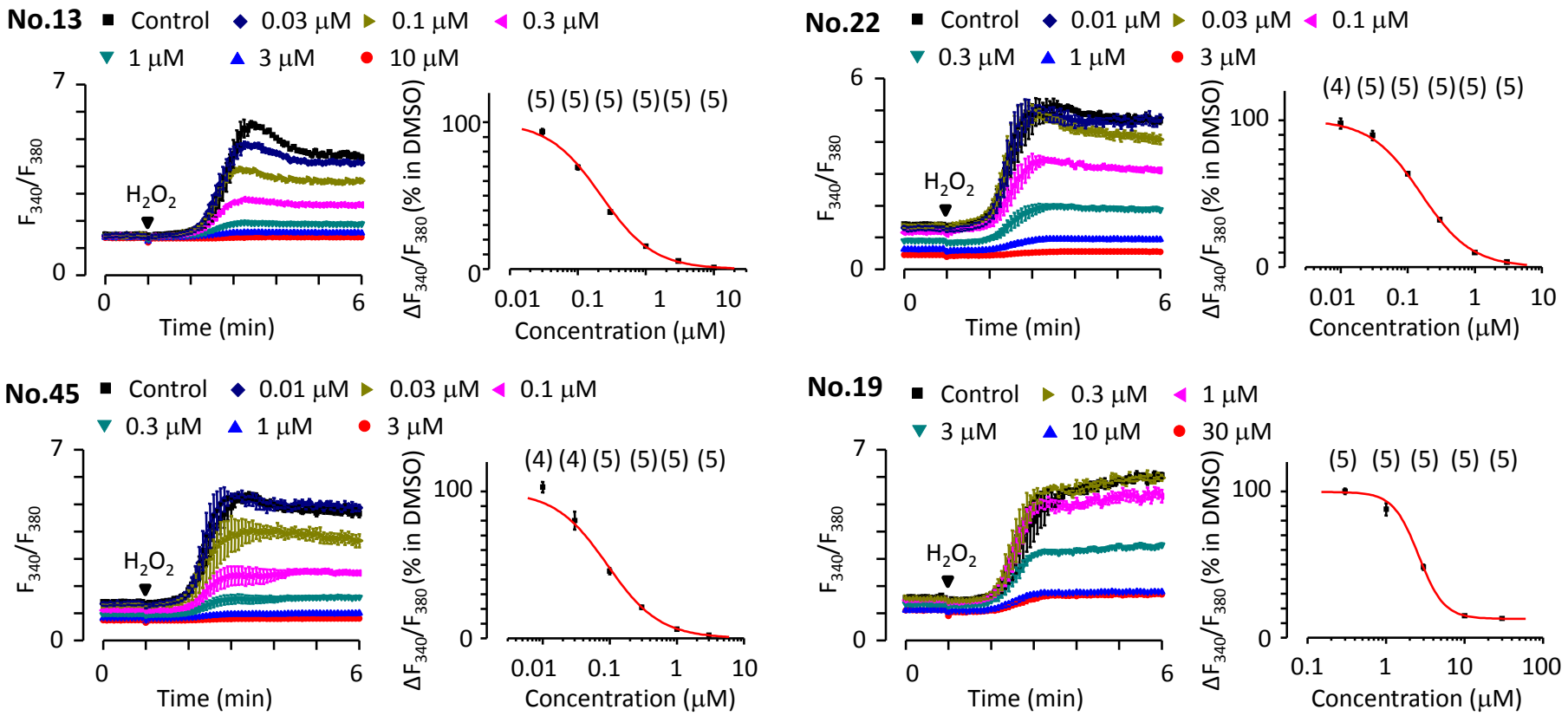

Figure 4.5 Concentration-dependent inhibition of H_2O_2-induced increases in the $[Ca^{2+}]_c$

For each compound are shown the time courses of the concentration-dependent effects on H_2O_2-induced Ca^{2+} response (*left*) and the concentration-inhibition relationship curve (*right*) in tetracycline-induced hTRPM2-expressing HEK293 cells using Flex-station. The red lines represent the fitting curves to Hill equation. Cells were pre-treated with SBS containing DMSO at related concentrations (black square) or the indicated compound at different concentrations (indicated by the symbols on the top of each panel) for 30 min, and then exposed to 1 mM H_2O_2 for 5 min. The numbers of wells examined for each compound are indicated in parenthesis.

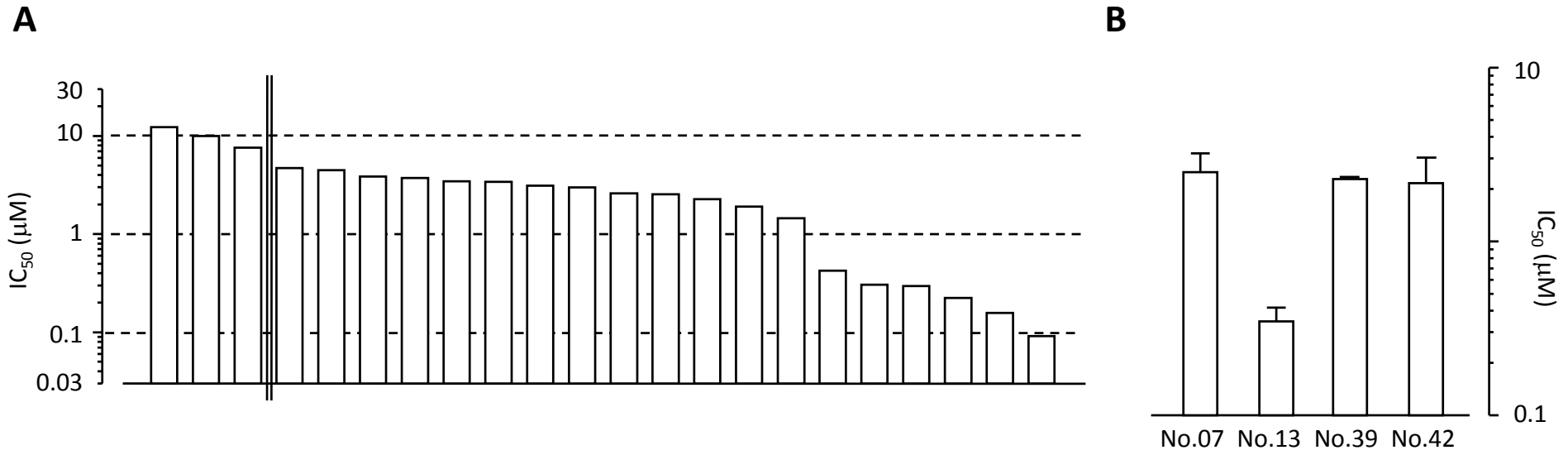

Figure 4.6 IC_{50} values of the tested compounds inhibiting H_2O_2-induced increases in the $[Ca^{2+}]_c$

A, summary of the IC_{50}s of compound tested in Fig. 4.5. The compounds are arranged according to their IC_{50} in a descending order. The dotted-lines show 5, 10 and 15 μM. The chemicals on the right of the double-line exhibit IC_{50}s lower than 5 μM. **B**, the mean data of IC_{50}s for compounds No.07, No.13, No.39 and No.42. The data show mean ± sem value from three independent experiments.

TRPM2 channel currents were noticeably various from almost complete abolition (No.07, No.13, No.39, and No.42) to modest inhibition (Fig. 4.8). The mean inhibition by No.07, No.13, No.39 and No.42 was 100% ± 0.6%, 98% ± 0.7%, 97% ± 1.7% and 92% ± 1.8%, respectively. The inhibition by all these four compounds was similar at positive and negative membrane potentials, indicating voltage-independent inhibition (Fig. 4.7B-E). However, there were significant differences in the inhibition kinetics and reversibility among these four compounds. The inhibition by No.07 and No.42 (Fig. 4.7B and Fig. 4.7C) was similar; the inhibition was relatively fast, with $\tau_{90\%}$ of 77.0 ± 39.5 s and 121.3 ± 38,3 s, respectively (Fig. 4.8C). The inhibitions by No.07 and No.42 were substantially reversible (75.3% ± 13.6% and 81.2% ± 4.3%, respectively) (Fig. 4.8B). In contrast, the inhibition by No.39 (Fig. 4.7D) was quick, with $\tau_{90\%}$ of 32.5 ± 6.0 s, but the recovery from the inhibition was slow, and only partial current (31.2% ± 7.2%) recovered after washout for 5 min. The inhibition by No.13 (Fig. 4.7E) was also slow, with $\tau_{90\%}$ of (196.4 ± 45.8 s) (Fig. 4.8C) and virtually irreversible (1.3% ± 1.0%) (Fig. 4.8B). I repeated the above-described Flex-station experiments for No.07, No.13 and No.39 and No.42. The results from three independent experiments (Fig. 4.6B) confirm the potency of inhibiting the hTRPM2 channels, with mean IC_{50} values of 0.35 ± 0.07 μM, 2.5 ± 0.7 μM, 2.3 ± 0.06 μM and 2.3 ± 0.9 μM, for N0.13, No.07, No.39 and No.42, respectively. Of notice, the IC_{50} of No.13 was nearly 10-fold lower than that of No.07, No.42 and No.39, indicating that this compound is more potent than the other three (Fig. 4.6B).

Taken together, the results from the Flex-station and patch-clamp recording show that No.07, No.42, No.13 and No.39 are potent TRPM2 channel inhibitors and particularly No.13 is the first compound to be identified so far that inhibits the hTRPM2 channel with a submicromolar potency.

4.2.4 Derivatives of No.13 and No.07

Thirteen compounds, eleven of which are structurally related to No.13 and two to No.07 were synthesized by Dr. Foster's group to better understand the structure-activity relationship of No.13 and No.07 compounds. The key structural characteristics of these derivative compounds are highlighted in Fig. 4.9, with an exception of CG-050, a derivative of No. 07 whose structure has not been fully determined.

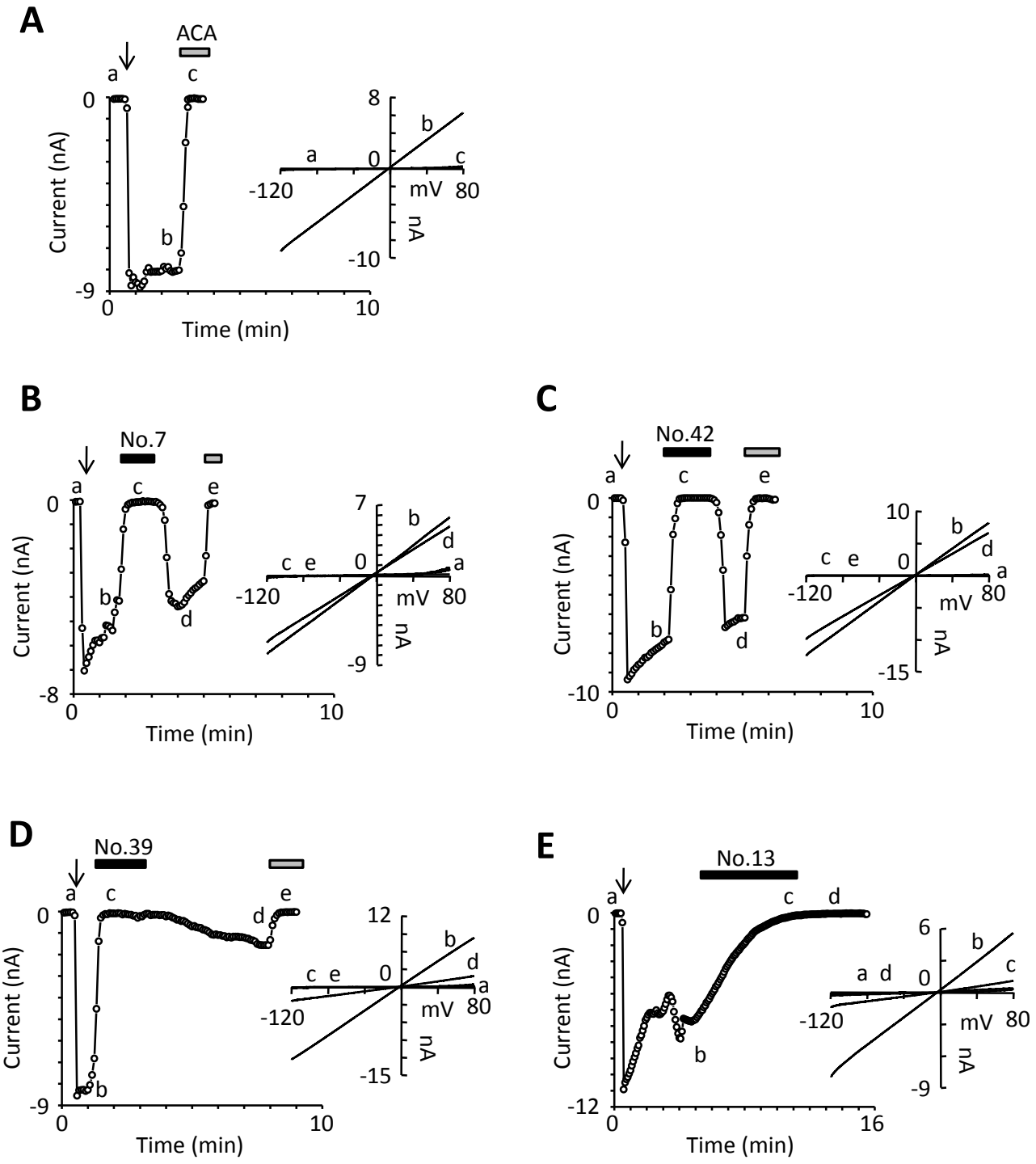
A
ACA
a
c
0
-9
Current (nA)
b
0
10
Time (min)
8
b
a
0
c
-120
mV
80
nA
-10
B
No.7
a
c
e
0
-8
b
d
Current (nA)
0
10
Time (min)
7
b
d
c e
0
a
-120
mV
80
nA
-9
C
No.42
a
c
e
0
-10
b
d
Current (nA)
0
10
Time (min)
10
b
d
c e
0
a
-120
mV
80
nA
-15
D
No.39
a
c
e
0
d
-9
b
Current (nA)
0
10
Time (min)
12
b
d
c e
0
a
-120
mV
80
nA
-15
E
No.13
a
c
d
0
-12
b
Current (nA)
0
16
Time (min)
6
b
c
a d
0
-120
mV
80
nA
-9

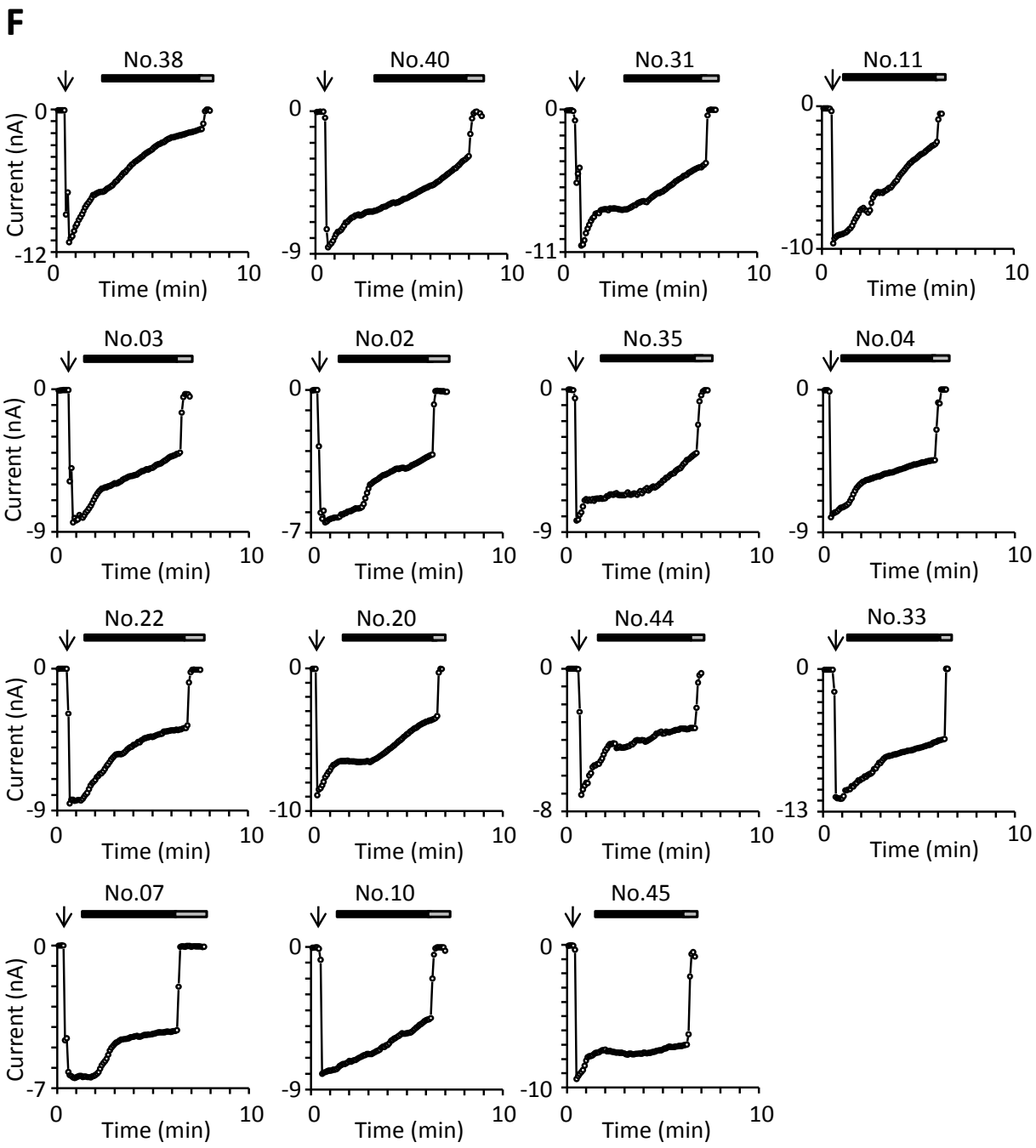

Figure 4.7 Effects of tested compounds on ADPR-induced TRPM2 channels currents

A-E, representative recordings of 1 mM ADPR-induced currents before and after application of 20 μM ACA (**A**) or 10 μM No.07, No.42, No.39 and No.13 (**B-E**) at−80 mV (*left*) and I–V relationship curves (*right*) in tetracycline-induced hTRPM2-expressing HEK293 cells using whole-cell patch clamp recording. The chemicals were washed for up to 5 min after maximum inhibition was observed. **F**, representative recordings for ADPR-induced currents before and after application of each indicated compounds at 10 μM. The TRPM2 channel currents were verified by the complete inhibition by application of 20 μM ACA (grey bar).

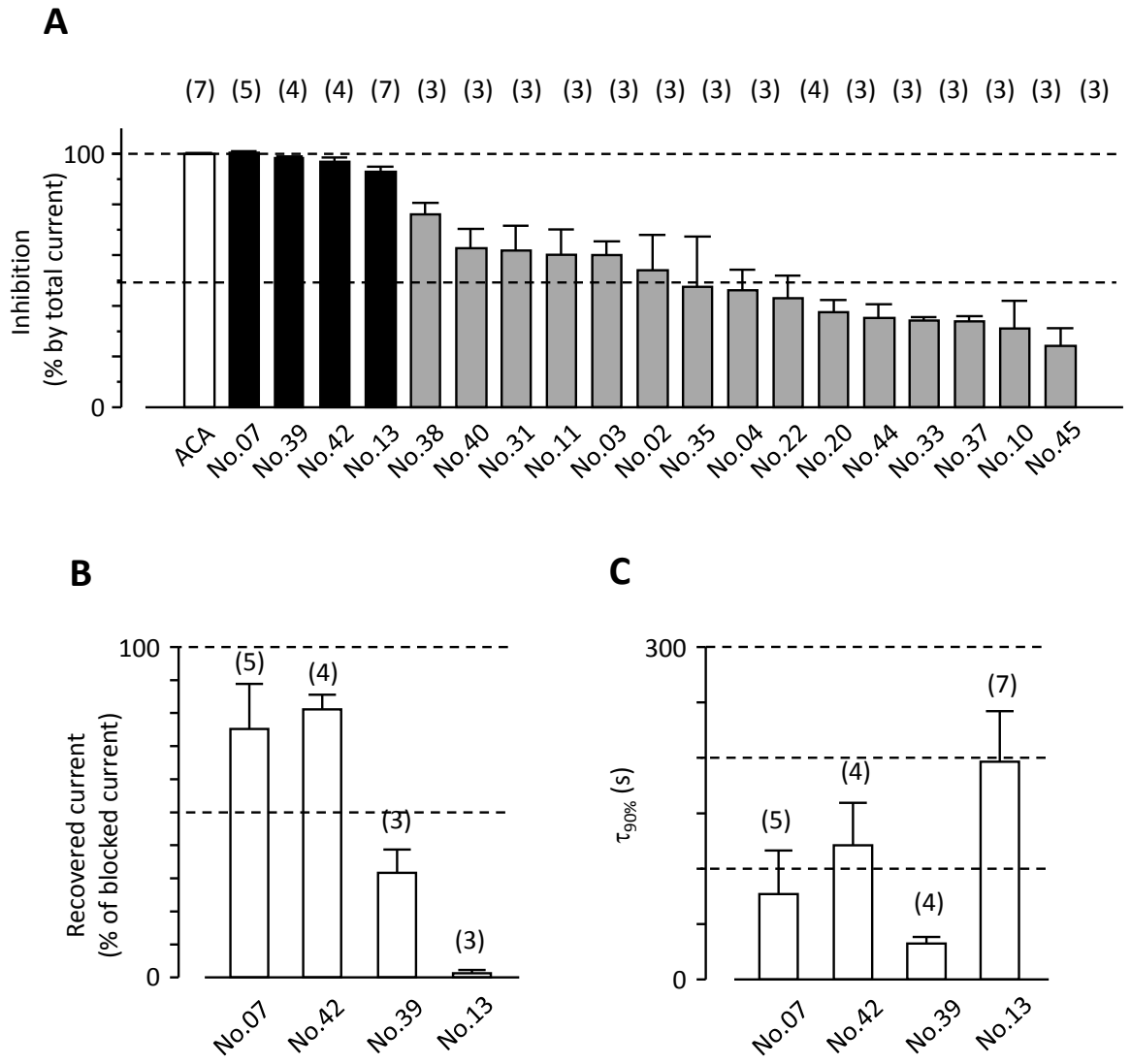

Figure 4.8 Inhibition of ADPR-induced whole cell currents by tested compounds

A, summary of the inhibition of 1 mM ADPR-induced whole cell currents by 20 μM ACA (open bar) and 10 μM indicated compounds, which almost completely (black bar) or partially (grey bar) blocked ADPR-induced currents in tetracycline-induced hTRPM2-expressing HEK293 cells. The compounds are arranged according to their percentage of inhibition in a descending order. **B**, the mean currents recovered after removal of the compounds for up to 5 min. **C**, the mean data of $\tau_{90\%}$. The data show mean ± sem; numbers of cells examined for each compound are indicated in parenthesis.

The eleven No.13 derivatives can be divided into 4 groups, according to the substitutions introduced to the three key functional groups (R1, R2 and R3) in the molecule of No.13. CG-046 and CG-045, belong to group 1. In these two compounds, R2 is substituted by 2-methylalkoxy-3-hydroxyphenyland; meanwhile the cyclopentyl in R1 in No.13 is changed into cyclohexyl and butly in CG-046 and CG-045, respectively. Group 2 has five members, CG-006, CG-013, CG-036, CG-008 andCG-040, in which R1 is all replaced by amino, and R2 is substituted by functional groups detailed in Fig. 4.9A. There are three compounds in group3, CG-011, CG-038 and CG-039; R1 is replaced by neobutly, and R2 is substituted by 3-pyridyl, 2-thienyl and 2-Furyl in CG-011, CG-038 and CG-039, respectively. CG-001 is the only one member belonging to group 4. In this compound, R1, R2 and R3 are changed into phenylmethylamino, 2-methylalkoxy-3-hydroxyphenyl and pyridobismdiazole, respectively.

Using Flex-station and hTRPM2-expressing HEK293 cells, the inhibition of H_2O_2-induced increases in the $[Ca^{2+}]_c$ by these compounds at more than six different concentrations were determined. The time courses and the concentration-inhibition relationship curves are shown in Fig. 4.10A, and the derived IC_{50}s are summarized in Fig. 4.11. GC-045 and GC-046, the compounds in group1, exhibited slightly lower IC_{50}s than that of No.13 (Fig. 4.11). The IC_{50}s of the five compounds in group 2 were similar or 10-fold lower than that of No.13 (Fig. 4.11). In addition, almost no or little change in the basal $[Ca^{2+}]_c$ was induced by any of these compounds (Fig. 4.10A). Among the compounds in group 3, the IC_{50}s of GC-038 and GC-039 were similar to that of No.13 and no change in the basal $[Ca^{2+}]_c$ by these two compounds was observed, and, by contrast, the potency of GC-011 was strongly reduced and this compound significantly altered the basal $[Ca^{2+}]_c$ (Fig. 4.10A and Fig. 4.11). Finally, compound GC-001 exhibited a reduced potency and introduced dramatic change in the basal $[Ca^{2+}]_c$ (Fig. 4.10A and Fig. 4.11).

The results of examining CG-058 and CG-050, the derivatives of No.07, are shown in Fig. 4.10B and Fig. 4.11. CG-058, exhibited about 10-fold higher potency than No. 07, with an IC_{50} of 0.17 μM. CG-050 was ineffective, resulting in partial inhibition of H_2O_2-induced increases in the $[Ca^{2+}]_c$ at even 30 μM, and thus, its IC_{50} of CG-050 was not calculated.

Taken together, four derivatives of No.13 (CG-013, CG-036, CG-040 and CG-008) and one of No.07 (CG-058) show improved potency than their parent compounds.

A

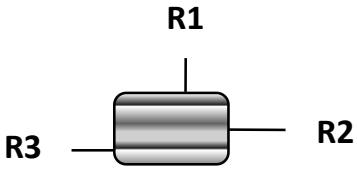

Chemicals	R1	R2	R3
No.13	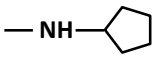	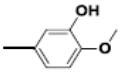	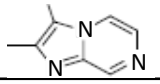
Group 1			
CG-046	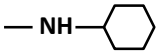	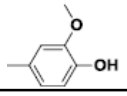	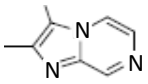
CG-045	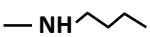	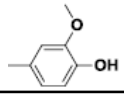	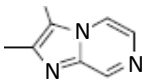
Group 2			
CG-006	—NH_2	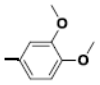	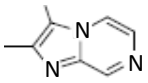
CG-013	—NH_2	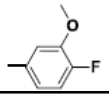	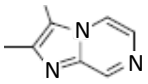
CG-036	—NH_2	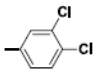	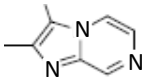
CG-008	—NH_2		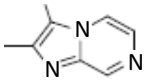
CG-040	—NH_2	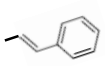	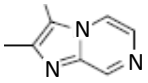
Group 3			
CG-011	—NH	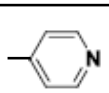	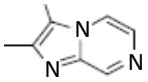
CG-038	—NH		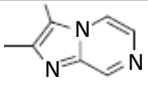
CG-039	—NH		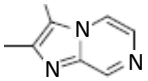
Group 4			
CG-001	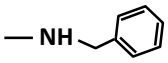	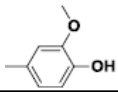	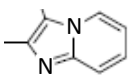

B

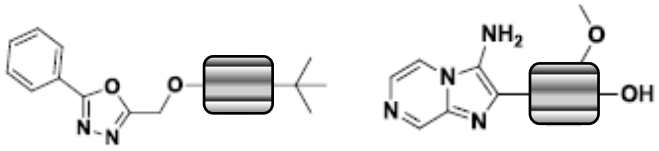

No.07 CG-058

Figure 4.9 The chemical structures of the derivatives of compounds No.13 and No.07

A, the derivatives of compound No.13, which are divided into four groups depending on the substitutions introduced to the R1, R2 and R3 functional groups in No.13. **B**, compound No.07 and its derivative CG-058. The boxes represent the parts of No.13 and No.07 whose structures are not revealed.

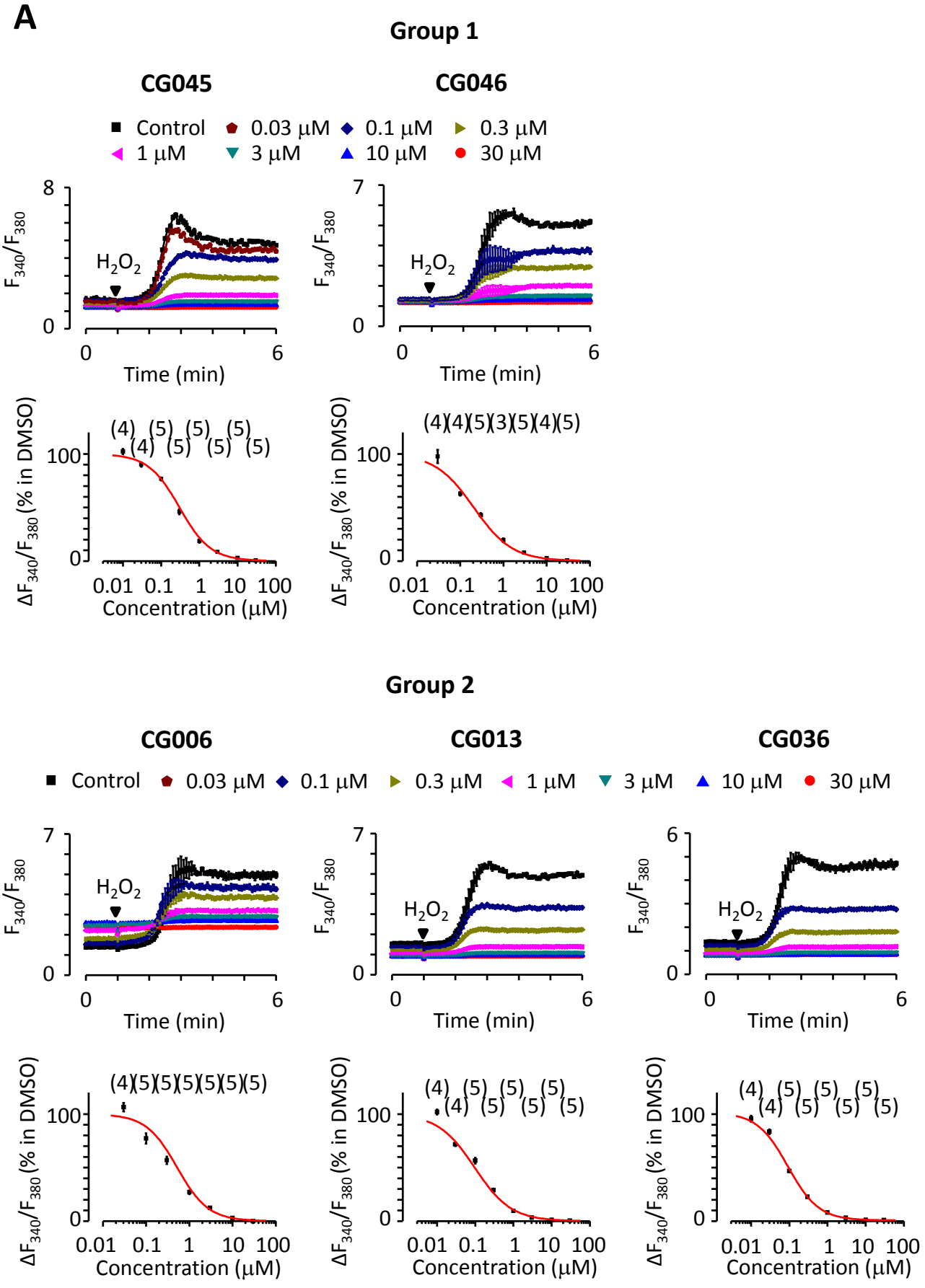
A
Group 1
CG045
CG046
Control
0.03 μM
0.1 μM
0.3 μM
1 μM
3 μM
10 μM
30 μM
F340/F380
H2O2
Time (min)
ΔF340/F380 (% in DMSO)
Concentration (μM)
(4) (5) (5) (5)
(4) (5) (5) (5)
(4)(4)(5)(3)(5)(4)(5)
Group 2
CG006
CG013
CG036
(4)(5)(5)(5)(5)(5)(5)

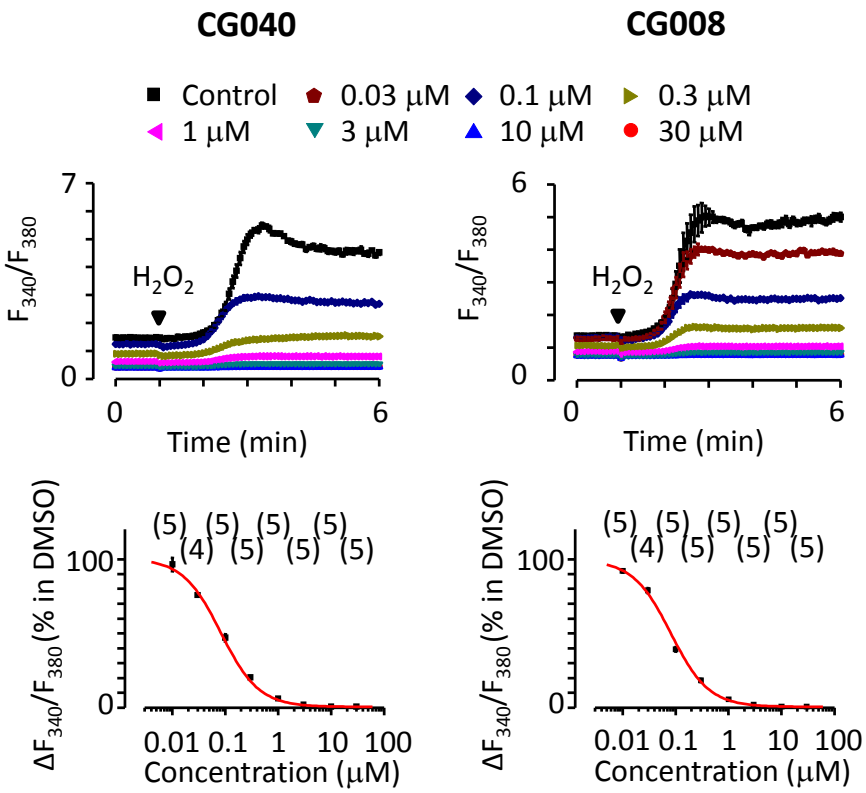
CG040
CG008
Control
0.03 μM
0.1 μM
0.3 μM
1 μM
3 μM
10 μM
30 μM
F340/F380
H2O2
Time (min)
ΔF340/F380 (% in DMSO)
(5) (5) (5) (5)
(4) (5) (5) (5)
Concentration (μM)

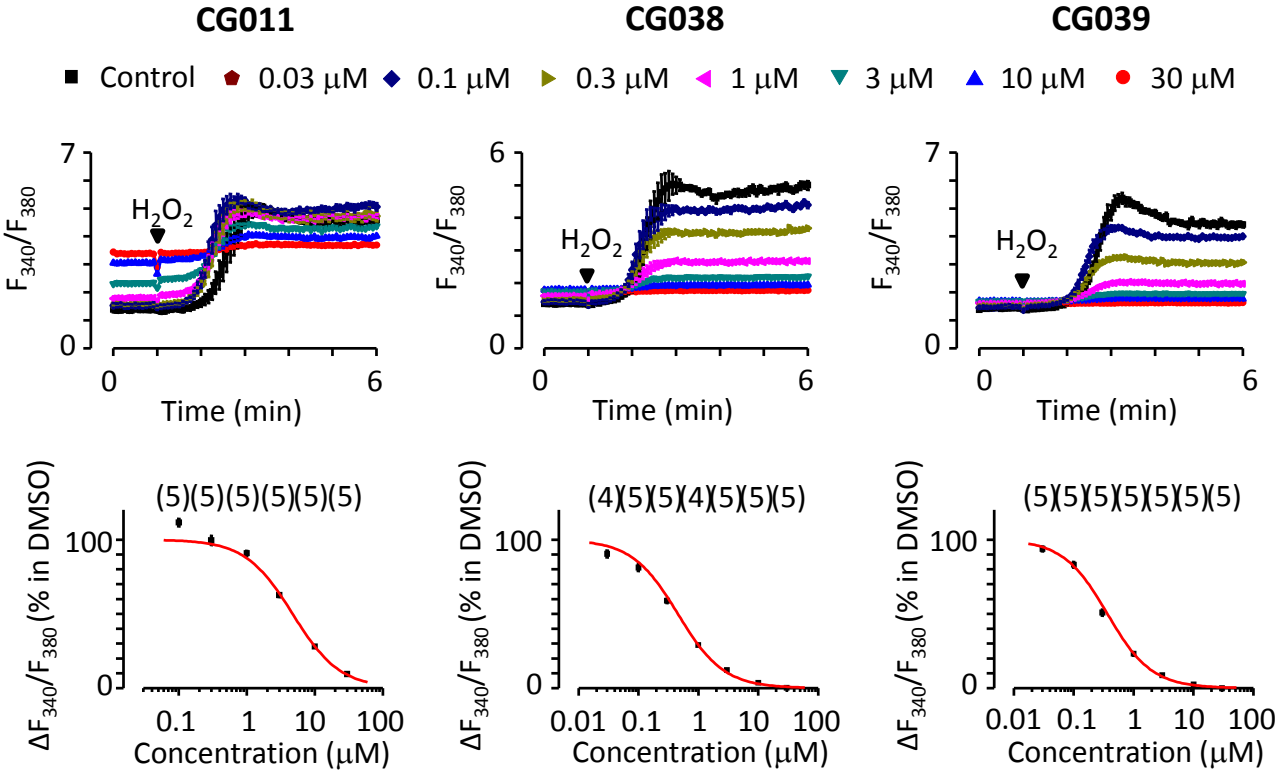
Group 3
CG011
CG038
CG039
Control
0.03 μM
0.1 μM
0.3 μM
1 μM
3 μM
10 μM
30 μM
F340/F380
H2O2
Time (min)
ΔF340/F380 (% in DMSO)
(5)(5)(5)(5)(5)(5)
(4)(5)(5)(4)(5)(5)(5)
(5)(5)(5)(5)(5)(5)(5)
Concentration (μM)

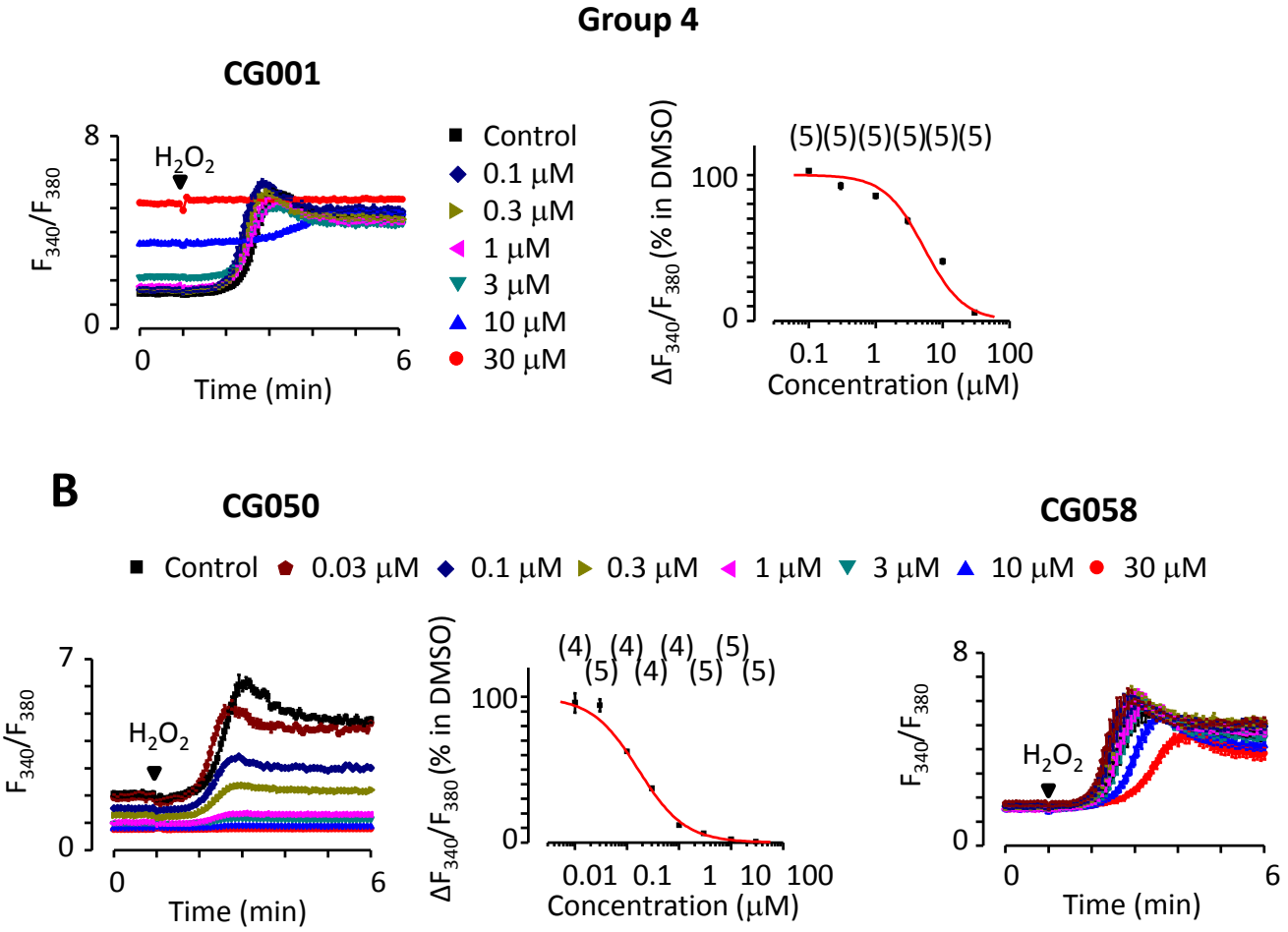

Figure 4.10 The effects of the derivatives of No.13 and No.07 on H_2O_2-induced Ca^{2+} responses

A-B, H_2O_2-induced Ca^{2+} responses in the absence (control) and presence of indicated concentrations of compounds related to No.13 (**A**) or No.07 (**B**) in tetracycline-induced hTRPM2-expressing HEK293 cells using Flex-station. The concentration-inhibition relationship curves are shown at the bottom or on the right for each chemical and the solid red lines represent the fitting curves to the Hill equation to calculate the IC_{50}. The cells were pre-treated with SBS with DMSO at related concentrations (black square) or compounds at indicated concentrations (shown by the symbols) for 30 min, and then exposed to 1 mM H_2O_2 for 5 min. The derivatives of No.13 are divided into 4 groups depending on their chemical structures (shown in Fig. 4.9). The numbers of wells examined for each compound are indicated in parenthesis

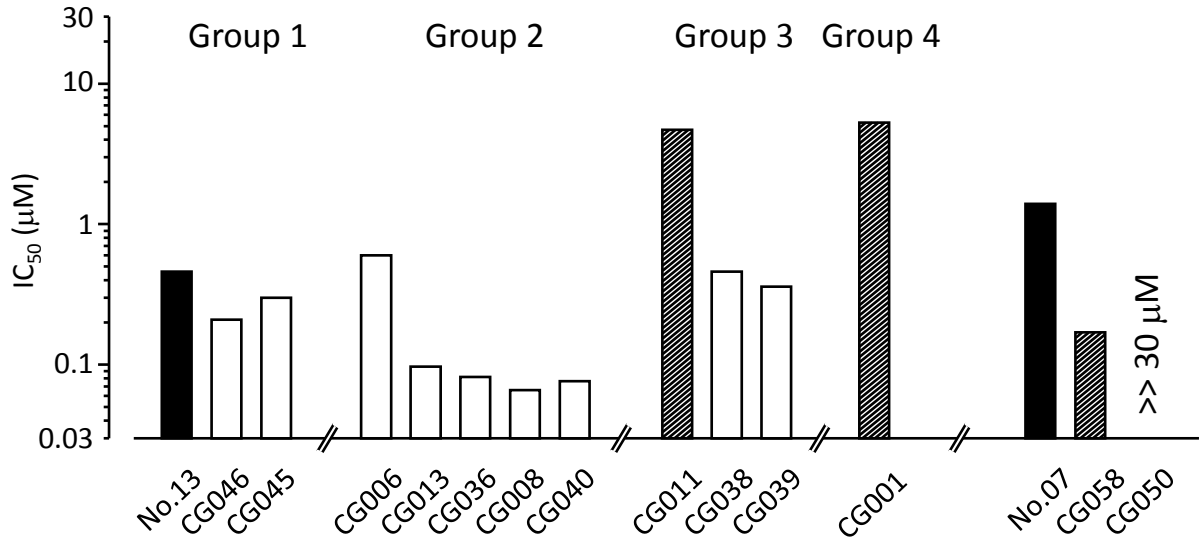

Figure 4.11 The IC_{50} values of the derivatives of compounds No.13 and No.07 in inhibiting H_2O_2-induced increases in the $[Ca^{2+}]_c$

Summary of the IC_{50}s of No.13 and No.07 derivatives, obtained from the data shown in Fig. 4.10. The derivatives of No.13 are divided into four groups according to their R1, R2 and R3 groups (details shown in figure 4.9). The oblique line bars show that the compounds alone cause a substantial change in the basal $[Ca^{2+}]_c$ at high concentrations.

4.3 Discussion

In the study described in this chapter, the effects of 48 hit compounds initially identified by screening chemical libraries on H_2O_2-induced increases in the $[Ca^{2+}]_c$ in tetracycline-induced hTRPM2-expressing HEK293 cells were investigated using Flex-station. Nineteen compounds exhibited potency with IC_{50}s lower than 5 μM. Subsequent experiments using whole-cell patch clamp recordings showed that four compounds, No.13, No.07, No.39 and No.42, almost completely abolished ADPR-induced currents, confirming them as novel TRPM2 channel inhibitors. Furthermore, the results in the structure-activity study demonstrated that four derivatives of No.13, CG-013, CG-036, CG-040 and CG-008, and one of No.07, CG-058, exhibited improved potency.

In whole-cell patch clamp recordings, No.07, No.42, No.13 and No.39 were verified to be the TRPM2 channel inhibitors, since they almost abolished ADPR-induced currents (Fig. 4.7 and Fig. 4.8). The inhibition by all of these four compounds was voltage-independent. However, they exhibited remarkable differences in the inhibition kinetics and reversibility. The inhibitions by No.07, No.39 and No.42 were relatively fast, in contrast to the slow and gradual inhibition caused by No.13. In addition, the inhibitions by No.07 and No.42 were almost completely reversible, whereas No.39 exhibited very slow and partially reversible inhibition, and No.13 induced a completely irreversible blockage. The mechanism underlying their actions is different but remains currently unclear. Further investigations are required.

The effects of eleven derivatives of No.13 and two of No.07 on H_2O_2-induced increases in the $[Ca^{2+}]_c$ were examined to better understand the structure-activity relationships (Fig. 4.9 and Fig. 4.10). The derivatives of No.13 resulted from substitutions of the key functional groups R1, R2 and R3 and accordingly are divided into four groups (Fig. 4.9). Group 1 containing two compounds, CG-046 and CG-045. In these two compounds, R2 is substituted by 2-methylalkoxy-3-hydroxyphenyl and, and the cyclopentyl in R1 in No.13 is changed into cyclohexyl and butly in CG-046 and CG-045, respectively (Fig. 4.9A). According to the data showing in Fig. 4.11, the IC_{50}s of CG-046 and CG-045 are only slightly smaller than that of No.13, implying that such substitutions in these two compounds have no or little effect on the potency of the inhibition of H_2O_2-induced Ca^{2+}-response. The results for group 2 are most remarkable. Group 2 has five members, CG-006, CG-013, CG-036, CG-008 and CG-040,

in which R1 is all replaced by amino, and R2 is substituted by functional groups detailed in Fig. 4.9A. Four of the five compounds, CG-013, CG-036, CG-040 and CG-008, exhibited a potency that is about 10-fold higher than that of No.13 (Fig 4.11). These results suggest an important role of amino in determining the potency. The other compound, CG-006, which also contains an amino in R1, exhibited a similar IC_{50} as that of No.13. This could result from the strongly reduction of the potency by the R2 in CG-006. The results for group 3 are also informative. There are three compounds in group 3, CG-011, CG-038 and CG-039; R1 is replaced by neobutly, and R2 is substituted by 3-pyridyl, 2-thienyl and 2-Furyl in CG-011, CG-038 and CG-039, respectively (Fig 4.9). GC-038 and GC-039 showed similar IC_{50}s as that of No.13, whereas GC-011 exhibited strongly reduced potency (Fig 4.10 and 4.11). These results imply the expectation of the improved potency by five-member rings, such as thienyl and furyl in GC-038 and GC-039, but not by the six-member rings, such as the pyridyl in GC-011. CG-001 is the sole member in group 4. In this compound, R1, R2 and R3 are changed into phenylmethylamino, 2-methylalkoxy-3-hydroxyphenyl and pyridobismdiazole, respectively (Fig. 4.9). CG-001 exhibited a dramatically reduced potency and significant alteration in the basal $[Ca^{2+}]_c$ (Fig. 4.11). CG-046 and CG-045, the compounds in group 1, which contain the same R2 as in CG-001, exhibit similar effect as compound No.13 on H_2O_2-induced Ca^{2+} response. Thus, the phenylmethylamino in R1 and/or pyridobismdiazole R3 could crucially result in the reduction of the inhibition potency of the compound. CG-058, the derivative of No.07, exhibited approximately 10-fold higher potency than No. 07 (Fig. 4.11). As the structure showing in Fig. 4.9B, there is a large difference between the molecular structure of CG-058 and No.13. Thus, the contribution of the functional groups in CG-001 to the inhibition potency is complex or difficult to determine. The other derivative of No. 07, CG-050, was ineffective, since it induced only partial inhibition of H_2O_2-induced increases in the $[Ca^{2+}]_c$ at even 30 μM (Fig. 4.11). However, the structure-activity cannot be analyzed, because structure of CG-050 has not been fully determined. Due to time constraint, patch clamp recording was not carried out to examine the effects of these compounds on ADPR-induced currents. Thus it is still unknown whether these derivatives can directly inhibit the TRPM2 channels as No.13. Such studies are clearly needed to better understand whether and how these compounds inhibit the hTRPM2 channels.

Besides No.07, No.42, No.13 and No.39, 15 other compounds also strongly and potently inhibited H_2O_2-induced increases in the $[Ca^{2+}]_c$ (Fig 4.6), but they induced partial inhibition of ADPR-induced currents (Fig. 4.8). From the discussion described in the introduction chapter (see section 1.2.5.1.6), H_2O_2 activates the TRPM2 channels via several indirect signalling mechanisms including ADPR generation that requires activation of PARP and CD38. For these compounds that completely blocked the H_2O_2-induced increases in the $[Ca^{2+}]_c$ but not ADPR-induced currents, it is possible that they inhibit the signalling pathways engaged in generation of ADPR, as well as directly blocking the TRPM2 channels.

The results from measuring H_2O_2-induced increases in the $[Ca^{2+}]_c$ using Fura-2 as the Ca^{2+} indicator show noticeable or even dramatic changes the basal value of F_{340}/F_{380} by some of the compounds (Figs. 4.1 to 4.6). The exact causes are not known and there are several factors that may contribute to such changes. For example, the changes may result from alterations in properties of Fura-2, include the binding affinity for Ca^{2+} and the excitation or emission fluorescence. It also remains possible that the compounds changing the basal intracellular $[Ca^{2+}]_c$ by altering the cell membrane permeability to increase or reduce Ca^{2+} influx or intracellular Ca^{2+} release or Ca^{2+} refilling in the ER.

In summary, the results in this chapter identified four structurally different compounds as four novel TRPM2 channel inhibitors with a potency of micromolar or submicromolar concentrations. Furthermore, five structurally related compounds exhibited improved potency. Further experiments are required to determine whether these novel inhibitors are specific to the TRPM2 channels and can inhibit the TRPM2 channels in different species such as human and rodent TRPM2 channels. If this is the case, it is interesting to know whether they provide the eagerly-awaited pharmacological tools to study TRPM2-mediated physiological or pathological functions and new therapeutics treating TRPM2-related diseases.

Chapter 5

Expression of TRPM2 channels and their role in H_2O_2-induced Ca^{2+} responses and cell death in macrophage cells

5.1 Introduction

As described in the introduction chapter (section 1.2.5.1.6, section 1.2.7 and section 1.2.8), ROS and particularly H_2O_2 are important signalling molecules that trigger or regulate a diversity of physiological functions and also potent agents causing oxidative damages associated with inflammatory, cardiovascular, and neurodegenerative diseases (Forman et al., 2010, Forstermann, 2008, Giorgio et al., 2007). One common cellular event during the early responses to ROS is the increase in the $[Ca^{2+}]_c$, resulting from activation of not yet fully characterized mechanisms leading to intracellular Ca^{2+} release and, more frequently and significantly, extracellular Ca^{2+} influx.

Macrophages play an important role in both innate and adaptive immunity. Their functions are to engulf and digest the pathogens and cellular debris, and generate ROS or pro-inflammatory mediators, such as IL-1β and TNF-α, to regulate the immunity response (Giorgio et al., 2007, Kashio et al., 2012, Kregel and Zhang, 2007). It is well-known that ROS produced by macrophages can in turn stimulate ROS generation to form positive feedback, and furthermore, regulates macrophage cell functions in diverse physiological and pathological conditions (Kregel and Zhang, 2007).

As also discussed in the introduction chapter (section 1.2.5.1.6), TRPM2 channel exhibits substantial Ca^{2+} permeability (Togashi et al., 2006, Xia et al., 2008) and strong sensitivity to activation by ROS via mechanisms primarily promoting ADPR generation (Perraud et al., 2005), and thus it is an important cellular sensor for ROS (Jiang et al., 2010). The most well-known role of TRPM2 channel is to mediate ROS-induced cell death, as shown in pancreatic β-cell (Lange et al., 2009), monocytic cell (Hara et al., 2002) and endothelial cell (Sun et al., 2012). Nonetheless, the exact contribution of the TRPM2 channel in ROS-induced cell death has not been well defined. It is known that ROS regulates macrophage functions by inducing cell death via stimulating PARP (Xu et al., 2006). PARP activation and ADPR generation represent the primary mechanism underlying activation of the TRPM2 channel by ROS (Buelow et al., 2008, Perraud et al., 2005). However, the role of the TRPM2 channel in mediating ROS-induced macrophage cell death is largely unclear.

In addition, many previous studies have reported that TRPM2 channel function as a cell surface Ca^{2+}-permeable cationic channel. However, it has become increasingly clear that TRPM2 also form as a Ca^{2+} channel mediating intracellular Ca^{2+} release. This study aimed to investigate the contribution and mechanisms of the TRPM2 channels in macrophage cells in mediating Ca^{2+} signaling and cell death during early response to biologically relevant concentrations of H_2O_2. Our results show that the TRPM2 channels operate as a cell surface Ca^{2+}-permeable channel that mediates Ca^{2+} influx and constitutes the principal Ca^{2+} signaling mechanism but has a limited, albeit significant, role in cell death.

5.2 Results

5.2.1 Optimization of the working conditions of anti-TRPM2 antibody

Immunofluorescent confocal imaging together with anti-TRPM2 antibody was used to investigate whether TRPM2 proteins were expressed in macrophage cells. I started with optimization of the working conditions of antibodies in HEK293 cells transiently transfected with the TRPM2 plasmid, because only a subset of HEK293 cells were expected to be transfected and thus express the TRPM2 proteins. Only these cells should exhibit immunofluorescence. I initially kept the dilution of primary anti-TRPM2 antibody at 1:500, and used 1:200 to 1:1000 dilution of the FITC-conjugated secondary antibody. In the second set of experiments, I used a dilution of the secondary antibody at 1:400 or 1:600, and the dilution of primary antibody changed from 1:200 to 1:1000. As the results shown in Fig. 5.1, under the conditions where the primary and secondary antibody antibodies were 1:500-1:1000 and 1:400-1:600, respectively, only some cells exhibited strong immunofluorescence, whereas the other cells were weakly or not stained. Thus, these antibody dilutions were used in the following immunofluorescent confocal imaging to examine TRPM2 protein expression in macrophage cells.

5.2.2 TRPM2 protein expression in RAW264.7, PMA-differentiated THP-1 and peritoneal macrophage cells

In order to examine TRPM2 protein expression in macrophage cells, I used two macrophage cell lines, RAW264.7 cells and PMA-differentiated THP-1 cells, two widely-used model cells to study macrophage cell functions and also peritoneal macrophage cells isolated from WT ($TRPM2^{+/+}$) mice. Representative images are shown in Fig. 5.2. There was strong immunostanining of RAW264.7, PMA-differentiated THP-1 and peritoneal macrophage cells (*up*), whereas no staining was observed in the absence of the primary antibody in all these three types of cells (*bottom*). These results suggest that the TRPM2 proteins are expressed in these three types of macrophage cells.

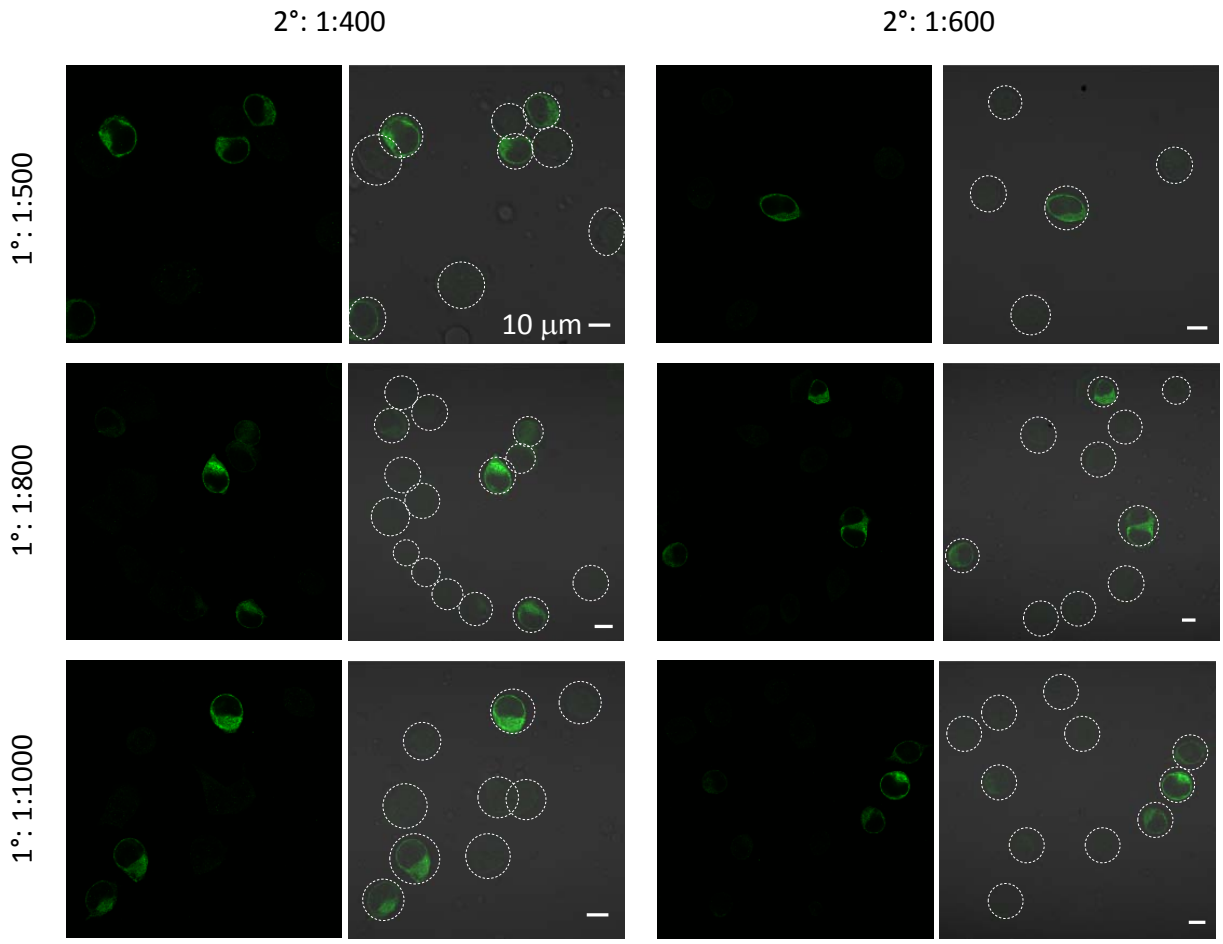

Figure 5.1 Immunofluorescence in HEK293 cells transiently transfected with hTRPM2 plasmid

Representative confocal images of HEK293 cells transiently transfected with hTRPM2 plasmid and stained with primary anti-TRPM2 antibody produced in rabbit (1°) and secondary goat anti-rabbit IgG-FITC antibody (2°). The dilution of primary and secondary antibody is indicated on the left and top, respectively. For each condition, the *left* image presents the fluorescence; *right* image presents the merged image of fluorescence and white light, with the cells highlighted in white dotted circles.

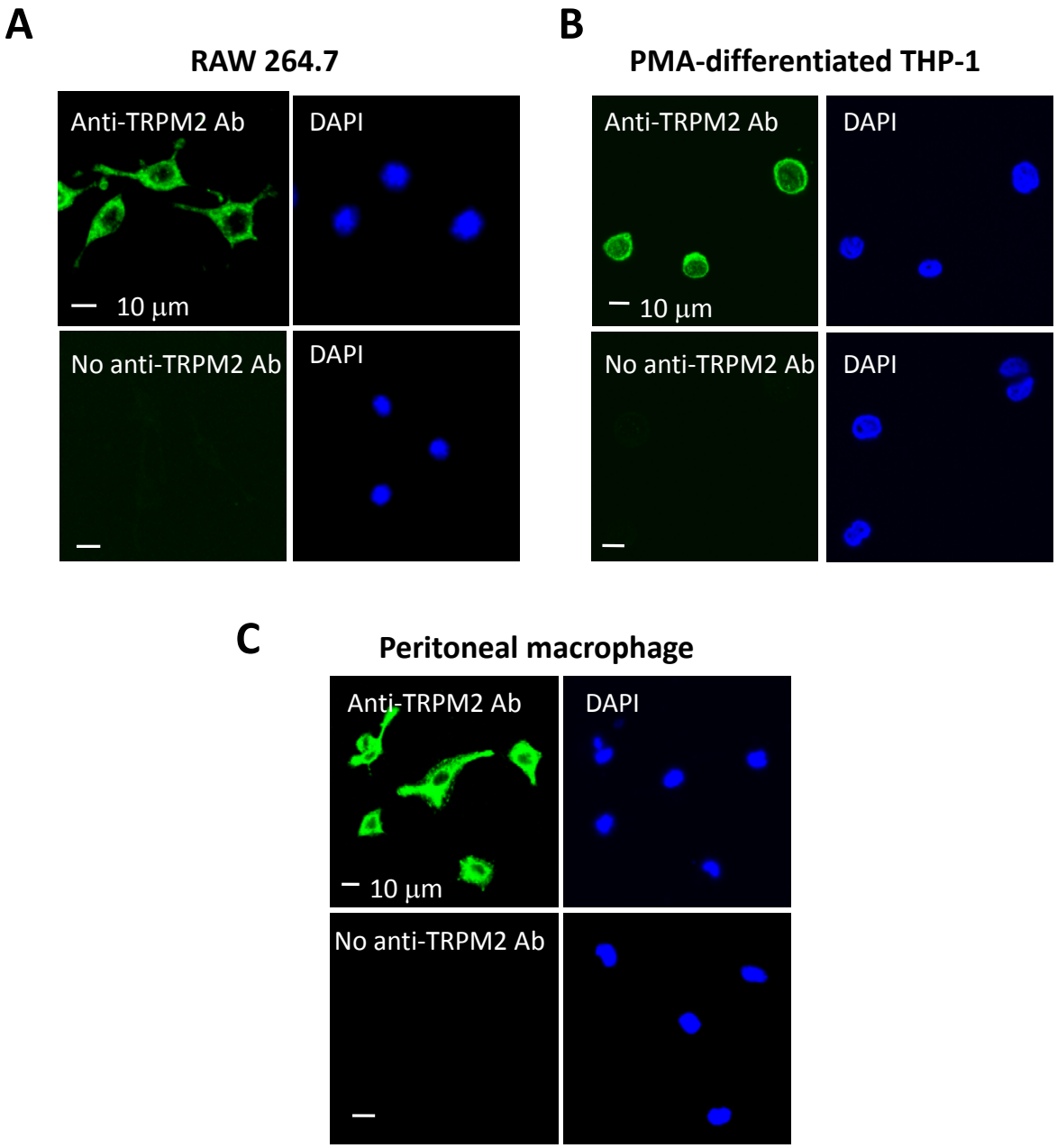

Figure 5.2 Expression of TRPM2 proteins in macrophage cells

A-C, representative immunofluorescent confocal images of RAW264.7 (**A**), PMA-differentiated THP-1 (**B**) or peritoneal macrophage cells (**C**). Cells were treated with (*up*) or without (*bottom*) of primary anti-TRPM2 antibody produced in rabbit. Each panel is accompanied with a DAPI-stained image showing all the cells (*right*). Similar results were obtained in at least three independent experiments.

5.2.3 H_2O_2-induced increases in the $[Ca^{2+}]_c$ in macrophage cells mainly result from extracellular Ca^{2+} influx and are temperature dependent

I next used single cell imaging to monitor the changes in the $[Ca^{2+}]_c$ in response to H_2O_2 at biologically relevant concentrations (300 μM) in RAW264.7, PMA-differentiated THP-1 and peritoneal macrophage cells. H_2O_2 at 300 μM induced consistent and robust increases in the $[Ca^{2+}]_c$. Noticeably, in peritoneal macrophage cells, the H_2O_2-induced Ca^{2+} responses occurred relatively earlier and took relatively shorter times to reach the maximum than in RAW264.7 and PMA-differentiated THP-1 cells (Fig. 5.3). In some experiments, cells were exposed to 5 μM ionomycin in the end of experimentation to compare H_2O_2-induced Ca^{2+} responses to ionomycin-induced Ca^{2+} responses.

To further elaborate whether the H_2O_2-induced increases in the $[Ca^{2+}]_c$ resulted from extracellular Ca^{2+} influx, intracellular Ca^{2+} release, or both, I used the Ca^{2+} add-back protocols (Fig. 5.4). In extracellular Ca^{2+}-free solution, H_2O_2 induced no consistent change in the $[Ca^{2+}]_c$. Subsequent introduction of extracellular Ca^{2+}-containing solution resulted in no or a small increase in the $[Ca^{2+}]_c$ in cells that were not treated with H_2O_2, and in striking contrast, there were rapid and robust increases in the $[Ca^{2+}]_c$ in H_2O_2-treated cells (Fig. 5.4). These results taken together indicate that extracellular Ca^{2+} influx represents a predominant mechanism for elevation in the $[Ca^{2+}]_c$ in macrophage cells in response to H_2O_2.

The TRPM2 channel is thermosensitive with an activation threshold of ≥40°C but can open at body temperature in the presence of subthreshold concentrations of agonist (Kashio et al., 2012, Togashi et al., 2006). We were interested in whether H_2O_2-induced increases in the $[Ca^{2+}]_c$ in macrophage cells were enhanced at body temperature. For this, I compared H_2O_2-induced Ca^{2+} responses at room temperature (22°C) and body temperature (37°C). As shown in Fig. 5.5, H_2O_2-induced increases in the $[Ca^{2+}]_c$ at 37°C were significantly greater than at 22°C. Furthermore, such responses were strongly inhibited by pre-treatment with 10 μM PJ-34, a PARP inhibitor known to block H_2O_2-induced TRPM2 channel activation (Fonfria et al., 2004). These results are consistent with the idea that the TRPM2 channel has a role in mediating H_2O_2-induced Ca^{2+} influx.

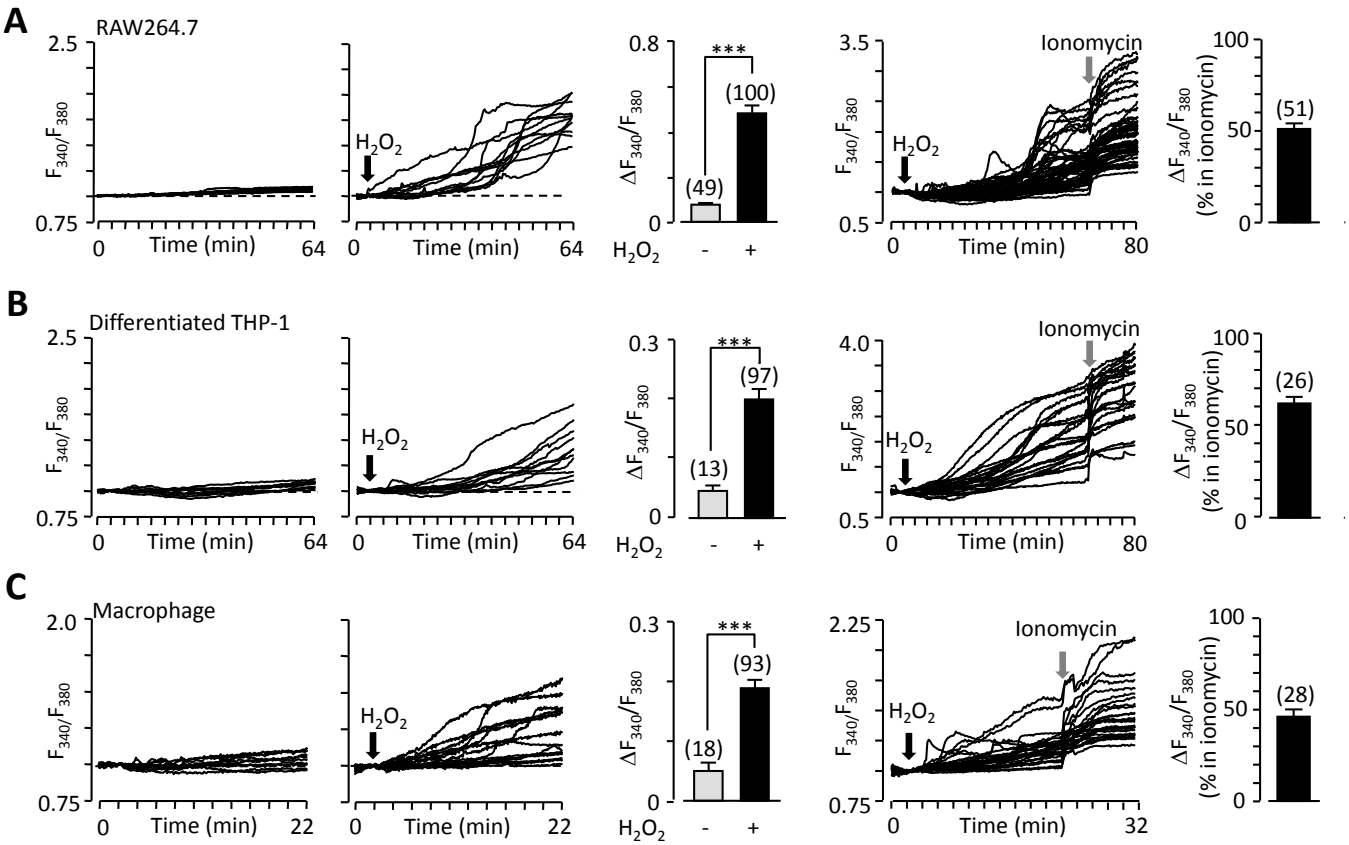

Figure 5.3 Exposure to H_2O_2 elevates the $[Ca^{2+}]_c$ in macrophage cells.

Left, representative single cell Ca^{2+} imaging recordings of individual RAW264.7 (**A**), PMA-differentiated THP-1 cells (**B**), and peritoneal macrophage (**C**) in response to perfusion with extracellular Ca^{2+}-containing solution alone or containing 300 μM H_2O_2. *Right*, cells were exposed to 300 μM H_2O_2 and then 5 μM ionomycin in extracellular Ca^{2+}-containing solutions. Dashed lines indicate the basal $[Ca^{2+}]_c$ when the solution perfusion started. Mean changes in the F_{340}/F_{380} under indicated conditions are also shown. Number of cells examined in each case is shown in parentheses. ***P < 0.005, significant difference.

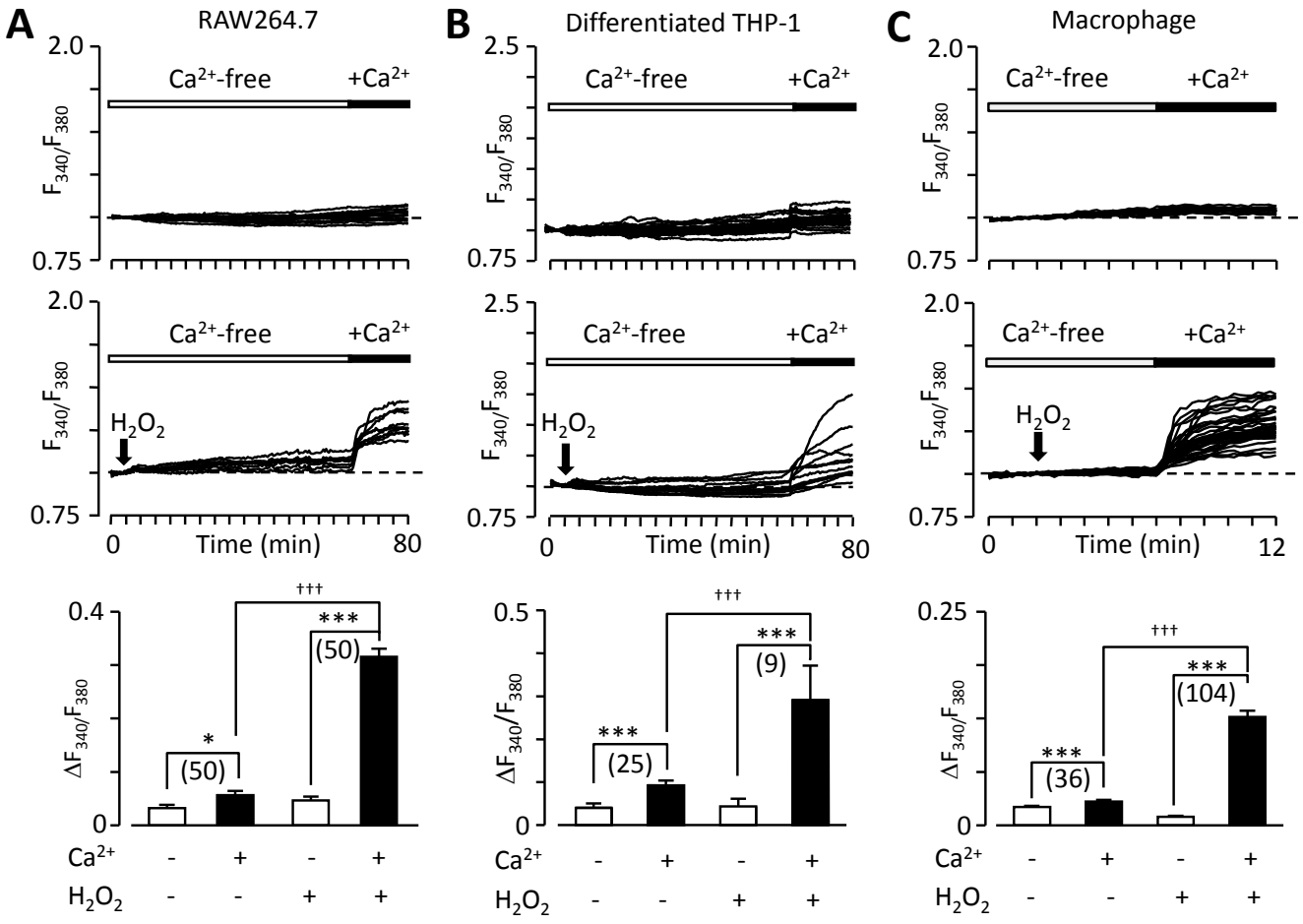

Figure 5.4 H_2O_2-induced increases in the $[Ca^{2+}]_c$ in macrophage cells primarily results from extracellular Ca^{2+} influx.

Representative single cell Ca^{2+} imaging recordings of individual RAW264.7 (**A**), PMA-differentiated THP-1 cells (**B**), and peritoneal macrophage (**C**) in response to perfusion initially with extracellular Ca^{2+}-free solutions and then with extracellular Ca^{2+}-containing solutions without (*top*) and with 300 μM H_2O_2 (*bottom*). Dashed lines indicate the basal $[Ca^{2+}]_c$ when the solution perfusion started. The mean changes in the F_{340}/F_{380} during the periods in extracellular Ca^{2+}-free solutions (-) or Ca^{2+}-containing solutions (+), respectively, are shown. The number of cells examined in each case is shown in parentheses. ***p < 0.05 and ***p < 0.005, significant difference between cells in the absence and presence of extracellular Ca^{2+}. †††p < 0.005, significant difference between untreated and H_2O_2-treated cells in the presence of extracellular Ca^{2+}.

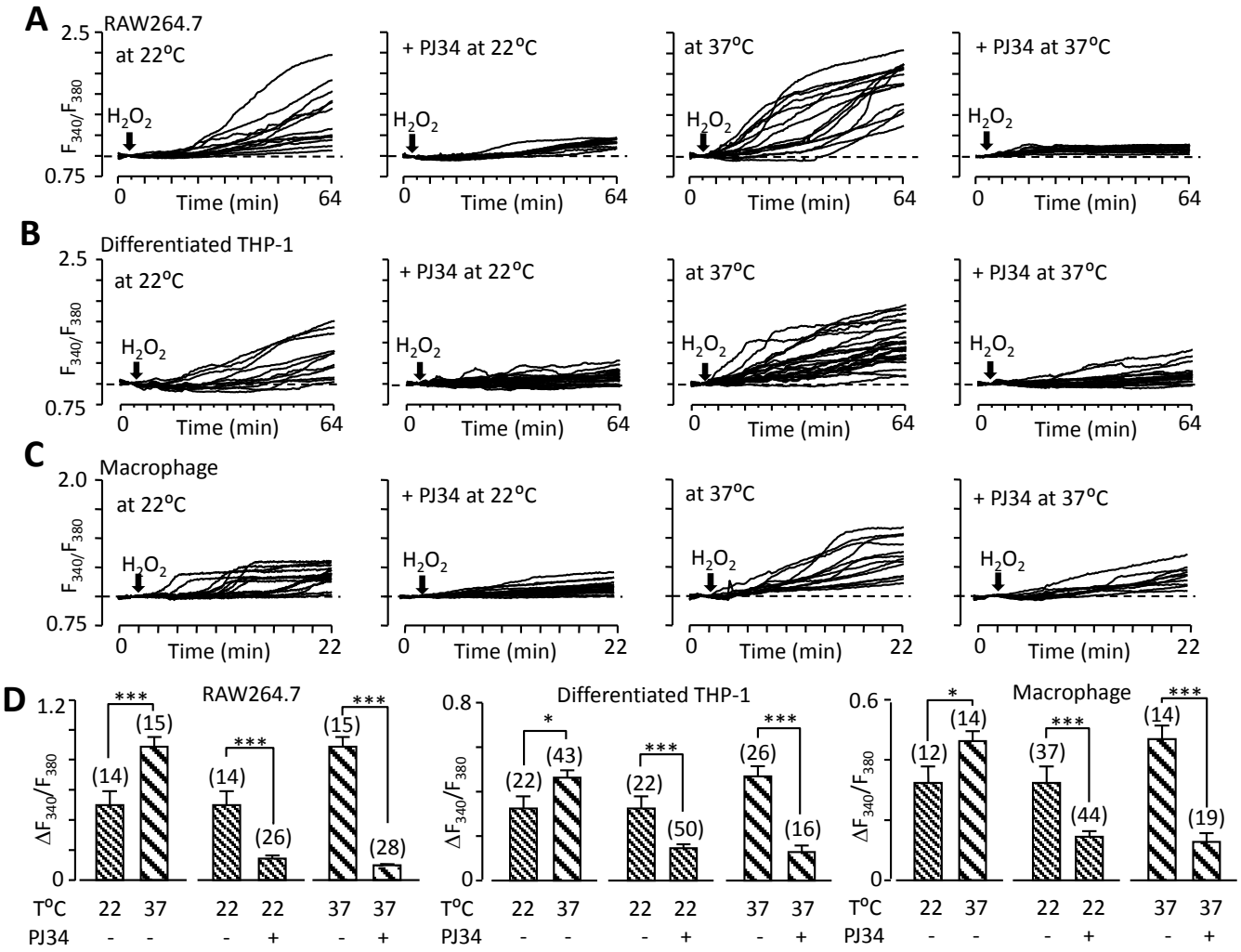

Figure 5.5 H_2O_2-induced increases in the $[Ca^{2+}]_c$ in macrophage cells are facilitated by body temperature.

A–C, representative single cell Ca^{2+} imaging recordings of individual RAW264.7 (**A**), PMA-differentiated THP-1 (**B**), and peritoneal macrophage cells (**C**) in response to perfusion with 300 μM H_2O_2 in extracellular Ca^{2+}-containing solution at room temperature (*left*) and body temperature (*right*). In each set of experiments, some cells were pre-treated with 10 μM PJ-34. Dashed lines indicate the basal $[Ca^{2+}]_c$ when the solution perfusion started. **D**, mean changes in the F_{340}/F_{380} in experiments shown in **A–C**, Number of cells examined in each case is shown in parentheses. *P < 0.05 and ***P < 0.005, significant difference for the paired groups.

5.2.4 Functional expression of the TRPM2 channels in peritoneal macrophage cells

Currently, there is no TRPM2 specific inhibitor as described above (see section 1.2.5.2). To provide defining evidence for the role of the TRPM2 channels in H_2O_2-induced Ca^{2+} responses in macrophage cells, I introduced the generated transgenic mice, $TRPM2^{-/-}$ mice, which were well established in our lab previously. These mice express mutated alleles without exons 17 and 18 of the *Trpm2* gene. The remaining sequence encodes an internally deleted TRPM2 protein lacking the Leu-843-Met-931 segment.

I compared H_2O_2-induced increases in the $[Ca^{2+}]_c$ in macrophage cells from the WT ($TRPM2^{+/+}$) and $TRPM2^{-/-}$ mice. The H_2O_2-induced increases in the $[Ca^{2+}]_c$ in extracellular Ca^{2+}-containing solution observed in the $TRPM2^{+/+}$ macrophage cells were completely lost in the $TRPM2^{-/-}$ macrophage cells (Fig. 5.6A and C), clearly indicating a key role for the TRPM2 channels in mediating H_2O_2-evoked increases in the $[Ca^{2+}]_c$ in macrophage cells. Similarly, the Ca^{2+} add-back experiments showed that H_2O_2 induced no change in the $[Ca^{2+}]_c$ in the $TRPM2^{-/-}$ macrophage cells in the absence or presence of extracellular Ca^{2+} (Fig. 5.6 B).

These results clearly indicate that TRPM2-mediated Ca^{2+} influx is the principal Ca^{2+} signalling mechanism in macrophage cells during initial response to H_2O_2. I was interested in whether PJ-34-insensitive PARPs contributed to H_2O_2-induced TRPM2 channel activation. For this, I compared H_2O_2-induced increases in the $[Ca^{2+}]_c$ in the $TRPM2^{+/+}$ and $TRPM2^{-/-}$ macrophage cells that were pre-treated with PJ-34. The residual H_2O_2-induced Ca^{2+} responses in the WT macrophage cells were significantly higher than those in the $TRPM2^{-/-}$ macrophage cells (Fig. 5.6 B and E), suggesting involvement of the PJ-34-insensitive PARPs in H_2O_2-induced TRPM2 channel activation.

Then, I investigated ADPR-induced currents in peritoneal macrophages from $TRPM2^{+/+}$ and $TRPM2^{-/-}$ mice. According to the results showing in Fig. 5.7, there were large ADPR-induced currents with a typical linear current-voltage relationship for the TRPM2 channels in macrophage cells isolated from the $TRPM2^{+/+}$ mice but such currents were undetectable in macrophage cells from the $TRPM2^{-/-}$ mice. Taken together with the study in single cell Ca^{2+} imaging, the data provide compelling evidence for functional expression of the TRPM2 channels in macrophage cells.

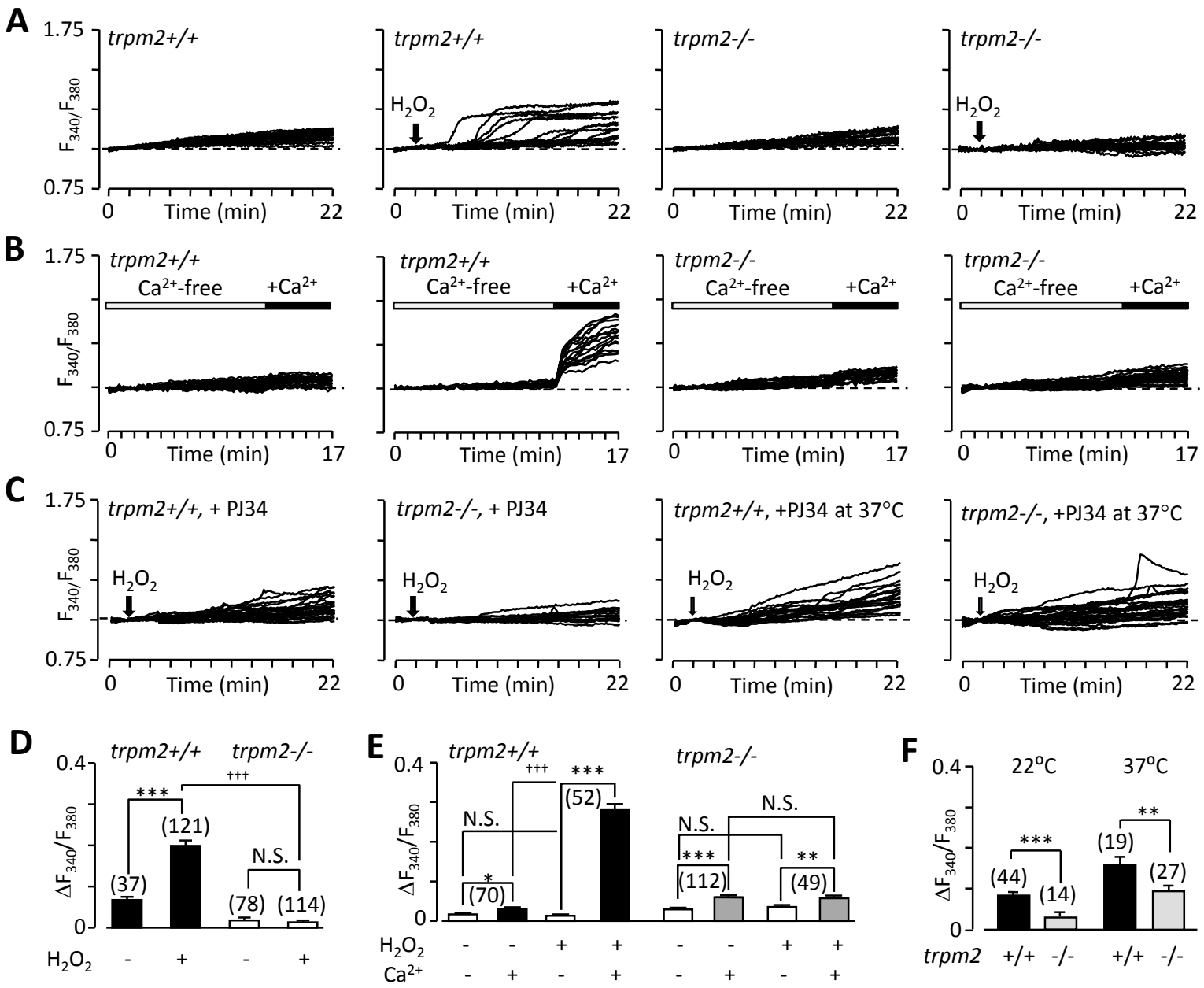
A
1.75
0.75
F340/F380
trpm2+/+
trpm2+/+
trpm2-/-
trpm2-/-
H2O2
0
Time (min)
22
B
trpm2+/+
trpm2+/+
trpm2-/-
trpm2-/-
Ca2+-free
+Ca2+
17
C
trpm2+/+, + PJ34
trpm2-/-, + PJ34
trpm2+/+, +PJ34 at 37°C
trpm2-/-, +PJ34 at 37°C
D
ΔF340/F380
0.4
0
trpm2+/+
trpm2-/-
***
†††
(37)
(121)
N.S.
(78)
(114)
H2O2
E
trpm2+/+
trpm2-/-
(70)
(52)
(112)
(49)
*
**
Ca2+
F
22°C
37°C
(44)
(14)
(19)
(27)
trpm2
+/+
-/-

Figure 5.6 TRPM2 channel mediates H_2O_2-induced extracellular Ca^{2+} influx in macrophage cells.

A and **B**, representative single cell Ca^{2+} imaging recordings of individual peritoneal macrophage from $trpm2^{+/+}$ and $trpm2^{-/-}$ mice, in responses to perfusion with extracellular Ca^{2+}-containing solution alone or containing 300 μM H_2O_2 (**A**) or perfusion initially with extracellular Ca^{2+}-free solutions and then with extracellular Ca^{2+}-containing solutions alone or containing 300 μM H_2O_2 (**B**). **C,** representative single cell Ca^{2+} imaging recordings of individual peritoneal macrophage from $TRPM2^{+/+}$ and $TRPM2^{-/-}$ mice in response to perfusion with 300 μM H_2O_2 in extracellular Ca^{2+}-containing solutions at room temperature and body temperature. All cells were pre-treated with 10 μM PJ-34. Dashed lines indicate the basal $[Ca^{2+}]_c$ when the solution perfusion started. **D–F**, mean changes in the F_{340}/F_{380} under indicated conditions. Number of cells examined in each case is shown in parentheses. **p < 0.01, ***p < 0.005, and †††p < 0.005, significant difference for the paired groups; N.S., no significant difference for the paired groups.

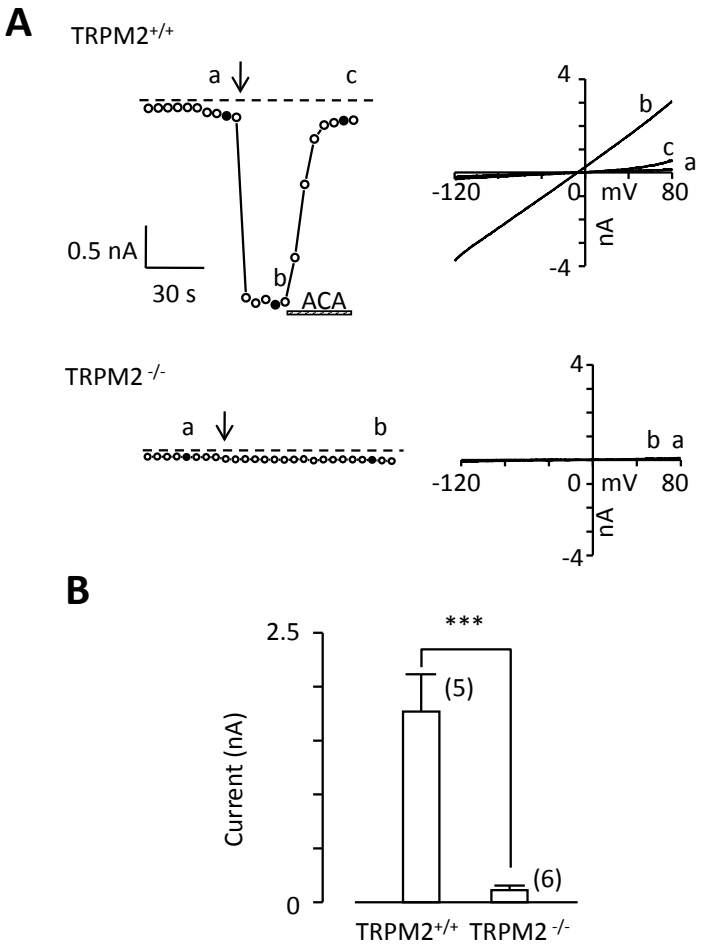

Figure 5.7 ADPR-induced whole-cell currents in peritoneal macrophage cells

A, representative ADPR-induced whole cell currents at −80 mV (*left*) and the I–V relationship curves (*right*) in peritoneal macrophage isolated from TRPM2$^{+/+}$ (*top*) and TRPM2$^{-/-}$ (*bottom*) mice. 1-s voltage ramps from −120 mV to +80 mV were applied in every 5 s. Arrows indicate the transition from cell-attached to whole cell configurations. 20 μM ACA was used to inhibit ADPR-induced currents. **B**, mean ADPR-induced peak currents at -80 mV. The data show mean ± sem; the number of cells examined in each case is shown in parentheses. *** p< 0.005 significant difference for the paired groups

5.2.5 Contribution of TRPM2 channel in H_2O_2-induced cell death in RAW264.7, PMA-differentiated THP-1 and peritoneal macrophage cells

I conducted the XTT cell viability assay to determine macrophage cell death during early response to H_2O_2. Exposure to 300 μM H_2O_2 for up to 60 min reduced the cell viability by 50% for RAW264.7 and peritoneal macrophage cells, and 20–30% for PMA-differentiated THP-1 cells, indicating significant macrophage cell death (Fig. 5.8). The relatively high viability for PMA-differentiated THP-1cells may relate to the difference in the level of macrophage differentiation and the resistance to cell death (Daigneault et al., 2010). The effects of exposure to H_2O_2 on the cell viability exhibited strong dependence on duration (5–60 min) and H_2O_2concentration (30 μM-3 mM) (Fig. 5.8).

To gain an insight into the role of the PARP activation and potential TRPM2 channel activation in H_2O_2-induced cell death, I examined the effect of PJ-34. Pretreatment with PJ-34 resulted in a general tendency of attenuating H_2O_2-induced reduction in the cell viability; the protective effect varied among the three cell types and reached statistical significance for exposures with relatively long durations or to relatively high concentrations of H_2O_2 (denoted by the symbol + in Fig. 5.8). In addition, PJ-34 prevented significant reduction in the viability of RAW264.7 and THP-1 cells by low concentrations of H_2O_2 (30–100 μM; Fig. 5.8). These results support that PARP activation and TRPM2 channel activation contribute to, but are not fully responsible for, macrophage cell death during initial exposure to H_2O_2.

A recent study has shown that the protective effects of PARP inhibition on H_2O_2-induced cardiomyocyte death can arise from TRPM2-independent mechanisms (Yang et al., 2006). To further define the role of the TRPM2 channels in H_2O_2-induced macrophage cell death, I finally compared the effects of H_2O_2 on the viability of $TRPM2^{+/+}$ and $TRPM2^{-/-}$ macrophage cells (Fig. 5.9). The TRPM2 channel deficiency conferred a general and consistent tendency of decreasing H_2O_2-induced reduction in macrophage cell viability; the effects were significant under most of the conditions examined (denoted by the symbol + in Fig. 5.9). The overall protective effects resulting from the genetic ablation of the TRPM2 channel function were similar to but noticeably more salient than those from pre-treatment with PJ-34 (Fig. 5.8); this is not surprising, considering that PJ-34-insensitive PARPs are involved in H_2O_2-induced TRPM2 channel activation (Fig. 5.6). There was a modest but statistically significant

increase in cell viability in response to 30-min exposure to 30 μM H_2O_2 (Fig. 5.9). It was also noted that the reduction in the cell viability by 1-3 mM H_2O_2, which are of less or no biological relevance, remained significantly different in$TRPM2^{+/+}$and $TRPM2^{-/-}$macrophage cells, but the difference diminished (Fig. 5.9), suggesting that the TRPM2 channel has a less or no significant role in macrophage cell death induced by such high concentrations of H_2O_2. There was strong and persistent H_2O_2-induced cell death in cells pre-treated with PJ-34 (Fig. 5.8) or TRPM2 channel-deficient macrophage cells (Fig. 5.9), consistently indicating a limited role for the TRPM2 channel in H_2O_2-inducedcell death in striking contrast with the key role in mediating H_2O_2-induced Ca^{2+} responses.

Cells die through either necrosis or apoptosis. The membrane integrity of necrotic cells is lost, so the trypan blue can enter into the necrotic cells, in contrast to the living and apoptotic cells that cannot be dyed because of the intactness of the cell membrane. Thus, I examined whether the H_2O_2-induced macrophage cell death is due necrosis or apoptosis, using trypan blue exclusion assay. As shown in Fig. 5.10, exposure to 300 μM H_2O_2 for 60 min induced a small necrosis in RAW264.7 cells, PMA-differentiated THP-1 cells and peritoneal macrophage cells. In RAW264.7 and peritoneal macrophage cells, there was substantial necrosis with 32.1% and 36.9% of dye-stained cells, respectively, after exposure to 3 mM H_2O_2 for 60 min. However, necrosis in PMA-differentiated THP-1 cells induced by 3 mM H_2O_2 was very low (5.4%). These results suggested that the macrophage cell death induced by relatively short exposure (≤ 60 min) to H_2O_2 at low concentration (≤300 μM) is mainly due to apoptosis, but not necrosis.

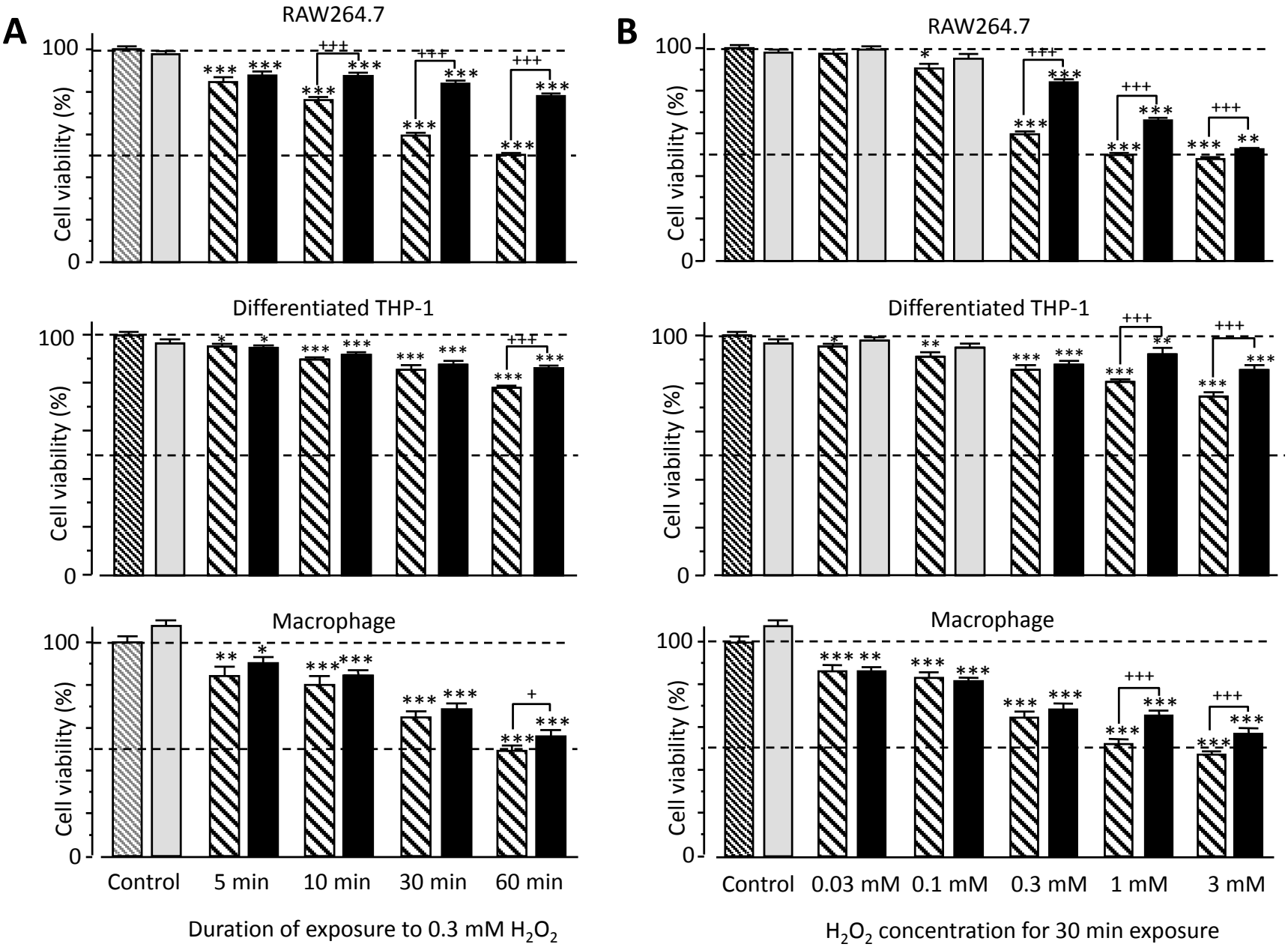
A
RAW264.7
Differentiated THP-1
Macrophage
Cell viability (%)
100
0
Control
5 min
10 min
30 min
60 min
Duration of exposure to 0.3 mM H_2O_2
B
RAW264.7
Differentiated THP-1
Macrophage
Cell viability (%)
100
0
Control
0.03 mM
0.1 mM
0.3 mM
1 mM
3 mM
H_2O_2 concentration for 30 min exposure

Figure 5.8 PJ-34 attenuates H_2O_2-induced reduction in macrophage cell viability.

Summary of the viability of RAW264.7, PMA-differentiated THP-1 and peritoneal macrophage cells after exposure to 300 μM H_2O_2 for indicated durations (**A**) for untreated cell (hatched columns) and cells pre-treated with 10 μM PJ-34 (black columns) or after exposure to indicated H_2O_2 concentrations (**B**) for 30 min for untreated cells (hatched columns) and cells pre-treated with 10 μM PJ-34 (grey and black columns). Dashed lines indicate the 50 and 100% levels. Data were obtained from 18 wells from three independent experiments, and expressed as percentage of the control without PJ-34 treatment. *P < 0.05, **P < 0.01, and ***P < 0.005, denote difference compared with their respective control. Grey bars indicate no difference from the control. †P < 0.05 and †††P < 0.005, denote difference for the paired groups.

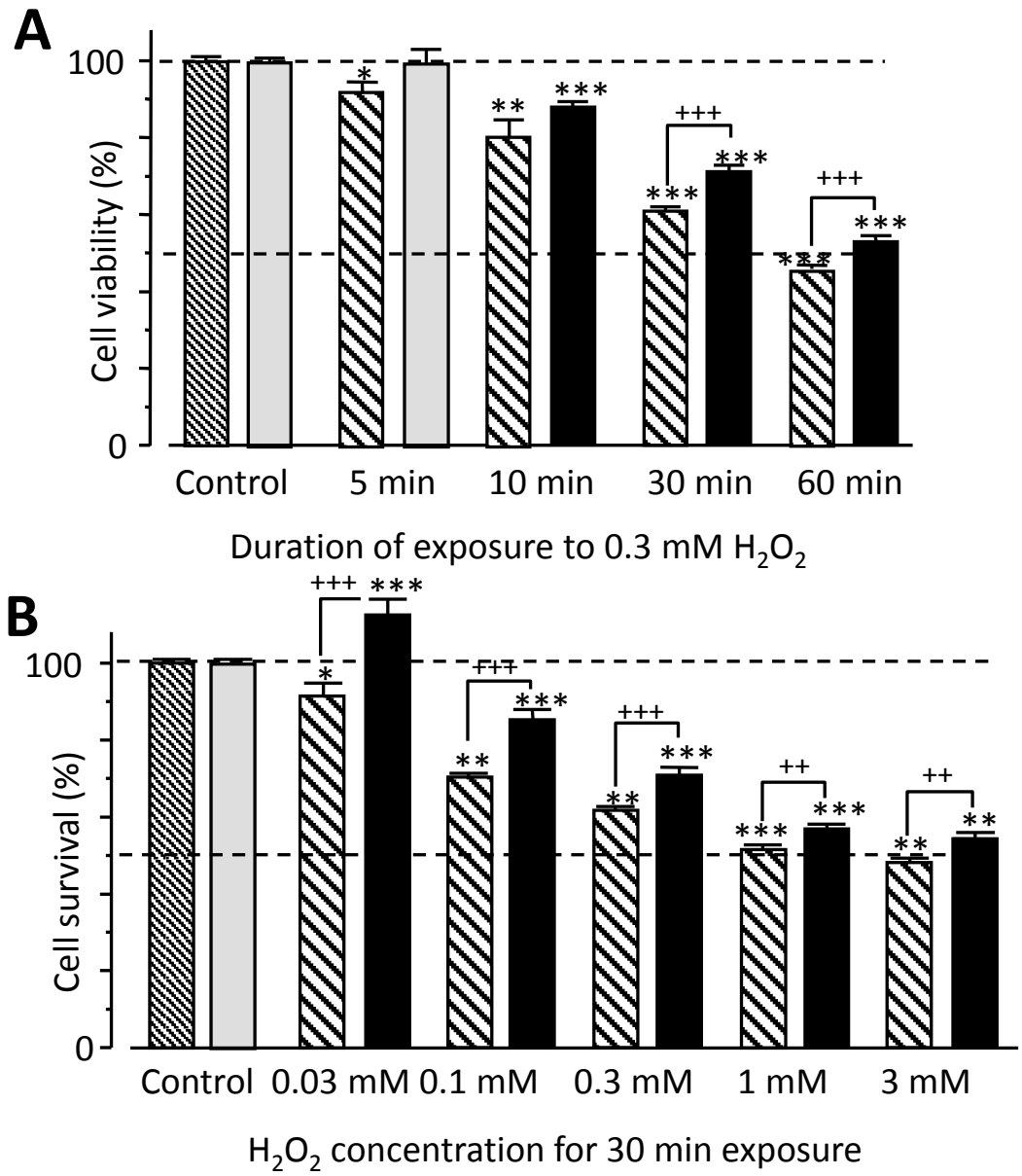

Figure 5.9 TRPM2 deficiency suppresses H_2O_2-induced reduction in macrophage cell viability.

Summary of the viability of macrophage cells from TRPM2$^{+/+}$ (hatched columns) and TRPM2$^{-/-}$ mice (grey and black columns), after exposure to 300 μM H_2O_2 for indicated durations (**A**) or after exposure to indicated concentrations of $H_2O_2$for 30 min (**B**). Dashed lines indicate the 50 and 100% levels. Data were obtained from 18 wells from 3 independent experiments, and expressed as percentage of the respective control. *P < 0.05 and **P < 0.001, difference compared with their respective control. Grey bars indicate no difference from the control. ††P < 0.01 and †††P < 0.005, difference for the paired groups.

A

RAW 264.7

0.3 mM 3 mM

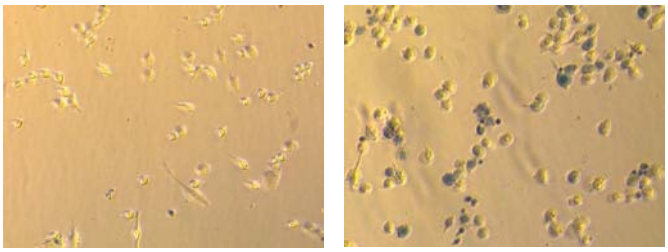

B

PMA-differentiated THP-1

0.3 mM 3 mM

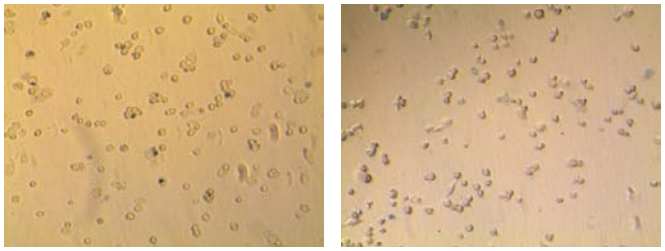

C

Peritoneal macrophage

0 mM 0.3 mM 3 mM

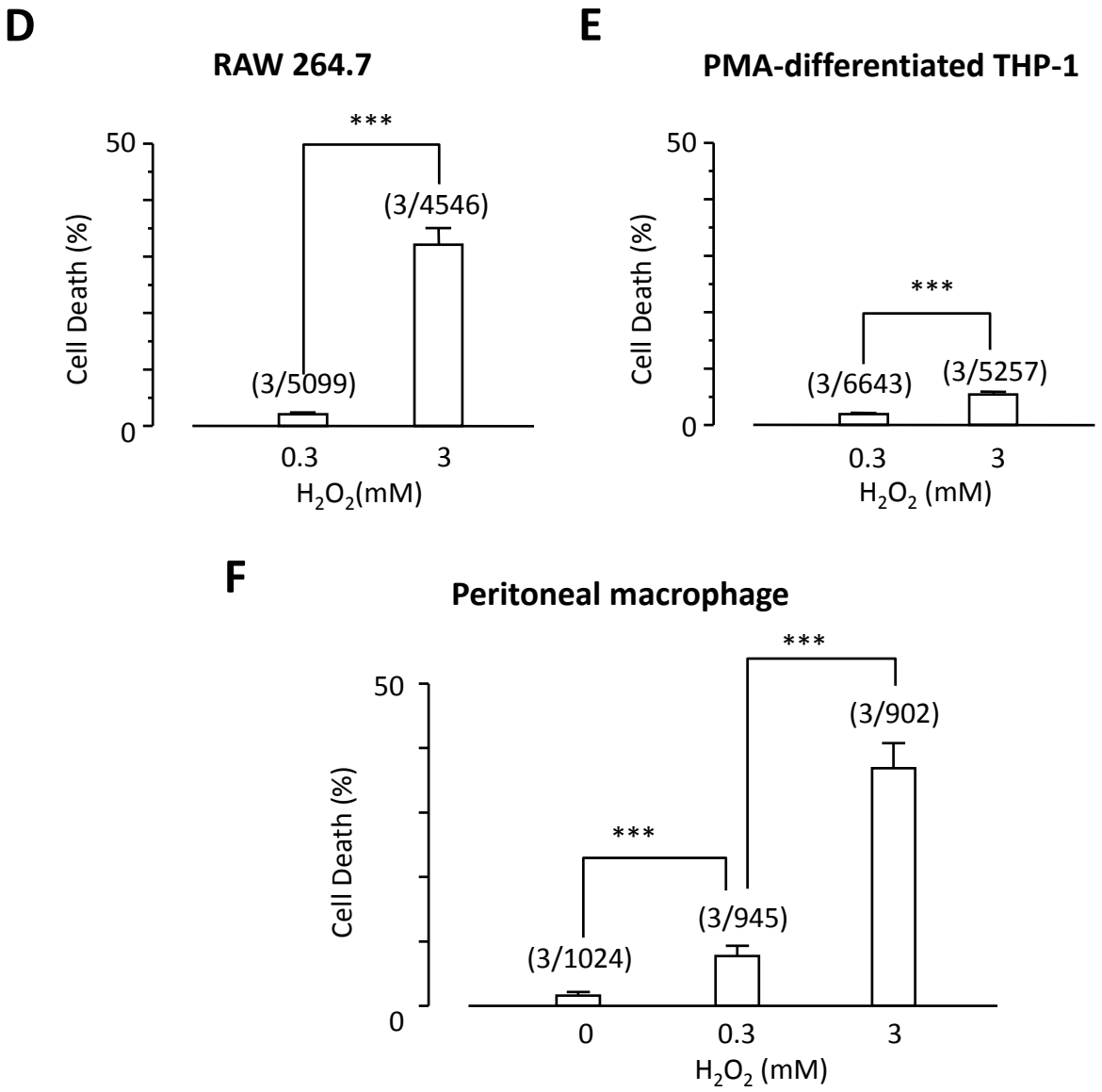

Figure 5.10 H_2O_2-induced necrosis in macrophage cells

A, representative images of H_2O_2-induced necrosis in RAW264.7 (**A**), PMA-differentiated THP-1 cells (**B**), and peritoneal macrophage (**C**) in trypan blue exclusion assays. Cells were pre-treated with H_2O_2 at indicated concentrations for 60 min. **B**, mean percentage of dye-stained RAW264.7 (**D**), PMA-differentiated THP-1 cells (**E**), and peritoneal macrophage (**F**) under the indicated conditions. The data show mean ± sem; the number of cells examined in three independent experiments in each case is shown in parentheses. *** $p< 0.005$ significant difference for the paired groups.

5.3 Discussion

The results from the study described in this chapter have provided evidence to support functional expression of the TRPM2 channels and a crucial role in mediating H_2O_2-induced increases in the $[Ca^{2+}]_c$ in macrophage cells. More specifically, the TRPM2 channels function as a cell surface Ca^{2+}-permeable channel that mediates extracellular Ca^{2+} influx and constitutes the principal mechanism elevating the $[Ca^{2+}]_c$ during early response to H_2O_2 at biologically relevant concentrations. The study has also shown that the TRPM2 channel or TRPM2-mediated Ca^{2+} influx has a limited role in H_2O_2-induced macrophage cell death.

It has become increasingly clear from numerous recent studies using transgenic TRPM2 deficient mice that theTRPM2 channels in immune cells plays a crucial role in immune responses and inflammatory diseases. However, the current picture with respect to the subcellular localization of the TRPM2 channels and associated Ca^{2+} signaling mechanisms and cell functions in these cells is intriguing; the TRPM2 channels on the one hand function as a Ca^{2+}-permeable channel in the plasma membrane mediating Ca^{2+} influx in monocytes, macrophages and microglia (Yamamoto et al., 2008) and, on the other, operate as a lysosomal Ca^{2+} release channel in dendritic cells (Sumoza-Toledo et al., 2011). In this study, we showed that H_2O_2 increased the $[Ca^{2+}]_c$ in macrophage cells and such responses were strongly attenuated by inhibiting the TRPM2 channel activation by PJ-34 (Fig. 5.5), prevented by removing extracellular Ca^{2+} (Fig. 5.4) or by genetically deleting the TRPM2 channel function (Fig. 5.6). These results provide consistent evidence to indicate that the TRPM2 channels in macrophage cells functions as a cell surface Ca^{2+}-permeable channel and TRPM2-mediated extracellular Ca^{2+} influx constitutes the principal mechanism elevating the $[Ca^{2+}]_c$ in early response to H_2O_2. Such information helps to fully understand the TRPM2-mediated disease mechanisms and the molecular mechanisms determining cell type-specific subcellular compartmentalization of the TRPM2 channels and thereby to identify druggable targets and develop therapeutics.

One interesting and physiologically relevant finding from this study is that the TRPM2-mediated H_2O_2-induced increases in the $[Ca^{2+}]_c$ in macrophage cells were significantly greater at body temperature than at room temperature (Fig. 5.5). TRPM2 channels heterologously expressed in HEK cells and endogenously expressed in insulin-secreting cells

are temperature-sensitive with an opening threshold of 40°C and thus remains closed at body temperature in the absence of agonist but can open in the presence of subthreshold concentrations of agonist, such as cADPR (Kashio et al., 2012, Togashi et al., 2006). Our results suggest that activation of the TRPM2 channel by H_2O_2 in macrophage cells is strongly facilitated at body temperature (Fig. 5.5). A recent thermodynamic study has postulated that the thermosensitivity of the TRP channels is in principle governed by temperature-dependent conformational changes (Clapham and Miller, 2011). As one plausible interpretation, the temperature induced potentiation of activation of the TRPM2 channel by H_2O_2 observed in this study may result from a synergy between ADPR and temperature in promoting the conformational transitions that lead to channel opening. The higher PARP activities and thus more ADPR generation at body temperature may also contribute. A recent study has shown that prior exposure to H_2O_2 increases the thermosensitivity of the TRPM2 channel (Kashio et al., 2012). Such H_2O_2-induced sensitization, despite being in a large part prevented by pre-treatment with PJ-34, has, however, been attributed to TRPM2 protein oxidation. Regardless, the synergy between H_2O_2 and body temperature is important for TRPM2-mediated macrophage cell functions in vivo.

TRPM2-mediated cell death is largely characteristic of cell death caused by oxidative, ischemic, and inflammatory damage (see section 1.2.8). The present study has revealed a significant but limited role for the TRPM2 channel in macrophage cell death induced by biologically relevant concentrations of H_2O_2 within 1 hr (Fig. 5.8 and 5.9), in contrast with the principal role in Ca^{2+}signaling. These findings are consistent with the idea that TRPM2-mediated Ca^{2+} signaling plays a more critical role in other macrophage cell functions in responses to early or initial exposure to ROS, for example, inflammasome activation and cytokine generation (Kashio et al., 2012, Zhong et al., 2013). Intriguingly, brief exposure to 30 μM H_2O_2 increased macrophage cell viability (Fig. 5.9). The reason for this is currently unclear. The increase in cell viability could result from increased cell proliferation as previously reported for microglia (Mander et al., 2006). A recent study has reported that TRPM2 expression renders SH-SY5Y cells to be less prone to cell death induced by 6- to 24-hr exposure to 50–100 μM H_2O_2 due to enhanced expression of FOXO3a (forkhead box O3) and SOD2 (superoxide dismutase 2) (Zhang et al., 2012). Further investigation is required.

In conclusion, the TRPM2 channel in macrophage cells functions as a Ca^{2+}-permeable channel in the plasma membrane and constitutes the principal Ca^{2+} signaling mechanism responsible for the increases in the $[Ca^{2+}]_c$ and has a significant but limited role in cell death during early response to H_2O_2. Such knowledge will help to evolve a full understanding of the TRPM2 channel in ROS-related immune responses and inflammatory diseases.

Chapter 6

Summary and conclusions

6.1 Summary of findings

6.1.1 The crucial contribution of a pore residue in determining species-dependent inhibition of TRPM2 channels by extracellular acidic pH

Several recent studies have shown the inhibition of hTRPM2 channel by extracellular acidic pH (Du et al., 2009b, Starkus et al., 2007, Starkus et al., 2010, Yang et al., 2010). However, there is significant discrepancy in the reversibility of the inhibition and the underlying mechanisms. In the previous study of our group, the state-dependent inhibition of hTRPM2 channel by extracellular acidic pH was postulated to result from initial reversible inhibition and subsequent conformational changes leading to largely irreversible TRPM2 channel inactivation (Yang et al., 2010).

Using whole-cell patch clamp recordings, I further investigated the reversibility of the inhibition of ADPR-induced TRPM2 channel currents by extracellular acidic pH 5.5 in HEK293 cells transiently transfected with hTRPM2 plasmid. The results showed that short exposure duration caused strong reversible inhibition of ADPR-induced currents; whereas the inhibition became irreversible after long exposure duration. These results are consistent with the two sequential steps hypothesis for the inhibition of hTRPM2 channels by extracellular acidic pH.

Studies using mice are important to infer the physiological functions proteins and the mechanisms responsible for associated pathologies and conduct preclinical testing of new therapeutic drugs, but species difference between humans and rodent animals may bear significant limitations (Chen and Kym, 2009). I conducted experiments to determine how the mouse TRPM2 channels respond to acidic pH. For this, I investigated the effects of extracellular acidic pH on both hTRPM2 and mTRPM2 channels at range of pH 4.0-6.0. The results showed that the steady-state inhibition of both hTRPM2 and mTRPM2 channels were complete and pH-independent. In addition, the lower acidic pH induced quicker inhibition of both hTRPM2 and mTRPM2 channel currents, indicating that the inhibition kinetics is pH-dependent. However, the inhibition kinetics at the mTRPM2 channels by acidic pH was significantly slower than that at the hTRPM2 channels. Strikingly, where

completely abolishing the hTRPM2 channels pH 6.0 hardly suppressed the mTRPM2 channel currents. These results demonstrated clear species-dependent sensitivity of the human and mouse TRPM2 channels in response to extracellular acidic pH.

In the further study of the molecular basis and mechanism of this species-dependent inhibition, residues Arg-961 and His-995 in the outer pore region of the hTRPM2 channel were substituted individually by Ser-958 and Gln-992, their equivalent residues in the mTRPM2 channel. The reciprocal mutations were also introduced in the mTRPM2 channel. Then, the effects of extracellular acidic pH on the inhibition of ADPR-induced current in these mutants have been investigated. The data show that H995Q mutation in the hTRPM2 channel strongly slowed down, and its reciprocal mutation Q992H in the mTRPM2 channel dramatically accelerated the inhibition kinetics, as anticipated if this residue is critical. In contrast, the R961S and S958R mutations resulted in no significant effect on the inhibition kinetics. Thus, these results has shown a crucial role for residue His-995/Gln-992 in the outer pore region in determining such species differences of TRPM2 channels in response to extracellular acidic pH. These results also provide further evidence to support the notion that extracellular acidic pH inhibit the TRPM2 channels by interacting with the ion-conducting pore (Yang et al., 2010).

6.1.2 Identification of novel and potent TRPM2 channel inhibitors

Currently, there is a lack of specific TRPM2 channel inhibitors, which makes it difficult to study the functions of the hTRPM2 channel. In order to search for novel TRPM2 inhibitors, screening of 14,000 compounds on H_2O_2-induced increases in the $[Ca^{2+}]_c$ in hTRPM2-expressing HEK293 cells have led to identification of 48 hit compounds that may inhibit the hTRPM2 channel. Using Flex-station and tetracycline-induced hTRPM2-expressing HEK293 cells, the effects of these 48 compounds on H_2O_2-induced increases in the $[Ca^{2+}]_c$ were investigated in detail. 24 compounds have been verified to strongly inhibit H_2O_2-induced Ca^{2+} responses and 19 of them exhibit a micromolar or submicromolar potency in inhibiting H_2O_2-induced Ca^{2+} responses. However, whole-cell patch clamp recording show four compounds, No.07, No.42, No.13 and No.39 at 10 μM can completely inhibit ADPR-induced TRPM2 channel currents. Their inhibition in terms of kinetics and irreversibility is noticeably

different. The inhibition by No.07 and No.42 was relatively quick and largely reversible. The inhibition by NO.39 is fast but hardly reversible, whereas the inhibition by No.13 was slow and irreversible. These results may indicate despite potent inhibition of the TRPM2 channels, mechanisms of actions of these four compounds appear different. Further investigations are required to understand how they inhibit the hTRPM2 channels.

In the further efforts to better the structure-activity relationships, eleven and two derivatives of No.13 and No.07, respectively, were tested for their inhibition of H_2O_2-induced increases in the $[Ca^{2+}]_c$. The results based on the IC_{50}s showed that four derivatives of No.13, CG-013, CG-036, CG-040 and CG-008, and one of No.07, CG-058, exhibited about 10-fold higher potency then No.39 and No.07, respectively.

Taken together, these results identified four novel and structurally different TRPM2 channels inhibitors. Further studies are required to determine their specificity and metabolically stability. Nonetheless, identification of such compounds may provide new tools to better understand the physiological and pathological functions of the human TRPM2 channels and develop therapeutics to treat TRPM2-related diseases.

6.1.3 Expression of TRPM2 channels and their role in H_2O_2–induced Ca^{2+} responses and cell death in macrophage cells

ROS, particularly H_2O_2, is important signaling molecule that regulates a diversity of physiological functions and is related to several diseases, such as inflammatory, cardiovascular, and neurodegenerative diseases. TRPM2 channel is an important cellular sensor for ROS. The early event of TRPM2 channel activation by H_2O_2 is to increase the $[Ca^{2+}]_c$. The most well-known role of the TRPM2 channel is to mediate ROS-induced cell death. However, the function expression of TRPM2 channel and its role in mediating H_2O_2-induced Ca^{2+} signaling and cell death in macrophage cells is not well understood. This study investigate the contribution and mechanisms of the TRPM2 channel in macrophage cells in mediating Ca^{2+} signaling and cell death during early response to biologically relevant concentrations of H_2O_2.

The TRPM2 protein expression was detected in RAW264.7 cells, PMA-differentiated THP-1 cells and peritoneal macrophage cells, using anti-TRPM2 antibody and immunofluorescent confocal imaging. The results showed the expression of TRPM2 proteins in all these three types of macrophage cells both on the cell surface and inside the cells. H_2O_2 induced robust increases in the $[Ca^{2+}]_c$ in RAW264.7 cells, PMA-differentiated THP-1 cells and peritoneal macrophage cells using single cell Ca^{2+} imaging. The role of TRPM2 channels in mediating these H_2O_2-induced Ca^{2+}responses were supported by their sensitivity to inhibition to PJ34, a PARP inhibitor known to prevent H_2O_2-induced TRPM2 channels, their sensitivity to facilitation by temperature. Furthermore, H_2O_2-induced Ca^{2+} responses were virtually lost in macrophages isolated from $TRPM2^{-/-}$ mice, providing compelling evidence to support the functional expression of TRPM2 channels in macrophage cells. In addition, H_2O_2-induced increases in the $[Ca^{2+}]_c$ almost exclusively result from extracellular Ca^{2+} influx, suggesting that TRPM2 channels function as a Ca^{2+}-permeable channel at the cell surface, which is different from the lysosomal location of TRPM2 channels as an intracellular Ca^{2+} release channel in dendrite cells. .

The role of TRPM2 channels in H_2O_2-induced macrophages cell death in RAW264.7 cells, PMA-differentiated THP-1 cells and peritoneal macrophage cells were investigated using the XTT assays. The data show that H_2O_2 at biologically relevant concentrations induced macrophage cell death in both exposure duration- and H_2O_2 concentration-dependent manner in all three types of macrophage cells. Further experiments using trypan blue exclusion assays show that H_2O_2-induced cell death by mainly due to the apoptosis, but not necrosis. Both pre-treatment with PJ-34 and TRPM2 channel deficiency partially reduced but not prevented H_2O_2-induced cell death. Taken together, these results indicate that the TRPM2 channels play a crucial role in mediating H_2O_2-induced increases in the $[Ca^{2+}]_c$ in macrophage cells and contributed to cell death.

6.2 General discussion

Inflammation is a complex response to the infection and tissue injury, which is characterized by redness, swelling, heat and pain. The leukocytes, such as macrophages, neutrophils and lymphocytes, are activated and recruited to the sites of infection and injured tissues to

eliminate the pathogens in the immune response. However, the leukocyte population needs to be controlled; otherwise the excessive immune response will damage the healthy cells and tissues and result in the inflammation.

Macrophage plays an important role in phagocytosis, antigen presentation and cytokine release in the immune response. Its population is reduced by apoptosis to prevent inflammation. TRPM2 channels have already been identified in macrophages. My study demonstrates that, although TRPM2-independent mechanism exists, the TRPM2 channel is involved in mediating the apoptosis in macrophage cell induced by biologically relevant concentrations of H_2O_2. My study also shows the essential role of TRPM2 channel in mediating the H_2O_2-induced Ca^{2+} influx in macrophage cells. These results indicate the limited contribution of TRPM2 channel to macrophage cell apoptosis through Ca^{2+}-depended pathway, and imply the role of TRPM2 channel in preventing of the induction of inflammation in the physiological condition.

However, several studies have reported the contribution of TRPM2 channel to promote the inflammation in the pathological condition, although the underlying mechanism is not fully understood (Melzer et al., 2012, Haraguchi et al., 2012, Yamamoto et al., 2008). The reduced pH is one of the characteristics in the inflammation. My study in TRPM2 channel-expressing HEK293 cells shows that extracellular acidic pH can induce TRPM2 channel inhibition, which is mainly caused by the channel inactivation when the exposure to acidic pH is prolonged. In addition, the inhibition kinetics is pH-dependent. The acidic pH-induced inhibition of TRPM2 channel results in a reduction of Ca^{2+} influx, which could further regulate the downstream cellular functions in the inflammatory condition.

Since TRPM2 channel has been reported to be involved in inflammation, it may be a target for development of therapy treating inflammatory diseases. In addition, as shown in my study, the hTRPM2 and mTRPM2 channel exhibit different sensitivity to, and slower kinetics of, inhibition in response to extracellular acidic pH. These results imply the distinct features of TRPM2 channels in two different species. Thus, the specific TRPM2 inhibitors are eagerly required in the research because of the limitation of the animal models. In my study, four novel TRPM2 inhibitors have been identified. These inhibitors can provide pharmacological

tools to study TRPM2 channel functions and new therapeutics treating TRPM2-related diseases, including inflammation.

6.3 Conclusions

The studies described in this thesis provide evidence to support the following conclusions:

(1) State-dependent and irreversible inhibition of the TRPM2 channels by extracellular acidic pH results from initial reversible inhibition and subsequent irreversible inactivation. The human and mouse TRPM2 channels exhibit species- difference in the sensitivity to extracellular acidic pH. Residue His-996/Gln-992 in the pore region is an important molecular determinant for such species difference.

(2) Four structurally different compounds No.13, No.07, No. 39 and No.42, have been identified as novel TRPM2 channels inhibitors, that with a micromolar and sub-micromolar potency.

(3) The TRPM2 channel is functionally expressed in macrophage cells and functions as a Ca^{2+}-permeable channel at the cell surface which play an essential role in mediating H_2O_2-induced Ca^{2+} influx and thereby contributing to H_2O_2-induced increases in the $[Ca^{2+}]_c$. The TRPM2 channel has also contributed to H_2O_2-induced macrophage cell death, but its role is limited.

References

ABAAN, O. D., LEVENSON, A., KHAN, O., FURTH, P. A., UREN, A. & TORETSKY, J. A. 2005. PTPL1 is a direct transcriptional target of EWS-FLI1 and modulates Ewing's Sarcoma tumorigenesis. *Oncogene,* 24**,** 2715-22.

ALY, D. G. & SHAHIN, R. S. 2010. Oxidative stress in lichen planus. *Acta Dermatovenerol Alp Panonica Adriat,* 19**,** 3-11.

ATIBA-DAVIES, M. & NOBEN-TRAUTH, K. 2007. TRPML3 and hearing loss in the varitint-waddler mouse. *Biochim Biophys Acta,* 1772**,** 1028-31.

BABES, A., ZORZON, D. & REID, G. 2004. Two populations of cold-sensitive neurons in rat dorsal root ganglia and their modulation by nerve growth factor. *Eur J Neurosci,* 20**,** 2276-82.

BAE, Y. S., OH, H., RHEE, S. G. & YOO, Y. D. 2011. Regulation of reactive oxygen species generation in cell signaling. *Mol Cells,* 32**,** 491-509.

BAHRA, P., MESHER, J., LI, S., POLL, C. T. & DANAHAY, H. 2004. P2Y2-receptor-mediated activation of a contralateral, lanthanide-sensitive calcium entry pathway in the human airway epithelium. *Br J Pharmacol,* 143**,** 91-8.

BAI, J. Z. & LIPSKI, J. 2010. Differential expression of TRPM2 and TRPV4 channels and their potential role in oxidative stress-induced cell death in organotypic hippocampal culture. *Neurotoxicology,* 31**,** 204-14.

BANDELL, M., STORY, G. M., HWANG, S. W., VISWANATH, V., EID, S. R., PETRUS, M. J., EARLEY, T. J. & PATAPOUTIAN, A. 2004. Noxious cold ion channel TRPA1 is activated by pungent compounds and bradykinin. *Neuron,* 41**,** 849-57.

BANVILLE, D., AHMAD, S., STOCCO, R. & SHEN, S. H. 1994. A novel protein-tyrosine phosphatase with homology to both the cytoskeletal proteins of the band 4.1 family and junction-associated guanylate kinases. *J Biol Chem,* 269**,** 22320-7.

BARBET, G., DEMION, M., MOURA, I. C., SERAFINI, N., LEGER, T., VRTOVSNIK, F., MONTEIRO, R. C., GUINAMARD, R., KINET, J. P. & LAUNAY, P. 2008. The calcium-activated nonselective cation channel TRPM4 is essential for the migration but not the maturation of dendritic cells. *Nat Immunol,* 9**,** 1148-56.

BARGAL, R., AVIDAN, N., BEN-ASHER, E., OLENDER, Z., ZEIGLER, M., FRUMKIN, A., RAAS-ROTHSCHILD, A., GLUSMAN, G., LANCET, D. & BACH, G. 2000. Identification of the gene causing mucolipidosis type IV. *Nat Genet,* 26**,** 118-23.

BARGAL, R., GOEBEL, H. H., LATTA, E. & BACH, G. 2002. Mucolipidosis IV: novel mutation and diverse ultrastructural spectrum in the skin. *Neuropediatrics,* 33**,** 199-202.

BARI, M. R., AKBAR, S., EWEIDA, M., KUHN, F. J., GUSTAFSSON, A. J., LUCKHOFF, A. & ISLAM, M. S. 2009. H2O2-induced Ca2+ influx and its inhibition by N-(p-amylcinnamoyl) anthranilic acid in the beta-cells: involvement of TRPM2 channels. *J Cell Mol Med,* 13**,** 3260-7.

BAUTISTA, D. M., JORDT, S. E., NIKAI, T., TSURUDA, P. R., READ, A. J., POBLETE, J., YAMOAH, E. N., BASBAUM, A. I. & JULIUS, D. 2006. TRPA1 mediates the inflammatory actions of environmental irritants and proalgesic agents. *Cell,* 124**,** 1269-82.

BECK, A., KOLISEK, M., BAGLEY, L. A., FLEIG, A. & PENNER, R. 2006. Nicotinic acid adenine dinucleotide phosphate and cyclic ADP-ribose regulate TRPM2 channels in T lymphocytes. *FASEB J,* 20**,** 962-4.

BEECH, D. J., MURAKI, K. & FLEMMING, R. 2004. Non-selective cationic channels of smooth muscle and the mammalian homologues of Drosophila TRP. *J Physiol,* 559**,** 685-706.

BEHRENDT, H. J., GERMANN, T., GILLEN, C., HATT, H. & JOSTOCK, R. 2004. Characterization of the mouse cold-menthol receptor TRPM8 and vanilloid receptor type-1 VR1 using a fluorometric imaging plate reader (FLIPR) assay. *Br J Pharmacol,* 141**,** 737-45.

BERGERON, C. 1990. Alzheimer's disease--neuropathological aspects. *Can J Vet Res,* 54**,** 58-64.

BERNUCCI, L., HENRIQUEZ, M., DIAZ, P. & RIQUELME, G. 2006. Diverse calcium channel types are present in the human placental syncytiotrophoblast basal membrane. *Placenta,* 27**,** 1082-95.

BESSMAN, M. J., FRICK, D. N. & O'HANDLEY, S. F. 1996. The MutT proteins or "Nudix" hydrolases, a family of versatile, widely distributed, "housecleaning" enzymes. *J Biol Chem,* 271**,** 25059-62.

BISHNOI, M., BOSGRAAF, C. A., ABOOJ, M., ZHONG, L. & PREMKUMAR, L. S. 2011. Streptozotocin-induced early thermal hyperalgesia is independent of glycemic state of rats: role of transient receptor potential vanilloid 1(TRPV1) and inflammatory mediators. *Mol Pain,* 7**,** 52.

BODDING, M. 2007. TRPM6: A Janus-like protein. *Handb Exp Pharmacol***,** 299-311.

BOUSQUET, S. M., MONET, M. & BOULAY, G. 2010. Protein kinase C-dependent phosphorylation of transient receptor potential canonical 6 (TRPC6) on serine 448 causes channel inhibition. *J Biol Chem,* 285**,** 40534-43.

BRAUCHI, S., ORIO, P. & LATORRE, R. 2004. Clues to understanding cold sensation: thermodynamics and electrophysiological analysis of the cold receptor TRPM8. *Proc Natl Acad Sci U S A,* 101**,** 15494-9.

BUELOW, B., SONG, Y. & SCHARENBERG, A. M. 2008. The Poly(ADP-ribose) polymerase PARP-1 is required for oxidative stress-induced TRPM2 activation in lymphocytes. *J Biol Chem,* 283**,** 24571-83.

BUIJS, J. T., CLETON, A. M., SMIT, V. T., LOWIK, C. W., S, E. P. & PLUIJM, G. 2004. Prognostic significance of periodic acid-Schiff-positive patterns in primary breast cancer and its lymph node metastases. *Breast Cancer Res Treat,* 84**,** 117-30.

CAMPBELL, E. M. & FARES, H. 2010. Roles of CUP-5, the Caenorhabditis elegans orthologue of human TRPML1, in lysosome and gut granule biogenesis. *BMC Cell Biol,* 11**,** 40.

CATERINA, M. J., LEFFLER, A., MALMBERG, A. B., MARTIN, W. J., TRAFTON, J., PETERSEN-ZEITZ, K. R., KOLTZENBURG, M., BASBAUM, A. I. & JULIUS, D. 2000. Impaired nociception and pain sensation in mice lacking the capsaicin receptor. *Science,* 288**,** 306-13.

CATERINA, M. J., SCHUMACHER, M. A., TOMINAGA, M., ROSEN, T. A., LEVINE, J. D. & JULIUS, D. 1997. The capsaicin receptor: a heat-activated ion channel in the pain pathway. *Nature,* 389**,** 816-24.

CAYOUETTE, S., LUSSIER, M. P., MATHIEU, E. L., BOUSQUET, S. M. & BOULAY, G. 2004. Exocytotic insertion of TRPC6 channel into the plasma membrane upon Gq protein-coupled receptor activation. *J Biol Chem,* 279**,** 7241-6.

CHEN, G. L., ZENG, B., EASTMOND, S., ELSENUSSI, S. E., BOA, A. N. & XU, S. Z. 2012. Pharmacological comparison of novel synthetic fenamate analogues with econazole and 2-APB on the inhibition of TRPM2 channels. *Br J Pharmacol,* 167**,** 1232-43.

CHEN, J. & BARRITT, G. J. 2003. Evidence that TRPC1 (transient receptor potential canonical 1) forms a Ca(2+)-permeable channel linked to the regulation of cell volume in liver cells obtained using small interfering RNA targeted against TRPC1. *Biochem J,* 373**,** 327-36.

CHEN, J. & KYM, P. R. 2009. TRPA1: the species difference. *J Gen Physiol,* 133**,** 623-5.

CHEN, Y., ZHANG, Z., LV, X. Y., WANG, Y. D., HU, Z. G., SUN, H., TAN, R. Z., LIU, Y. H., BIAN, G. H., XIAO, Y., LI, Q. W., YANG, Q. T., AI, J. Z., FENG, L., YANG, Y., WEI, Y. Q. & ZHOU, Q. 2008. Expression of Pkd2l2 in testis is implicated in spermatogenesis. *Biol Pharm Bull,* 31**,** 1496-500.

CHIU, L. L., PERNG, D. W., YU, C. H., SU, S. N. & CHOW, L. P. 2007. Mold allergen, pen C 13, induces IL-8 expression in human airway epithelial cells by activating protease-activated receptor 1 and 2. *J Immunol,* 178**,** 5237-44.

CHOKSHI, R., FRUASAHA, P. & KOZAK, J. A. 2012. 2-aminoethyl diphenyl borinate (2-APB) inhibits TRPM7 channels through an intracellular acidification mechanism. *Channels (Austin),* 6**,** 362-9.

CHRISTENSEN, K. A., MYERS, J. T. & SWANSON, J. A. 2002. pH-dependent regulation of lysosomal calcium in macrophages. *J Cell Sci,* 115**,** 599-607.

CHUBANOV, V., WALDEGGER, S., MEDEROS Y SCHNITZLER, M., VITZTHUM, H., SASSEN, M. C., SEYBERTH, H. W., KONRAD, M. & GUDERMANN, T. 2004. Disruption of

TRPM6/TRPM7 complex formation by a mutation in the TRPM6 gene causes hypomagnesemia with secondary hypocalcemia. *Proc Natl Acad Sci U S A,* 101**,** 2894-9.

CHUNG, K. K., FREESTONE, P. S. & LIPSKI, J. 2011. Expression and functional properties of TRPM2 channels in dopaminergic neurons of the substantia nigra of the rat. *J Neurophysiol,* 106**,** 2865-75.

CHUNG, M. K., GULER, A. D. & CATERINA, M. J. 2005. Biphasic currents evoked by chemical or thermal activation of the heat-gated ion channel, TRPV3. *J Biol Chem,* 280**,** 15928-41.

CLAPHAM, D. E. & MILLER, C. 2011. A thermodynamic framework for understanding temperature sensing by transient receptor potential (TRP) channels. *Proc Natl Acad Sci U S A,* 108**,** 19492-7.

COHEN, C. & PARRY, D. A. 1990. Alpha-helical coiled coils and bundles: how to design an alpha-helical protein. *Proteins,* 7**,** 1-15.

COREY, D. P., GARCIA-ANOVEROS, J., HOLT, J. R., KWAN, K. Y., LIN, S. Y., VOLLRATH, M. A., AMALFITANO, A., CHEUNG, E. L., DERFLER, B. H., DUGGAN, A., GELEOC, G. S., GRAY, P. A., HOFFMAN, M. P., REHM, H. L., TAMASAUSKAS, D. & ZHANG, D. S. 2004. TRPA1 is a candidate for the mechanosensitive transduction channel of vertebrate hair cells. *Nature,* 432**,** 723-30.

COSENS, D. J. & MANNING, A. 1969. Abnormal electroretinogram from a Drosophila mutant. *Nature,* 224**,** 285-7.

CRIVICI, A. & IKURA, M. 1995. Molecular and structural basis of target recognition by calmodulin. *Annu Rev Biophys Biomol Struct,* 24**,** 85-116.

CROUSILLAC, S., LEROUGE, M., RANKIN, M. & GLEASON, E. 2003. Immunolocalization of TRPC channel subunits 1 and 4 in the chicken retina. *Vis Neurosci,* 20**,** 453-63.

CSANADY, L. & TOROCSIK, B. 2009. Four Ca2+ ions activate TRPM2 channels by binding in deep crevices near the pore but intracellularly of the gate. *J Gen Physiol,* 133**,** 189-203.

DAIGNEAULT, M., PRESTON, J. A., MARRIOTT, H. M., WHYTE, M. K. & DOCKRELL, D. H. 2010. The identification of markers of macrophage differentiation in PMA-stimulated THP-1 cells and monocyte-derived macrophages. *PLoS One,* 5**,** e8668.

DAVARE, M. A., FORTIN, D. A., SANEYOSHI, T., NYGAARD, S., KAECH, S., BANKER, G., SODERLING, T. R. & WAYMAN, G. A. 2009. Transient receptor potential canonical 5 channels activate Ca2+/calmodulin kinase Igamma to promote axon formation in hippocampal neurons. *J Neurosci,* 29**,** 9794-808.

DE BLAS, G. A., ROGGERO, C. M., TOMES, C. N. & MAYORGA, L. S. 2005. Dynamics of SNARE assembly and disassembly during sperm acrosomal exocytosis. *PLoS Biol,* 3**,** e323.

DEN DEKKER, E., HOENDEROP, J. G., NILIUS, B. & BINDELS, R. J. 2003. The epithelial calcium channels, TRPV5 & TRPV6: from identification towards regulation. *Cell Calcium,* 33**,** 497-507.

DERBENEV, A. V., MONROE, M. J., GLATZER, N. R. & SMITH, B. N. 2006. Vanilloid-mediated heterosynaptic facilitation of inhibitory synaptic input to neurons of the rat dorsal motor nucleus of the vagus. *J Neurosci,* 26**,** 9666-72.

DERBENEV, A. V., STUART, T. C. & SMITH, B. N. 2004. Cannabinoids suppress synaptic input to neurones of the rat dorsal motor nucleus of the vagus nerve. *J Physiol,* 559**,** 923-38.

DEVI, S., KEDLAYA, R., MADDODI, N., BHAT, K. M., WEBER, C. S., VALDIVIA, H. & SETALURI, V. 2009. Calcium homeostasis in human melanocytes: role of transient receptor potential melastatin 1 (TRPM1) and its regulation by ultraviolet light. *Am J Physiol Cell Physiol,* 297**,** C679-87.

DI, A., GAO, X. P., QIAN, F., KAWAMURA, T., HAN, J., HECQUET, C., YE, R. D., VOGEL, S. M. & MALIK, A. B. 2012. The redox-sensitive cation channel TRPM2 modulates phagocyte ROS production and inflammation. *Nat Immunol,* 13**,** 29-34.

DI PALMA, F., BELYANTSEVA, I. A., KIM, H. J., VOGT, T. F., KACHAR, B. & NOBEN-TRAUTH, K. 2002. Mutations in Mcoln3 associated with deafness and pigmentation defects in varitint-waddler (Va) mice. *Proc Natl Acad Sci U S A,* 99**,** 14994-9.

DIETRICH, A. & GUDERMANN, T. 2008. Another TRP to endothelial dysfunction: TRPM2 and endothelial permeability. *Circ Res,* 102**,** 275-7.

DING, Y., WINTERS, A., DING, M., GRAHAM, S., AKOPOVA, I., MUALLEM, S., WANG, Y., HONG, J. H., GRYCZYNSKI, Z., YANG, S. H., BIRNBAUMER, L. & MA, R. 2011. Reactive oxygen species-mediated TRPC6 protein activation in vascular myocytes, a mechanism for vasoconstrictor-regulated vascular tone. *J Biol Chem,* 286**,** 31799-809.

DIVER, J. M., SAGE, S. O. & ROSADO, J. A. 2001. The inositol trisphosphate receptor antagonist 2-aminoethoxydiphenylborate (2-APB) blocks Ca2+ entry channels in human platelets: cautions for its use in studying Ca2+ influx. *Cell Calcium,* 30**,** 323-9.

DOERNER, J. F., GISSELMANN, G., HATT, H. & WETZEL, C. H. 2007. Transient receptor potential channel A1 is directly gated by calcium ions. *J Biol Chem,* 282**,** 13180-9.

DONG, X. P., CHENG, X., MILLS, E., DELLING, M., WANG, F., KURZ, T. & XU, H. 2008. The type IV mucolipidosis-associated protein TRPML1 is an endolysosomal iron release channel. *Nature,* 455**,** 992-6.

DU, J., XIE, J. & YUE, L. 2009a. Intracellular calcium activates TRPM2 and its alternative spliced isoforms. *Proc Natl Acad Sci U S A,* 106**,** 7239-44.

DU, J., XIE, J. & YUE, L. 2009b. Modulation of TRPM2 by acidic pH and the underlying mechanisms for pH sensitivity. *J Gen Physiol,* 134**,** 471-88.

DU, W., HUANG, J., YAO, H., ZHOU, K., DUAN, B. & WANG, Y. 2010. Inhibition of TRPC6 degradation suppresses ischemic brain damage in rats. *J Clin Invest,* 120**,** 3480-92.

DUNCAN, L. M., DEEDS, J., HUNTER, J., SHAO, J., HOLMGREN, L. M., WOOLF, E. A., TEPPER, R. I. & SHYJAN, A. W. 1998. Down-regulation of the novel gene melastatin correlates with potential for melanoma metastasis. *Cancer Res,* 58**,** 1515-20.

EISFELD, J. & LUCKHOFF, A. 2007. Trpm2. *Handb Exp Pharmacol***,** 237-52.

FENG, S., RODAT-DESPOIX, L., DELMAS, P. & ONG, A. C. 2011. A single amino acid residue constitutes the third dimerization domain essential for the assembly and function of the tetrameric polycystin-2 (TRPP2) channel. *J Biol Chem,* 286**,** 18994-9000.

FOGGENSTEINER, L., BEVAN, A. P., THOMAS, R., COLEMAN, N., BOULTER, C., BRADLEY, J., IBRAGHIMOV-BESKROVNAYA, O., KLINGER, K. & SANDFORD, R. 2000. Cellular and subcellular distribution of polycystin-2, the protein product of the PKD2 gene. *J Am Soc Nephrol,* 11**,** 814-27.

FONFRIA, E., MARSHALL, I. C., BENHAM, C. D., BOYFIELD, I., BROWN, J. D., HILL, K., HUGHES, J. P., SKAPER, S. D. & MCNULTY, S. 2004. TRPM2 channel opening in response to oxidative stress is dependent on activation of poly(ADP-ribose) polymerase. *Br J Pharmacol,* 143**,** 186-92.

FONFRIA, E., MARSHALL, I. C., BOYFIELD, I., SKAPER, S. D., HUGHES, J. P., OWEN, D. E., ZHANG, W., MILLER, B. A., BENHAM, C. D. & MCNULTY, S. 2005. Amyloid beta-peptide(1-42) and hydrogen peroxide-induced toxicity are mediated by TRPM2 in rat primary striatal cultures. *J Neurochem,* 95**,** 715-23.

FONFRIA, E., MATTEI, C., HILL, K., BROWN, J. T., RANDALL, A., BENHAM, C. D., SKAPER, S. D., CAMPBELL, C. A., CROOK, B., MURDOCK, P. R., WILSON, J. M., MAURIO, F. P., OWEN, D. E., TILLING, P. L. & MCNULTY, S. 2006. TRPM2 is elevated in the tMCAO stroke model, transcriptionally regulated, and functionally expressed in C13 microglia. *J Recept Signal Transduct Res,* 26**,** 179-98.

FORMAN, H. J., MAIORINO, M. & URSINI, F. 2010. Signaling functions of reactive oxygen species. *Biochemistry,* 49**,** 835-42.

FORSTERMANN, U. 2008. Oxidative stress in vascular disease: causes, defense mechanisms and potential therapies. *Nat Clin Pract Cardiovasc Med,* 5**,** 338-49.

FREDERICK, J., BUCK, M. E., MATSON, D. J. & CORTRIGHT, D. N. 2007. Increased TRPA1, TRPM8, and TRPV2 expression in dorsal root ganglia by nerve injury. *Biochem Biophys Res Commun,* 358**,** 1058-64.

FROMTLING, R. A. 1988. Overview of medically important antifungal azole derivatives. *Clin Microbiol Rev,* 1**,** 187-217.

GARCIA-GUZMAN, M., SOTO, F., GOMEZ-HERNANDEZ, J. M., LUND, P. E. & STUHMER, W. 1997. Characterization of recombinant human P2X4 receptor reveals pharmacological differences to the rat homologue. *Mol Pharmacol,* 51**,** 109-18.

GARDAM, K. E., GEIGER, J. E., HICKEY, C. M., HUNG, A. Y. & MAGOSKI, N. S. 2008. Flufenamic acid affects multiple currents and causes intracellular Ca2+ release in Aplysia bag cell neurons. *J Neurophysiol,* 100**,** 38-49.

GATTONE, V. H., RICKER, J. L., TRAMBAUGH, C. M. & KLEIN, R. M. 2002. Multiorgan mRNA misexpression in murine autosomal recessive polycystic kidney disease. *Kidney Int,* 62**,** 1560-9.

GILBERT, B. J. 2013. The role of amyloid beta in the pathogenesis of Alzheimer's disease. *J Clin Pathol,* 66**,** 362-6.

GIORGIO, M., TRINEI, M., MIGLIACCIO, E. & PELICCI, P. G. 2007. Hydrogen peroxide: a metabolic by-product or a common mediator of ageing signals? *Nat Rev Mol Cell Biol,* 8**,** 722-8.

GRAHAM, S., DING, M., DING, Y., SOURS-BROTHERS, S., LUCHOWSKI, R., GRYCZYNSKI, Z., YORIO, T., MA, H. & MA, R. 2010. Canonical transient receptor potential 6 (TRPC6), a redox-regulated cation channel. *J Biol Chem,* 285**,** 23466-76.

GRIMM, C., KRAFT, R., SAUERBRUCH, S., SCHULTZ, G. & HARTENECK, C. 2003. Molecular and functional characterization of the melastatin-related cation channel TRPM3. *J Biol Chem,* 278**,** 21493-501.

GROSCHNER, K. & ROSKER, C. 2005. TRPC3: a versatile transducer molecule that serves integration and diversification of cellular signals. *Naunyn Schmiedebergs Arch Pharmacol,* 371**,** 251-6.

GRUBISHA, O., RAFTY, L. A., TAKANISHI, C. L., XU, X., TONG, L., PERRAUD, A. L., SCHARENBERG, A. M. & DENU, J. M. 2006. Metabolite of SIR2 reaction modulates TRPM2 ion channel. *J Biol Chem,* 281**,** 14057-65.

GRYNKIEWICZ, G., POENIE, M. & TSIEN, R. Y. 1985. A new generation of Ca2+ indicators with greatly improved fluorescence properties. *J Biol Chem,* 260**,** 3440-50.

GULER, A. D., LEE, H., IIDA, T., SHIMIZU, I., TOMINAGA, M. & CATERINA, M. 2002. Heat-evoked activation of the ion channel, TRPV4. *J Neurosci,* 22**,** 6408-14.

GUO, L., SCHREIBER, T. H., WEREMOWICZ, S., MORTON, C. C., LEE, C. & ZHOU, J. 2000. Identification and characterization of a novel polycystin family member, polycystin-L2, in mouse and human: sequence, expression, alternative splicing, and chromosomal localization. *Genomics,* 64**,** 241-51.

GUSE, A. H. 2005. Second messenger function and the structure-activity relationship of cyclic adenosine diphosphoribose (cADPR). *FEBS J,* 272**,** 4590-7.

GWANYANYA, A., AMUZESCU, B., ZAKHAROV, S. I., MACIANSKIENE, R., SIPIDO, K. R., BOLOTINA, V. M., VEREECKE, J. & MUBAGWA, K. 2004. Magnesium-inhibited, TRPM6/7-like channel in cardiac myocytes: permeation of divalent cations and pH-mediated regulation. *J Physiol,* 559**,** 761-76.

GWANYANYA, A., MACIANSKIENE, R., BITO, V., SIPIDO, K. R., VEREECKE, J. & MUBAGWA, K. 2010. Inhibition of the calcium-activated chloride current in cardiac ventricular myocytes by N-(p-amylcinnamoyl)anthranilic acid (ACA). *Biochem Biophys Res Commun,* 402**,** 531-6.

HALLER, T., DIETL, P., DEETJEN, P. & VOLKL, H. 1996. The lysosomal compartment as intracellular calcium store in MDCK cells: a possible involvement in InsP3-mediated Ca2+ release. *Cell Calcium,* 19**,** 157-65.

HALLIWELL, B. 2007. Oxidative stress and cancer: have we moved forward? *Biochem J,* 401**,** 1-11.

HAM, H. Y., HONG, C. W., LEE, S. N., KWON, M. S., KIM, Y. J. & SONG, D. K. 2012. Sulfur mustard primes human neutrophils for increased degranulation and stimulates cytokine release via TRPM2/p38 MAPK signaling. *Toxicol Appl Pharmacol,* 258**,** 82-8.

HAMILL, O. P., MARTY, A., NEHER, E., SAKMANN, B. & SIGWORTH, F. J. 1981. Improved patch-clamp techniques for high-resolution current recording from cells and cell-free membrane patches. *Pflugers Arch,* 391**,** 85-100.

HANAHAN, D. 1983. Studies on transformation of Escherichia coli with plasmids. *J Mol Biol,* 166**,** 557-80.

HARA, Y., WAKAMORI, M., ISHII, M., MAENO, E., NISHIDA, M., YOSHIDA, T., YAMADA, H., SHIMIZU, S., MORI, E., KUDOH, J., SHIMIZU, N., KUROSE, H., OKADA, Y., IMOTO, K. & MORI, Y. 2002. LTRPC2 Ca2+-permeable channel activated by changes in redox status confers susceptibility to cell death. *Mol Cell,* 9**,** 163-73.

HARAGUCHI, K., KAWAMOTO, A., ISAMI, K., MAEDA, S., KUSANO, A., ASAKURA, K., SHIRAKAWA, H., MORI, Y., NAKAGAWA, T. & KANEKO, S. 2012. TRPM2 contributes to inflammatory and neuropathic pain through the aggravation of pronociceptive inflammatory responses in mice. *J Neurosci,* 32**,** 3931-41.

HARDIE, R. C. & MINKE, B. 1992. The trp gene is essential for a light-activated Ca2+ channel in Drosophila photoreceptors. *Neuron,* 8**,** 643-51.

HARTENECK, C., FRENZEL, H. & KRAFT, R. 2007. N-(p-amylcinnamoyl)anthranilic acid (ACA): a phospholipase A(2) inhibitor and TRP channel blocker. *Cardiovasc Drug Rev,* 25**,** 61-75.

HARTENECK, C. & GOLLASCH, M. 2011. Pharmacological modulation of diacylglycerol-sensitive TRPC3/6/7 channels. *Curr Pharm Biotechnol,* 12**,** 35-41.

HECQUET, C. M., AHMMED, G. U. & MALIK, A. B. 2010. TRPM2 channel regulates endothelial barrier function. *Adv Exp Med Biol,* 661**,** 155-67.

HECQUET, C. M., AHMMED, G. U., VOGEL, S. M. & MALIK, A. B. 2008. Role of TRPM2 channel in mediating H2O2-induced Ca2+ entry and endothelial hyperpermeability. *Circ Res,* 102**,** 347-55.

HECQUET, C. M. & MALIK, A. B. 2009. Role of H(2)O(2)-activated TRPM2 calcium channel in oxidant-induced endothelial injury. *Thromb Haemost,* 101**,** 619-25.

HEINER, I., EISFELD, J., HALASZOVICH, C. R., WEHAGE, E., JUNGLING, E., ZITT, C. & LUCKHOFF, A. 2003. Expression profile of the transient receptor potential (TRP) family in neutrophil granulocytes: evidence for currents through long TRP channel 2 induced by ADP-ribose and NAD. *Biochem J,* 371**,** 1045-53.

HEINER, I., EISFELD, J., WARNSTEDT, M., RADUKINA, N., JUNGLING, E. & LUCKHOFF, A. 2006. Endogenous ADP-ribose enables calcium-regulated cation currents through TRPM2 channels in neutrophil granulocytes. *Biochem J,* 398**,** 225-32.

HENSHALL, S. M., AFAR, D. E., HILLER, J., HORVATH, L. G., QUINN, D. I., RASIAH, K. K., GISH, K., WILLHITE, D., KENCH, J. G., GARDINER-GARDEN, M., STRICKER, P. D., SCHER, H. I., GRYGIEL, J. J., AGUS, D. B., MACK, D. H. & SUTHERLAND, R. L. 2003. Survival analysis of genome-wide gene expression profiles of prostate cancers identifies new prognostic targets of disease relapse. *Cancer Res,* 63**,** 4196-203.

HERMOSURA, M. C., CUI, A. M., GO, R. C., DAVENPORT, B., SHETLER, C. M., HEIZER, J. W., SCHMITZ, C., MOCZ, G., GARRUTO, R. M. & PERRAUD, A. L. 2008. Altered functional properties of a TRPM2 variant in Guamanian ALS and PD. *Proc Natl Acad Sci U S A,* 105**,** 18029-34.

HILL, K., BENHAM, C. D., MCNULTY, S. & RANDALL, A. D. 2004a. Flufenamic acid is a pH-dependent antagonist of TRPM2 channels. *Neuropharmacology,* 47**,** 450-60.

HILL, K., MCNULTY, S. & RANDALL, A. D. 2004b. Inhibition of TRPM2 channels by the antifungal agents clotrimazole and econazole. *Naunyn Schmiedebergs Arch Pharmacol,* 370**,** 227-37.

HILL, K., TIGUE, N. J., KELSELL, R. E., BENHAM, C. D., MCNULTY, S., SCHAEFER, M. & RANDALL, A. D. 2006. Characterisation of recombinant rat TRPM2 and a TRPM2-like conductance in cultured rat striatal neurones. *Neuropharmacology,* 50**,** 89-97.

HILLE, B. 1992. Axons, ions, and dons. *Science,* 258**,** 144-5.

HISATSUNE, C., KURODA, Y., NAKAMURA, K., INOUE, T., NAKAMURA, T., MICHIKAWA, T., MIZUTANI, A. & MIKOSHIBA, K. 2004. Regulation of TRPC6 channel activity by tyrosine phosphorylation. *J Biol Chem,* 279**,** 18887-94.

HOEFLICH, K. P. & IKURA, M. 2002. Calmodulin in action: diversity in target recognition and activation mechanisms. *Cell,* 108**,** 739-42.

HOENDEROP, J. G., HARTOG, A., STUIVER, M., DOUCET, A., WILLEMS, P. H. & BINDELS, R. J. 2000. Localization of the epithelial Ca(2+) channel in rabbit kidney and intestine. *J Am Soc Nephrol,* 11**,** 1171-8.

HOENDEROP, J. G., NILIUS, B. & BINDELS, R. J. 2003. Epithelial calcium channels: from identification to function and regulation. *Pflugers Arch,* 446**,** 304-8.

HOENDEROP, J. G., NILIUS, B. & BINDELS, R. J. 2005. Calcium absorption across epithelia. *Physiol Rev,* 85**,** 373-422.

HOFMANN, T., CHUBANOV, V., GUDERMANN, T. & MONTELL, C. 2003. TRPM5 is a voltage-modulated and Ca(2+)-activated monovalent selective cation channel. *Curr Biol,* 13**,** 1153-8.

HOFMANN, T., OBUKHOV, A. G., SCHAEFER, M., HARTENECK, C., GUDERMANN, T. & SCHULTZ, G. 1999. Direct activation of human TRPC6 and TRPC3 channels by diacylglycerol. *Nature,* 397**,** 259-63.

HONG, E. G., NOH, H. L., LEE, S. K., CHUNG, Y. S., LEE, K. W. & KIM, H. M. 2002. Insulin and glucagon secretions, and morphological change of pancreatic islets in OLETF rats, a model of type 2 diabetes mellitus. *J Korean Med Sci,* 17**,** 34-40.

HU, H., TIAN, J., ZHU, Y., WANG, C., XIAO, R., HERZ, J. M., WOOD, J. D. & ZHU, M. X. 2010. Activation of TRPA1 channels by fenamate nonsteroidal anti-inflammatory drugs. *Pflugers Arch,* 459**,** 579-92.

HU, H. Z., GU, Q., WANG, C., COLTON, C. K., TANG, J., KINOSHITA-KAWADA, M., LEE, L. Y., WOOD, J. D. & ZHU, M. X. 2004. 2-aminoethoxydiphenyl borate is a common activator of TRPV1, TRPV2, and TRPV3. *J Biol Chem,* 279**,** 35741-8.

HUANG, A. L., CHEN, X., HOON, M. A., CHANDRASHEKAR, J., GUO, W., TRANKNER, D., RYBA, N. J. & ZUKER, C. S. 2006. The cells and logic for mammalian sour taste detection. *Nature,* 442**,** 934-8.

INAMURA, K., SANO, Y., MOCHIZUKI, S., YOKOI, H., MIYAKE, A., NOZAWA, K., KITADA, C., MATSUSHIME, H. & FURUICHI, K. 2003. Response to ADP-ribose by activation of TRPM2 in the CRI-G1 insulinoma cell line. *J Membr Biol,* 191**,** 201-7.

INOUE, R., JENSEN, L. J., SHI, J., MORITA, H., NISHIDA, M., HONDA, A. & ITO, Y. 2006. Transient receptor potential channels in cardiovascular function and disease. *Circ Res,* 99**,** 119-31.

ISHII, M., SHIMIZU, S., HAGIWARA, T., WAJIMA, T., MIYAZAKI, A., MORI, Y. & KIUCHI, Y. 2006a. Extracellular-added ADP-ribose increases intracellular free Ca2+ concentration through Ca2+ release from stores, but not through TRPM2-mediated Ca2+ entry, in rat beta-cell line RIN-5F. *J Pharmacol Sci,* 101**,** 174-8.

ISHII, M., SHIMIZU, S., HARA, Y., HAGIWARA, T., MIYAZAKI, A., MORI, Y. & KIUCHI, Y. 2006b. Intracellular-produced hydroxyl radical mediates H2O2-induced Ca2+ influx and cell death in rat beta-cell line RIN-5F. *Cell Calcium,* 39**,** 487-94.

ISHIMARU, Y., INADA, H., KUBOTA, M., ZHUANG, H., TOMINAGA, M. & MATSUNAMI, H. 2006. Transient receptor potential family members PKD1L3 and PKD2L1 form a candidate sour taste receptor. *Proc Natl Acad Sci U S A,* 103**,** 12569-74.

JIANG, L. H., RASSENDREN, F., SURPRENANT, A. & NORTH, R. A. 2000. Identification of amino acid residues contributing to the ATP-binding site of a purinergic P2X receptor. *J Biol Chem,* 275**,** 34190-6.

JIANG, L. H., YANG, W., ZOU, J. & BEECH, D. J. 2010. TRPM2 channel properties, functions and therapeutic potentials. *Expert Opin Ther Targets,* 14**,** 973-88.

JORDT, S. E., TOMINAGA, M. & JULIUS, D. 2000. Acid potentiation of the capsaicin receptor determined by a key extracellular site. *Proc Natl Acad Sci U S A,* 97**,** 8134-9.

JOSSE, C., BOELAERT, J. R., BEST-BELPOMME, M. & PIETTE, J. 2001. Importance of post-transcriptional regulation of chemokine genes by oxidative stress. *Biochem J,* 360**,** 321-33.

KARACSONYI, C., MIGUEL, A. S. & PUERTOLLANO, R. 2007. Mucolipin-2 localizes to the Arf6-associated pathway and regulates recycling of GPI-APs. *Traffic,* 8**,** 1404-14.

KARASHIMA, Y., TALAVERA, K., EVERAERTS, W., JANSSENS, A., KWAN, K. Y., VENNEKENS, R., NILIUS, B. & VOETS, T. 2009. TRPA1 acts as a cold sensor in vitro and in vivo. *Proc Natl Acad Sci U S A,* 106**,** 1273-8.

KASHIO, M., SOKABE, T., SHINTAKU, K., UEMATSU, T., FUKUTA, N., KOBAYASHI, N., MORI, Y. & TOMINAGA, M. 2012. Redox signal-mediated sensitization of transient receptor potential melastatin 2 (TRPM2) to temperature affects macrophage functions. *Proc Natl Acad Sci U S A,* 109**,** 6745-50.

KATANO, M., NUMATA, T., AGUAN, K., HARA, Y., KIYONAKA, S., YAMAMOTO, S., MIKI, T., SAWAMURA, S., SUZUKI, T., YAMAKAWA, K. & MORI, Y. 2012. The juvenile myoclonic epilepsy-related protein EFHC1 interacts with the redox-sensitive TRPM2 channel linked to cell death. *Cell Calcium,* 51**,** 179-85.

KIM, H. J., LI, Q., TJON-KON-SANG, S., SO, I., KISELYOV, K., SOYOMBO, A. A. & MUALLEM, S. 2008. A novel mode of TRPML3 regulation by extracytosolic pH absent in the varitint-waddler phenotype. *EMBO J,* 27**,** 1197-205.

KIM, H. J., SOYOMBO, A. A., TJON-KON-SANG, S., SO, I. & MUALLEM, S. 2009. The Ca(2+) channel TRPML3 regulates membrane trafficking and autophagy. *Traffic,* 10**,** 1157-67.

KIM, M. Y., ZHANG, T. & KRAUS, W. L. 2005. Poly(ADP-ribosyl)ation by PARP-1: 'PAR-laying' NAD+ into a nuclear signal. *Genes Dev,* 19**,** 1951-67.

KINNEAR, N. P., BOITTIN, F. X., THOMAS, J. M., GALIONE, A. & EVANS, A. M. 2004. Lysosome-sarcoplasmic reticulum junctions. A trigger zone for calcium signaling by nicotinic acid adenine dinucleotide phosphate and endothelin-1. *J Biol Chem,* 279**,** 54319-26.

KINNEAR, N. P., WYATT, C. N., CLARK, J. H., CALCRAFT, P. J., FLEISCHER, S., JEYAKUMAR, L. H., NIXON, G. F. & EVANS, A. M. 2008. Lysosomes co-localize with ryanodine receptor subtype 3 to form a trigger zone for calcium signalling by NAADP in rat pulmonary arterial smooth muscle. *Cell Calcium,* 44**,** 190-201.

KISELYOV, K., XU, X., MOZHAYEVA, G., KUO, T., PESSAH, I., MIGNERY, G., ZHU, X., BIRNBAUMER, L. & MUALLEM, S. 1998. Functional interaction between InsP3 receptors and store-operated Htrp3 channels. *Nature,* 396**,** 478-82.

KLIONSKY, L., TAMIR, R., GAO, B., WANG, W., IMMKE, D. C., NISHIMURA, N. & GAVVA, N. R. 2007. Species-specific pharmacology of Trichloro(sulfanyl)ethyl benzamides as transient receptor potential ankyrin 1 (TRPA1) antagonists. *Mol Pain,* 3**,** 39.

KLOSE, C., STRAUB, I., RIEHLE, M., RANTA, F., KRAUTWURST, D., ULLRICH, S., MEYERHOF, W. & HARTENECK, C. 2011. Fenamates as TRP channel blockers: mefenamic acid selectively blocks TRPM3. *Br J Pharmacol,* 162**,** 1757-69.

KNOWLES, H., HEIZER, J. W., LI, Y., CHAPMAN, K., OGDEN, C. A., ANDREASEN, K., SHAPLAND, E., KUCERA, G., MOGAN, J., HUMANN, J., LENZ, L. L., MORRISON, A. D. & PERRAUD, A. L. 2011. Transient Receptor Potential Melastatin 2 (TRPM2) ion channel is required for innate immunity against Listeria monocytogenes. *Proc Natl Acad Sci U S A,* 108**,** 11578-83.

KOBAYASHI, K., FUKUOKA, T., OBATA, K., YAMANAKA, H., DAI, Y., TOKUNAGA, A. & NOGUCHI, K. 2005. Distinct expression of TRPM8, TRPA1, and TRPV1 mRNAs in rat primary afferent neurons with adelta/c-fibers and colocalization with trk receptors. *J Comp Neurol,* 493**,** 596-606.

KOLISEK, M., BECK, A., FLEIG, A. & PENNER, R. 2005. Cyclic ADP-ribose and hydrogen peroxide synergize with ADP-ribose in the activation of TRPM2 channels. *Mol Cell,* 18**,** 61-9.

KOSTER, J. C., PERMUTT, M. A. & NICHOLS, C. G. 2005. Diabetes and insulin secretion: the ATP-sensitive K+ channel (K ATP) connection. *Diabetes,* 54**,** 3065-72.

KOVACS, G., MONTALBETTI, N., SIMONIN, A., DANKO, T., BALAZS, B., ZSEMBERY, A. & HEDIGER, M. A. 2012. Inhibition of the human epithelial calcium channel TRPV6 by 2-aminoethoxydiphenyl borate (2-APB). *Cell Calcium,* 52**,** 468-80.

KRAFT, R., GRIMM, C., GROSSE, K., HOFFMANN, A., SAUERBRUCH, S., KETTENMANN, H., SCHULTZ, G. & HARTENECK, C. 2004. Hydrogen peroxide and ADP-ribose induce TRPM2-mediated calcium influx and cation currents in microglia. *Am J Physiol Cell Physiol,* 286**,** C129-37.

KREGEL, K. C. & ZHANG, H. J. 2007. An integrated view of oxidative stress in aging: basic mechanisms, functional effects, and pathological considerations. *Am J Physiol Regul Integr Comp Physiol,* 292**,** R18-36.

KUHN, F. J., KUHN, C., NAZIROGLU, M. & LUCKHOFF, A. 2009. Role of an N-terminal splice segment in the activation of the cation channel TRPM2 by ADP-ribose and hydrogen peroxide. *Neurochem Res,* 34**,** 227-33.

KUHN, F. J. & LUCKHOFF, A. 2004. Sites of the NUDT9-H domain critical for ADP-ribose activation of the cation channel TRPM2. *J Biol Chem,* 279**,** 46431-7.

KURAS, Z., YUN, Y. H., CHIMOTE, A. A., NEUMEIER, L. & CONFORTI, L. 2012. KCa3.1 and TRPM7 channels at the uropod regulate migration of activated human T cells. *PLoS One,* 7**,** e43859.

LACY, P. & STOW, J. L. 2011. Cytokine release from innate immune cells: association with diverse membrane trafficking pathways. *Blood,* 118**,** 9-18.

LANGE, I., PENNER, R., FLEIG, A. & BECK, A. 2008. Synergistic regulation of endogenous TRPM2 channels by adenine dinucleotides in primary human neutrophils. *Cell Calcium,* 44**,** 604-15.

LANGE, I., YAMAMOTO, S., PARTIDA-SANCHEZ, S., MORI, Y., FLEIG, A. & PENNER, R. 2009. TRPM2 functions as a lysosomal Ca2+-release channel in beta cells. *Sci Signal,* 2**,** ra23.

LAPLANTE, J. M., FALARDEAU, J. L., BROWN, E. M., SLAUGENHAUPT, S. A. & VASSILEV, P. M. 2011. The cation channel mucolipin-1 is a bifunctional protein that facilitates membrane remodeling via its serine lipase domain. *Exp Cell Res,* 317**,** 691-705.

LARDNER, A. 2001. The effects of extracellular pH on immune function. *J Leukoc Biol,* 69**,** 522-30.

LEE-KWON, W., WADE, J. B., ZHANG, Z., PALLONE, T. L. & WEINMAN, E. J. 2005. Expression of TRPC4 channel protein that interacts with NHERF-2 in rat descending vasa recta. *Am J Physiol Cell Physiol,* 288**,** C942-9.

LEE, N., CHEN, J., SUN, L., WU, S., GRAY, K. R., RICH, A., HUANG, M., LIN, J. H., FEDER, J. N., JANOVITZ, E. B., LEVESQUE, P. C. & BLANAR, M. A. 2003. Expression and characterization of human transient receptor potential melastatin 3 (hTRPM3). *J Biol Chem,* 278**,** 20890-7.

LEV, S., ZEEVI, D. A., FRUMKIN, A., OFFEN-GLASNER, V., BACH, G. & MINKE, B. 2010. Constitutive activity of the human TRPML2 channel induces cell degeneration. *J Biol Chem,* 285**,** 2771-82.

LIEDTKE, W. 2006. Transient receptor potential vanilloid channels functioning in transduction of osmotic stimuli. *J Endocrinol,* 191**,** 515-23.

LIEVREMONT, J. P., NUMAGA, T., VAZQUEZ, G., LEMONNIER, L., HARA, Y., MORI, E., TREBAK, M., MOSS, S. E., BIRD, G. S., MORI, Y. & PUTNEY, J. W., JR. 2005. The role of canonical transient receptor potential 7 in B-cell receptor-activated channels. *J Biol Chem,* 280**,** 35346-51.

LIMAN, E. R. 2007. TRPM5 and taste transduction. *Handb Exp Pharmacol***,** 287-98.

LINTE, R. M., CIOBANU, C., REID, G. & BABES, A. 2007. Desensitization of cold- and menthol-sensitive rat dorsal root ganglion neurones by inflammatory mediators. *Exp Brain Res,* 178**,** 89-98.

LIU, D. & LIMAN, E. R. 2003. Intracellular Ca2+ and the phospholipid PIP2 regulate the taste transduction ion channel TRPM5. *Proc Natl Acad Sci U S A,* 100**,** 15160-5.

LOF, C., VIITANEN, T., SUKUMARAN, P. & TORNQUIST, K. 2011. TRPC2: of mice but not men. *Adv Exp Med Biol,* 704**,** 125-34.

LOPEZJIMENEZ, N. D., CAVENAGH, M. M., SAINZ, E., CRUZ-ITHIER, M. A., BATTEY, J. F. & SULLIVAN, S. L. 2006. Two members of the TRPP family of ion channels, Pkd1l3 and Pkd2l1, are co-expressed in a subset of taste receptor cells. *J Neurochem,* 98**,** 68-77.

LUND, F. E., MULLER-STEFFNER, H., ROMERO-RAMIREZ, H., MORENO-GARCIA, M. E., PARTIDA-SANCHEZ, S., MAKRIS, M., OPPENHEIMER, N. J., SANTOS-ARGUMEDO, L. & SCHUBER, F. 2006. CD38 induces apoptosis of a murine pro-B leukemic cell line by a tyrosine kinase-dependent but ADP-ribosyl cyclase- and NAD glycohydrolase-independent mechanism. *Int Immunol,* 18**,** 1029-42.

LUND, F. E., SOLVASON, N. W., COOKE, M. P., HEALTH, A. W., GRIMALDI, J. C., PARKHOUSE, R. M., GOODNOW, C. C. & HOWARD, M. C. 1995. Signaling through murine CD38 is impaired in antigen receptor-unresponsive B cells. *Eur J Immunol,* 25**,** 1338-45.

MAEKAWA, K., IMAGAWA, N., NAGAMATSU, M. & HARADA, S. 1994. Molecular cloning of a novel protein-tyrosine phosphatase containing a membrane-binding domain and GLGF repeats. *FEBS Lett,* 337**,** 200-6.

MAGNONE, M., BAUER, I., POGGI, A., MANNINO, E., STURLA, L., BRINI, M., ZOCCHI, E., DE FLORA, A., NENCIONI, A. & BRUZZONE, S. 2012. NAD+ levels control Ca2+ store replenishment and mitogen-induced increase of cytosolic Ca2+ by Cyclic ADP-ribose-dependent TRPM2 channel gating in human T lymphocytes. *J Biol Chem,* 287**,** 21067-81.

MALAVASI, F., DEAGLIO, S., FERRERO, E., FUNARO, A., SANCHO, J., AUSIELLO, C. M., ORTOLAN, E., VAISITTI, T., ZUBIAUR, M., FEDELE, G., AYDIN, S., TIBALDI, E. V., DURELLI, I., LUSSO, R., COZNO, F. & HORENSTEIN, A. L. 2006. CD38 and CD157 as receptors of the immune system: a bridge between innate and adaptive immunity. *Mol Med,* 12**,** 334-41.

MALKIA, A., PERTUSA, M., FERNANDEZ-BALLESTER, G., FERRER-MONTIEL, A. & VIANA, F. 2009. Differential role of the menthol-binding residue Y745 in the antagonism of thermally gated TRPM8 channels. *Mol Pain,* 5**,** 62.

MANDER, P. K., JEKABSONE, A. & BROWN, G. C. 2006. Microglia proliferation is regulated by hydrogen peroxide from NADPH oxidase. *J Immunol,* 176**,** 1046-52.

MARCHAND, F., PERRETTI, M. & MCMAHON, S. B. 2005. Role of the immune system in chronic pain. *Nat Rev Neurosci,* 6**,** 521-32.

MARTINA, J. A., LELOUVIER, B. & PUERTOLLANO, R. 2009. The calcium channel mucolipin-3 is a novel regulator of trafficking along the endosomal pathway. *Traffic,* 10**,** 1143-56.

MARUYAMA, Y., OGURA, T., MIO, K., KIYONAKA, S., KATO, K., MORI, Y. & SATO, C. 2007. Three-dimensional reconstruction using transmission electron microscopy reveals a swollen, bell-shaped structure of transient receptor potential melastatin type 2 cation channel. *J Biol Chem,* 282**,** 36961-70.

MCGHEE, D. J., ROYLE, P. L., THOMPSON, P. A., WRIGHT, D. E., ZAJICEK, J. P. & COUNSELL, C. E. 2013. A systematic review of biomarkers for disease progression in Parkinson's disease. *BMC Neurol,* 13**,** 35.

MCHUGH, D., FLEMMING, R., XU, S. Z., PERRAUD, A. L. & BEECH, D. J. 2003. Critical intracellular Ca2+ dependence of transient receptor potential melastatin 2 (TRPM2) cation channel activation. *J Biol Chem,* 278**,** 11002-6.

MCKEMY, D. D., NEUHAUSSER, W. M. & JULIUS, D. 2002. Identification of a cold receptor reveals a general role for TRP channels in thermosensation. *Nature,* 416**,** 52-8.

MEI, Z. Z. & JIANG, L. H. 2009. Requirement for the N-terminal coiled-coil domain for expression and function, but not subunit interaction of, the ADPR-activated TRPM2 channel. *J Membr Biol,* 230**,** 93-9.

MEI, Z. Z., MAO, H. J. & JIANG, L. H. 2006a. Conserved cysteine residues in the pore region are obligatory for human TRPM2 channel function. *Am J Physiol Cell Physiol,* 291**,** C1022-8.

MEI, Z. Z., XIA, R., BEECH, D. J. & JIANG, L. H. 2006b. Intracellular coiled-coil domain engaged in subunit interaction and assembly of melastatin-related transient receptor potential channel 2. *J Biol Chem,* 281**,** 38748-56.

MELZER, N., HICKING, G., GOBEL, K. & WIENDL, H. 2012. TRPM2 cation channels modulate T cell effector functions and contribute to autoimmune CNS inflammation. *PLoS One,* 7**,** e47617.

MINKE, B., WU, C. & PAK, W. L. 1975. Induction of photoreceptor voltage noise in the dark in Drosophila mutant. *Nature,* 258**,** 84-7.

MISHRA, R., RAO, V., TA, R., SHOBEIRI, N. & HILL, C. E. 2009. Mg2+- and MgATP-inhibited and Ca2+/calmodulin-sensitive TRPM7-like current in hepatoma and hepatocytes. *Am J Physiol Gastrointest Liver Physiol,* 297**,** G687-94.

MOCHIZUKI, T., WU, G., HAYASHI, T., XENOPHONTOS, S. L., VELDHUISEN, B., SARIS, J. J., REYNOLDS, D. M., CAI, Y., GABOW, P. A., PIERIDES, A., KIMBERLING, W. J., BREUNING, M. H., DELTAS, C. C., PETERS, D. J. & SOMLO, S. 1996. PKD2, a gene for polycystic kidney disease that encodes an integral membrane protein. *Science,* 272**,** 1339-42.

MONET, M., FRANCOEUR, N. & BOULAY, G. 2012. Involvement of phosphoinositide 3-kinase and PTEN protein in mechanism of activation of TRPC6 protein in vascular smooth muscle cells. *J Biol Chem,* 287**,** 17672-81.

MONTELL, C. 2005. The TRP superfamily of cation channels. *Sci STKE,* 2005**,** re3.

MONTELL, C. & RUBIN, G. M. 1989. Molecular characterization of the Drosophila trp locus: a putative integral membrane protein required for phototransduction. *Neuron,* 2**,** 1313-23.

MONTELL, D. J. & GOODMAN, C. S. 1989. Drosophila laminin: sequence of B2 subunit and expression of all three subunits during embryogenesis. *J Cell Biol,* 109**,** 2441-53.

MONTELL, E., LERIN, C., NEWGARD, C. B. & GOMEZ-FOIX, A. M. 2002. Effects of modulation of glycerol kinase expression on lipid and carbohydrate metabolism in human muscle cells. *J Biol Chem,* 277**,** 2682-6.

MOORE, T. M., CHETHAM, P. M., KELLY, J. J. & STEVENS, T. 1998. Signal transduction and regulation of lung endothelial cell permeability. Interaction between calcium and cAMP. *Am J Physiol,* 275**,** L203-22.

MUNSCH, T., FREICHEL, M., FLOCKERZI, V. & PAPE, H. C. 2003. Contribution of transient receptor potential channels to the control of GABA release from dendrites. *Proc Natl Acad Sci U S A,* 100**,** 16065-70.

MURAKAMI, M., OHBA, T., XU, F., SHIDA, S., SATOH, E., ONO, K., MIYOSHI, I., WATANABE, H., ITO, H. & IIJIMA, T. 2005. Genomic organization and functional analysis of murine PKD2L1. *J Biol Chem,* 280**,** 5626-35.

MURAKI, K., IWATA, Y., KATANOSAKA, Y., ITO, T., OHYA, S., SHIGEKAWA, M. & IMAIZUMI, Y. 2003. TRPV2 is a component of osmotically sensitive cation channels in murine aortic myocytes. *Circ Res,* 93**,** 829-38.

NADLER, M. J., HERMOSURA, M. C., INABE, K., PERRAUD, A. L., ZHU, Q., STOKES, A. J., KUROSAKI, T., KINET, J. P., PENNER, R., SCHARENBERG, A. M. & FLEIG, A. 2001. LTRPC7 is a Mg.ATP-regulated divalent cation channel required for cell viability. *Nature,* 411**,** 590-5.

NAGAMINE, K., KUDOH, J., MINOSHIMA, S., KAWASAKI, K., ASAKAWA, S., ITO, F. & SHIMIZU, N. 1998. Molecular cloning of a novel putative Ca2+ channel protein (TRPC7) highly expressed in brain. *Genomics,* 54**,** 124-31.

NAGATA, K., DUGGAN, A., KUMAR, G. & GARCIA-ANOVEROS, J. 2005. Nociceptor and hair cell transducer properties of TRPA1, a channel for pain and hearing. *J Neurosci,* 25**,** 4052-61.

NAKAYAMA, H., WILKIN, B. J., BODI, I. & MOLKENTIN, J. D. 2006. Calcineurin-dependent cardiomyopathy is activated by TRPC in the adult mouse heart. *FASEB J,* 20**,** 1660-70.

NARGI, F. E. & YANG, T. J. 1993. Optimization of the L-M cell bioassay for quantitating tumor necrosis factor alpha in serum and plasma. *J Immunol Methods,* 159**,** 81-91.

NATH, A. K., KRAUTHAMMER, M., LI, P., DAVIDOV, E., BUTLER, L. C., COPEL, J., KATAJAMAA, M., ORESIC, M., BUHIMSCHI, I., BUHIMSCHI, C., SNYDER, M. & MADRI, J. A. 2009. Proteomic-based detection of a protein cluster dysregulated during cardiovascular development identifies biomarkers of congenital heart defects. *PLoS One,* 4**,** e4221.

NAULI, S. M., ALENGHAT, F. J., LUO, Y., WILLIAMS, E., VASSILEV, P., LI, X., ELIA, A. E., LU, W., BROWN, E. M., QUINN, S. J., INGBER, D. E. & ZHOU, J. 2003. Polycystins 1 and 2 mediate mechanosensation in the primary cilium of kidney cells. *Nat Genet,* 33**,** 129-37.

NAYLOR, J., LI, J., MILLIGAN, C. J., ZENG, F., SUKUMAR, P., HOU, B., SEDO, A., YULDASHEVA, N., MAJEED, Y., BERI, D., JIANG, S., SEYMOUR, V. A., MCKEOWN, L., KUMAR, B., HARTENECK, C., O'REGAN, D., WHEATCROFT, S. B., KEARNEY, M. T., JONES, C., PORTER, K. E. & BEECH, D. J. 2010. Pregnenolone sulphate- and cholesterol-regulated TRPM3 channels coupled to vascular smooth muscle secretion and contraction. *Circ Res,* 106**,** 1507-15.

NAZIROGLU, M., OZGUL, C., CIG, B., DOGAN, S. & UGUZ, A. C. 2011. Glutathione modulates Ca(2+) influx and oxidative toxicity through TRPM2 channel in rat dorsal root ganglion neurons. *J Membr Biol,* 242**,** 109-18.

NAZIROGLU, M., OZGUL, C., KUCUKAYAZ, M., CIG, B., HEBEISEN, S. & BAL, R. 2013. Selenium modulates oxidative stress-induced TRPM2 cation channel currents in transfected Chinese hamster ovary cells. *Basic Clin Pharmacol Toxicol,* 112**,** 96-102.

NEEPER, M. P., LIU, Y., HUTCHINSON, T. L., WANG, Y., FLORES, C. M. & QIN, N. 2007. Activation properties of heterologously expressed mammalian TRPV2: evidence for species dependence. *J Biol Chem,* 282**,** 15894-902.

NEHER, E. & SAKMANN, B. 1992. The patch clamp technique. *Sci Am,* 266**,** 44-51.

NIJENHUIS, T., HOENDEROP, J. G. & BINDELS, R. J. 2005. TRPV5 and TRPV6 in Ca(2+) (re)absorption: regulating Ca(2+) entry at the gate. *Pflugers Arch,* 451**,** 181-92.

NIJENHUIS, T., HOENDEROP, J. G., VAN DER KEMP, A. W. & BINDELS, R. J. 2003. Localization and regulation of the epithelial Ca2+ channel TRPV6 in the kidney. *J Am Soc Nephrol,* 14**,** 2731-40.

NIJENHUIS, T., RENKEMA, K. Y., HOENDEROP, J. G. & BINDELS, R. J. 2006. Acid-base status determines the renal expression of Ca2+ and Mg2+ transport proteins. *J Am Soc Nephrol,* 17**,** 617-26.

NILIUS, B. 2007. Transient receptor potential (TRP) cation channels: rewarding unique proteins. *Bull Mem Acad R Med Belg,* 162**,** 244-53.

NILIUS, B., OWSIANIK, G., VOETS, T. & PETERS, J. A. 2007. Transient receptor potential cation channels in disease. *Physiol Rev,* 87**,** 165-217.

NILIUS, B., PRENEN, J., DROOGMANS, G., VOETS, T., VENNEKENS, R., FREICHEL, M., WISSENBACH, U. & FLOCKERZI, V. 2003a. Voltage dependence of the Ca2+-activated cation channel TRPM4. *J Biol Chem,* 278**,** 30813-20.

NILIUS, B., PRENEN, J., VENNEKENS, R., HOENDEROP, J. G., BINDELS, R. J. & DROOGMANS, G. 2001a. Modulation of the epithelial calcium channel, ECaC, by intracellular Ca2+. *Cell Calcium,* 29**,** 417-28.

NILIUS, B., PRENEN, J., VENNEKENS, R., HOENDEROP, J. G., BINDELS, R. J. & DROOGMANS, G. 2001b. Pharmacological modulation of monovalent cation currents through the epithelial Ca2+ channel ECaC1. *Br J Pharmacol,* 134**,** 453-62.

NILIUS, B., VENNEKENS, R., PRENEN, J., HOENDEROP, J. G., BINDELS, R. J. & DROOGMANS, G. 2000. Whole-cell and single channel monovalent cation currents through the novel rabbit epithelial Ca2+ channel ECaC. *J Physiol,* 527 Pt 2**,** 239-48.

NILIUS, B., VRIENS, J., PRENEN, J., DROOGMANS, G. & VOETS, T. 2004. TRPV4 calcium entry channel: a paradigm for gating diversity. *Am J Physiol Cell Physiol,* 286**,** C195-205.

NILIUS, B., WATANABE, H. & VRIENS, J. 2003b. The TRPV4 channel: structure-function relationship and promiscuous gating behaviour. *Pflugers Arch,* 446**,** 298-303.

NOBEN-TRAUTH, K. 2011. The TRPML3 channel: from gene to function. *Adv Exp Med Biol,* 704**,** 229-37.

NOMOTO, Y., YOSHIDA, A., IKEDA, S., KAMIKAWA, Y., HARADA, K., OHWATASHI, A. & KAWAHIRA, K. 2008. Effect of menthol on detrusor smooth-muscle contraction and the micturition reflex in rats. *Urology,* 72**,** 701-5.

NOMURA, H., TURCO, A. E., PEI, Y., KALAYDJIEVA, L., SCHIAVELLO, T., WEREMOWICZ, S., JI, W., MORTON, C. C., MEISLER, M., REEDERS, S. T. & ZHOU, J. 1998. Identification of PKDL, a novel polycystic kidney disease 2-like gene whose murine homologue is deleted in mice with kidney and retinal defects. *J Biol Chem,* 273**,** 25967-73.

NUMATA, T., SATO, K., CHRISTMANN, J., MARX, R., MORI, Y., OKADA, Y. & WEHNER, F. 2012. The DeltaC splice-variant of TRPM2 is the hypertonicity-induced cation channel in HeLa cells, and the ecto-enzyme CD38 mediates its activation. *J Physiol,* 590**,** 1121-38.

NUMBERGER, M. & DRAGUHN, A. 1996. Patch-Clamp-Technik. *Spektrum Akademischer Verlag*.

OANCEA, E., VRIENS, J., BRAUCHI, S., JUN, J., SPLAWSKI, I. & CLAPHAM, D. E. 2009. TRPM1 forms ion channels associated with melanin content in melanocytes. *Sci Signal,* 2**,** ra21.

OBERWINKLER, J., LIS, A., GIEHL, K. M., FLOCKERZI, V. & PHILIPP, S. E. 2005. Alternative splicing switches the divalent cation selectivity of TRPM3 channels. *J Biol Chem,* 280**,** 22540-8.

ODELL, A. F., SCOTT, J. L. & VAN HELDEN, D. F. 2005. Epidermal growth factor induces tyrosine phosphorylation, membrane insertion, and activation of transient receptor potential channel 4. *J Biol Chem,* 280**,** 37974-87.

OKADA, T., INOUE, R., YAMAZAKI, K., MAEDA, A., KUROSAKI, T., YAMAKUNI, T., TANAKA, I., SHIMIZU, S., IKENAKA, K., IMOTO, K. & MORI, Y. 1999. Molecular and functional characterization of a novel mouse transient receptor potential protein homologue TRP7. Ca(2+)-permeable cation channel that is constitutively activated and enhanced by stimulation of G protein-coupled receptor. *J Biol Chem,* 274**,** 27359-70.

OKADA, Y., REINACH, P. S., SHIRAI, K., KITANO, A., KAO, W. W., FLANDERS, K. C., MIYAJIMA, M., LIU, H., ZHANG, J. & SAIKA, S. 2011. TRPV1 involvement in inflammatory tissue fibrosis in mice. *Am J Pathol,* 178**,** 2654-64.

OLAH, M. E., JACKSON, M. F., LI, H., PEREZ, Y., SUN, H. S., KIYONAKA, S., MORI, Y., TYMIANSKI, M. & MACDONALD, J. F. 2009. Ca2+-dependent induction of TRPM2 currents in hippocampal neurons. *J Physiol,* 587**,** 965-79.

OLSON, T. M. & TERZIC, A. 2010. Human K(ATP) channelopathies: diseases of metabolic homeostasis. *Pflugers Arch,* 460**,** 295-306.

PARAKH, S., SPENCER, D. M., HALLORAN, M. A., SOO, K. Y. & ATKIN, J. D. 2013. Redox regulation in amyotrophic lateral sclerosis. *Oxid Med Cell Longev,* 2013**,** 408681.

PARTIDA-SANCHEZ, S., COCKAYNE, D. A., MONARD, S., JACOBSON, E. L., OPPENHEIMER, N., GARVY, B., KUSSER, K., GOODRICH, S., HOWARD, M., HARMSEN, A., RANDALL, T. D. & LUND, F. E. 2001. Cyclic ADP-ribose production by CD38 regulates intracellular calcium release, extracellular calcium influx and chemotaxis in neutrophils and is required for bacterial clearance in vivo. *Nat Med,* 7**,** 1209-16.

PARTIDA-SANCHEZ, S., RIVERO-NAVA, L., SHI, G. & LUND, F. E. 2007. CD38: an ecto-enzyme at the crossroads of innate and adaptive immune responses. *Adv Exp Med Biol,* 590**,** 171-83.

PEDERSEN, S. F., OWSIANIK, G. & NILIUS, B. 2005. TRP channels: an overview. *Cell Calcium,* 38**,** 233-52.

PEIER, A. M., MOQRICH, A., HERGARDEN, A. C., REEVE, A. J., ANDERSSON, D. A., STORY, G. M., EARLEY, T. J., DRAGONI, I., MCINTYRE, P., BEVAN, S. & PATAPOUTIAN, A. 2002a. A TRP channel that senses cold stimuli and menthol. *Cell,* 108**,** 705-15.

PEIER, A. M., REEVE, A. J., ANDERSSON, D. A., MOQRICH, A., EARLEY, T. J., HERGARDEN, A. C., STORY, G. M., COLLEY, S., HOGENESCH, J. B., MCINTYRE, P., BEVAN, S. & PATAPOUTIAN, A. 2002b. A heat-sensitive TRP channel expressed in keratinocytes. *Science,* 296**,** 2046-9.

PEREZ, C. A., HUANG, L., RONG, M., KOZAK, J. A., PREUSS, A. K., ZHANG, H., MAX, M. & MARGOLSKEE, R. F. 2002. A transient receptor potential channel expressed in taste receptor cells. *Nat Neurosci,* 5**,** 1169-76.

PERRAUD, A. L., FLEIG, A., DUNN, C. A., BAGLEY, L. A., LAUNAY, P., SCHMITZ, C., STOKES, A. J., ZHU, Q., BESSMAN, M. J., PENNER, R., KINET, J. P. & SCHARENBERG, A. M. 2001. ADP-ribose gating of the calcium-permeable LTRPC2 channel revealed by Nudix motif homology. *Nature,* 411**,** 595-9.

PERRAUD, A. L., TAKANISHI, C. L., SHEN, B., KANG, S., SMITH, M. K., SCHMITZ, C., KNOWLES, H. M., FERRARIS, D., LI, W., ZHANG, J., STODDARD, B. L. & SCHARENBERG, A. M. 2005. Accumulation of free ADP-ribose from mitochondria mediates oxidative stress-induced gating of TRPM2 cation channels. *J Biol Chem,* 280**,** 6138-48.

PHILIPP, S., HAMBRECHT, J., BRASLAVSKI, L., SCHROTH, G., FREICHEL, M., MURAKAMI, M., CAVALIE, A. & FLOCKERZI, V. 1998. A novel capacitative calcium entry channel expressed in excitable cells. *EMBO J,* 17**,** 4274-82.

PINGLE, S. C., JAJOO, S., MUKHERJEA, D., SNIDERHAN, L. F., JHAVERI, K. A., MARCUZZI, A., RYBAK, L. P., MAGGIRWAR, S. B. & RAMKUMAR, V. 2007. Activation of the adenosine A1 receptor inhibits HIV-1 tat-induced apoptosis by reducing nuclear factor-kappaB activation and inducible nitric-oxide synthase. *Mol Pharmacol,* 72**,** 856-67.

PIPER, R. C. & LUZIO, J. P. 2004. CUPpling calcium to lysosomal biogenesis. *Trends Cell Biol,* 14**,** 471-3.

PLANELLS-CASES, R., GARCIA-SANZ, N., MORENILLA-PALAO, C. & FERRER-MONTIEL, A. 2005. Functional aspects and mechanisms of TRPV1 involvement in neurogenic inflammation that leads to thermal hyperalgesia. *Pflugers Arch,* 451**,** 151-9.

PLANT, T. D. & SCHAEFER, M. 2003. TRPC4 and TRPC5: receptor-operated Ca2+-permeable nonselective cation channels. *Cell Calcium,* 33**,** 441-50.

POTESER, M., GRAZIANI, A., ROSKER, C., EDER, P., DERLER, I., KAHR, H., ZHU, M. X., ROMANIN, C. & GROSCHNER, K. 2006. TRPC3 and TRPC4 associate to form a redox-sensitive cation channel. Evidence for expression of native TRPC3-TRPC4 heteromeric channels in endothelial cells. *J Biol Chem,* 281**,** 13588-95.

PREMKUMAR, L. S., RAISINGHANI, M., PINGLE, S. C., LONG, C. & PIMENTEL, F. 2005. Downregulation of transient receptor potential melastatin 8 by protein kinase C-mediated dephosphorylation. *J Neurosci,* 25**,** 11322-9.

PRICE, D. L., BORCHELT, D. R. & SISODIA, S. S. 1993. Alzheimer disease and the prion disorders amyloid beta-protein and prion protein amyloidoses. *Proc Natl Acad Sci U S A,* 90**,** 6381-4.

RAMSEY, I. S., DELLING, M. & CLAPHAM, D. E. 2006. An introduction to TRP channels. *Annu Rev Physiol,* 68**,** 619-47.

RICCIO, A., LI, Y., MOON, J., KIM, K. S., SMITH, K. S., RUDOLPH, U., GAPON, S., YAO, G. L., TSVETKOV, E., RODIG, S. J., VAN'T VEER, A., MELONI, E. G., CARLEZON, W. A., JR., BOLSHAKOV, V. Y. & CLAPHAM, D. E. 2009. Essential role for TRPC5 in amygdala function and fear-related behavior. *Cell,* 137**,** 761-72.

ROEDDING, A. S., GAO, A. F., AU-YEUNG, W., SCARCELLI, T., LI, P. P. & WARSH, J. J. 2012. Effect of oxidative stress on TRPM2 and TRPC3 channels in B lymphoblast cells in bipolar disorder. *Bipolar Disord,* 14**,** 151-61.

ROGER, S., MEI, Z. Z., BALDWIN, J. M., DONG, L., BRADLEY, H., BALDWIN, S. A., SURPRENANT, A. & JIANG, L. H. 2010. Single nucleotide polymorphisms that were identified in affective mood disorders affect ATP-activated P2X7 receptor functions. *J Psychiatr Res,* 44**,** 347-55.

RYCHKOV, G. & BARRITT, G. J. 2007. TRPC1 Ca(2+)-permeable channels in animal cells. *Handb Exp Pharmacol***,** 23-52.

SABNIS, A. S., SHADID, M., YOST, G. S. & REILLY, C. A. 2008. Human lung epithelial cells express a functional cold-sensing TRPM8 variant. *Am J Respir Cell Mol Biol,* 39**,** 466-74.

SANO, Y., INAMURA, K., MIYAKE, A., MOCHIZUKI, S., YOKOI, H., MATSUSHIME, H. & FURUICHI, K. 2001. Immunocyte Ca2+ influx system mediated by LTRPC2. *Science,* 293**,** 1327-30.

SATO, T., IRIE, S., KITADA, S. & REED, J. C. 1995. FAP-1: a protein tyrosine phosphatase that associates with Fas. *Science,* 268**,** 411-5.

SCHAEFER, M., PLANT, T. D., OBUKHOV, A. G., HOFMANN, T., GUDERMANN, T. & SCHULTZ, G. 2000. Receptor-mediated regulation of the nonselective cation channels TRPC4 and TRPC5. *J Biol Chem,* 275**,** 17517-26.

SCHMIDT, T. M. 2009. Role of melastatin-related transient receptor potential channel TRPM1 in the retina: Clues from horses and mice. *J Neurosci,* 29**,** 11720-2.

SCHWENDE, H., FITZKE, E., AMBS, P. & DIETER, P. 1996. Differences in the state of differentiation of THP-1 cells induced by phorbol ester and 1,25-dihydroxyvitamin D3. *J Leukoc Biol,* 59**,** 555-61.

SHEN, B. W., PERRAUD, A. L., SCHARENBERG, A. & STODDARD, B. L. 2003. The crystal structure and mutational analysis of human NUDT9. *J Mol Biol,* 332**,** 385-98.

SHI, J., GESHI, N., TAKAHASHI, S., KIYONAKA, S., ICHIKAWA, J., HU, Y., MORI, Y., ITO, Y. & INOUE, R. 2013. Molecular determinants for cardiovascular TRPC6 channel regulation by Ca2+/calmodulin-dependent kinase II. *J Physiol,* 591**,** 2851-66.

SHIMOSATO, G., AMAYA, F., UEDA, M., TANAKA, Y., DECOSTERD, I. & TANAKA, M. 2005. Peripheral inflammation induces up-regulation of TRPV2 expression in rat DRG. *Pain,* 119**,** 225-32.

SIFLINGER-BIRNBOIM, A., LUM, H., DEL VECCHIO, P. J. & MALIK, A. B. 1996. Involvement of Ca2+ in the H2O2-induced increase in endothelial permeability. *Am J Physiol,* 270**,** L973-8.

SIMARD, C., HOF, T., KEDDACHE, Z., LAUNAY, P. & GUINAMARD, R. 2013. The TRPM4 non-selective cation channel contributes to the mammalian atrial action potential. *J Mol Cell Cardiol,* 59**,** 11-9.

SMITH, G. D., GUNTHORPE, M. J., KELSELL, R. E., HAYES, P. D., REILLY, P., FACER, P., WRIGHT, J. E., JERMAN, J. C., WALHIN, J. P., OOI, L., EGERTON, J., CHARLES, K. J., SMART, D., RANDALL, A. D., ANAND, P. & DAVIS, J. B. 2002. TRPV3 is a temperature-sensitive vanilloid receptor-like protein. *Nature,* 418**,** 186-90.

SONG, Y., BUELOW, B., PERRAUD, A. L. & SCHARENBERG, A. M. 2008. Development and validation of a cell-based high-throughput screening assay for TRPM2 channel modulators. *J Biomol Screen,* 13**,** 54-61.

SONODA, Y., MUKAIDA, N., WANG, J. B., SHIMADA-HIRATSUKA, M., NAITO, M., KASAHARA, T., HARADA, A., INOUE, M. & MATSUSHIMA, K. 1998. Physiologic regulation of postovulatory neutrophil migration into vagina in mice by a C-X-C chemokine(s). *J Immunol,* 160**,** 6159-65.

SOSSEY-ALAOUI, K., LYON, J. A., JONES, L., ABIDI, F. E., HARTUNG, A. J., HANE, B., SCHWARTZ, C. E., STEVENSON, R. E. & SRIVASTAVA, A. K. 1999. Molecular cloning and characterization of TRPC5 (HTRP5), the human homologue of a mouse brain receptor-activated capacitative Ca2+ entry channel. *Genomics,* 60**,** 330-40.

STARKUS, J., BECK, A., FLEIG, A. & PENNER, R. 2007. Regulation of TRPM2 by extra- and intracellular calcium. *J Gen Physiol,* 130**,** 427-40.

STARKUS, J. G., FLEIG, A. & PENNER, R. 2010. The calcium-permeable non-selective cation channel TRPM2 is modulated by cellular acidification. *J Physiol,* 588**,** 1227-40.

STORY, G. M., PEIER, A. M., REEVE, A. J., EID, S. R., MOSBACHER, J., HRICIK, T. R., EARLEY, T. J., HERGARDEN, A. C., ANDERSSON, D. A., HWANG, S. W., MCINTYRE, P., JEGLA, T., BEVAN, S. & PATAPOUTIAN, A. 2003. ANKTM1, a TRP-like channel expressed in nociceptive neurons, is activated by cold temperatures. *Cell,* 112**,** 819-29.

STROTMANN, R., HARTENECK, C., NUNNENMACHER, K., SCHULTZ, G. & PLANT, T. D. 2000. OTRPC4, a nonselective cation channel that confers sensitivity to extracellular osmolarity. *Nat Cell Biol,* 2**,** 695-702.

SU, L. T., AGAPITO, M. A., LI, M., SIMONSON, W. T., HUTTENLOCHER, A., HABAS, R., YUE, L. & RUNNELS, L. W. 2006. TRPM7 regulates cell adhesion by controlling the calcium-dependent protease calpain. *J Biol Chem,* 281**,** 11260-70.

SUKUMAR, P. & BEECH, D. J. 2010. Stimulation of TRPC5 cationic channels by low micromolar concentrations of lead ions (Pb2+). *Biochem Biophys Res Commun,* 393**,** 50-4.

SUMOZA-TOLEDO, A., LANGE, I., CORTADO, H., BHAGAT, H., MORI, Y., FLEIG, A., PENNER, R. & PARTIDA-SANCHEZ, S. 2011. Dendritic cell maturation and chemotaxis is regulated by TRPM2-mediated lysosomal Ca2+ release. *FASEB J,* 25**,** 3529-42.

SUMOZA-TOLEDO, A. & PENNER, R. 2011. TRPM2: a multifunctional ion channel for calcium signalling. *J Physiol,* 589**,** 1515-25.

SUN, L., YAU, H. Y., WONG, W. Y., LI, R. A., HUANG, Y. & YAO, X. 2012. Role of TRPM2 in H(2)O(2)-induced cell apoptosis in endothelial cells. *PLoS One,* 7**,** e43186.

SUN, M., GOLDIN, E., STAHL, S., FALARDEAU, J. L., KENNEDY, J. C., ACIERNO, J. S., JR., BOVE, C., KANESKI, C. R., NAGLE, J., BROMLEY, M. C., COLMAN, M., SCHIFFMANN, R. & SLAUGENHAUPT, S. A. 2000. Mucolipidosis type IV is caused by mutations in a gene encoding a novel transient receptor potential channel. *Hum Mol Genet,* 9**,** 2471-8.

SUTTON, K. A., JUNGNICKEL, M. K., WANG, Y., CULLEN, K., LAMBERT, S. & FLORMAN, H. M. 2004. Enkurin is a novel calmodulin and TRPC channel binding protein in sperm. *Dev Biol,* 274**,** 426-35.

TAKAHASHI, N., KOZAI, D., KOBAYASHI, R., EBERT, M. & MORI, Y. 2011. Roles of TRPM2 in oxidative stress. *Cell Calcium,* 50**,** 279-87.

TALAVERA, K., YASUMATSU, K., VOETS, T., DROOGMANS, G., SHIGEMURA, N., NINOMIYA, Y., MARGOLSKEE, R. F. & NILIUS, B. 2005. Heat activation of TRPM5 underlies thermal sensitivity of sweet taste. *Nature,* 438**,** 1022-5.

THEBAULT, S., CAO, G., VENSELAAR, H., XI, Q., BINDELS, R. J. & HOENDEROP, J. G. 2008. Role of the alpha-kinase domain in transient receptor potential melastatin 6 channel and regulation by intracellular ATP. *J Biol Chem,* 283**,** 19999-20007.

TOGASHI, K., HARA, Y., TOMINAGA, T., HIGASHI, T., KONISHI, Y., MORI, Y. & TOMINAGA, M. 2006. TRPM2 activation by cyclic ADP-ribose at body temperature is involved in insulin secretion. *EMBO J,* 25**,** 1804-15.

TOGASHI, K., INADA, H. & TOMINAGA, M. 2008. Inhibition of the transient receptor potential cation channel TRPM2 by 2-aminoethoxydiphenyl borate (2-APB). *Br J Pharmacol,* 153**,** 1324-30.

TOMINAGA, M., CATERINA, M. J., MALMBERG, A. B., ROSEN, T. A., GILBERT, H., SKINNER, K., RAUMANN, B. E., BASBAUM, A. I. & JULIUS, D. 1998. The cloned capsaicin receptor integrates multiple pain-producing stimuli. *Neuron,* 21**,** 531-43.

TOMINAGA, M. & TOMINAGA, T. 2005. Structure and function of TRPV1. *Pflugers Arch,* 451**,** 143-50.

TONG, Q., ZHANG, W., CONRAD, K., MOSTOLLER, K., CHEUNG, J. Y., PETERSON, B. Z. & MILLER, B. A. 2006. Regulation of the transient receptor potential channel TRPM2 by the Ca2+ sensor calmodulin. *J Biol Chem,* 281**,** 9076-85.

TOTH, B. & CSANADY, L. 2010. Identification of direct and indirect effectors of the transient receptor potential melastatin 2 (TRPM2) cation channel. *J Biol Chem,* 285**,** 30091-102.

TOTH, B. & CSANADY, L. 2012. Pore collapse underlies irreversible inactivation of TRPM2 cation channel currents. *Proc Natl Acad Sci U S A,* 109**,** 13440-5.

TSAVALER, L., SHAPERO, M. H., MORKOWSKI, S. & LAUS, R. 2001. Trp-p8, a novel prostate-specific gene, is up-regulated in prostate cancer and other malignancies and shares high homology with transient receptor potential calcium channel proteins. *Cancer Res,* 61**,** 3760-9.

TSUKIMI, Y., MIZUYACHI, K., YAMASAKI, T., NIKI, T. & HAYASHI, F. 2005. Cold response of the bladder in guinea pig: involvement of transient receptor potential channel, TRPM8. *Urology,* 65**,** 406-10.

TSURUDA, P. R., JULIUS, D. & MINOR, D. L., JR. 2006. Coiled coils direct assembly of a cold-activated TRP channel. *Neuron,* 51**,** 201-12.

TSUTSUI, H., KINUGAWA, S. & MATSUSHIMA, S. 2011. Oxidative stress and heart failure. *Am J Physiol Heart Circ Physiol,* 301**,** H2181-90.

TURNER, K. L. & SONTHEIMER, H. 2013. KCa3.1 Modulates Neuroblast Migration Along the Rostral Migratory Stream (RMS) In Vivo. *Cereb Cortex*.

UCHIDA, K., DEZAKI, K., DAMDINDORJ, B., INADA, H., SHIUCHI, T., MORI, Y., YADA, T., MINOKOSHI, Y. & TOMINAGA, M. 2011. Lack of TRPM2 impaired insulin secretion and glucose metabolisms in mice. *Diabetes,* 60**,** 119-26.

UCHIDA, K. & TOMINAGA, M. 2011. TRPM2 modulates insulin secretion in pancreatic beta-cells. *Islets,* 3**,** 209-11.

UEHARA, K. 2005. Localization of TRPC1 channel in the sinus endothelial cells of rat spleen. *Histochem Cell Biol,* 123**,** 347-56.

UEMURA, T., KUDOH, J., NODA, S., KANBA, S. & SHIMIZU, N. 2005. Characterization of human and mouse TRPM2 genes: identification of a novel N-terminal truncated protein specifically expressed in human striatum. *Biochem Biophys Res Commun,* 328**,** 1232-43.

ULLRICH, N. D., VOETS, T., PRENEN, J., VENNEKENS, R., TALAVERA, K., DROOGMANS, G. & NILIUS, B. 2005. Comparison of functional properties of the Ca2+-activated cation channels TRPM4 and TRPM5 from mice. *Cell Calcium,* 37**,** 267-78.

VALKO, M., LEIBFRITZ, D., MONCOL, J., CRONIN, M. T., MAZUR, M. & TELSER, J. 2007. Free radicals and antioxidants in normal physiological functions and human disease. *Int J Biochem Cell Biol,* 39**,** 44-84.

VAN DE GRAAF, S. F., HOENDEROP, J. G., VAN DER KEMP, A. W., GISLER, S. M. & BINDELS, R. J. 2006. Interaction of the epithelial Ca2+ channels TRPV5 and TRPV6 with the intestine- and kidney-enriched PDZ protein NHERF4. *Pflugers Arch,* 452**,** 407-17.

VENKATACHALAM, K., HOFMANN, T. & MONTELL, C. 2006. Lysosomal localization of TRPML3 depends on TRPML2 and the mucolipidosis-associated protein TRPML1. *J Biol Chem,* 281**,** 17517-27.

VENKATACHALAM, K. & MONTELL, C. 2007. TRP channels. *Annu Rev Biochem,* 76**,** 387-417.

VENKATACHALAM, K., ZHENG, F. & GILL, D. L. 2003. Regulation of canonical transient receptor potential (TRPC) channel function by diacylglycerol and protein kinase C. *J Biol Chem,* 278**,** 29031-40.

VENNEKENS, R., HOENDEROP, J. G., PRENEN, J., STUIVER, M., WILLEMS, P. H., DROOGMANS, G., NILIUS, B. & BINDELS, R. J. 2000. Permeation and gating properties of the novel epithelial Ca(2+) channel. *J Biol Chem,* 275**,** 3963-9.

VERMA, S., QUILLINAN, N., YANG, Y. F., NAKAYAMA, S., CHENG, J., KELLEY, M. H. & HERSON, P. S. 2012. TRPM2 channel activation following in vitro ischemia contributes to male hippocampal cell death. *Neurosci Lett,* 530**,** 41-6.

VOGT-EISELE, A. K., WEBER, K., SHERKHELI, M. A., VIELHABER, G., PANTEN, J., GISSELMANN, G. & HATT, H. 2007. Monoterpenoid agonists of TRPV3. *Br J Pharmacol,* 151**,** 530-40.

VRIENS, J., OWSIANIK, G., FISSLTHALER, B., SUZUKI, M., JANSSENS, A., VOETS, T., MORISSEAU, C., HAMMOCK, B. D., FLEMING, I., BUSSE, R. & NILIUS, B. 2005. Modulation of the Ca2 permeable cation channel TRPV4 by cytochrome P450 epoxygenases in vascular endothelium. *Circ Res,* 97**,** 908-15.

WAGNER, T. F., LOCH, S., LAMBERT, S., STRAUB, I., MANNEBACH, S., MATHAR, I., DUFER, M., LIS, A., FLOCKERZI, V., PHILIPP, S. E. & OBERWINKLER, J. 2008. Transient receptor potential M3 channels are ionotropic steroid receptors in pancreatic beta cells. *Nat Cell Biol,* 10**,** 1421-30.

WALKER, K. M., URBAN, L., MEDHURST, S. J., PATEL, S., PANESAR, M., FOX, A. J. & MCINTYRE, P. 2003. The VR1 antagonist capsazepine reverses mechanical hyperalgesia in models of inflammatory and neuropathic pain. *J Pharmacol Exp Ther,* 304**,** 56-62.

WANG, B., LI, W., MENG, X. & ZOU, F. 2009. Hypoxia up-regulates vascular endothelial growth factor in U-87 MG cells: involvement of TRPC1. *Neurosci Lett,* 459**,** 132-6.

WANG, J., SHIMODA, L. A. & SYLVESTER, J. T. 2004. Capacitative calcium entry and TRPC channel proteins are expressed in rat distal pulmonary arterial smooth muscle. *Am J Physiol Lung Cell Mol Physiol,* 286**,** L848-58.

WATANABE, H., VRIENS, J., PRENEN, J., DROOGMANS, G., VOETS, T. & NILIUS, B. 2003. Anandamide and arachidonic acid use epoxyeicosatrienoic acids to activate TRPV4 channels. *Nature,* 424**,** 434-8.

WEHAGE, E., EISFELD, J., HEINER, I., JUNGLING, E., ZITT, C. & LUCKHOFF, A. 2002. Activation of the cation channel long transient receptor potential channel 2 (LTRPC2) by hydrogen peroxide. A splice variant reveals a mode of activation independent of ADP-ribose. *J Biol Chem,* 277**,** 23150-6.

WEHRHAHN, J., KRAFT, R., HARTENECK, C. & HAUSCHILDT, S. 2010. Transient receptor potential melastatin 2 is required for lipopolysaccharide-induced cytokine production in human monocytes. *J Immunol,* 184**,** 2386-93.

WINKING, M., HOFFMANN, D. C., KUHN, C., HILGERS, R. D., LUCKHOFF, A. & KUHN, F. J. 2012. Importance of a conserved sequence motif in transmembrane segment S3 for the gating of human TRPM8 and TRPM2. *PLoS One,* 7**,** e49877.

WISSENBACH, U., BODDING, M., FREICHEL, M. & FLOCKERZI, V. 2000. Trp12, a novel Trp related protein from kidney. *FEBS Lett,* 485**,** 127-34.

WOLF, F. I., TRAPANI, V., SIMONACCI, M., MASTROTOTARO, L., CITTADINI, A. & SCHWEIGEL, M. 2010. Modulation of TRPM6 and Na(+)/Mg(2+) exchange in mammary epithelial cells in response to variations of magnesium availability. *J Cell Physiol,* 222**,** 374-81.

WORLEY, P. F., ZENG, W., HUANG, G. N., YUAN, J. P., KIM, J. Y., LEE, M. G. & MUALLEM, S. 2007. TRPC channels as STIM1-regulated store-operated channels. *Cell Calcium,* 42**,** 205-11.

WU, G., HAYASHI, T., PARK, J. H., DIXIT, M., REYNOLDS, D. M., LI, L., MAEDA, Y., CAI, Y., COCA-PRADOS, M. & SOMLO, S. 1998. Identification of PKD2L, a human PKD2-related gene: tissue-specific expression and mapping to chromosome 10q25. *Genomics,* 54**,** 564-8.

WUENSCH, T., THILO, F., KRUEGER, K., SCHOLZE, A., RISTOW, M. & TEPEL, M. 2010. High glucose-induced oxidative stress increases transient receptor potential channel expression in human monocytes. *Diabetes,* 59**,** 844-9.

XIA, R., MEI, Z. Z., MAO, H. J., YANG, W., DONG, L., BRADLEY, H., BEECH, D. J. & JIANG, L. H. 2008. Identification of pore residues engaged in determining divalent cationic permeation in transient receptor potential melastatin subtype channel 2. *J Biol Chem,* 283**,** 27426-32.

XIAO, Y., LV, X., CAO, G., BIAN, G., DUAN, J., AI, J., SUN, H., LI, Q., YANG, Q., CHEN, T., ZHAO, D., TAN, R., LIU, Y., WANG, Y., ZHANG, Z., YANG, Y., WEI, Y. & ZHOU, Q. 2010.

Overexpression of Trpp5 contributes to cell proliferation and apoptosis probably through involving calcium homeostasis. *Mol Cell Biochem,* 339**,** 155-61.

XING, J. & LI, J. 2007. TRPV1 receptor mediates glutamatergic synaptic input to dorsolateral periaqueductal gray (dl-PAG) neurons. *J Neurophysiol,* 97**,** 503-11.

XU, H., RAMSEY, I. S., KOTECHA, S. A., MORAN, M. M., CHONG, J. A., LAWSON, D., GE, P., LILLY, J., SILOS-SANTIAGO, I., XIE, Y., DISTEFANO, P. S., CURTIS, R. & CLAPHAM, D. E. 2002. TRPV3 is a calcium-permeable temperature-sensitive cation channel. *Nature,* 418**,** 181-6.

XU, S. Z., ZENG, F., BOULAY, G., GRIMM, C., HARTENECK, C. & BEECH, D. J. 2005. Block of TRPC5 channels by 2-aminoethoxydiphenyl borate: a differential, extracellular and voltage-dependent effect. *Br J Pharmacol,* 145**,** 405-14.

XU, X. Z., MOEBIUS, F., GILL, D. L. & MONTELL, C. 2001. Regulation of melastatin, a TRP-related protein, through interaction with a cytoplasmic isoform. *Proc Natl Acad Sci U S A,* 98**,** 10692-7.

XU, Y., KIM, S. O., LI, Y. & HAN, J. 2006. Autophagy contributes to caspase-independent macrophage cell death. *J Biol Chem,* 281**,** 19179-87.

YAMAMOTO, S., SHIMIZU, S., KIYONAKA, S., TAKAHASHI, N., WAJIMA, T., HARA, Y., NEGORO, T., HIROI, T., KIUCHI, Y., OKADA, T., KANEKO, S., LANGE, I., FLEIG, A., PENNER, R., NISHI, M., TAKESHIMA, H. & MORI, Y. 2008. TRPM2-mediated Ca2+influx induces chemokine production in monocytes that aggravates inflammatory neutrophil infiltration. *Nat Med,* 14**,** 738-47.

YANG, K. T., CHANG, W. L., YANG, P. C., CHIEN, C. L., LAI, M. S., SU, M. J. & WU, M. L. 2006. Activation of the transient receptor potential M2 channel and poly(ADP-ribose) polymerase is involved in oxidative stress-induced cardiomyocyte death. *Cell Death Differ,* 13**,** 1815-26.

YANG, W., MANNA, P. T., ZOU, J., LUO, J., BEECH, D. J., SIVAPRASADARAO, A. & JIANG, L. H. 2011. Zinc inactivates melastatin transient receptor potential 2 channels via the outer pore. *J Biol Chem,* 286**,** 23789-98.

YANG, W., ZOU, J., XIA, R., VAAL, M. L., SEYMOUR, V. A., LUO, J., BEECH, D. J. & JIANG, L. H. 2010. State-dependent inhibition of TRPM2 channel by acidic pH. *J Biol Chem,* 285**,** 30411-8.

YILDIRIM, E. & BIRNBAUMER, L. 2007. TRPC2: molecular biology and functional importance. *Handb Exp Pharmacol***,** 53-75.

YUASA, K., MATSUDA, T. & TSUJI, A. 2011. Functional regulation of transient receptor potential canonical 7 by cGMP-dependent protein kinase Ialpha. *Cell Signal,* 23**,** 1179-87.

ZAN, Y., HAAG, J. D., CHEN, K. S., SHEPEL, L. A., WIGINGTON, D., WANG, Y. R., HU, R., LOPEZ-GUAJARDO, C. C., BROSE, H. L., PORTER, K. I., LEONARD, R. A., HITT, A. A., SCHOMMER, S. L., ELEGBEDE, A. F. & GOULD, M. N. 2003. Production of knockout rats using ENU mutagenesis and a yeast-based screening assay. *Nat Biotechnol,* 21**,** 645-51.

ZENG, B., CHEN, G. L. & XU, S. Z. 2012. Divalent copper is a potent extracellular blocker for TRPM2 channel. *Biochem Biophys Res Commun,* 424**,** 279-84.

ZENG, F., XU, S. Z., JACKSON, P. K., MCHUGH, D., KUMAR, B., FOUNTAIN, S. J. & BEECH, D. J. 2004. Human TRPC5 channel activated by a multiplicity of signals in a single cell. *J Physiol,* 559**,** 739-50.

ZENG, X., SIKKA, S. C., HUANG, L., SUN, C., XU, C., JIA, D., ABDEL-MAGEED, A. B., POTTLE, J. E., TAYLOR, J. T. & LI, M. 2010. Novel role for the transient receptor potential channel TRPM2 in prostate cancer cell proliferation. *Prostate Cancer Prostatic Dis,* 13**,** 195-201.

ZHANG, W., CHU, X., TONG, Q., CHEUNG, J. Y., CONRAD, K., MASKER, K. & MILLER, B. A. 2003. A novel TRPM2 isoform inhibits calcium influx and susceptibility to cell death. *J Biol Chem,* 278**,** 16222-9.

ZHANG, W., HIRSCHLER-LASZKIEWICZ, I., TONG, Q., CONRAD, K., SUN, S. C., PENN, L., BARBER, D. L., STAHL, R., CAREY, D. J., CHEUNG, J. Y. & MILLER, B. A. 2006. TRPM2 is an ion channel that modulates hematopoietic cell death through activation of caspases and PARP cleavage. *Am J Physiol Cell Physiol,* 290**,** C1146-59.

ZHANG, X., HUANG, J. & MCNAUGHTON, P. A. 2005. NGF rapidly increases membrane expression of TRPV1 heat-gated ion channels. *EMBO J,* 24**,** 4211-23.

ZHANG, Z., ZHANG, W., JUNG, D. Y., KO, H. J., LEE, Y., FRIEDLINE, R. H., LEE, E., JUN, J., MA, Z., KIM, F., TSITSILIANOS, N., CHAPMAN, K., MORRISON, A., COOPER, M. P., MILLER, B. A. & KIM, J. K. 2012. TRPM2 Ca2+ channel regulates energy balance and glucose metabolism. *Am J Physiol Endocrinol Metab,* 302**,** E807-16.

ZHONG, Z., ZHAI, Y., LIANG, S., MORI, Y., HAN, R., SUTTERWALA, F. S. & QIAO, L. 2013. TRPM2 links oxidative stress to NLRP3 inflammasome activation. *Nat Commun,* 4**,** 1611.

ZHU, J., YU, Y., ULBRICH, M. H., LI, M. H., ISACOFF, E. Y., HONIG, B. & YANG, J. 2011. Structural model of the TRPP2/PKD1 C-terminal coiled-coil complex produced by a combined computational and experimental approach. *Proc Natl Acad Sci U S A,* 108**,** 10133-8.

ZOU, J., YANG, W., BEECH, D. J. & JIANG, L. H. 2011. A residue in the TRPM2 channel outer pore is crucial in determining species-dependent sensitivity to extracellular acidic pH. *Pflugers Arch,* 462**,** 293-302.

ZUFALL, F. 2005. The TRPC2 ion channel and pheromone sensing in the accessory olfactory system. *Naunyn Schmiedebergs Arch Pharmacol,* 371**,** 245-50.

ZUFALL, F., UKHANOV, K., LUCAS, P., LIMAN, E. R. & LEINDERS-ZUFALL, T. 2005. Neurobiology of TRPC2: from gene to behavior. *Pflugers Arch,* 451**,** 61-71.

ZURBORG, S., YURGIONAS, B., JIRA, J. A., CASPANI, O. & HEPPENSTALL, P. A. 2007. Direct activation of the ion channel TRPA1 by Ca2+. *Nat Neurosci,* 10**,** 277-9.